

# **INVESTIGATING THE USE OF A NEW UNIVERSAL BREAKAWAY STEEL POST**

## Submitted by

Steven W. Arens, M.S.C.E., E.I.T.  
Graduate Research Assistant

Dean L. Sicking, Ph.D., P.E.  
Professor and MwRSF Director

Ronald K. Faller, Ph.D., P.E.  
Research Assistant Professor

John D. Reid, Ph.D.  
Professor

Robert W. Bielenberg, M.S.M.E., E.I.T.  
Research Associate Engineer

John R. Rohde, Ph.D., P.E.  
Associate Professor

Karla A. Lechtenberg, M.S.M.E., E.I.T.  
Research Associate Engineer

## **MIDWEST ROADSIDE SAFETY FACILITY**

University of Nebraska-Lincoln  
527 Nebraska Hall  
Lincoln, Nebraska 68588-0529  
(402) 472-0965

## Submitted to

### **MINNESOTA DEPARTMENT OF TRANSPORTATION (MnDOT)**

Transportation Building  
395 John Ireland Boulevard  
Saint Paul, Minnesota 55155

MwRSF Research Report No. TRP-03-218-09

August 3, 2009

## TECHNICAL REPORT DOCUMENTATION PAGE

1. Report No. <b>TRP-03-218-09</b>	2.	3. Recipient's Accession No.	
4. Title and Subtitle <b>INVESTIGATING THE USE OF A NEW UNIVERSAL BREAKAWAY STEEL POST</b>		5. Report Date <b>August 3, 2009</b>	
		6.	
7. Author(s) <b>Arens, S.W., Sicking, D.L., Faller, R.K., Reid, J.D., Bielenberg, R.W., Rohde, J.R., and Lechtenberg, K.A.</b>		8. Performing Organization Report No. <b>TRP-03-218-09</b>	
9. Performing Organization Name and Address <b>Midwest Roadside Safety Facility (MwRSF) University of Nebraska-Lincoln 527 Nebraska Hall Lincoln, Nebraska 68588-0529</b>		10. Project/Task/Work Unit No.	
		11. Contract © or Grant (G) No. <b>SPR-3(017)</b>	
12. Sponsoring Organization Name and Address <b>Minnesota Department of Transportation (MnDOT) Transportation Building 395 John Ireland Boulevard Saint Paul, Minnesota 55155</b>		13. Type of Report and Period Covered <b>Final Report 2007-2009</b>	
		14. Sponsoring Agency Code <b>SPR-3(017) Supplement #39</b>	
15. Supplementary Notes <b>Prepared in cooperation with U.S. Department of Transportation, Federal Highway Administration.</b>			
16. Abstract (Limit: 200 words) A new fracturing-bolt, universal breakaway steel post was developed and evaluated for use as a replacement for the wood CRT post currently used in the thrie beam bullnose system. It was the intent that the new universal breakaway steel post would also become a replacement for wood CRT posts used in other guardrail systems. This research study focused only on a steel post for the thrie beam bullnose system. After investigating numerous candidate steel post concepts, bogie testing was used to select the most promising design, a fracturing-bolt steel post. The fracturing-bolt, steel post successfully matched the strength and dynamic behavior of the wood CRT post in three different impact orientations. Preliminary LS-DYNA simulation modeling was also performed to analyze the fracturing-bolt, steel post. Subsequently, the breakaway steel post was implemented into the thrie beam bullnose barrier system and subjected to one 2000P full-scale vehicle crash test according to the TL-3 of NCHRP Report No. 350. Test no. USPBN-1 demonstrated that the breakaway steel post did not perform satisfactory in the bullnose system as the pickup truck was not captured and later overrode the guardrail system. The fracturing-bolt posts did not absorb sufficient energy to safely capture and contain the vehicle. Post no. 2 did not break away quickly, thus causing the pickup to redirect more than observed in prior wood-post, bullnose testing. Based on the unsatisfactory results, two research plans were proposed for continuing the research and development of a breakaway steel post for use in bullnose barriers.			
17. Document Analysis/Descriptors <b>Highway Safety, Guardrail Posts, Wood Posts, Breakaway Steel Posts, Bogie Testing, Bullnose Barrier, Median Barrier, Crash Test, Compliance Test</b>		18. Availability Statement <b>No restrictions. Document available from: National Technical Information Services, Springfield, Virginia 22161</b>	
19. Security Class (this report) <b>Unclassified</b>	20. Security Class (this page) <b>Unclassified</b>	21. No. of Pages <b>311</b>	22. Price

## **DISCLAIMER STATEMENT**

The contents of this report reflect the views of the authors who are responsible for the facts and the accuracy of the data presented herein. The contents do not necessarily reflect the official views nor policies of Minnesota Department of Transportation, the United States Department of Transportation, nor the Federal Highway Administration. This report does not constitute a standard, specification, regulation, product, or endorsement.

## **UNCERTAINTY OF MEASUREMENT STATEMENT**

The Midwest Roadside Safety Facility (MwRSF) has determined the uncertainty of measurement for several parameters involved in non-standard testing of roadside safety hardware as well as in standard full-scale crash testing of roadside safety features. Information regarding the uncertainty of measurement for critical parameters is available upon request by the sponsor and the Federal Highway Administration.

## **ACKNOWLEDGMENTS**

The authors wish to acknowledge several sources that made a contribution to this project:

(1) Minnesota Department of Transportation for sponsoring this project; and (2) MwRSF personnel for constructing the barrier and conducting the crash test.

Acknowledgment is also given to the following individuals who made a contribution to the completion of this research project.

### **Midwest Roadside Safety Facility**

J.C. Holloway, M.S.C.E., E.I.T., Research Manager  
S.K. Rosenbaugh, M.S.C.E., E.I.T., Research Associate Engineer  
C.L. Meyer, B.S.M.E., E.I.T., Research Engineer II  
A.T. Russell, B.S.B.A., Laboratory Mechanic II  
K.L. Krenk, B.S.M.A., Field Operations Manager  
A.T. McMaster, Laboratory Mechanic I  
Undergraduate and Graduate Assistants

### **Dunlap Photography**

James Dunlap, President and Owner

## TABLE OF CONTENTS

DISCLAIMER STATEMENT .....	ii
UNCERTAINTY OF MEASUREMENT STATEMENT .....	ii
ACKNOWLEDGMENTS .....	iii
TABLE OF CONTENTS.....	iv
LIST OF FIGURES .....	viii
LIST OF TABLES .....	xv
1 INTRODUCTION .....	1
1.1 Background.....	1
1.2 Objective.....	2
1.3 Research Approach.....	3
2 LITERATURE REVIEW .....	4
2.1 Previous CRT Wood Post Testing.....	4
2.2 Previous Breakaway Steel Post Testing.....	5
3 CRT PHYSICAL TESTING DETAILS.....	13
3.1 Introduction.....	13
3.2 CRT Wood Post Details.....	13
3.3 CRT Bogie Test Results.....	17
3.3.1 Test Nos. MNCRT-1, MNCRT-2, and MNCRT-3.....	17
3.3.2 Test Nos. MNCRT-4, MNCRT-5, and MNCRT-6.....	22
3.3.3 Test Nos. MNCRT-7, MNCRT-8, and MNCRT-9.....	27
3.4 Conclusion/Recommendations .....	34
4 PRELIMINARY BREAKAWAY POST DESIGNS.....	36
4.1 Introduction.....	36
4.2 Preliminary Breakaway Post Ideas .....	36
4.2.1 Steel Breakaway Post Ideas .....	37
4.2.2 Brittle Material Post Ideas .....	38
4.3 Options for First Round of Bogie Testing .....	45
5 BREAKAWAY POST BOGIE TESTING – ROUND 1.....	47
5.1 Purpose.....	47
5.2 Scope.....	47
5.3 Post Details .....	48
5.3.1 Steel Tube in Steel Tube.....	48
5.3.2 Steel Tube in Steel Tube With Thru Bolt .....	53
5.3.3 Upper FRP Post.....	57
5.3.4 Fracturing Bolt (Slipbase).....	61
5.3.5 Circular Fillet Weld .....	66
5.4 Equipment and Instrumentation.....	71
5.4.1 Bogie.....	71
5.4.2 Accelerometer.....	72
5.4.3 Pressure Tape Switches.....	73
5.4.4 Photography Cameras .....	73
5.5 Methodology of Testing.....	73
5.6 End of Test Determination.....	74

5.7 Data Processing.....	75
5.8 Round 1 Bogie Testing Results.....	77
5.8.1 Test UBSP-1 – Steel Tube in Steel Tube.....	78
5.8.2 Test UBSP-2 – Steel Tube in Steel Tube with Thru Bolt.....	81
5.8.3 Test UBSP-3 – Upper FRP Tube.....	84
5.8.4 Test UBSP-4 – Upper FRP Tube.....	87
5.8.5 Test UBSP-5 – Fracturing Bolt (Slipbase).....	90
5.8.6 Test UBSP-6 – Fracturing Bolt (Slipbase).....	93
5.8.7 Test UBSP-7 – Circular Fillet Weld.....	96
5.8.8 Test UBSP-8 – Circular Fillet Weld.....	98
5.9 Round 1 Summary and Conclusions.....	101
<b>6 BREAKAWAY POST BOGIE TESTING – ROUND 2.....</b>	<b>104</b>
6.1 Purpose.....	104
6.2 Scope.....	104
6.3 Post Details.....	105
6.3.1 Fracturing Bolt.....	105
6.3.2 Circular Fillet Weld.....	111
6.4 Equipment and Instrumentation.....	116
6.5 Round 2 Bogie Testing Results.....	117
6.5.1 Test UBSP-9 – Fracturing Bolt.....	118
6.5.2 Test UBSP-10 – Fracturing Bolt.....	121
6.5.3 Test UBSP-11 – Circular Fillet Weld.....	124
6.5.4 Test UBSP-12 – Circular Fillet Weld.....	127
6.5.5 Test UBSP-13 – Fracturing Bolt.....	130
6.6 Test UBSP-9 versus Test UBSP-13.....	133
6.7 Round 2 Summary and Conclusions.....	136
<b>7 WOOD CRT POST BOGIE TESTING IN SOIL.....</b>	<b>139</b>
7.1 Purpose.....	139
7.2 Scope.....	139
7.3 Post Details.....	140
7.4 Equipment and Instrumentation.....	140
7.5 Test Results for Wood CRT Posts in Soil.....	143
7.5.1 Test UBSP-14 – Strong Axis (0 Degree) Impact on CRT Post.....	144
7.5.2 Test UBSP-15 – Strong-Axis (0 Degree) Impact on CRT Post.....	147
7.5.3 Test UBSP-16 – Weak-Axis (90 Degree) Impact on CRT Post.....	150
7.5.4 Test UBSP-17 – Weak-Axis (90 Degree) Impact on CRT Post.....	153
7.5.5 Test UBSP-18 – Diagonal-Axis (45 Degree) Impact on CRT Post.....	156
7.5.6 Test UBSP-19 – Diagonal-Axis (45 Degree) Impact on CRT Post.....	159
7.6 Summary and Conclusions.....	162
<b>8 BREAKAWAY POST BOGIE TESTING – ROUND 3.....</b>	<b>165</b>
8.1 Purpose.....	165
8.2 Scope.....	165
8.3 Post Details.....	166
8.4 Equipment and Instrumentation.....	166
8.5 Test Results for Fracturing Bolt Concept – Round 3.....	171

8.5.1 Test UBSP-20 – Fracturing Bolt – Strong Axis.....	172
8.5.2 Test UBSP-21 – Fracturing Bolt – 45-Degree Angle .....	176
8.6 Round 3 Summary and Conclusions.....	180
9 COMPUTER SIMULATION.....	182
9.1 Introduction.....	182
9.2 Previous LS-DYNA Modeling .....	182
9.3 Fracturing Bolt Model Details .....	183
9.3.1 Part Details.....	183
9.3.2 Connection Details.....	185
9.4 Initial Simulation Results – Rigid Cylinder Impacts .....	185
9.4.1 Contact and Prestressing Issues .....	186
9.4.2 Prestressing Results .....	186
9.4.3 Rigid Cylinder Impact Results.....	187
9.5 Bogie and Soil Model Details.....	188
9.5.1 Bogie Model.....	188
9.5.2 Soil Model.....	189
9.6 Final Simulation Results.....	190
9.6.1 Soil Loading Curve .....	191
9.6.2 Final Bolt Material Properties.....	192
9.6.3 Strong-Axis Impact Results .....	192
9.6.4 Weak-Axis Impact Results .....	197
9.6.5 Diagonal (45-Degree) Axis Impact Results.....	200
9.7 Conclusions/Recommendations.....	203
10 FULL-SCALE CRASH TEST PROGRAM.....	205
10.1 Test Requirements .....	205
10.2 Evaluation Criteria.....	206
10.3 Bullnose Median Barrier Design Details .....	210
10.3.1 Revised Weld Details for Fracturing Bolt Post.....	210
10.4 Test Facility .....	230
10.5 Vehicle Tow and Guidance System.....	230
10.6 Test Vehicle .....	230
10.7 Data Acquisition Systems .....	235
10.7.1 Accelerometers .....	235
10.7.2 Rate Transducers.....	236
10.7.3 High-Speed Photography.....	237
10.7.4 Pressure Tape Switches.....	237
10.8 Crash Test No. USPBN-1 .....	239
10.8.1 Weather Conditions .....	239
10.8.2 Test Description .....	239
10.8.3 Vehicle Damage.....	240
10.8.4 Barrier Damage.....	241
10.8.5 Occupant Risk Values.....	242
10.8.6 Discussion of Results.....	243
11 COMPARISON OF CRASH TESTS USING TEST DESIGNATION NO. 3-38 .....	258
11.1 Comparison of Crash Tests Designation No. 3-38 .....	258

12 SUMMARY AND CONCLUSIONS .....265  
    12.1 Summary ..... 265  
13 RECOMMENDATIONS .....269  
    13.1 Future Work ..... 269  
        13.1.1 - Plan No. 1 – Implement Modifications and Re-run Full-Scale Crash Test..... 269  
        13.1.2 - Plan No. 2 – Refocus Effort on More Research and Development ..... 271  
14 REFERENCES .....272  
15 APPENDICES .....275  
    Appendix A. Bogie Testing Results..... 276  
    Appendix B. Occupant Compartment Deformation, Test USPBN-1 ..... 297  
    Appendix C. Accelerometer Data Analysis, Test USPBN-1 ..... 301  
    Appendix D. Summary of Test USPBN-1 in Metric Units ..... 309



## LIST OF FIGURES

Figure 1. CRT Wood Post in Rigid Sleeve.....	14
Figure 2a. Cross-Sectional Dimensions for CRT Wood Posts – English.....	15
Figure 2b. Cross-Sectional Dimensions for CRT Wood Posts – Metric.....	15
Figure 3a. Force versus Deflection Curves for MNCRT-1, 2, and 3 – English.....	20
Figure 3b. Force versus Deflection Curves for MNCRT-1, 2, and 3 – Metric.....	20
Figure 4a. Energy versus Deflection Curves for MNCRT-1, 2, and 3 – English.....	21
Figure 4b. Energy versus Deflection Curves for MNCRT-1, 2, and 3 – Metric.....	21
Figure 5a. Force versus Deflection Curves for MNCRT-4, 5, and 6 – English.....	25
Figure 5b. Force versus Deflection Curves for MNCRT-4, 5, and 6 – Metric.....	25
Figure 6a. Energy versus Deflection Curves for MNCRT-4, 5, and 6 – English.....	26
Figure 6b. Energy versus Deflection Curves for MNCRT-4, 5, and 6 – Metric.....	26
Figure 7a. Force versus Deflection Curves for MNCRT-7, 8, and 9 – English.....	29
Figure 7b. Force versus Deflection Curves for MNCRT-7, 8, and 9 – Metric.....	29
Figure 8a. Energy versus Deflection Curves for MNCRT-7, 8, and 9 – English.....	30
Figure 8b. Energy versus Deflection Curves for MNCRT-7, 8, and 9 – Metric.....	30
Figure 9a. Force versus Deflection Curves Minus Fixture Effect– English.....	32
Figure 9b. Force versus Deflection Curves Minus Fixture Effect – Metric.....	32
Figure 10a. Energy versus Deflection Curves Minus Fixture Effect – English.....	33
Figure 10b. Energy versus Deflection Curves Minus Fixture Effect – Metric.....	33
Figure 11a. Peak Forces and Energy Levels of the CRT Post – English.....	35
Figure 11b. Peak Forces Energy and Levels of the CRT Post - Metric.....	35
Figure 12. Fiberglass Reinforced Plastic Structural Shape.....	39
Figure 13. Recycled Plastic Post Options.....	40
Figure 14. Preliminary Steel W8x10 (W203x14.9) Breakaway Post Designs.....	41
Figure 15a. Preliminary Tubular Breakaway Post Designs – English.....	42
Figure 15b. Preliminary Tubular Breakaway Post Designs – Metric.....	43
Figure 16a. Preliminary Slipbase Post Design - English.....	44
Figure 16b. Preliminary Slipbase Post Design - Metric.....	44
Figure 17. Steel Tube In Steel Tube Assembly Details.....	50
Figure 18. Steel Tube In Steel Tube Part Details.....	51
Figure 19. Steel Tube In Steel Tube Post Details.....	52
Figure 20. Steel Tube In Steel Tube With Thru Bolt Assembly Details.....	54
Figure 21. Steel Tube In Steel Tube With Thru Bolt Part Details.....	55
Figure 22. Steel Tube In Steel Tube With Thru Bolt Post Details.....	56
Figure 23. Upper FRP Post Assembly Details.....	58
Figure 24. Upper FRP Post Shim Details.....	59
Figure 25. Upper FRP Post Part Details.....	60
Figure 26. Assembled Fracturing Bolt (Slipbase) Design.....	61
Figure 27. Fracturing Bolt (Slipbase) Assembly Details.....	62
Figure 28. Fracturing Bolt (Slipbase) Steel Plate Details.....	63
Figure 29. Fracturing Bolt (Slipbase) Part Details.....	64
Figure 30. Fracturing Bolt (Slipbase) Post Details.....	65
Figure 31. Circular Fillet Weld Assembly Details.....	67

Figure 32. Circular Fillet Weld Connection Details .....	68
Figure 33. Circular Fillet Weld Post Details.....	69
Figure 34. Circular Fillet Weld Calculations.....	70
Figure 35. Rigid Frame Bogie on Guidance Track.....	72
Figure 36. General Bogie Test Setup.....	76
Figure 37a. Force versus Deflection Curve for UBSP-1 - English.....	79
Figure 37b. Force versus Deflection Curve for UBSP-1 - Metric .....	79
Figure 38a. Energy versus Deflection Curve for UBSP-1 - English .....	79
Figure 38b. Energy versus Deflection Curve for UBSP-1 - Metric.....	79
Figure 39. Time Sequential Photographs, Test UBSP-1.....	80
Figure 40. Post Impact Images of Test UBSP-1 .....	80
Figure 41a. Force versus Deflection Curve for UBSP-2 - English.....	82
Figure 41b. Force versus Deflection Curve for UBSP-2 - Metric .....	82
Figure 42a. Energy versus Deflection Curve for UBSP-2 - English .....	82
Figure 42b. Energy versus Deflection Curve for UBSP-2 - Metric.....	82
Figure 43. Time Sequential Images, Test UBSP-2 .....	83
Figure 44. Post-Impact Images of Test UBSP-2.....	83
Figure 45a. Force versus Deflection Curve for UBSP-3 - English.....	85
Figure 45b. Force versus Deflection Curve for UBSP-3 - Metric .....	85
Figure 46a. Energy versus Deflection Curve for UBSP-3 - English .....	85
Figure 46b. Energy versus Deflection Curve for UBSP-3 - Metric.....	85
Figure 47. Time Sequential Photographs, Test UBSP-3.....	86
Figure 48. Post-Impact Images of UBSP-3.....	86
Figure 49a. Force versus Deflection Curve for UBSP-4 - English.....	88
Figure 49b. Force versus Deflection Curve for UBSP-4 - Metric .....	88
Figure 50a. Energy versus Deflection Curve for UBSP-4 - English .....	88
Figure 50b. Energy versus Deflection Curve for UBSP-4 - Metric.....	88
Figure 51. Time Sequential Photographs, Test UBSP-4.....	89
Figure 52. Post-Impact Images of UBSP-4.....	89
Figure 53a. Force versus Deflection Curve for UBSP-5 - English.....	91
Figure 53b. Force versus Deflection Curve for UBSP-5 - Metric .....	91
Figure 54a. Energy versus Deflection Curve for UBSP-5 - English .....	91
Figure 54b. Energy versus Deflection Curve for UBSP-5 - Metric.....	91
Figure 55. Time Sequential Photographs, Test UBSP-5.....	92
Figure 56. Post-Impact Images of UBSP-5.....	92
Figure 57a. Force versus Deflection Curve for UBSP-6 - English.....	94
Figure 57b. Force versus Deflection Curve for UBSP-6 - Metric .....	94
Figure 58a. Energy versus Deflection Curve for UBSP-6 - English .....	94
Figure 58b. Energy versus Deflection Curve for UBSP-6 - Metric.....	94
Figure 59. Time Sequential Photographs, Test UBSP-6.....	95
Figure 60. Post-Impact Images of UBSP-6.....	95
Figure 61. Time Sequential Photographs, Test UBSP-7.....	97
Figure 62. Post-Impact Images of UBSP-7.....	97
Figure 63a. Force versus Deflection Curve for UBSP-8 - English.....	99
Figure 63b. Force versus Deflection Curve for UBSP-8 - Metric .....	99

Figure 64a. Energy versus Deflection Curve for UBSP-8 - English ..... 99  
Figure 64b. Energy versus Deflection Curve for UBSP-8 - Metric..... 99  
Figure 65. Time Sequential Photographs, Test UBSP-8..... 100  
Figure 66. Post-Impact Images of UBSP-8..... 100  
Figure 67. Fracturing Bolt Calculations..... 106  
Figure 68. Revised Fracturing Bolt Design Details ..... 107  
Figure 69. Revised Fracturing Bolt Design Details ..... 108  
Figure 70. Revised Fracturing Bolt Design Details ..... 109  
Figure 71. Revised Fracturing Bolt Design Details ..... 110  
Figure 72. Circular Fillet Weld Tear Out Calculations..... 112  
Figure 73. Revised Circular Fillet Weld Design Details ..... 113  
Figure 74. Revised Circular Fillet Weld Design Details ..... 114  
Figure 75. Revised Circular Fillet Weld Design Details ..... 115  
Figure 76a. Force versus Deflection Curve for UBSP-9 - English..... 119  
Figure 76b. Force versus Deflection Curve for UBSP-9 - Metric ..... 119  
Figure 77a. Energy versus Deflection Curve for UBSP-9 - English ..... 119  
Figure 77b. Energy versus Deflection Curve for UBSP-9 - Metric..... 119  
Figure 78. Time Sequential Photographs, Test UBSP-9..... 120  
Figure 79. Post-Impact Images of UBSP-9..... 120  
Figure 80a. Force versus Deflection Curve for UBSP-10 - English..... 122  
Figure 80b. Force versus Deflection Curve for UBSP-10 - Metric ..... 122  
Figure 81a. Energy versus Deflection Curve for UBSP-10 - English ..... 122  
Figure 81b. Energy versus Deflection Curve for UBSP-10 - Metric..... 122  
Figure 82. Time Sequential Photographs, Test UBSP-10..... 123  
Figure 83. Post-Impact Images of UBSP-10..... 123  
Figure 84a. Force versus Deflection Curve for UBSP-11 - English..... 125  
Figure 84b. Force versus Deflection Curve for UBSP-11 - Metric ..... 125  
Figure 85a. Energy versus Deflection Curve for UBSP-11 - English ..... 125  
Figure 85b. Energy versus Deflection Curve for UBSP-11 - Metric..... 125  
Figure 86. Time Sequential Photographs, Test UBSP-11..... 126  
Figure 87. Post-Impact Images of UBSP-11..... 126  
Figure 88a. Force versus Deflection Curve for UBSP-12 - English..... 128  
Figure 88b. Force versus Deflection Curve for UBSP-12 - Metric ..... 128  
Figure 89a. Energy versus Deflection Curve for UBSP-12 - English ..... 128  
Figure 89b. Energy versus Deflection Curve for UBSP-12 - Metric..... 128  
Figure 90. Time Sequential Photographs, Test UBSP-12..... 129  
Figure 91. Post-Impact Images of UBSP-12..... 129  
Figure 92a. Force versus Deflection Curve for UBSP-13 - English..... 131  
Figure 92b. Force versus Deflection Curve for UBSP-13 - Metric ..... 131  
Figure 93a. Energy versus Deflection Curve for UBSP-13 - English ..... 131  
Figure 93b. Energy versus Deflection Curve for UBSP-13 - Metric..... 131  
Figure 94. Time Sequential Photographs, Test UBSP-13..... 132  
Figure 95. Post-Impact Images of UBSP-13..... 132  
Figure 96a. Force versus Deflection Curves for UBSP-9 and 13 – English..... 134  
Figure 96b. Force versus Deflection Curves for UBSP-9 and 13 – Metric ..... 134

Figure 97a. Energy versus Deflection for UBSP-9 and 13 – English.....	135
Figure 97b. Energy versus Deflection for UBSP-9 and 13 – Metric .....	135
Figure 98a. Force versus Deflection Curve for UBSP-14 - English.....	145
Figure 98b. Force versus Deflection Curve for UBSP-14 - Metric .....	145
Figure 99a. Energy versus Deflection Curve for UBSP-14 - English .....	145
Figure 99b. Energy versus Deflection Curve for UBSP-14 - Metric.....	145
Figure 100. Time Sequential Photographs, Test UBSP-14.....	146
Figure 101. Post-Impact Images of UBSP-14.....	146
Figure 102a. Force versus Deflection Curve for UBSP-15 - English.....	148
Figure 102b. Force versus Deflection Curve for UBSP-15 - Metric .....	148
Figure 103a. Energy versus Deflection Curve for UBSP-15 - English .....	148
Figure 103b. Energy versus Deflection Curve for UBSP-15 - Metric.....	148
Figure 104. Time Sequential Photographs, Test UBSP-15.....	149
Figure 105. Post-Impact Images of UBSP-15.....	149
Figure 106a. Force versus Deflection Curve for UBSP-16 - English.....	151
Figure 106b. Force versus Deflection Curve for UBSP-16 - Metric .....	151
Figure 107a. Energy versus Deflection Curve for UBSP-16 - English .....	151
Figure 107b. Energy versus Deflection Curve for UBSP-16 - Metric.....	151
Figure 108. Post-Impact Images of UBSP-16.....	152
Figure 109a. Force versus Deflection Curve for UBSP-17 - English.....	154
Figure 109b. Force versus Deflection Curve for UBSP-17 - Metric .....	154
Figure 110a. Energy versus Deflection Curve for UBSP-17 - English .....	154
Figure 110b. Energy versus Deflection Curve for UBSP-17 - Metric.....	154
Figure 111. Time Sequential Photographs, Test UBSP-17.....	155
Figure 112. Post-Impact Images of UBSP-17.....	155
Figure 113a. Force versus Deflection Curve for UBSP-18 - English.....	157
Figure 113b. Force versus Deflection Curve for UBSP-18 - Metric .....	157
Figure 114a. Energy versus Deflection Curve for UBSP-18 - English .....	157
Figure 114b. Energy versus Deflection Curve for UBSP-18 - Metric.....	157
Figure 115. Time Sequential Photographs, Test UBSP-18.....	158
Figure 116. Post-Impact Images of UBSP-18.....	158
Figure 117a. Force versus Deflection Curve for UBSP-19 - English.....	160
Figure 117b. Force versus Deflection Curve for UBSP-19 - Metric .....	160
Figure 118a. Energy versus Deflection Curve for UBSP-19 - English .....	160
Figure 118b. Energy versus Deflection Curve for UBSP-19 - Metric.....	160
Figure 119. Time Sequential Photographs, Test UBSP-19.....	161
Figure 120. Post-Impact Images of UBSP-19.....	161
Figure 121. Fracturing Bolt Details .....	167
Figure 122. Fracturing Bolt Details .....	168
Figure 123. Fracturing Bolt Details .....	169
Figure 124. Fracturing Bolt Details .....	170
Figure 125a. Force versus Deflection Curve for UBSP-20 - English.....	173
Figure 125b. Force versus Deflection Curve for UBSP-20 - Metric .....	173
Figure 126a. Energy versus Deflection Curve for UBSP-20 - English .....	173
Figure 126b. Energy versus Deflection Curve for UBSP-20 - Metric.....	173

Figure 127. Time Sequential Photographs, Test UBSP-20.....	174
Figure 128. Post-Impact Images of UBSP-20.....	174
Figure 129. Additional Images of Bolt and Washer Damage of UBSP-20 .....	175
Figure 130a. Force versus Deflection Curve for UBSP-21 - English.....	177
Figure 130b. Force versus Deflection Curve for UBSP-21 - Metric .....	177
Figure 131a. Energy versus Deflection Curve for UBSP-21 - English .....	177
Figure 131b. Energy versus Deflection Curve for UBSP-21 - Metric.....	177
Figure 132. Time Sequential Photographs, Test UBSP-21.....	178
Figure 133. Post-Impact Images of UBSP-21.....	178
Figure 134. Additional Images of Bolt and Washer Damage of UBSP-21 .....	179
Figure 135. Hiser Slipbase Model .....	183
Figure 136. Meshed Fracturing Bolt Post.....	184
Figure 137. Rigid Cylinder Impact.....	185
Figure 138. Prestress Levels in One Bolt Shaft .....	187
Figure 139. Rigid Cylinder Impact Results .....	188
Figure 140. Fracturing Bolt Model with the Bogie Model Before Impact.....	189
Figure 141. Soil Springs and Rigid Soil Tube .....	190
Figure 142. Bolt Fracture Images of the Simulation and Actual Testing .....	194
Figure 143. Time Sequential Photographs – Strong-Axis Impact.....	195
Figure 144a. Force vs. Deflection Curve, UBSP-20 Comparison - English.....	196
Figure 144b. Force vs. Deflection Curve, UBSP-20 Comparison - Metric.....	196
Figure 145a. Energy vs. Deflection Curve, UBSP-20 Comparison - English.....	196
Figure 145b. Energy vs. Deflection Curve, UBSP-20 Comparison - Metric .....	196
Figure 146. Time Sequential Photographs – Weak Axis Impact.....	198
Figure 147a. Force vs. Deflection Curve, UBSP-10 Comparison - English.....	199
Figure 147b. Force vs. Deflection Curve, UBSP-10 Comparison - Metric.....	199
Figure 148a. Energy vs. Deflection Curve, UBSP-10 Comparison - English.....	199
Figure 148b. Energy vs. Deflection Curve, UBSP-10 Comparison - Metric .....	199
Figure 149. Time Sequential Photographs – Diagonal Axis Impact .....	201
Figure 150a. Force vs. Deflection Curve, UBSP-21 Comparison - English.....	202
Figure 150b. Force vs. Deflection Curve, UBSP-21 Comparison - Metric.....	202
Figure 151a. Energy vs. Deflection Curve, UBSP-21 Comparison - English.....	202
Figure 151b. Energy vs. Deflection Curve, UBSP-21 Comparison - Metric .....	202
Figure 152. Full-Scale Crash Test Matrix.....	208
Figure 153. Fracturing Bolt Recommended Welds .....	212
Figure 154. UBSP Bullnose Median Barrier System Layout .....	213
Figure 155. UBSP Bullnose Post Locations .....	214
Figure 156. USBP Bullnose Nose Section Detail.....	215
Figure 157. UBSP Bullnose Post Nos. 1 and 2 Details .....	216
Figure 158. UBSP Bullnose Post Nos. 3-8 and 9-12 Details.....	217
Figure 159. UBSP Bullnose End Rail Detail and Splice Detail .....	218
Figure 160. UBSP Bullnose Fracturing Bolt Details – As Tested.....	219
Figure 161. UBSP Bullnose W6x9 (W152x13.4) Post and Blockout Details.....	220
Figure 162. UBSP Bullnose BCT Wood Post and Foundation Tube Details.....	221
Figure 163. UBSP Bullnose BCT Anchor Cable and Nose Cable Detail.....	222

Figure 164. UBSP Bullnose BCT Anchorage Details .....	223
Figure 165. UBSP Bullnose Rail Section Details .....	224
Figure 166. UBSP Bullnose Rail Slot Patterns .....	225
Figure 167. UBSP Bullnose Bill of Materials .....	226
Figure 168. UBSP Bullnose Barrier.....	227
Figure 169. UBSP Bullnose Barrier.....	228
Figure 170. UBSP Bullnose Barrier.....	229
Figure 171. Test Vehicle, Test USPBN-1.....	232
Figure 172. Vehicle Dimensions, Test USPBN-1 .....	233
Figure 173. Vehicle Target Locations, Test USPBN-1 .....	234
Figure 174. Locations of High Speed Cameras, Test USPBN-1 .....	238
Figure 175. Impact Location, Test USPBN-1.....	245
Figure 176. Summary of Test Results and Sequential Photographs, Test USPBN-1 .....	246
Figure 177. Additional Sequential Photographs, Test USPBN-1 .....	247
Figure 178. Additional Sequential Photographs, Test USPBN-1 .....	248
Figure 179. Additional Sequential Photographs, Test USPBN-1 .....	249
Figure 180. Additional Sequential Photographs, Test USPBN-1 .....	250
Figure 181. Vehicle Trajectory, Test USPBN-1 .....	251
Figure 182. System Damage and Vehicle Final Position, Test USPBN-1 .....	252
Figure 183. System Damage, Test USPBN-1 .....	253
Figure 184. System Damage, Test USPBN-1 .....	254
Figure 185. System Damage, Test USPBN-1 .....	255
Figure 186. Vehicle Damage, Test USPBN-1 .....	256
Figure 187. Vehicle Damage, Test USPBN-1 .....	257
Figure 188. Sequential Photographs, Test USPBN-1 .....	260
Figure 189. Sequential Photographs, Test MBN-8.....	261
Figure 190. Sequential Photographs, Test USPBN-1 .....	262
Figure 191. Sequential Photographs, Test MBN-8.....	263
Figure A-1. Results of UBSP-1 (EDR3).....	277
Figure A-2. Results of UBSP-2 (EDR3).....	278
Figure A-3. Results of UBSP-3 (EDR3).....	279
Figure A-4. Results of UBSP-4 (EDR3).....	280
Figure A-5. Results of UBSP-5 (EDR3).....	281
Figure A-6. Results of UBSP-6 (EDR3).....	282
Figure A-7. Results of UBSP-8 (EDR3).....	283
Figure A-8. Results of UBSP-9 (EDR3).....	284
Figure A-9. Results of UBSP-10 (EDR3).....	285
Figure A-10. Results of UBSP-11 (EDR3).....	286
Figure A-11. Results of USBP-12 (EDR3).....	287
Figure A-12. Results of UBSP-13 (EDR3).....	288
Figure A-13. Results of UBSP-14 (EDR3).....	289
Figure A-14. Results of UBSP-15 (EDR3).....	290
Figure A-15. Results of UBSP-16 (EDR3).....	291
Figure A-16. Results of UBSP-17 (EDR3).....	292
Figure A-17. Results of UBSP-18 (EDR3).....	293

Figure A-18. Results of UBSP-19 (EDR3)..... 294  
Figure A-19. Results of UBSP-20 (EDR3)..... 295  
Figure A-20. Results of UBSP-21 (EDR3)..... 296  
Figure B-1. Occupant Compartment Deformation, Set 1 ..... 298  
Figure B-2. Occupant Compartment Deformation, Set 2 ..... 299  
Figure B-3. Occupant Compartment Deformation Index (OCDI)..... 300  
Figure C-1. Graph of Longitudinal Deceleration – Filtered Data, Test USPBN-1..... 302  
Figure C-2. Graph of Longitudinal Occupant Impact Velocity – Filtered Data, Test USPBN-1303  
Figure C-3. Graph of Longitudinal Occupant Displacement – Filtered Data, Test USPBN-1... 304  
Figure C-4. Graph of Lateral Deceleration – Filtered Data, Test USPBN-1 ..... 305  
Figure C-5. Graph of Lateral Occupant Impact Velocity – Filtered Data, Test USPBN-1 ..... 306  
Figure C-6. Graph of Lateral Occupant Displacement – Filtered Data, Test USPBN-1 ..... 307  
Figure C-7. Rate Transducer Data, Test USPBN-1 ..... 308  
Figure D-1. Summary of Test Results and Sequential Photographs (Metric), Test USPBN-1 .. 310

## LIST OF TABLES

Table 1. Breakaway Steel Post Patents .....	10
Table 1. Breakaway Steel Post Patents Cont'd .....	11
Table 1. Breakaway Steel Post Patents Cont'd.....	12
Table 2a. Wood CRT Post Peak Load Capacities - English.....	16
Table 2b. Wood CRT Post Peak Load Capacities – Metric.....	16
Table 3a. Test Results for MNCRT-1, MNCRT-2, and MNCRT-3 – English.....	19
Table 3b. Test Results for MNCRT-1, MNCRT-2, and MNCRT-3 – Metric .....	19
Table 4a. Test Results for MNCRT-4, MNCRT-5, and MNCRT-6 – English.....	24
Table 4b. Test Results for MNCRT-4, MNCRT-5, and MNCRT-6 – Metric .....	24
Table 5a. Test Results for MNCRT-7, MNCRT-8, and MNCRT-9 – English.....	28
Table 5b. Test Results for MNCRT-7, MNCRT-8, and MNCRT-9 – Metric .....	28
Table 6a. Test Results Without Fixture Effect for MNCRT-7, MNCRT-8, and MNCRT-9 – English .....	31
Table 6b. Test Results Without Fixture Effect for MNCRT-7, MNCRT-8, and MNCRT-9 – Metric.....	31
Table 7. Round 1 Bogie Testing Concepts .....	46
Table 8. Test Matrix for Round 1 Bogie Testing.....	48
Table 9. Test Parameters.....	74
Table 10a. Summary of Round 1 Bogie Testing Results – English.....	103
Table 10b. Summary of Round 1 Bogie Testing Results – Metric.....	103
Table 11. Test Matrix for Round 2 Bogie Testing.....	104
Table 12a. Summary of Round 2 Bogie Testing Results – English.....	138
Table 12b. Summary of Round 2 Bogie Testing Results – Metric.....	138
Table 13. Test Matrix for Wood CRT Post Bogie Testing In Soil .....	140
Table 14a. CRT Wood Post Details – English.....	142
Table 14b. CRT Wood Post Details – Metric .....	142
Table 15a. Test Results for CRT Wood Posts In Soil – English .....	164
Table 15b. Test Results for CRT Wood Posts In Soil - Metric .....	164
Table 16. Test Matrix for Round 3 Bogie Testing.....	165
Table 17a. Summary of Round 3 Bogie Testing Results – English.....	181
Table 17b. Summary of Round 3 Bogie Testing Results – Metric.....	181
Table 18. Model Parts, Element Types, and Materials .....	184
Table 19. Soil Loading Curve.....	191
Table 20. Final ASTM A325 Bolt Material Properties – MAT_024.....	192
Table 21. NCHRP Report No. 350 Evaluation Criteria for Crash Tests .....	209
Table 22. Weather Conditions, Test No. USPBN-1 .....	239
Table 23. Summary of OIV, ORA, THIV, and PHD Values, Test USPBN-1 .....	243
Table 24. General Behavior and Comparison of Test Designation No. 3-38 Tests.....	259
Table 25. Comparison of Fracture Times for Wood and Steel Posts.....	264
Table 26. Comparison of Pickup Location versus Time.....	264
Table A-1. Post Testing Summary .....	276
Table A-2. Post Testing Results Reference .....	276



## 1 INTRODUCTION

### 1.1 Background

From 1997 through 2000, the Midwest Roadside Safety Facility (MwRSF) developed a three-beam bullnose guardrail system for shielding median hazards found between divided highways [1-3]. The new, non-proprietary bullnose guardrail system was successfully developed, full-scale vehicle crash tested, and evaluated according to the Test Level 3 (TL-3) safety performance evaluation criteria provided in National Cooperative Highway Research Program (NCHRP) Report No. 350 [4].

Controlled release terminal (CRT) wood posts were used in the bullnose guardrail system. Although the CRT posts adequately met the TL-3 safety requirements, these wood posts have several drawbacks. First, the properties and performance of wood posts is highly variable due to the existence of knots, checks, and splits, thus leading to the necessity of grading and inspection requirements. Also, two holes are drilled in the CRT posts to allow it to break away upon impact. These holes further expose the interior of the wood to the environment, which can accelerate deterioration. Wood posts can also swell under certain environmental conditions, causing difficulty in the removal of broken posts from steel foundation tubes after impact. Chemical preservatives used to treat the wood posts have been identified as harmful to the environment by some government agencies. Thus, the treated wood posts may require special consideration during disposal. As a result of these concerns regarding the use of wood CRT posts, there existed a need for a breakaway steel post option for use in the Thrie-Beam Bullnose guardrail systems.

First, due to cost efficiency and viability of the design, existing proprietary steel breakaway posts were investigated and tested in the “Evaluation of an Existing Steel Post Alternative for the Thrie-Beam Bullnose Guardrail System” [5]. After several proprietary steel post designs were reviewed and tested, a Road Systems, Inc. (RSI) Hinged Steel Post was chosen as the best alternative post option for the bullnose system. Two full-scale tests were performed on the bullnose system with the breakaway hinged steel posts, and both tests were unsuccessful due to the pickup truck overriding the system.

After the two failed full-scale tests, focus shifted to the development of a new Universal Breakaway Steel Post to replace the CRT wood posts in the Thrie-Beam Bullnose system. While the previously designed proprietary steel breakaway posts had been successfully used for guardrail end terminals, the bullnose system appeared to be more sensitive to subtle differences between wooden and steel breakaway posts. The new, non-proprietary, Universal Breakaway Steel Post was to be designed to mimic the strength and behavior of the wooden CRT post in order to function properly in the bullnose system. In addition, if successfully developed, the new post could provide a replacement option for the CRT wood post in a wide variety of roadside hardware systems.

## **1.2 Objective**

The objective of the research project was to develop a generic steel replacement post for the wood CRT post. First, the new Universal Breakaway Steel Post was to match the cantilevered bending capacities about the strong and weak axis as well as for a biaxial loading condition for the existing wood CRT post. Second, the embedded portion of the post would need to have the same geometry in order to assure comparable rotational resistance in the soil. Third,

the mass, general geometry, and the breakaway characteristics of the upper post section were to be similar to the CRT wood post. If these behavior characteristics could be achieved, it was believed that the Universal Breakaway Steel Post could be used as a replacement for CRT posts in any application.

### **1.3 Research Approach**

This report is divided into thirteen chapters plus references and appendices. This study began with a literature review, as seen in Chapter 2, to review any previous CRT wood post testing and to identify any previous steel breakaway posts concepts that may be appropriate for use as a replacement for the wood CRT post. Next, Chapter 3 describes CRT wood post bogie testing in a rigid sleeve. Chapter 4 presents all of the breakaway post design concepts that were developed for possible use as the universal breakaway steel post.

Chapter 5 contains information on the first round of bogie testing on breakaway posts. The physical testing setup, details of the testing, and the results of the first round of tests are all discussed. Chapter 6 contains information on the second round of bogie testing on the breakaway post concepts. Next, chapter 7 discusses the bogie testing on CRT wood posts placed in soil. Finally, chapter 8 discusses the third and final rounds of bogie testing on breakaway post concepts.

After the bogie testing, focus shifted to preliminary simulation work as described in Chapter 9. Next, all of the details and results of full-scale crash test no. USPBN-1 are discussed in Chapter 10. Chapter 11 compares test no. USPBN-1 to all previous crash tests designation no. 3-38 on the bullnose barrier. Finally, Chapter 12 and Chapter 13 provide the conclusions and recommended future work, respectively, for this project.

## 2 LITERATURE REVIEW

### 2.1 Previous CRT Wood Post Testing

Many studies of guardrail posts have been performed previously. Hascall et al. [6] reviewed and summarized the previous post studies completed from 1960 through 2004. The only relevant study pertaining to CRT post properties was performed by Ensco Inc. and was titled “Safety Modification of Turned-Down Guardrail Terminals” in which the CRT post was developed [7]. This report consisted of three volumes and described the development of a safer turned-down guardrail terminal. The CRT wood post was developed for use as a breakaway post in the turned-down terminal to allow the rail to fall freely when impacted near the terminal and to redirect impacts occurring downstream of the first post.

In the development of the CRT wood post, a 6-in. x 8-in. (152-mm x 203-mm) cross section was utilized. It was found that drilling the two 3 1/2-in. (89-mm) holes in the middle region of the post allowed the post to break off with a low magnitude of force in the weak axis for varying soil strengths. For very strong soils, or frozen soils, failure would occur through the upper hole at ground level, and for more typical soil, the failure would occur at the lower hole or 15 3/4 in. (400 mm) below ground. Drilling the 3 1/2-in. (89-mm) holes parallel to the weak axis of the post reduced the section modulus by 46 percent in the weak axis but only by 14 percent in the strong axis. Thus, with the drilled holes, the strong axis of the CRT wood post was 2.2 times stronger than the weak axis, which was desirable for breaking away near the terminal and redirecting impacts downstream. Also, it was found that the hole size should not exceed 3 1/2 in. (89 mm) so the post could still be driven.

## 2.2 Previous Breakaway Steel Post Testing

A review was also conducted on prior breakaway post concepts. Many private companies have developed proprietary steel posts, commonly utilized in guardrail end terminals. Some of these concepts may be suitable for use as the universal breakaway post. There are a significant number of patents protecting these proprietary breakaway posts, and a patent review was performed to identify the relevant post concepts. As shown in Table 1, the numerous patents cover a broad range of breakaway mechanisms for signs, terminals, and guardrail posts. After compiling all of the patents, applicable breakaway concepts were chosen as possibilities for the universal breakaway post. However, permission would first need to be granted from the owner of the intellectual property in order to use an existing patented concept. For the preliminary stages of design, most of the relevant ideas were considered for use as the universal steel breakaway post, and the owner's permission would be checked if a concept was selected for further investigation and use. The relevant patents can be seen in bold and in italics in Table 1 and are described below.

When considering breakaway posts for signs, several patents were deemed relevant for the universal breakaway post. Patent no. 5,535,555 describes a breakaway coupler with a hollow, tubular sleeve which breaks at a weakened shear point when struck by a vehicle. The tubular design could be used to connect a lower foundation tube that was anticipated in the universal breakaway steel post. However, this patent used numerous pins to connect the post together, and this design may be difficult to sufficiently weaken under weak-axis impact loading.

In patent no. 5,855,443, shearing plate washers form a shear plane to shear fasteners connecting a support surface to a sign support. This breakaway connection breaks away cleanly,

but it is omni-directional meaning it would need to be modified to provide strength in a strong axis impact and be weakened for weak axis impacts. Also, the desired universal breakaway steel post may be more flexural controlled instead of shear controlled and the shearing plate washers would not be needed.

Patent nos. 6,264,162 and 6,390,436 both describe a breakaway collar surrounding a sign support post. The sidewall of the collar includes at least one vertical line of weakness to facilitate a portion of the sidewall to break away. This design could break away cleanly as desired, but the collar would need to be large to be placed around a 6-in. x 8-in. (152-mm x 203-mm) foundation tube. Also, it may prove difficult to significantly reduce the strength of the design for weak-axis impacts, while maintaining its strength in strong-axis impacts.

The last relevant breakaway sign post, patent no. 6,409,156, describes a breakaway bracket assembly connecting two structural members with a central section having a V-shaped, pre-formed break point. Although this bracket has the potential to break away cleanly as desired, the custom V-shape may be costly to manufacture.

Next, most of the breakaway steel posts that were developed for end terminals were relevant for the universal breakaway steel post. In patent no. 6,065,894, a molded coupling unit with an intermediate fracture zone allows C-channel post segments to separate when subjected to a vehicle impact greater than a predetermined severity. A thermoplastic or formed-up thermosetting compound is molded into the coupling unit, which could break away cleanly, but it may be costly to produce and design.

Patent nos. 6,398,192 and 6,619,630 both describe a breakaway support post with a releasable coupling assembly consisting of a shear pin designed to break away in a weak-axis

impact. Although this post has low strength in the weak axis, the post does not break away cleanly as it rotates around a second bolt down to the ground.

In patent nos. 6,488,268, 6,793,204, and 6,886,813, several breakaway support posts are described that resist impact in a strong direction and yield to impact in a weak direction. Two different breakaway support posts have elongated slots cut in flanges of an I-beam to form a yieldable connection in the weak direction. Also, two different posts involve a shear and pivot pin, where the shear pin breaks away in the weak direction and the post rotates to the ground around the pivot pin. The last breakaway post has a connection of two rods, or bolts, aligned in the strong direction with spacing from breaker bars or nuts allowing the post to bend and fail the rods. Although these breakaway posts do have a different strong axis and weak axis as desired, most of these designs may not break away cleanly in weak- or diagonal-axis impacts.

The last relevant patent for a terminal breakaway post is detailed in patent no. 6,729,607. A cable release anchor is described that has bearing plates with U-shaped cutouts to hold a tension cable. The post breaks away cleanly when impacted in the weak axis by shearing bolts, but it is set up for anchorage to react to tensile loads from the tension cable.

Finally, there were numerous applicable patents describing breakaway steel posts for guardrail. In patent no. 4,330,106, a steel channel member with fastening bolts connects an upper and lower I-beam member. The steel channel connection breaks away when impacted in the weak axis, but it does not break away in the strong axis as desired. Patent no. 5,664,905 describes a post with V-shaped or U-shaped notches or cut-outs to have the notches close together. Although this post has a weakened section, it does not break away cleanly as it just collapses over on itself.

In patent nos. 5,988,598 and 6,254,063, a breakaway steel guardrail post is described that includes upper and lower post sections connected by different breakaway joints. One joint consisted of through bolts designed to either break or tear out. Another embodiment includes two U- or channel-shaped steel plates with the flanges of the channel designed to yield upon impact in the weak axis, while a large diameter steel pin provides strength in the strong axis. The last embodiment relies on weld failures in the breakaway joint to control the post strength. These posts all have a strong and weak axis as desired, but they may not break away cleanly. Only the welded connection may break away cleanly as long as the weld is consistent.

Patent no. 6,902,150 and application nos. 20070063177, 20070063178, and 20070063179 all describe steel breakaway posts with cutouts in the flanges of I-beams. Various cutouts including circular cutouts and sawcuts are all detailed to weaken the post and create a failure point in the post. Similarly, patent application no. 20070102689 also describes cutouts but for cable guardrail posts. One weakness is that these designs would not break away cleanly as desired in the universal breakaway post.

Last, in patent application nos. 20060027797 and 20060038164, an energy absorbing post is described where impact energy is absorbed by out-of-plane deformation. The energy is either absorbed through bolt tear-out or by Mode 3 out-of-plane tearing in a splice plate. Although these posts absorb energy as desired, they would not break away cleanly in the universal breakaway post.

In addition to all the proprietary steel posts found in the patent search, another relevant steel breakaway post was the steel slipbase breakaway cable terminal (BCT) post [8-10]. These posts consisted of three ASTM 325 bolts in a triangular slipbase configuration. However, the



design never did gain wide acceptance due to high initial costs and maintenance issues when compared to the BCT wood post.

**Table 1. Breakaway Steel Post Patents**

Signs		Title	Authors	Notes
Patent No.	Date			
3,308,584	03/14/67	Highway Guide Post	Graham	Iron tubing joined w/ ball and socket and sheared rivets
3,332,666	07/25/67	Guard Rail Assembly	Gray	Arm assemblies pivotally mounted on anchor posts
3,349,531	10/31/67	Frangible Connector Assembly For Stanchions, Poles, And Standards	Watson	Impact frangible and bendable connector assembly
3,355,998	12/05/67	Highway Marker Device	Roemisch	Support and base member connected w/ wooden plug
3,385,564	05/28/68	Highway Guard Rail Supports	Persicke	Arm pivotally mounted to base w/ pivotal guard rail mount
3,417,965	12/24/68	Vehicle Guard Rail	Gray	Pivotaly supported guard rail w/ torque tube
3,499,630	03/10/70	Posts For Highway Safety Rails	Dashio	Posts w/ shearing coupling of V shape
3,521,917	07/28/70	Positive Action Clamp	King	Breakaway signpost w/ butt joint overlapped by opposed plates
3,606,222	09/20/71	Support Construction for Signs	Howard	Breakaway street sign support w/ three posts
3,628,296	12/21/71	Breakaway Sign Support	Henry	Assembly w/ ground anchor, reinforcing sleeve, & post member
3,637,244	01/25/72	Load Concentrated Breakaway Coupling	Strizki	Circumferentially spaced breakaway couplings
3,820,906	06/28/74	Highway Sign Post	Katt	Two sections coupled together by a clamp
3,846,030	11/05/74	Post	Katt	Tubular clamp coupling the post and base
3,912,404	10/14/75	Highway Post Construction	Katt	Hollow centrally frangible coupling
3,951,556	04/20/76	Load Concentrated Breakaway Coupling Apparatus	Strizki	Platform w/ breakaway coupling members
3,967,906	07/06/76	Safety Breakaway Ground Mounted Post Support Assemblies	Strizki	Upper and lower members connected w/ breakaway coupling members
4,071,970	02/07/78	Hinge Plate For Roadside Post Safety Breakaway System For Sign Panels And The Like	Strizki	Rectangular hinge w/ notch or groove
4,126,403	11/21/78	Post Construction	Sweeney, MacDonald	Upper and lower posts overlapped, connected w/ breakaway elements
4,236,843	12/02/80	Sign Post Couplings	Chisholm	Coupling webs w/ high stress concentration for horizontal impact
4,310,979	01/19/82	Breakaway Dual-Legged Sign Support	Bloom	Support post w/ hinge behind vertical center of area of the sign
4,850,565	07/25/89	Post Support	Moreno	Breakaway connection between ground support and post
4,923,319	05/08/90	Breakaway Connector	Dent	Breakaway bolt w/ reduced diameters to form cones
4,926,592	05/02/90	Breakaway Sign Post Coupling	Nehls	Horizontal plate coupling between mounting and support post
4,928,446	05/29/90	Breakaway Sign Post And Post Ground Anchor	Alexander	Breakaway post w/ two channel members & a stud
5,004,366	04/02/91	Breakaway Coupling	Simmons	Breakaway coupling for connecting two members end to end
5,160,111	11/03/92	Collapsible Signaling Post	Hugron	Weakened section w/ a helical groove on a tubular member
5,214,886	06/01/93	Breakaway Connection For Post	Hugron	Breakaway connection w/ U-shape cross-section and flanges
5,480,121	01/02/96	Breakaway Connector For Sign Post	Rice, Alexander	Stud rigidly welded to two spaced-apart channel members
5,481,835	01/09/96	Breakaway Base and Upper-Separation Joint	Bloom	Circular breakaway base for luminaire supports
5,484,217	01/16/96	Restorable Breakaway Post	Carroll, Frejd	Base post and breakaway post secured w/ flexible member
<b>5,535,555</b>	<b>07/16/96</b>	<b>Breakaway Post Coupling</b>	<b>Boyd, Akana</b>	<b>Hollow, tubular sleeve w/ cutouts creating a shear point</b>

**\*Most Relevant Patents Bolded and in Italics**

Table 1. Breakaway Steel Post Patents Cont'd

Signs Continued		Title	Authors	Notes
Patent No.	Date			
D0389252	01/13/98	Traffic Sign Post Slip Splice Connection Base Piece	Alberson, Bullard	Ornamental traffic sign post slip splice base piece
D0389253	01/13/98	Traffic Sign Post Slip Splice Connection Base Piece	Alberson, Bullard	Ornamental traffic sign post slip splice base piece
<b>5,855,443</b>	<b>01/05/99</b>	<b>Breakaway Connection System For Roadside Use</b>	<b>Faller, Reid, Paulsen, Krenk</b>	<b>Breakaway mounting system w/ shearing plates</b>
6,113,055	09/05/00	Sign Post Coupler	Salmán	Hollow, tubular, integral coupler w/ two sockets and shear section
<b>6,264,162</b>	<b>07/24/01</b>	<b>Breakaway Sign Post</b>	<b>Barnes, Potter</b>	<b>Assembly w/ support post, anchoring post, &amp; breakaway collar</b>
6,308,927	10/30/01	Breakaway Sign Post Connector	Leahy	Breakaway sign post connector w/ shear member and bushing
<b>6,390,436</b>	<b>05/21/02</b>	<b>Breakaway Sign Post</b>	<b>Barnes, Potter</b>	<b>Assembly w/ support post, anchoring post, &amp; breakaway collar</b>
<b>6,409,156</b>	<b>06/25/02</b>	<b>Breakaway Bracket</b>	<b>Dent</b>	<b>Breakaway bracket assembly w/ two straps and flange section</b>
6,422,783	07/23/02	Breakaway Post Slipbase	Jordan	Triangular slip base support system for tubular posts
20020122693	09/05/02	Breakaway Post Slipbase	Jordan	Triangular slip base support system for tubular posts
6,457,885	10/01/02	Flush Mount Breakaway Post Coupler	Salmán	Coupler for connecting a post to ground anchor
6,516,573	02/11/03	Integrated Breakaway For Support Posts	Fairrell, Stallman II, Kuhn, Berkemeier	Post or coupling w/ an integrated weakened region
6,540,196	04/01/03	Breakaway Support Structure Coupling	Ellsworth	Breakaway coupling w/ two plates and bearing
6,739,567	05/25/04	Separable Magnetic Attachment Assembly	Curtis	Magnetic assembly and base plate attract and hold together
6,868,641	03/22/05	Breakaway Post Base	Conner, Partee	Breakaway post base w/ pair of adjacent triangular slip planes
20060107572	05/25/06	Breakaway Sign Post With Magnetically Coupled Sections	Barnes	Sign post assembly w/ a magnetic coupling assembly
7,051,466	05/30/06	Breakaway Sign Post With Magnetically Coupled Sections	Barnes	Sign post assembly w/ a magnetic coupling assembly
7,056,056	06/06/06	Collision Safety Device Having A Breakaway Shear Coupling	Wiegand, Larsen	Breakaway coupling w/ two shearing plates and a band
20060228165	10/12/06	Reusable, Breakaway Connector Section For Highway Sign Posts	Yonan III	Reusable breakaway connector w/ female & male ends
20060236619	10/26/06	Breakaway Sign Post With Magnetically Coupled Sections	Barnes	Sign post assembly w/ a magnetic coupling assembly
7,188,821	03/13/07	Magnetic Assembly For Reversibly Securing A Post	Curtis	Magnetic assembly and base plate attract and hold together
Terminals				
Patent No.	Date	Title	Authors	Notes
4,607,824	08/26/86	Guardrail End Terminal	Krage, Denman	Fender panels on vertical legs with slip bases
<b>6,065,894</b>	<b>05/23/00</b>	<b>Breakaway Post Connector</b>	<b>Wasson, Melrose</b>	<b>Coupling unit adapted for an intermediate fracture zone</b>
<b>6,398,192</b>	<b>06/04/02</b>	<b>Breakaway Support Post For Highway Guardrail End Treatments</b>	<b>Albritton</b>	<b>Breakaway support post w/ releasable coupling assembly</b>
<b>6,488,268</b>	<b>12/02/02</b>	<b>Breakaway Support Post For Highway Guardrail End Treatments</b>	<b>Albritton</b>	<b>Breakaway support post that yields in weak direction</b>
6,554,256	04/29/03	Highway Guardrail End Terminal Assembly	Ochoa	End terminal assembly w/ plurality of posts
<b>6,619,630</b>	<b>09/16/03</b>	<b>Breakaway Support Post For Highway Guardrail End Treatments</b>	<b>Albritton</b>	<b>Breakaway support post w/ releasable coupling assembly</b>
<b>6,729,607</b>	<b>05/04/04</b>	<b>Cable Release Anchor</b>	<b>Alberson, Bullard, Bligh, Burth</b>	<b>Cable release anchor w/ improved breakaway post design</b>
<b>6,793,204</b>	<b>09/21/04</b>	<b>Breakaway Support Post For Highway Guardrail End Treatments</b>	<b>Albritton</b>	<b>Breakaway support post that yields in weak direction</b>
<b>6,886,813</b>	<b>05/03/05</b>	<b>Breakaway Support Post For Highway Guardrail End Treatments</b>	<b>Albritton</b>	<b>Breakaway support post that yields in weak direction</b>

\*Most Relevant Patents Bolded and in Italics

**Table 1. Breakaway Steel Post Patents Cont'd**

Guardrail		Title	Authors	Notes
No.	Date			
3,353,795	11/21/67	Safety Fence For Roads	Muller	Safety fence w/ post and socket connected by a shear pin
<b>4,330,106</b>	<b>05/18/82</b>	<b>Guard Rail Construction</b>	<b>Chisholm</b>	<b>Breakaway I-beam posts coupled w/ a channel member</b>
4,784,515	11/15/88	Collapsible Highway Barrier	Krage, Denman	Collapsible guardrail assembly and rotatable beam
<b>5,664,905</b>	<b>09/09/97</b>	<b>Fence</b>	<b>Thompson, McGregor</b>	<b>Post w/ notches in rear face</b>
<b>5,988,598</b>	<b>11/23/99</b>	<b>Breakaway Steel Guardrail Post</b>	<b>Sicking, Reid, Rohde</b>	<b>Breakaway post connected with fastener sets</b>
<b>6,254,063</b>	<b>07/03/01</b>	<b>Energy Absorbing Breakaway Steel Guardrail Post</b>	<b>Rohde, Reid, Sicking</b>	<b>Breakaway post for use in dissipation of impact energy</b>
6,644,888	11/11/03	Roadway Guardrail Structure	Ochoa	Posts w/ flanges having free edge portions
<b>6,902,150</b>	<b>06/07/05</b>	<b>Steel Yielding Guardrail Support Post</b>	<b>Alberson, Bullard, Buth,</b>	<b>Guardrail support post w/ cutouts in the flanges</b>
<b>20060027797</b>	<b>02/09/06</b>	<b>Energy Absorbing Post For Roadside Safety Devices</b>	<b>Sicking, Rohde, Reid, Mak</b>	<b>Energy absorbed by out-of-plane deformation</b>
<b>20060038164</b>	<b>02/23/06</b>	<b>Energy Absorbing Post For Roadside Safety Devices</b>	<b>Sicking, Rohde, Reid, Mak</b>	<b>Energy absorbed by out-of-plane deformation</b>
<b>20070063177</b>	<b>03/22/07</b>	<b>Yielding Post Guardrail Safety System</b>	<b>Alberson, Bullard, Buth,</b>	<b>Steel post mid portion weakened about first axis only</b>
<b>20070063178</b>	<b>03/22/07</b>	<b>Guardrail Flange Protector</b>	<b>Alberson, Bullard, Buth,</b>	<b>Steel post mid portion weakened about first axis only</b>
<b>20070063179</b>	<b>03/22/07</b>	<b>A Weakened Guardrail Mounting Connection</b>	<b>Alberson, Bullard, Buth,</b>	<b>Plurality of steel weakened support posts</b>
20070102689	05/10/07	Cable Barrier Guardrail System With Steel Yielding Support Posts	Alberson, Bligh, Bullard, Buth	Upper, mid, & lower sections - Mid portion is weakened longitudinally

**\*Most Relevant Patents Bolded and in Italics**

### **3 CRT PHYSICAL TESTING DETAILS**

#### **3.1 Introduction**

The next step in the research was determining the dynamic properties of the controlled releasing terminal (CRT) wood post under various loading conditions. Dynamic impact testing was performed on 6-in. x 8-in. (152-mm x 203-mm) CRT wood posts placed in a rigid sleeve at three different angles. A total of nine bogie tests were performed with three tests each at 0, 45, and 90 degree angles relative to the strong axis. For each bogie test, raw acceleration data, obtained from accelerometers, was filtered with a CFC 60 filter. Using initial velocity and measured accelerations, the force-displacement and energy-displacement graphs were plotted. Thus, the energy dissipation and capacity of the CRT wood posts at the different impact angles were determined [11]. A brief summary of the properties of the CRT wood post and results of the nine bogie tests are presented below.

#### **3.2 CRT Wood Post Details**

Controlled releasing terminal (CRT) wood posts were fabricated from grade No. 1 or better, non-dense southern yellow pine (SYP) wood material. The 72-in. (1,829-mm) long, CRT wood post was designed to break away when impacted about its weak axis of bending in turned-down guardrail applications. A standard 6-in. x 8-in. (152-mm x 203-mm) cross section was utilized and weakened by drilling out two 3 1/2-in. (89-mm) holes in the middle region of the post. A CRT wood post is shown in Figure 1 with the cross section shown in Figure 2.

From the cross-sectional dimensions and the properties of the wood CRT posts, a reasonable estimate was made for the peak load capacities about both axes of bending. As shown in Table 2, the peak load is a function of the estimated modulus of rupture, which was chosen as

5,400 psi (37,232 MPa) [12] to accurately represent properties of the SYP wood being tested. The results from Table 2 show that the strong axis should absorb approximately twice the peak load as the weak axis of the post.



**Figure 1. CRT Wood Post in Rigid Sleeve**

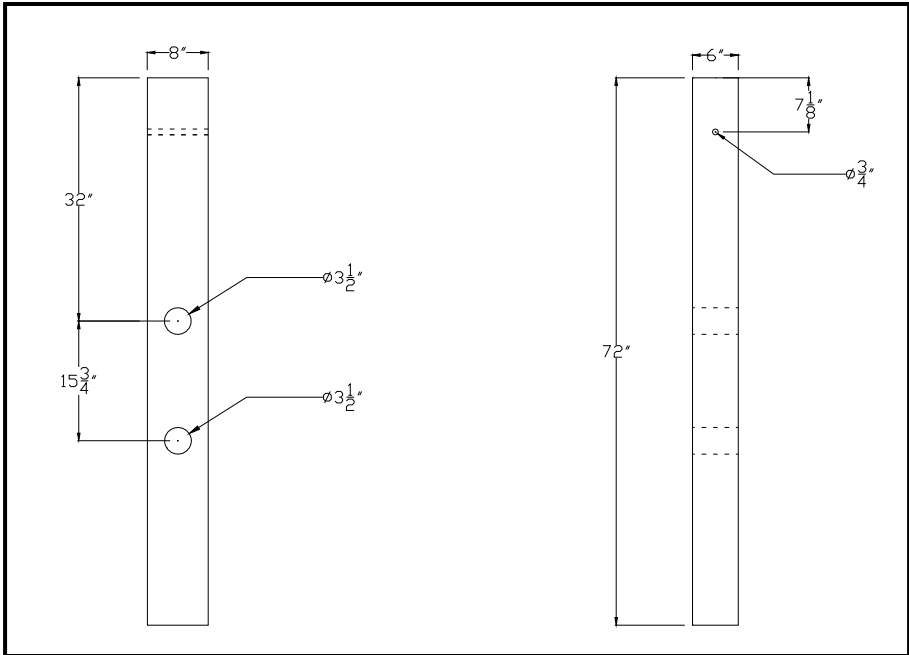


Figure 2a. Cross-Sectional Dimensions for CRT Wood Posts – English

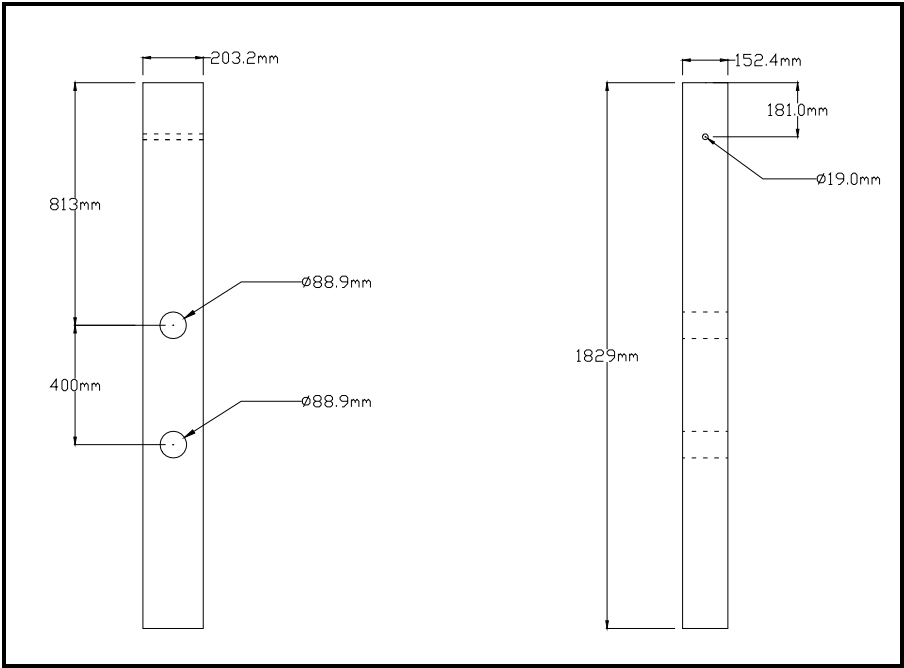


Figure 2b. Cross-Sectional Dimensions for CRT Wood Posts – Metric

**Table 2a. Wood CRT Post Peak Load Capacities - English**

CRT Post Properties				Strong Axis of Bending				Weak Axis of Bending								
Assumed Modulus of Rupture (psi)	Post Width (in.)	Post Depth (in.)	C x-x (in.)	C y-y (in.)	Hole Diameter (in.)	Load Height (in.)	I <sub>gross</sub> x-x (in. <sup>4</sup> )	I <sub>hole</sub> x-x (in. <sup>4</sup> )	I <sub>net</sub> x-x (in. <sup>4</sup> )	S <sub>net</sub> x-x (in. <sup>3</sup> )	Bending Moment x-x (Kip-In.)	I <sub>gross</sub> y-y (in. <sup>4</sup> )	I <sub>hole</sub> y-y (in. <sup>4</sup> )	I <sub>net</sub> y-y (in. <sup>4</sup> )	S <sub>net</sub> y-y (in. <sup>3</sup> )	Bending Moment y-y (Kip-In.)
5,400	6	8	4	3	3 1/2	24 7/8	256.00	21.44	234.56	58.64	317	144.00	63.00	81.00	27.00	146

Peak Load Capacities	
Strong Axis x-x (Kips)	Weak Axis y-y (Kips)
12.74	5.87

**Table 2b. Wood CRT Post Peak Load Capacities – Metric**

CRT Post Properties				Strong Axis of Bending				Weak Axis of Bending								
Assumed Modulus of Rupture (MPa)	Post Width (mm)	Post Depth (mm)	C x-x (mm)	C y-y (mm)	Hole Diameter (mm)	Load Height (mm)	I <sub>gross</sub> x-x (mm <sup>4</sup> )	I <sub>hole</sub> x-x (mm <sup>4</sup> )	I <sub>net</sub> x-x (mm <sup>4</sup> )	S <sub>net</sub> x-x (mm <sup>3</sup> )	Bending Moment x-x (k)	I <sub>gross</sub> y-y (mm <sup>4</sup> )	I <sub>hole</sub> y-y (mm <sup>4</sup> )	I <sub>net</sub> y-y (mm <sup>4</sup> )	S <sub>net</sub> y-y (mm <sup>3</sup> )	Bending Moment y-y (k)
37,232	152.4	203.2	101.6	76.2	88.9	631.8	1.066E+08	8.920E+06	9.763E+07	9.609E+05	35.82	5.994E+07	2.622E+07	3.371E+07	4.425E+05	16.50

Peak Load Capacities	
Strong Axis x-x (kN)	Weak Axis y-y (kN)
56.67	26.11



### **3.3 CRT Bogie Test Results**

The dynamic properties for the CRT wood post were determined through bogie testing with target impact conditions consisting of a speed of 15 mph (24.1 km/h), orientation angles of 0, 45, and 90 degrees relative to the strong axis, and a height of 24 7/8 in. (632 mm) above the ground line. Also, all the posts were placed in the rigid sleeve with an embedment of 40 in. (1016 mm). Test nos. MNCRT-1 through MNCRT-3 were impacted in the strong axis at an impact angle of 0 degrees. Test nos. MNCRT-4 through MNCRT-6 were impacted in the weak axis at an impact angle of 90 degrees. Finally, test nos. MNCRT-7 through MNCRT-9 were impacted in a diagonal axis at an impact angle of 45 degrees. The test results presented in this section are grouped according to impact angle and are used to provide insight into the properties of the CRT post at the three different impact orientations.

For all tests, the CRT posts exhibited an initial rise in the force level due to the inertial effects and initiation of post failure. This initial rise occurred before a deflection of 5 in. (127 mm) for every test. After the initial 5 in. (127 mm), the post had already fractured and had lost most of its resistance, as seen in the high-speed video. As a result, energy levels at 5 in. (127 mm) of deflection were chosen to provide a consistent position to compare the different tests. The energy dissipated during each test was calculated by integrating the area under its force-deflection curve.

#### **3.3.1 Test Nos. MNCRT-1, MNCRT-2, and MNCRT-3**

The first three bogie tests were performed on the strong axis of the CRT wood posts. The test summaries for all three tests are given in Table 3, while force versus displacement and energy versus displacement curves can be seen in Figure 3 and Figure 4 respectively. For all

three tests, the initial peak force occurred quickly at a similar displacement, averaging 1.45 in. (37 mm). The peak force levels had larger variability, ranging from 7.58 kips (33.72 kN) to 13.31 kips (59.21 kN). In tests MNCRT-1 and MNCRT-3, the energy levels showed similar results with 11.4 kip-in. (1.29 kJ) and 13.6 kip-in. (1.54 kJ), respectively. However, test MNCRT-2 had a significantly larger energy level of 23.9 kip-in. (2.70 kJ) at 5 in. (127 mm) of deflection. This difference can be attributed to a variation in the wood properties. The post in MNCRT-2 had no knots, while the other two posts in MNCRT-1 and MNCRT-3 had several knots that significantly reduced the strength, or energy levels, of both posts. With no post knots in MNCRT-2, the post broke differently by splitting down the middle before fracturing and finally failing near the breakaway hole. The posts in MNCRT-1 and MNCRT-3 fractured near the breakaway hole and broke off quickly.

**Table 3a. Test Results for MNCRT-1, MNCRT-2, and MNCRT-3 – English**

Test No.	Impact Velocity (mph)	Impact Angle (degrees)	Initial Peak Force		Energy @ 5" Displacement (kip-in.)	Final Total Energy	
			Displacement (in.)	Force (kips)		Displacement (in.)	Energy (kip-in.)
MNCRT-1	14.40	0	1.57	9.91	13.9	11.18	18.26
MNCRT-2	15.9	0	1.47	13.31	23.9	18.98	36.0
MNCRT-3	15.13	0	1.32	7.58	11.4	6.50	13.82
Average	15.14	0	1.45	10.27	16.4	12.22	22.69

\*Post knots in test nos. MNCRT-1 and MNCRT-3

**Table 3b. Test Results for MNCRT-1, MNCRT-2, and MNCRT-3 – Metric**

Test No.	Impact Velocity (m/s)	Impact Angle (degrees)	Initial Peak Force		Energy @ 127 mm Displacement (kJ)	Final Total Energy	
			Displacement (mm)	Force (kN)		Displacement (mm)	Energy (kJ)
MNCRT-1	6.44	0	39.9	44.08	1.57	284.0	2.06
MNCRT-2	7.11	0	37.3	59.21	2.70	482.1	4.07
MNCRT-3	6.76	0	33.5	33.72	1.29	165.1	1.56
Average	6.77	0	36.9	45.67	1.85	310.4	2.56

\*Post knots in test nos. MNCRT-1 and MNCRT-3

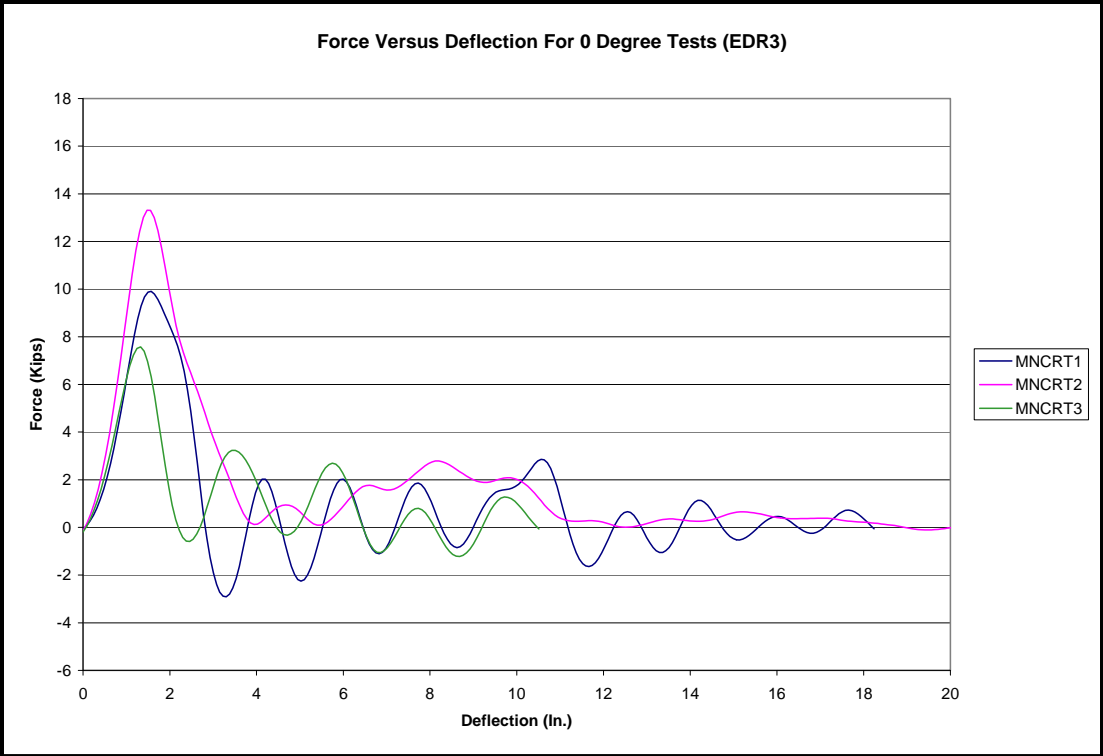


Figure 3a. Force versus Deflection Curves for MNCRT-1, 2, and 3 – English

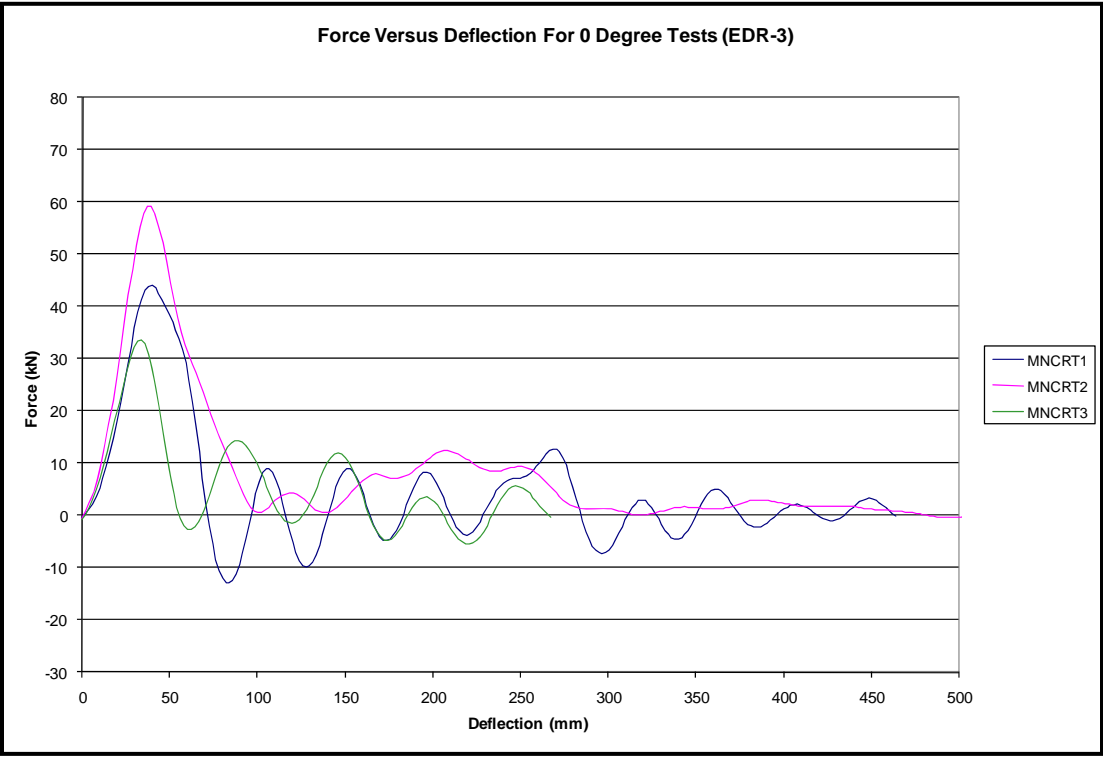


Figure 3b. Force versus Deflection Curves for MNCRT-1, 2, and 3 – Metric

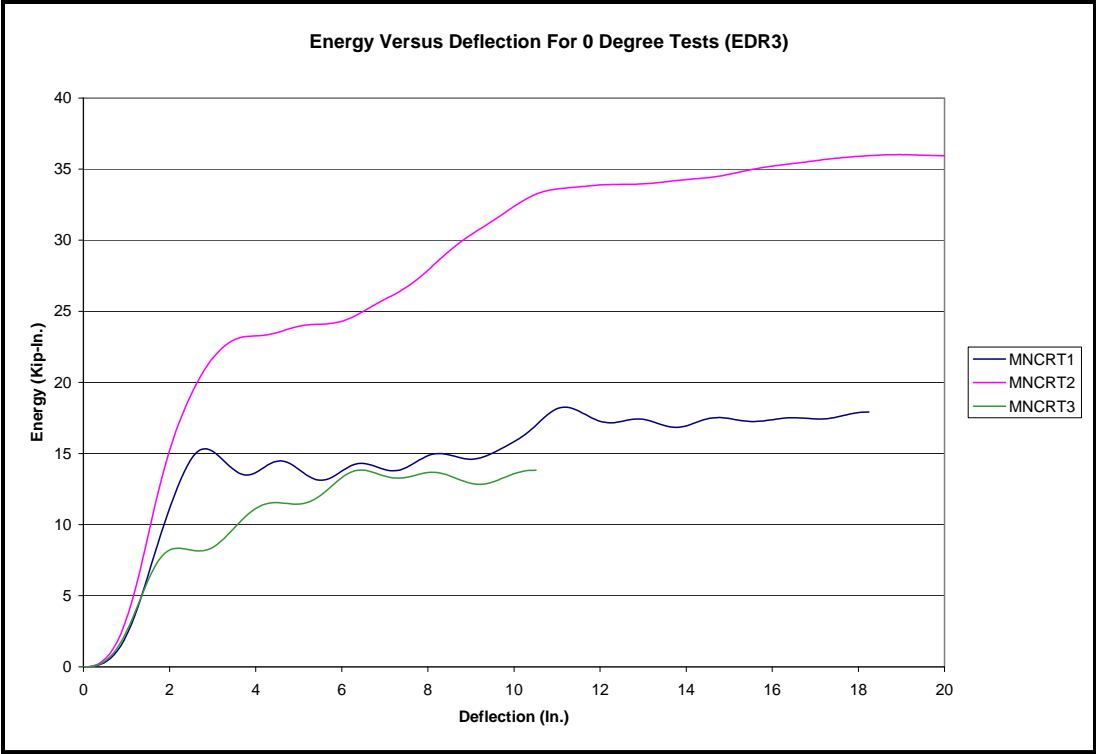


Figure 4a. Energy versus Deflection Curves for MNCRT-1, 2, and 3 – English

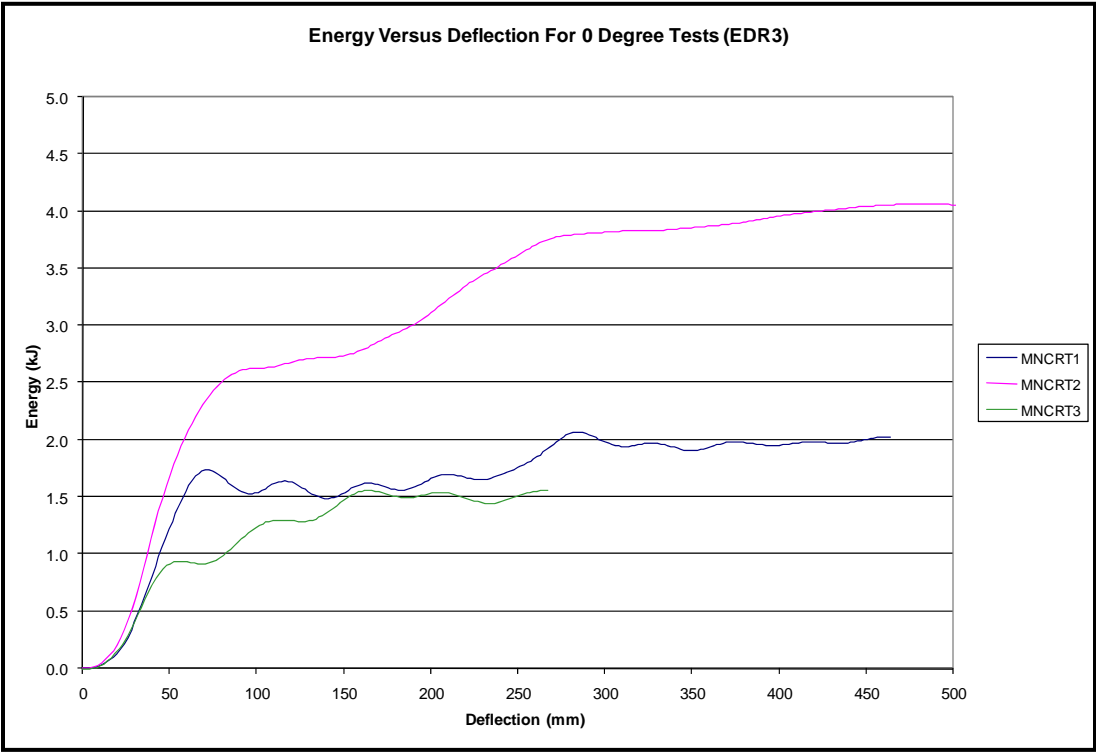


Figure 4b. Energy versus Deflection Curves for MNCRT-1, 2, and 3 – Metric

### 3.3.2 Test Nos. MNCRT-4, MNCRT-5, and MNCRT-6

The second set of three bogie tests was performed on the weak axis of the CRT wood posts. The test summaries for all three tests are given in Table 4, while force versus displacement and energy versus displacement curves can be seen in Figure 5 and Figure 6 respectively. For all three tests, failure resulted from the post breaking near ground level at the breakaway hole. The initial peak force occurred quickly at a similar displacement, averaging 1.50 in. (38.2 mm). The peak force levels were also similar, ranging from 7.67 kips (34.12 kN) to 10.34 kips (45.99 kN). Test MNCRT-4 had an energy level of 17.1 kip-in. (1.93 kJ), test MNCRT-5 had an energy level of 20.2 kip-in. (2.28 kJ), and test MNCRT-6 had an energy level of 13.4 kip-in. (1.51 kJ). Any differences can be attributed to variations in the wood material. The average energy level for these three weak-axis tests was 16.9 kip-in. (1.91 kJ), which was actually slightly higher than the average of 16.4 kip-in. (1.85 kJ) for the strong-axis tests.

Although the higher energies seen in the weak axis testing was not expected, a reason for the higher energies can be explained by the larger displacements before fracture seen in the testing. These larger displacements in the weak axis can be explained by the static, elastic deflection for a cantilever beam calculated from Equation 1.

$$\Delta = \frac{P * L^3}{3 * E * I} \quad \text{Eqn. 1}$$

Where: P=Applied Load, L=Length of Beam, E=Elastic Modulus, I=Moment of Inertia

For the same elastic modulus and based on the properties found in Table 2, the CRT wood post should have approximately 33 percent more deflection in the weak axis. Thus, with higher deflections, the weak axis absorbed similar energy even with the slightly lower peak force levels. Also, variations in the wood could explain the higher energies absorbed in the weak axis.

The modulus of rupture in the weak axis was nearly double the modulus of rupture seen in the strong-axis testing, 8,356 psi (57.6 GPa) compared to 4,357 psi (30.0 GPa). If more tests were conducted, it would be expected that the modulus of rupture in the weak axis testing would decrease to values seen in the strong-axis testing and also in other research studies involving post testing.

**Table 4a. Test Results for MNCRT-4, MNCRT-5, and MNCRT-6 – English**

Test No.	Impact Velocity (mph)	Impact Angle (degrees)	Initial Peak Force		Energy @ 5" Displacement	Final Total Energy	
			Displacement (in.)	Force (kips)		Displacement (in.)	Energy (kip-in.)
MNCRT-4	16.44	90	1.62	10.34	17.1	11.03	21.94
MNCRT-5	15.77	90	1.47	9.19	20.2	12.37	24.57
MNCRT-6	15.28	90	1.42	7.67	13.4	11.02	16.64
Average	15.82	90	1.50	9.07	16.9	11.47	21.05

**Table 4b. Test Results for MNCRT-4, MNCRT-5, and MNCRT-6 – Metric**

Test No.	Impact Velocity (m/s)	Impact Angle (degrees)	Initial Peak Force		Energy @ 127 mm Displacement	Final Total Energy	
			Displacement (mm)	Force (kN)		Displacement (mm)	Energy (kJ)
MNCRT-4	7.35	90	41.1	45.99	1.93	280.2	2.48
MNCRT-5	7.05	90	37.3	40.88	2.28	314.2	2.78
MNCRT-6	6.83	90	36.1	34.12	1.51	279.9	1.88
Average	7.08	90	38.2	40.33	1.91	291.4	2.38



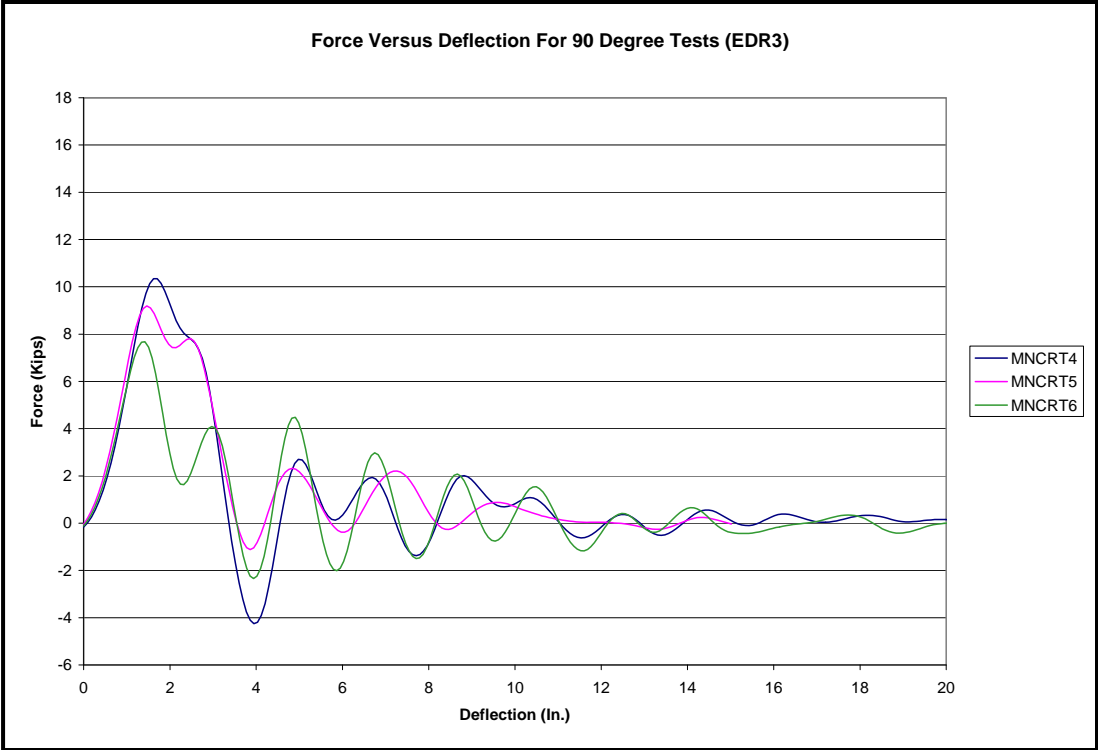


Figure 5a. Force versus Deflection Curves for MNCRT-4, 5, and 6 – English

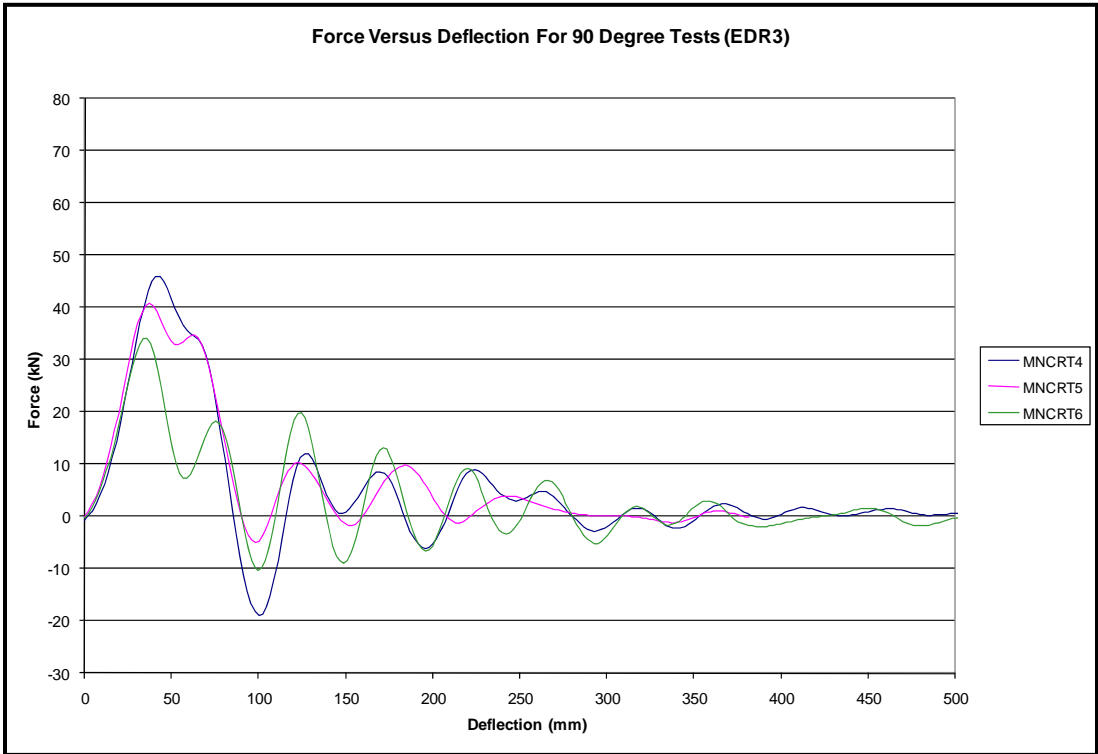


Figure 5b. Force versus Deflection Curves for MNCRT-4, 5, and 6 – Metric

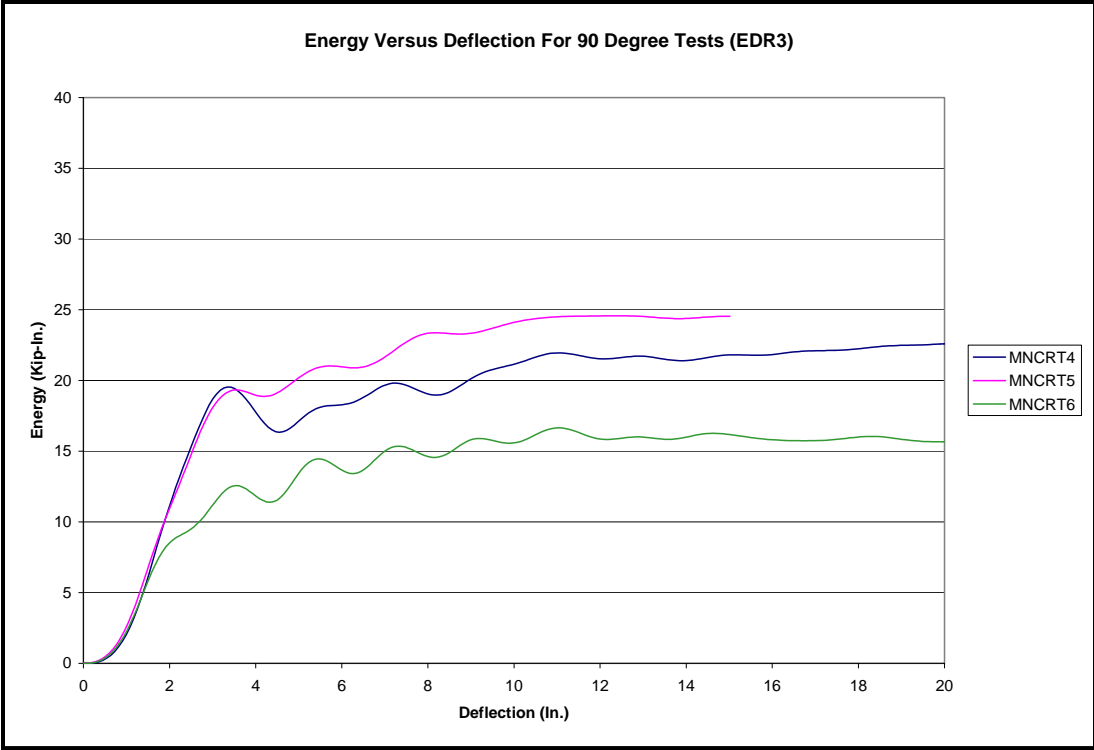


Figure 6a. Energy versus Deflection Curves for MNCRT-4, 5, and 6 – English

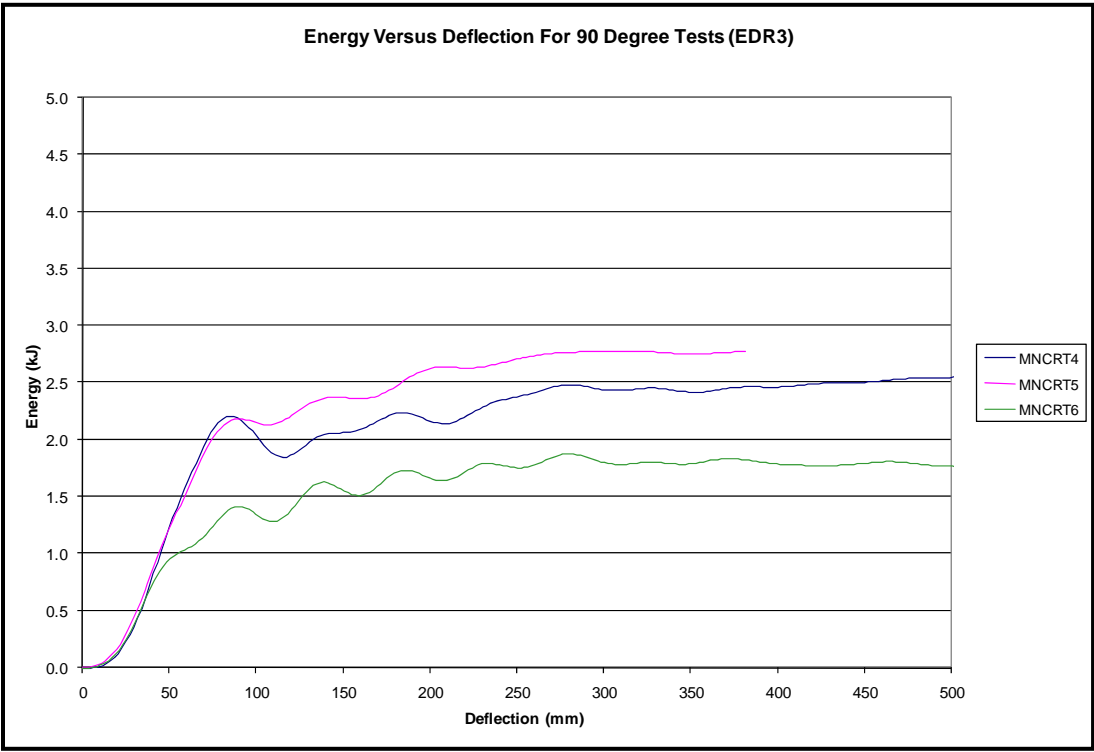


Figure 6b. Energy versus Deflection Curves for MNCRT-4, 5, and 6 – Metric

### **3.3.3 Test Nos. MNCRT-7, MNCRT-8, and MNCRT-9**

The final set of three bogie tests was performed on the diagonal axis (45°) of the CRT wood posts. The test summaries for all three tests are given in Table 5, while force versus displacement and energy versus displacement curves can be seen in Figure 7 and Figure 8 respectively. For all three tests, failure resulted from the post breaking near ground level at the breakaway hole. The initial peak force occurred at a displacement averaging 2.79 in. (70.8 mm). The peak force levels ranged from 6.98 kips (31.05 kN) to 16.11 kips (71.66 kN). The large differences in the peak forces again illustrate the high variability in the wood properties. Also, in MNCRT-8, the post rotated up in the rigid sleeve, so the breakaway hole moved above ground level causing more inconsistency as the post did not break away nearly as quickly. The energy versus deflection curves also were not as consistent as the previous impact angles. For these tests, there was a fixture issue in the rigid sleeve that had some affect on the consistency of the energy levels. It was observed that posts would shift in the rigid sleeve for the first 6 to 8 ms of the tests. This movement was unexpected and created some error as the wood posts were not properly held rigidly in place. The three tests averaged 23.13 kip-in. (2.61 kJ), which was higher than expected due to the fixture issue.

Due to the fixture issue, the data was also processed by cutting off the fixture effect, as seen in Table 6 and Figures 9 and 10. By cutting off the initial peak due to the fixture, both the energy levels and deflections of the post dropped to more expected results. Approximately 1 1/2 in. (38 mm) of deflection was cut off when subtracting off the fixture issue.

**Table 5a. Test Results for MNCRT-7, MNCRT-8, and MNCRT-9 – English**

Test No.	Impact Velocity (mph)	Impact Angle (degrees)	Initial Peak Force		Energy @ 5" Displacement		Final Total Energy	
			Displacement (in.)	Force (kips)	Energy (kip-in.)	Displacement (in.)	Energy (kip-in.)	
MNCRT-7	16.06	45	3.36	16.11	35.5	13.28	38.97	
MNCRT-8	16.02	45	3.38	9.24	22.4	19.93	36.0	
MNCRT-9	15.54	45	1.62	6.98	11.5	3.43	13.60	
Average	15.87	45	2.79	10.78	23.13	12.21	29.52	

**Table 5b. Test Results for MNCRT-7, MNCRT-8, and MNCRT-9 – Metric**

Test No.	Impact Velocity (m/s)	Impact Angle (degrees)	Initial Peak Force		Energy @ 127 mm Displacement		Final Total Energy	
			Displacement (mm)	Force (kN)	Energy (kJ)	Displacement (mm)	Energy (kJ)	
MNCRT-7	7.18	45	85.3	71.66	4.01	337.3	4.40	
MNCRT-8	7.16	45	85.9	41.10	2.53	506.2	4.07	
MNCRT-9	6.95	45	41.1	31.05	1.30	87.1	1.54	
Average	7.10	45	70.8	47.94	2.61	310.2	3.34	

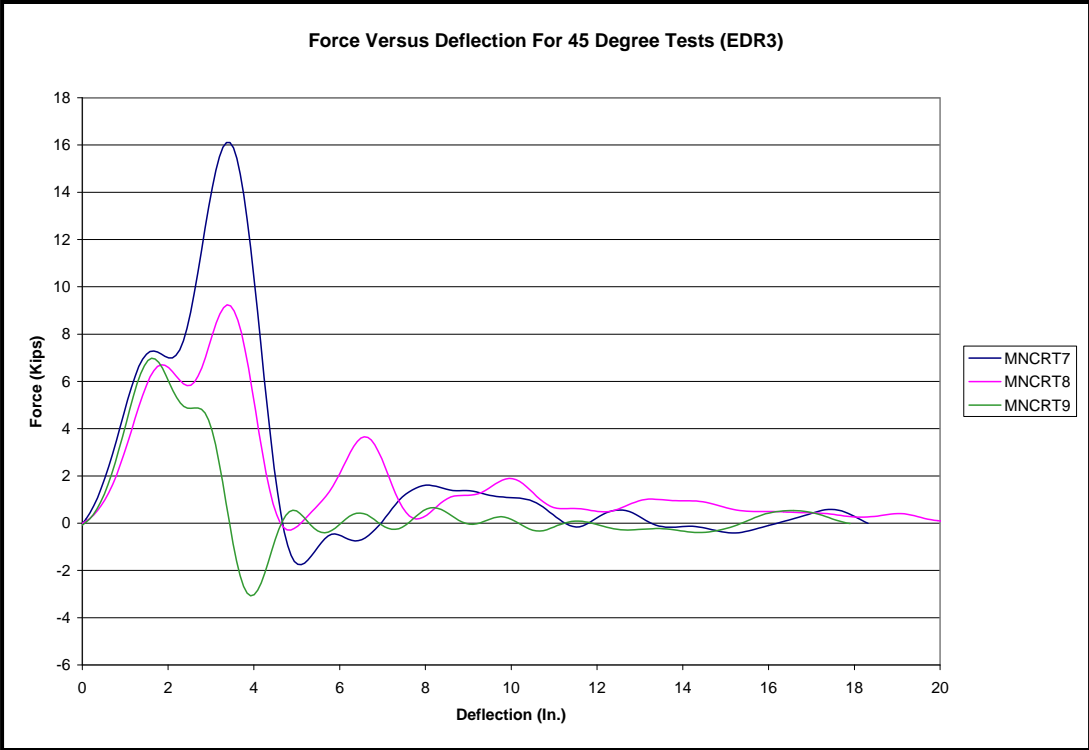


Figure 7a. Force versus Deflection Curves for MNCRT-7, 8, and 9 – English

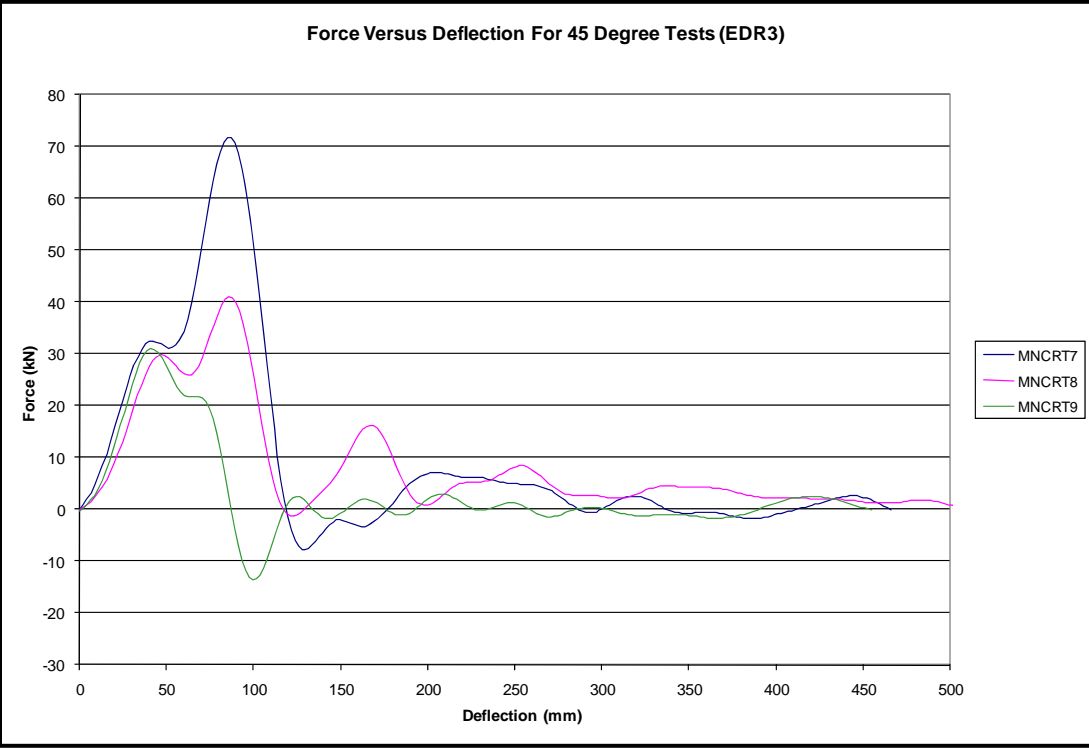


Figure 7b. Force versus Deflection Curves for MNCRT-7, 8, and 9 – Metric

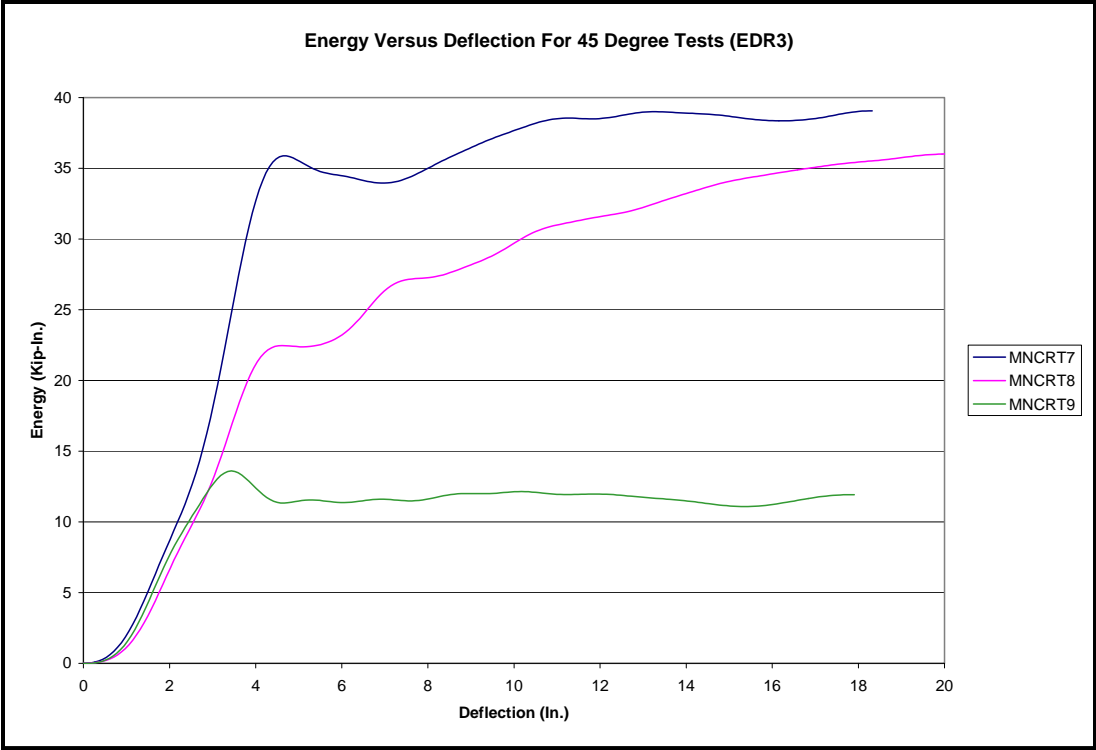


Figure 8a. Energy versus Deflection Curves for MNCRT-7, 8, and 9 – English

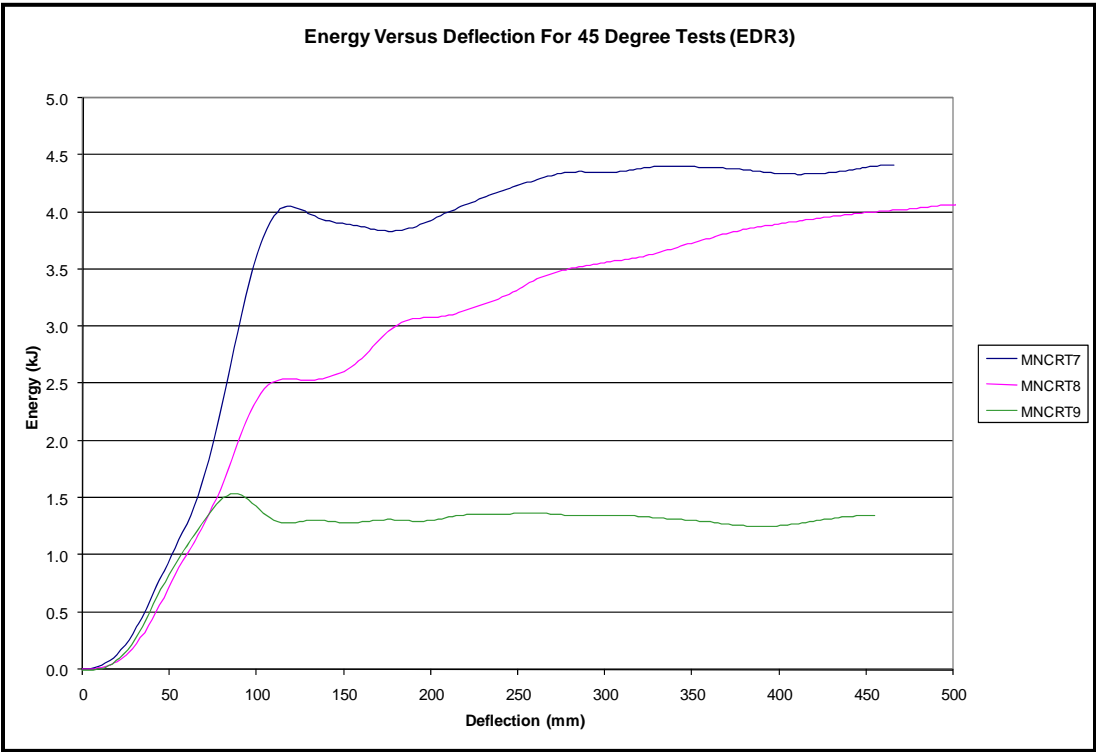


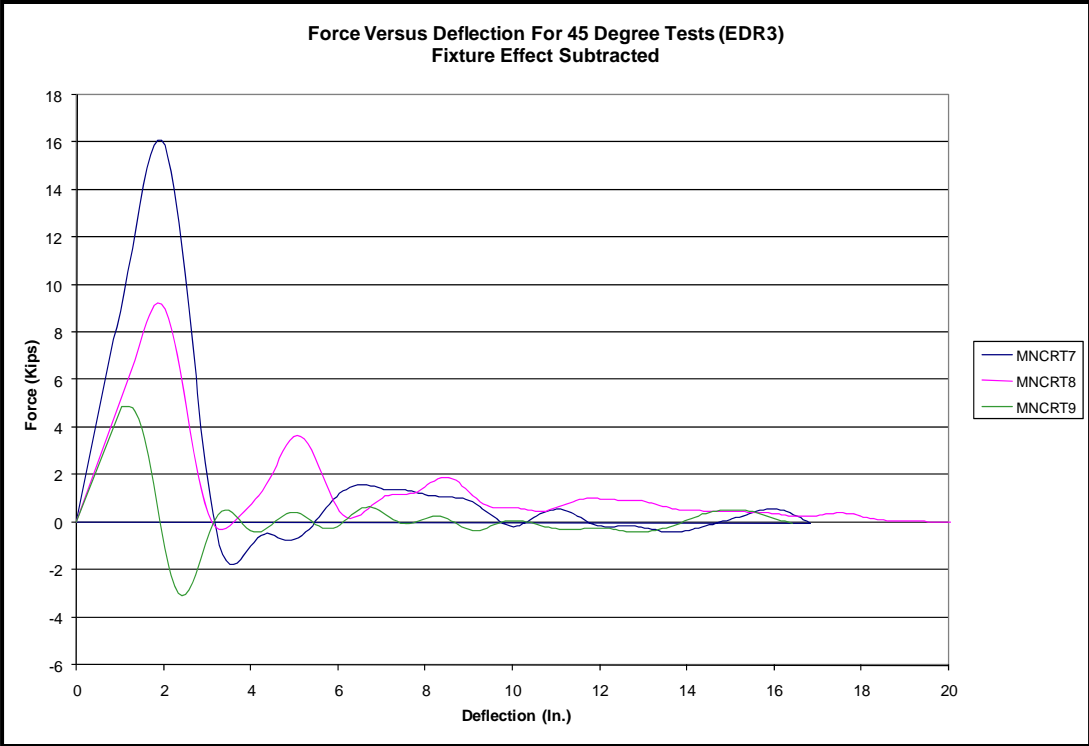
Figure 8b. Energy versus Deflection Curves for MNCRT-7, 8, and 9 – Metric

**Table 6a. Test Results Without Fixture Effect for MNCRT-7, MNCRT-8, and MNCRT-9 – English**

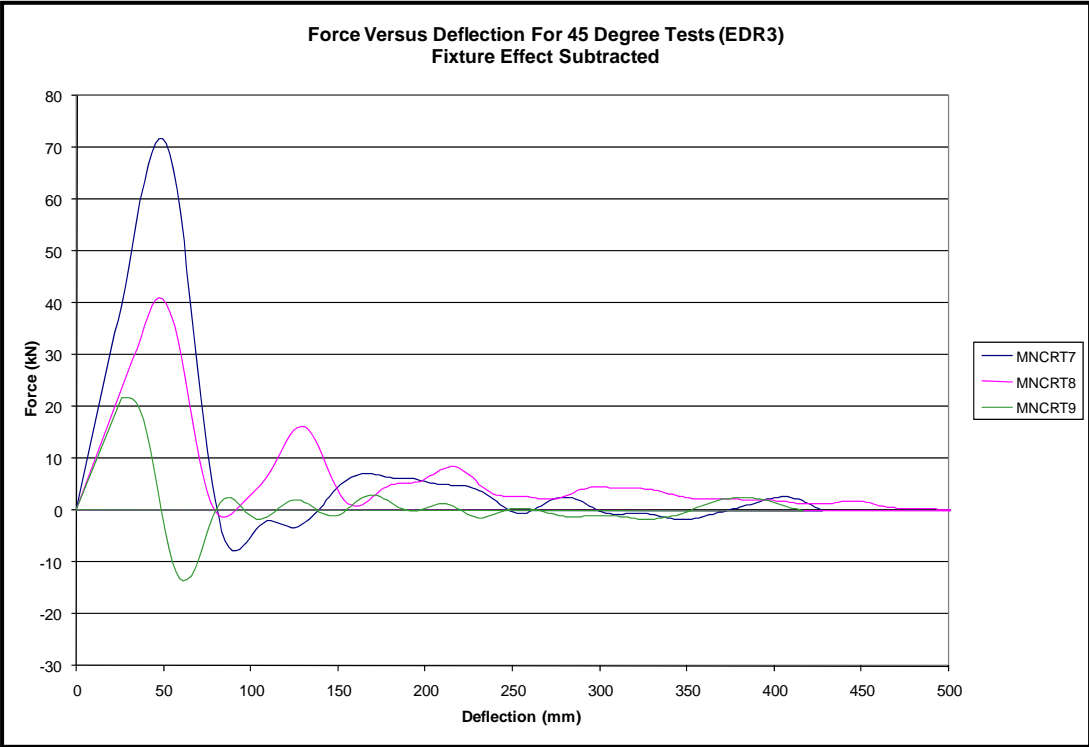
Test No.	Impact Velocity (mph)	Impact Angle (degrees)	Initial Peak Force		Energy @ 5" Displacement	Final Total Energy	
			Displacement (in.)	Force (kips)		Displacement (in.)	Energy (kip-in.)
MNCRT-7	16.06	45	1.86	16.11	26.2	11.8	31.1
MNCRT-8	16.02	45	1.88	9.24	18.0	18.5	29.4
MNCRT-9	15.54	45	1.20	4.88	3.97	1.93	6.07
Average	15.87	45	1.65	10.08	16.1	10.7	22.2

**Table 6b. Test Results Without Fixture Effect for MNCRT-7, MNCRT-8, and MNCRT-9 – Metric**

Test No.	Impact Velocity (m/s)	Impact Angle (degrees)	Initial Peak Force		Energy @ 127 mm Displacement	Final Total Energy	
			Displacement (mm)	Force (kN)		Displacement (mm)	Energy (kJ)
MNCRT-7	7.18	45	47.2	71.66	2.96	300	3.51
MNCRT-8	7.16	45	47.8	41.10	2.03	470	3.32
MNCRT-9	6.95	45	30.5	21.7	0.45	49.0	0.69
Average	7.10	45	41.9	49.2	1.81	273	2.51



**Figure 9a. Force versus Deflection Curves Minus Fixture Effect– English**



**Figure 9b. Force versus Deflection Curves Minus Fixture Effect – Metric**



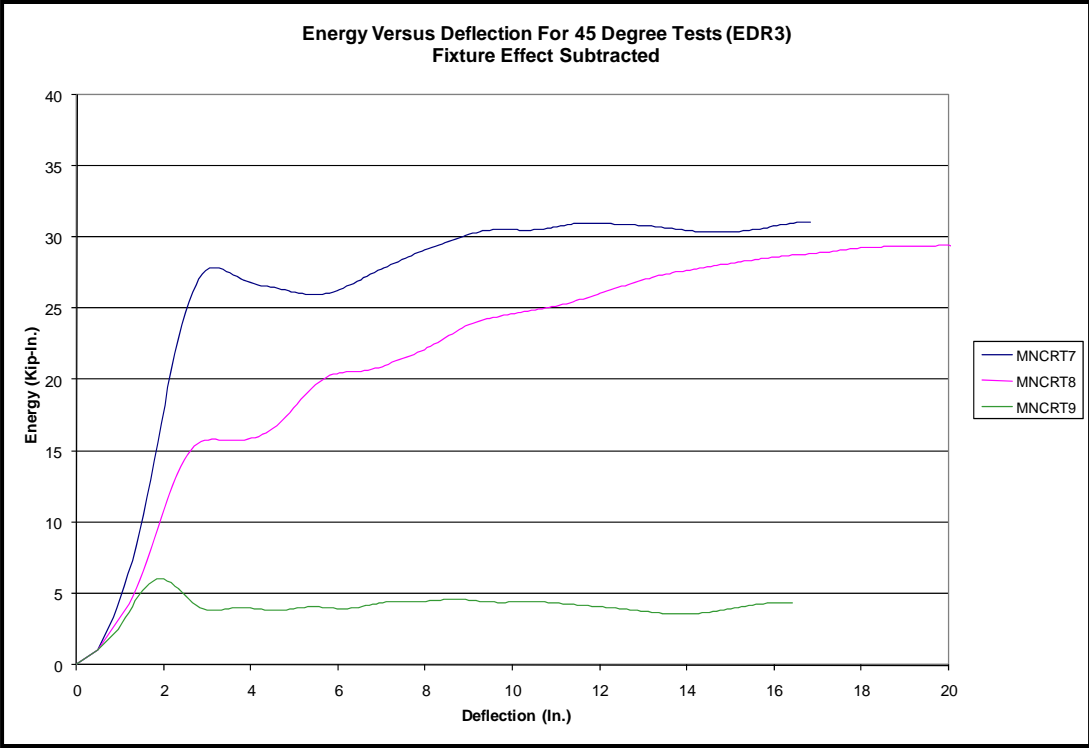


Figure 10a. Energy versus Deflection Curves Minus Fixture Effect – English

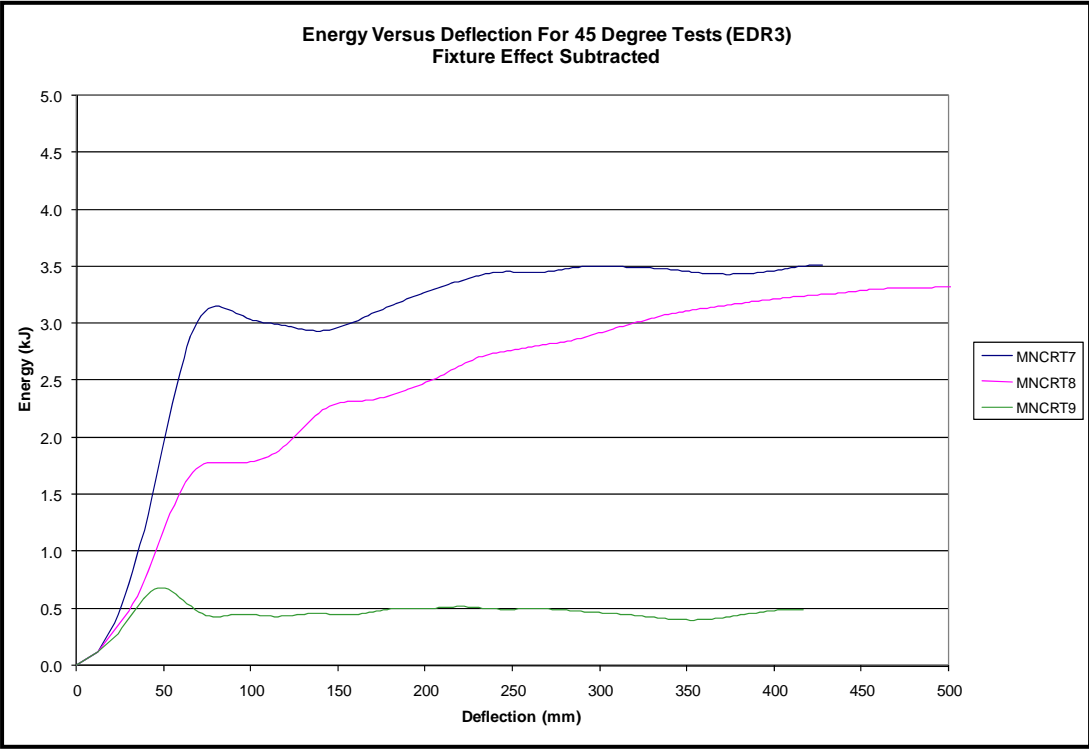


Figure 10b. Energy versus Deflection Curves Minus Fixture Effect – Metric

### 3.4 Conclusion/Recommendations

Although only nine bogie tests were performed with three tests at three different angles, the test results provided the basic properties of the CRT post under dynamic impact testing. Based on the bogie tests and the properties of the CRT post given in Table 2, the peak forces and total energy for the strong, weak, and diagonal axis were determined and are illustrated in Figure 11.

The strong-axis peak force of 12 kips (53.4 kN) was chosen based on the bogie testing that showed a similar average of 10.27 kips (45.7 kN). Although the bogie testing in the weak axis averaged 9.07 kips (40.3 kN), the weak-axis peak force was chosen as 6 kips (26.7 kN). This decision was based on knowing the modulus of rupture in the weak axis was nearly double the modulus of rupture seen in the strong axis testing, 8,356 psi (57.6 GPa) compared to 4,357 psi (30.0 GPa). If more tests were conducted, it would be expected that the modulus of rupture in the weak axis testing would decrease to values seen in the strong axis and in other testing and studies. Also, wood properties of a SYP CRT wood post found in Table 2 shows how the strong axis should have nearly double the peak force due to the different moment of inertias for the separate axes. This data from the moment of inertias was independent of the differences and variation in the wood that greatly affected the nine bogie tests.

For the energy levels, 2 in. (51 mm) of deflection at the peak force was chosen to be representative of the energy level. Thus, the target energy levels were 24 kip-in. (2.71 kJ) in the strong axis, 12 kip-in. (1.36 kJ) in the weak axis, and 16 kip-in. (1.81 kJ) in the diagonal axis. These values stemmed from the bogie results and also from previous experience with the CRT posts knowing that the posts fracture relatively quickly. From these results, there were now target

force and energy values to aim for in the development of preliminary breakaway post designs, as seen in Figure 11.

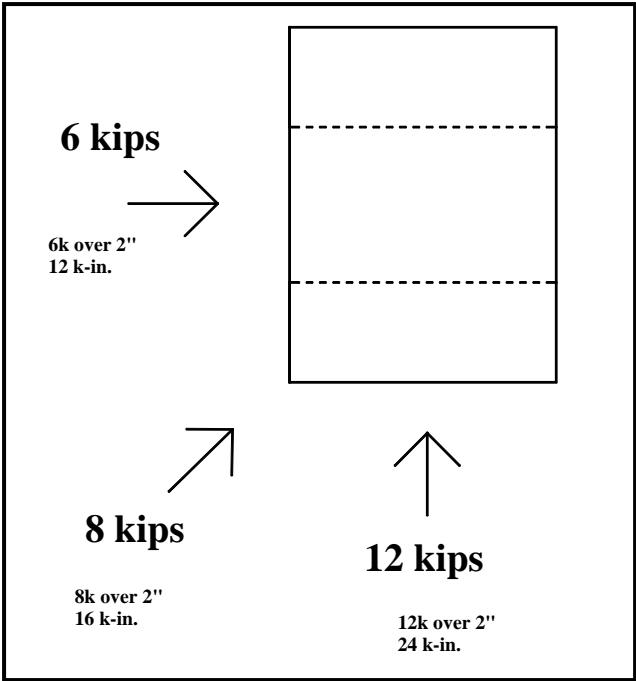


Figure 11a. Peak Forces and Energy Levels of the CRT Post – English

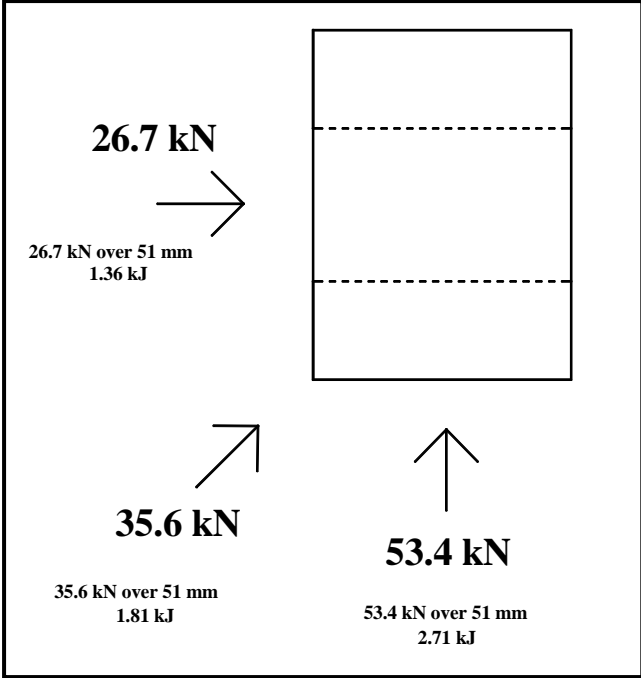


Figure 11b. Peak Forces Energy and Levels of the CRT Post - Metric

## **4 PRELIMINARY BREAKAWAY POST DESIGNS**

### **4.1 Introduction**

After observing and determining the dynamic properties of the CRT wood post, the next phase of research consisted of brainstorming possible breakaway post designs to match the properties and breakaway characteristics of the CRT post. The preliminary breakaway post designs needed to be tuned to the longitudinal, lateral, and oblique resistances of the CRT wood post, thus allowing it to replace the CRT post in several guardrail applications. In addition to developing new preliminary breakaway post concepts, previous breakaway post ideas were also examined.

### **4.2 Preliminary Breakaway Post Ideas**

As described in the literature review presented in Chapter 2, previous breakaway post designs were examined to determine concepts for consideration as the universal breakaway post. This section described the effort to develop new breakaway post concepts. A new design concept would eliminate any patent infringement concerns and would allow states to use the new post royalty free.

While brainstorming new designs, numerous concepts were identified that may replicate both the strength and failure properties that were observed in CRT wood posts. As mentioned earlier, the post must attach to a 6-in. x 8-in. (152-mm x 203-mm) steel foundation tube in order to maintain the same soil interaction as the 6-in. x 8-in. (152-mm x 203-mm) CRT wood post. Another important consideration was the need to maintain the brittle breakaway characteristics that were observed with the CRT wood posts.

At first, steel breakaway posts were the main focus. However, due to the ductile behavior of steel, other more brittle materials were also considered. Steel has difficulty matching the fracture behavior of the wood. Wood fibers can begin failing, which reduces the cross-section and weakens the post. As a result, even if force levels drop, the wood post can still break away due to the weakened cross section. In steel, even if some yielding begins to occur, the cross section does not weaken and the force levels must reach the full capacity of a steel section in order for a steel post to break away. All the preliminary breakaway post ideas can be seen in Figures 12 through 16.

#### **4.2.1 Steel Breakaway Post Ideas**

Numerous options, as shown in Figure 14, were considered for use with a steel W8x10 (W203x14.9) upper post connected to the steel foundation tube. With one exception, all of the W8x10 (W203x14.9) concepts used steel plates to create either a welded or bolted breakaway connection between the upper W8x10 (W203x14.9) post and the lower steel foundation tube. Some breakaway concepts pictured, including the plug weld post, the A325 bolt post, the circular fillet weld post, the two plug weld post, and the elliptical plug weld post, were possibly covered by existing patents and may require the owner's permission before their use in actual guardrail systems is considered. Also, two preliminary tubular steel post options are illustrated in Figure 15. Finally, a fracturing bolt (slipbase) option, shown in Figure 16, was also considered as a candidate for use as the universal breakaway post. All of these developed concepts utilized all steel parts, and each of these concepts, shown in Figures 14 through 16, is described in more detail below.

Beginning with welded connections in Figure 14, the plug weld concept, the groove weld concept, the circular fillet weld concept, the two plug weld concept, and the elliptical plug weld concept are all similar designs with comparable breakaway characteristics. All of these welded concepts have welds that are designed to shear and break away when impacted. Next, the A325 bolt post concept has a bolted connection designed to shear off the bolts and break away. The breakaway tab concept consists of a notched steel plate designed to fracture and break away when impacted.

In the steel tube in steel tube concept in Figure 15, an upper tube creates a “socket” with the lower tube. By just being embedded in the lower tube with no connection, the upper tube is able to be pulled up and out of the lower tube when impacted. Also, the weakened steel tube concept has a drilled hole out at the ground level of steel tube in order to weaken the steel tube and allow the tube to fail easier. Last, the fracturing bolt (slipbase) concept, shown in Figure 16, has four connecting bolts designed to fracture and break away due to tensile and shear forces.

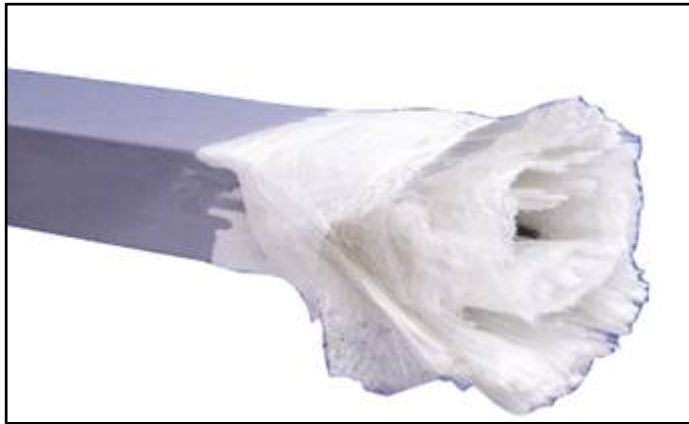
#### **4.2.2 Brittle Material Post Ideas**

The other preliminary tubular designs in Figure 15 capitalized on the brittleness of various other materials to better match the breakaway properties of wood. For the coupler designs, a cast steel, cast iron, or ceramic coupler was used as a “brittle” breakaway mechanism between the lower steel foundation tube and an upper steel tube. These cast steel, cast iron, or ceramic coupler designs could either be a tubular coupler as shown or plates attached to the outside of the upper tube and lower foundation tube.

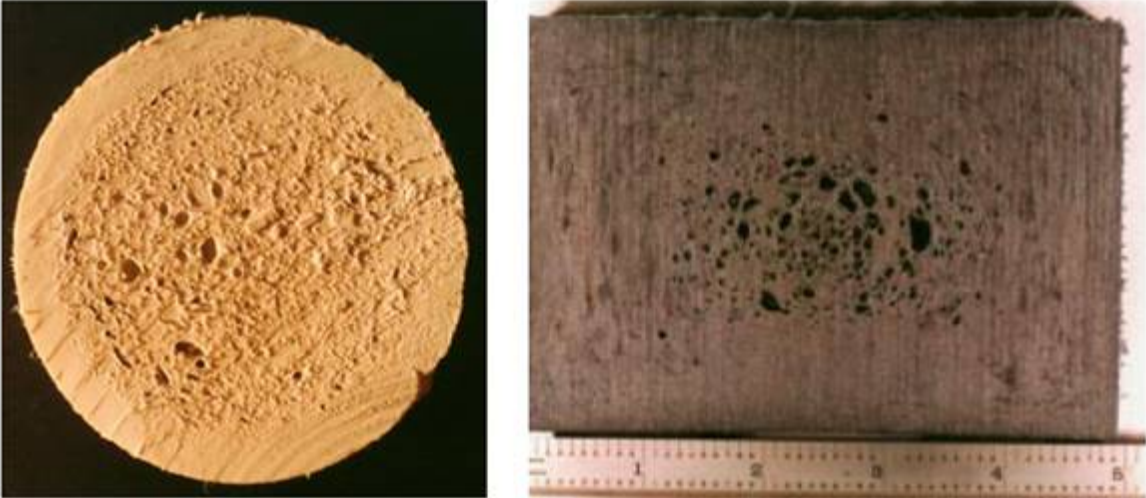
Another material considered was fiber reinforced plastic (FRP) in various structural shapes. The FRP component is a pultruded composite of E-glass fiber and thermosetting

isophthalic polyester resin with UV inhibitor [13]. As illustrated in Figure 12, the continuous strand mat and fiber reinforcements provide the strength for an FRP shape, while the resin binds the reinforcements and protects it from UV exposure. For the FRP material, both an upper post and a tubular coupler option, as visible in Figure 15, were considered as practical candidates for the universal breakaway post.

Lastly, recycled plastic was explored as a possible alternate coupler material. The recycled plastic consisted of various recycled high-density polyethylene mixed with sawdust and shaped into a guardrail post [14], as depicted in Figure 13.

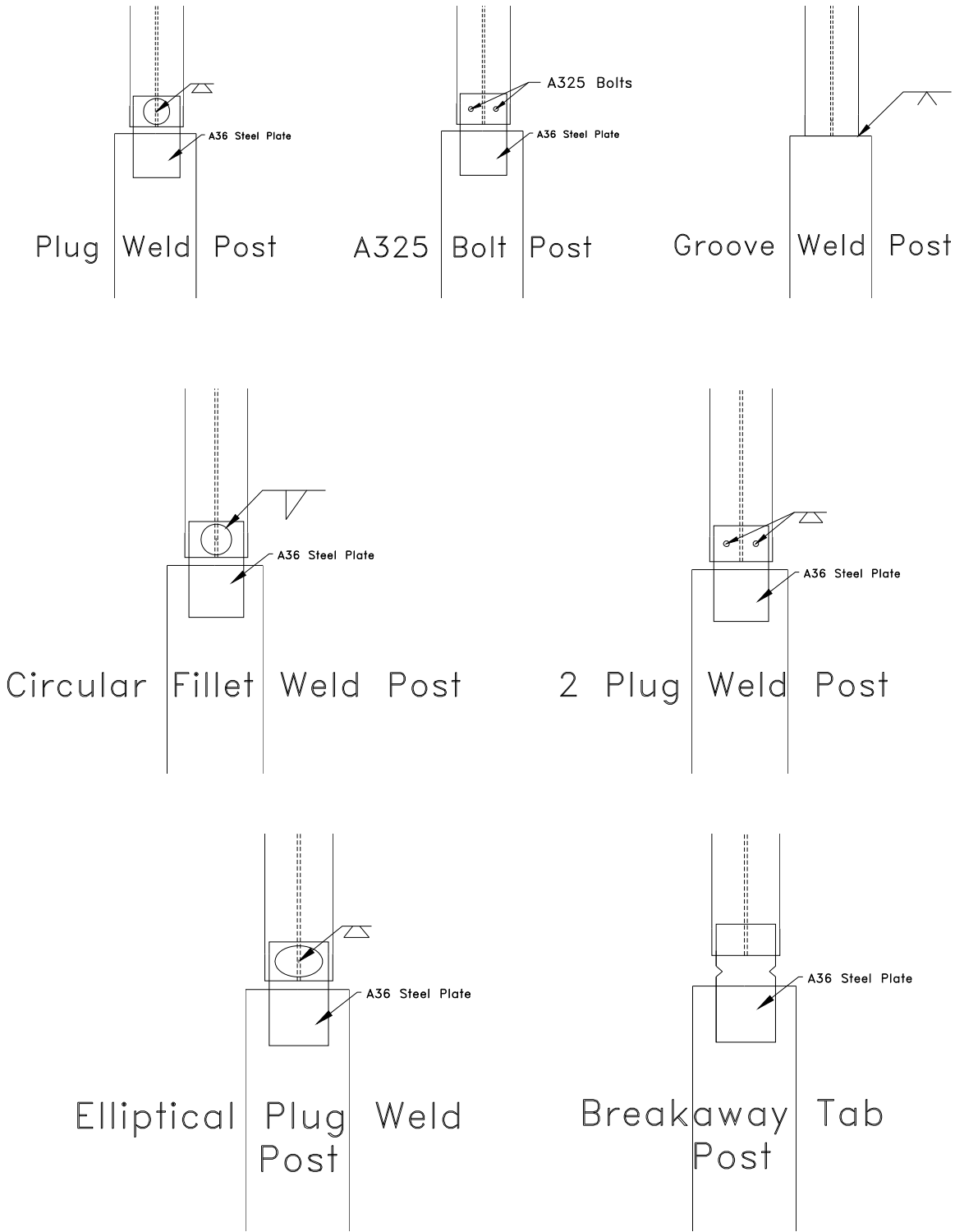


**Figure 12. Fiberglass Reinforced Plastic Structural Shape**

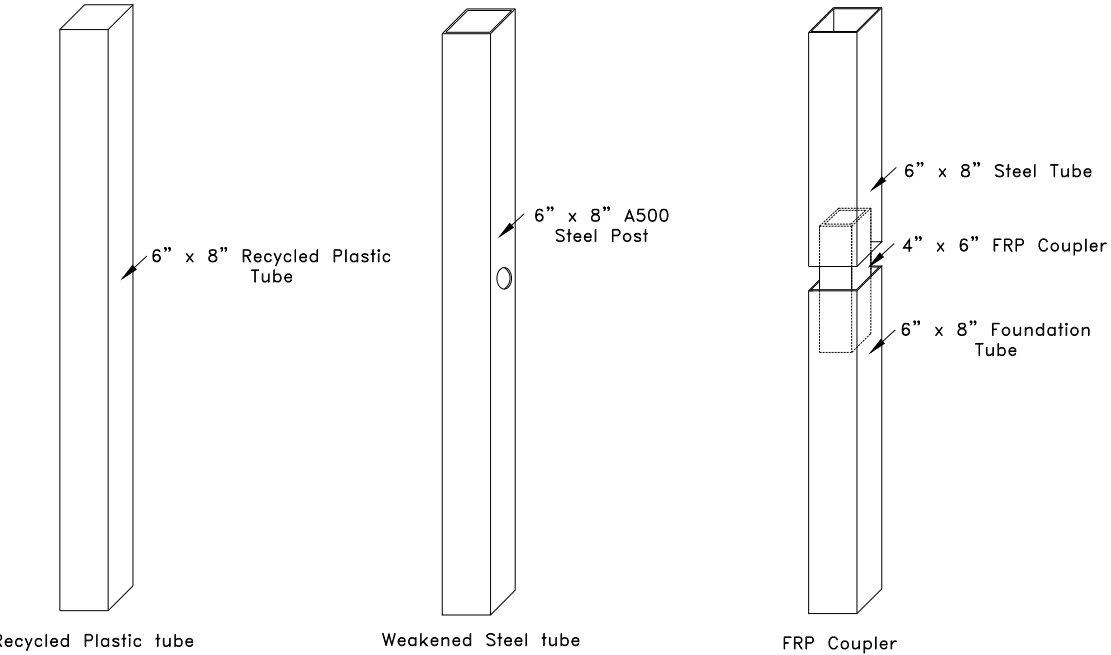
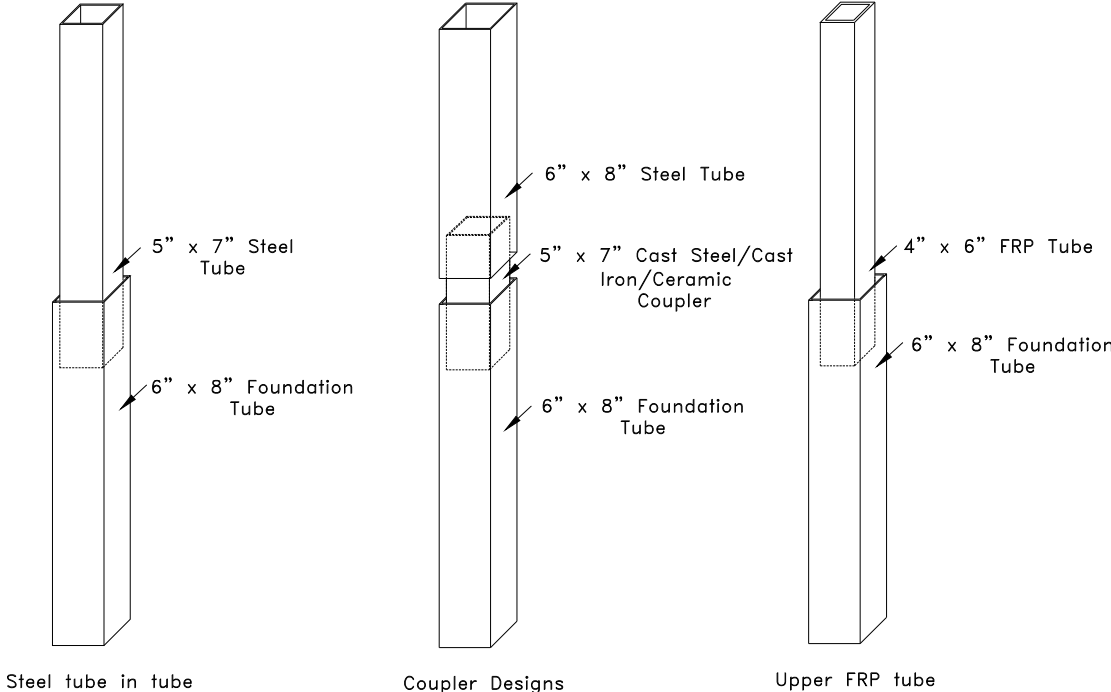


**Figure 13. Recycled Plastic Post Options**

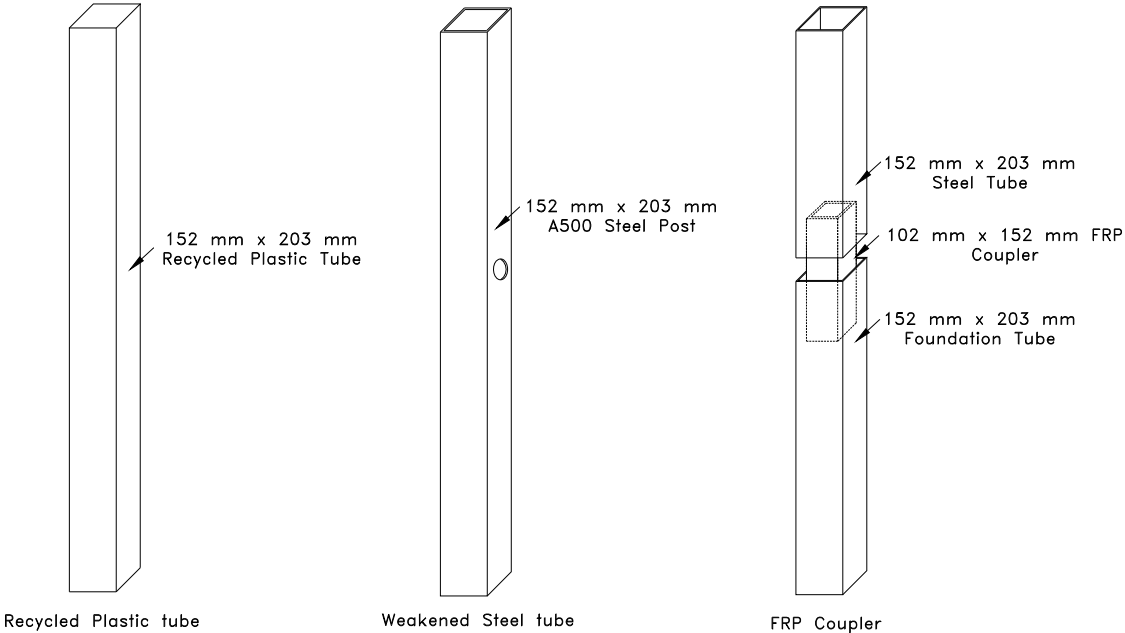
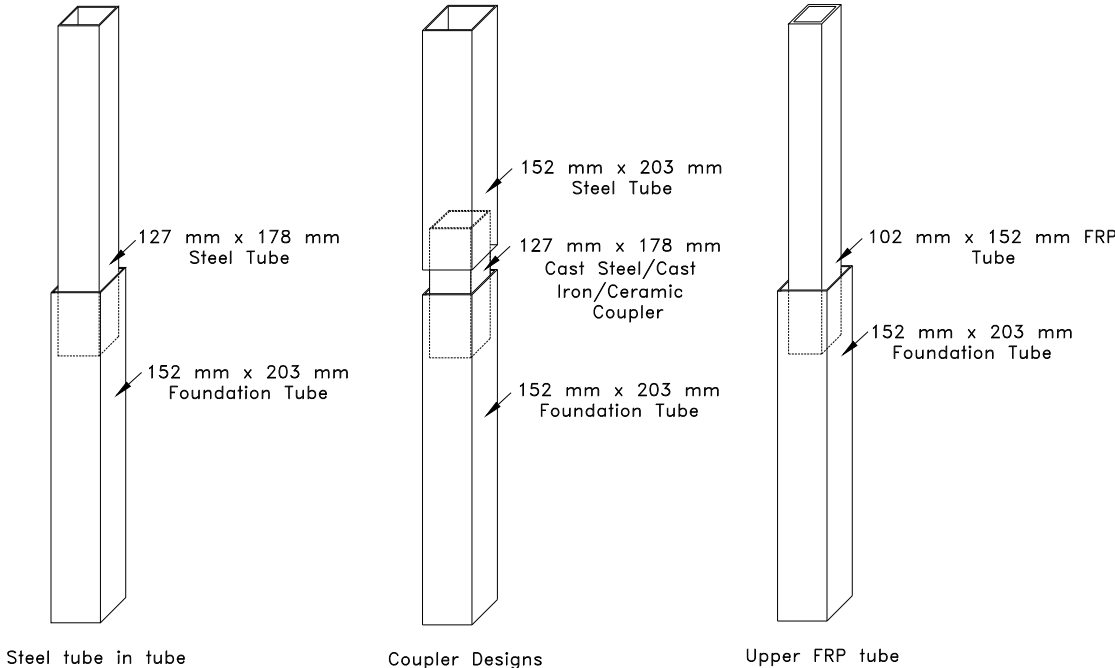




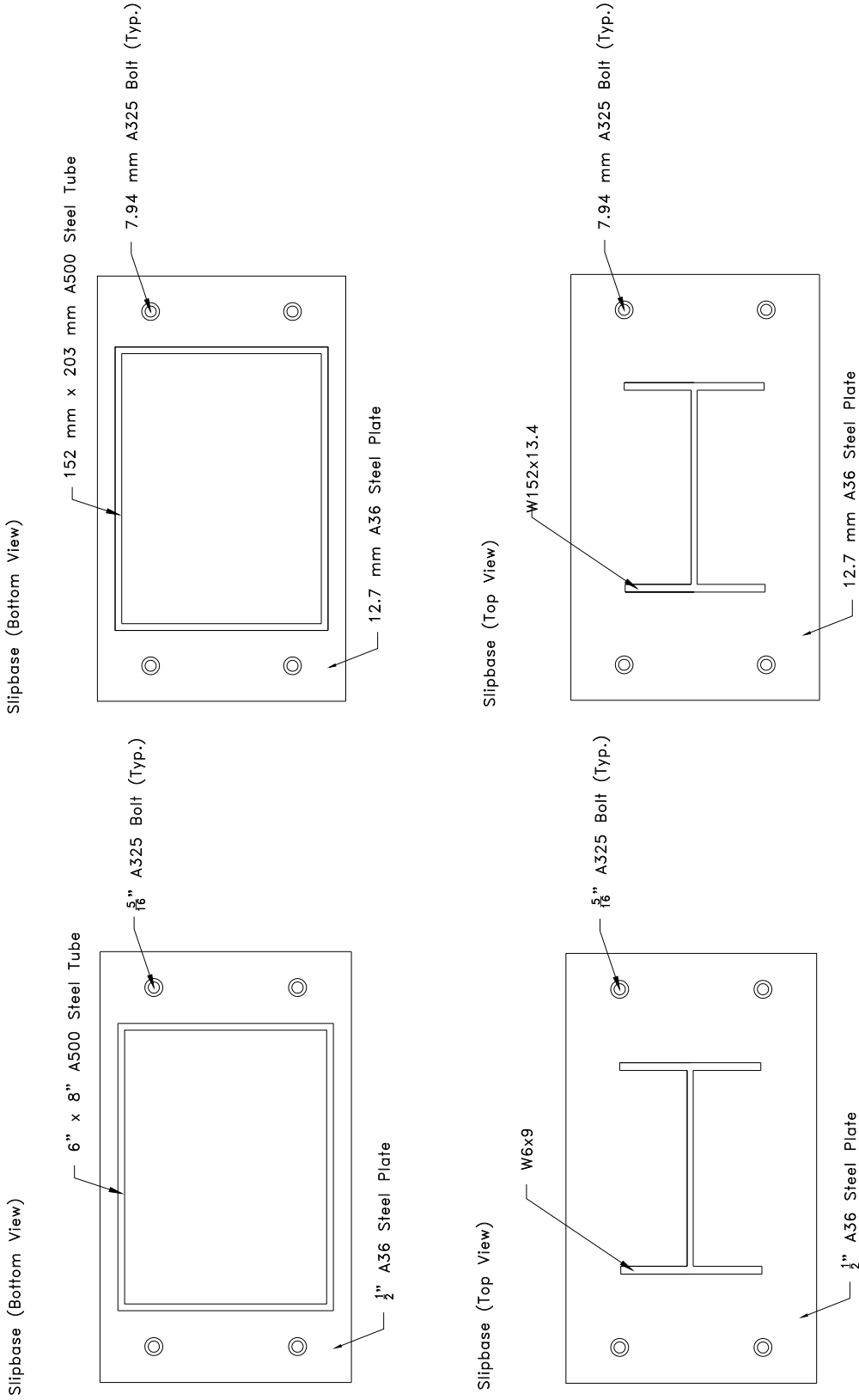
**Figure 14. Preliminary Steel W8x10 (W203x14.9) Breakaway Post Designs**



**Figure 15a. Preliminary Tubular Breakaway Post Designs – English**



**Figure 15b. Preliminary Tubular Breakaway Post Designs – Metric**



**Figure 16a. Preliminary Slipbase Post Design - English**      **Figure 16b. Preliminary Slipbase Post Design - Metric**

### 4.3 Options for First Round of Bogie Testing

After developing candidate posts for the universal breakaway post, the potential options needed to be narrowed down to the most promising designs for use in the initial round of bogie testing. Beginning with the steel W8x10 (W203x14.9) options listed in Figure 14, the plug weld post was discarded after evaluation of historical bogie tests. The post was found to absorb too much energy for strong-axis impacts when the back-side plug weld would not disengage from the foundation post. Also, from previous bogie tests, the A325 bolt option was dropped because the non-traffic side bolts would not break, and the post did not break away freely. Both the two plug weld and elliptical plug weld options were also deemed insufficient, as these designs would have similar behavior to the single plug weld. The groove weld option was also eliminated based upon concerns that variations in weld quality would lead to inconsistent behavior.

For the breakaway tab option, one concern was that the non-traffic-side tab would not break away as desired, since it would just bend over after the traffic-side plate fractured in tension. As a result, this option was also discarded. Finally, the circular fillet weld option seemed the most promising of the W8x10 (W203x14.9) designs to break away cleanly like wood, since it did not have a solid plug weld to get hung up on the non-traffic-side face. Thus, it was decided that a circular fillet had the best chance to break away on the non-impact side and to include this design in the first round of bogie testing.

Next, looking at the tubular designs in Figure 15, the steel tube in tube idea would be able to break away cleanly when the upper tube is pulled out of the lower tube. As a result, it was included in the bogie testing. For the coupler designs, the cast steel, cast iron, and ceramic options all provide acceptable breakaway behavior, but the cost of developing these options was

deemed to be high. There would be a need for a costly custom mold during development, and even minor revisions in the design would require a new mold. For the fiber reinforced plastic (FRP) concepts, the upper FRP post and FRP coupler options utilize the brittle characteristics of the FRP material. There are numerous standard FRP structural shapes, which can be used for the universal breakaway post. Thus, this concept was chosen for further study.

Next, the recycled plastic post option mixes polyethylene with sawdust. This mixture does not provide the preferred uniformity, and the polyethylene in the recycled plastic has a high toughness that will resist fracturing and breaking away when impacted. Another unacceptable factor of the recycled plastic is the sawdust, which is the same wood material that the breakaway post was intended to replace. The weakened steel tube would just bend over to the ground and would not break away cleanly due to the ductile behavior of the steel. Thus, the weakened steel tube was not considered for the first round of bogie testing. Finally, the fracturing bolt (slipbase) post in Figure 16 was included in the bogie testing, as it would be able to break away as desired when the bolts broke due to tensile and shear forces.

Thus, the number of preliminary concepts was narrowed down to the five options listed in Table 7. These concepts were tested in the first round of bogie testing to determine if they could replicate the strength and failure properties of the CRT post.

**Table 7. Round 1 Bogie Testing Concepts**

<b>Concept No.</b>	<b>Post Type</b>
1	Steel Tube In Steel Tube
2	Steel Tube In Steel Tube With Thru Bolt
3	Upper FRP Post
4	Fracturing Bolt (Slipbase)
5	Circular Fillet Weld

## **5 BREAKAWAY POST BOGIE TESTING – ROUND 1**

### **5.1 Purpose**

Physical component testing is an important aspect of any design process which is often used to gain practical insights into the behavior of the design. As such, bogie tests were undertaken on the selected post designs to verify fracture characteristics and determine if fracture forces could be tuned to match the behavior of the wood CRT post.

### **5.2 Scope**

Initial bogie tests were conducted on the five post concepts identified for further investigation, as shown in Table 7. For these bogie tests, the posts were embedded 40 in. (1,016 mm) in standard strong soil in order to match the conditions in the bullnose system, where the posts are embedded in soil. Earlier, the wood CRT posts were embedded in rigid sleeves to determine the strength of the post without the effect of soil. The coarse aggregate soil conformed to the American Association of State Highway Transportation Officials (AASHTO) standard specifications for “Materials for Aggregate and Soil Aggregate Sub-base, Base, and Surface Courses,” designation M 147-65 (1990) Grading B, as recommended in NCHRP Report No. 350 [4]. The target test conditions consisted of a impact speed of 20 mph (32 km/h) using a centerline contact with the bogie nose, approximately 24 7/8 in. (632 mm) above the ground. The weight (mass) of the bogie was 1841 lbs (835 kg). The test matrix for the first round of bogie testing is listed in Table 8.

**Table 8. Test Matrix for Round 1 Bogie Testing**

Test No.	Post Concept	Speed		Impact Axis
		mph (km/hr)	ft/s (m/s)	
UBSP-1	Steel Tube in Steel Tube	19.5 (31.3)	28.5 (8.70)	Strong
UBSP-2	Steel Tube in Steel Tube With Thru Bolt	19.3 (31.1)	28.3 (8.63)	Weak
UBSP-3	Upper FRP Post	19.7 (31.7)	28.9 (8.81)	Strong
UBSP-4	Upper FRP Post	19.6 (31.5)	28.7 (8.76)	Weak
UBSP-5	Fracturing Bolt (Slipbase)	19.4 (31.2)	27.6 (8.67)	Strong
UBSP-6	Fracturing Bolt (Slipbase)	18.5 (29.8)	27.1 (8.27)	Weak
UBSP-7	Circular Fillet Weld	19.4 (31.2)	23.6 (8.67)	Strong
UBSP-8	Circular Fillet Weld	20.2 (32.4)	29.6 (9.01)	Weak

### 5.3 Post Details

#### 5.3.1 Steel Tube in Steel Tube

The steel tube in steel tube concept utilized an upper 5-in. x 7-in. x 3/16-in. (127-mm x 178-mm x 4.8-mm) tube embedded 6 in. (152 mm) into the lower 6-in. x 8-in. x 3/16-in. (152-mm x 203-mm x 4.8-mm) foundation tube, as shown in Figures 17 through 19. This concept relied on the collapse of the upper tube, further initiating a pullout from the lower tube. The upper tube sat on top of a through bolt and was not connected to the lower foundation tube in order to allow the upper tube to easily pop out of the lower foundation tube and to release from the base.

The strength of this concept was dependent on numerous factors, including the embedment depth of upper post into the lower post. The depth of embedment controls the force required to initiate collapse of the upper post which leads to pop out. Clearance also affects the strength of the post. Shims were used to adjust the snugness, or clearance, between the two tubes. Other factors, including cutting corners or slotting the upper tube, were believed capable of altering the strength of the post but were not implemented at this time. Instead, they were



reserved for later use and refinement of the ratio of the post strengths in the weak and strong axis, if deemed necessary.

For the first round of bogie testing, it was decided that a strong-axis impact with an embedment depth of 6 in. (152 mm) and 1/8 in. (3.2 mm) clearance in the “socket” area would be sufficient to provide an understanding of the general behavior and strength of the steel tube in steel tube concept. Refinements and adjustments could easily be made based on this first run to adjust to the desired strength and behavior.

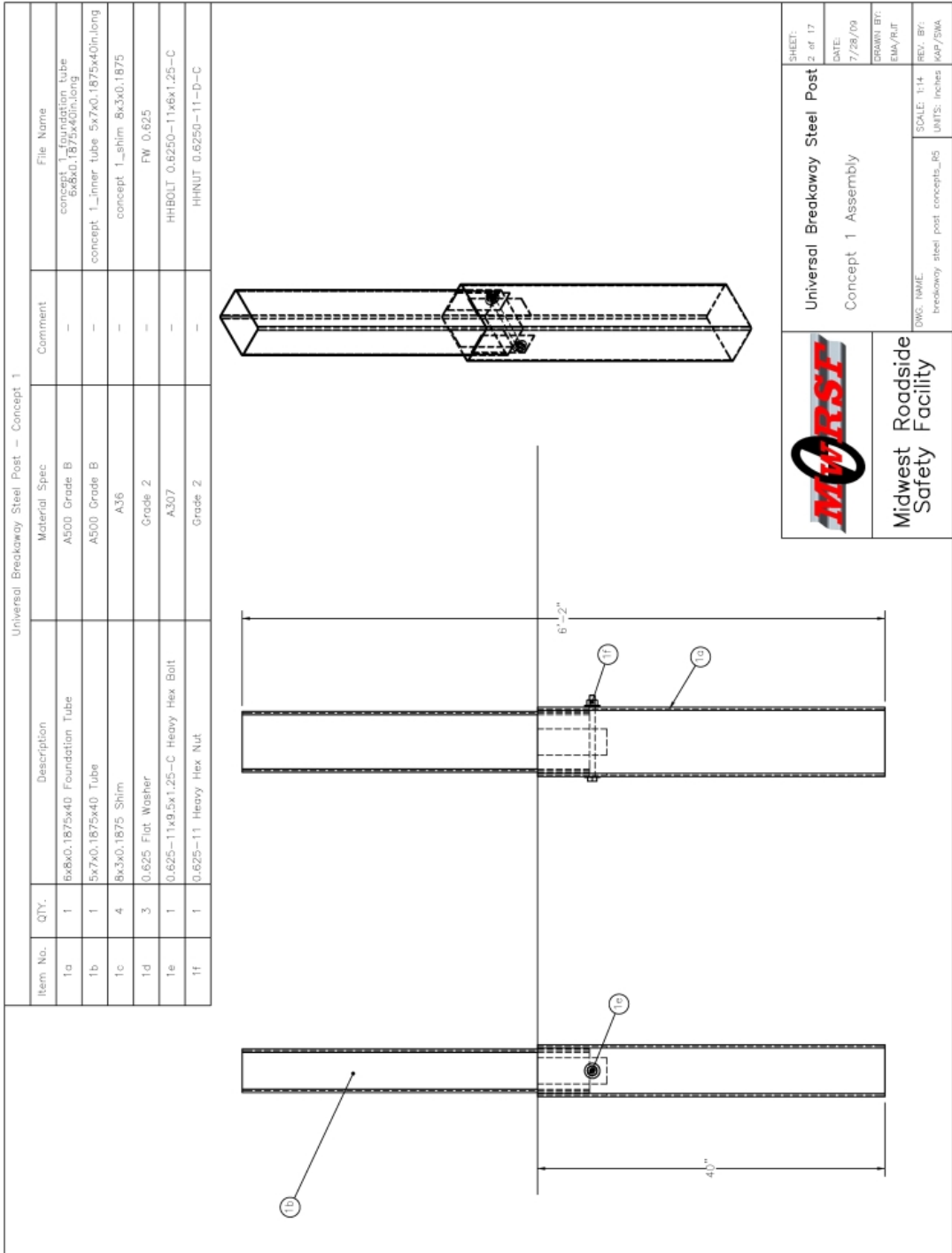
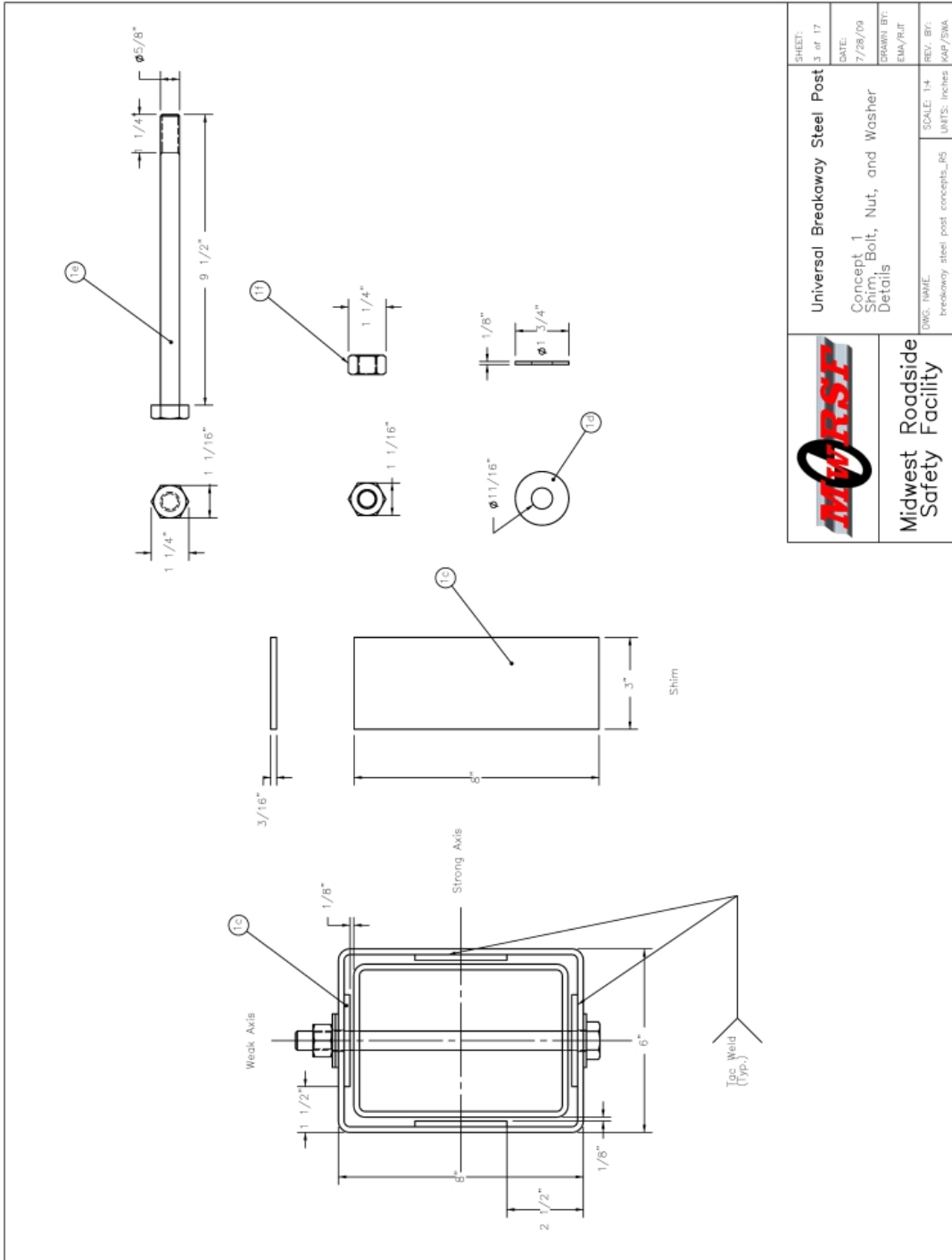


Figure 17. Steel Tube In Steel Tube Assembly Details




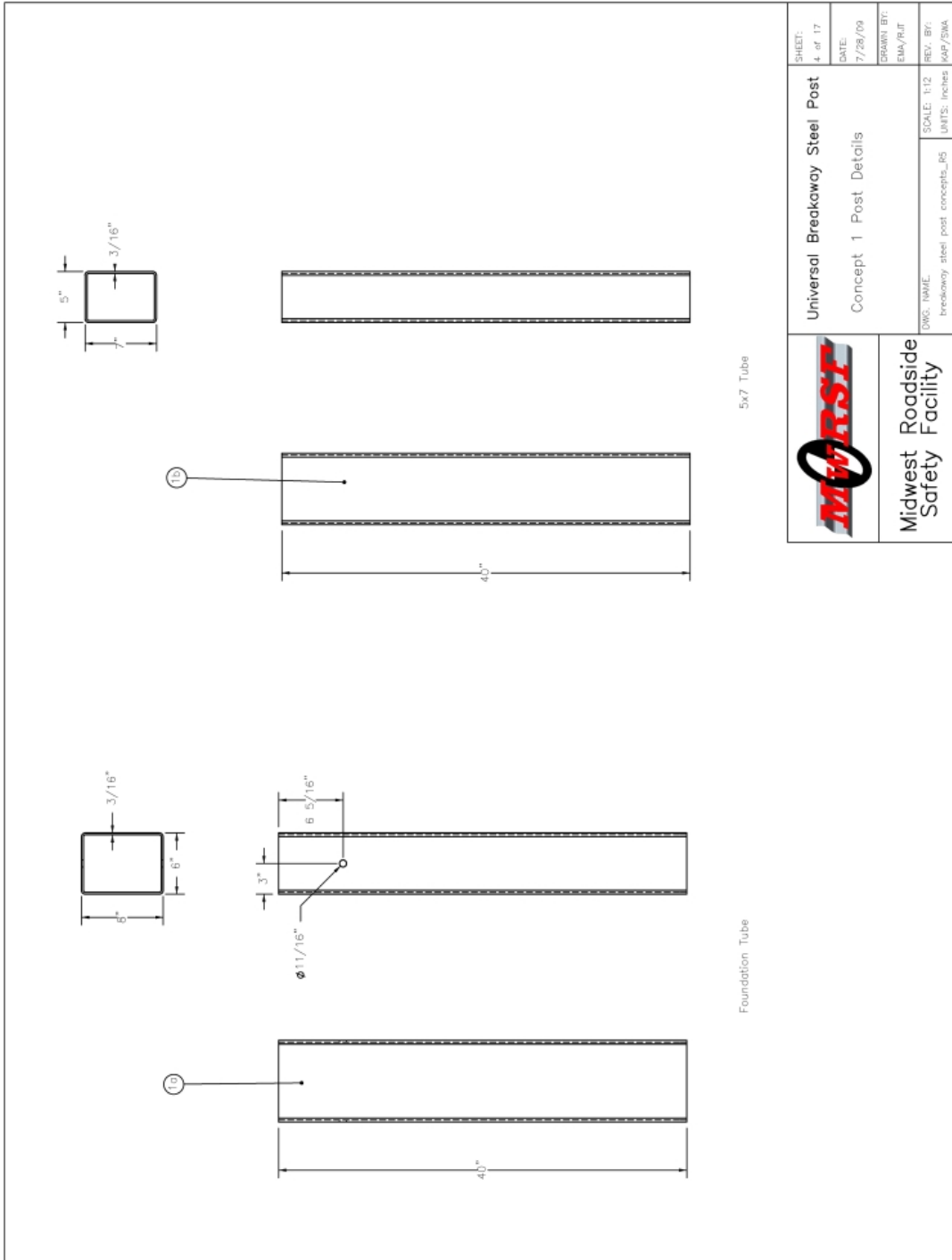

 Midwest Roadside Safety Facility	Universal Breakaway Steel Post Concept 1 Shim, Bolt, Nut, and Washer Details	SHEET: 3 of 17
	DWG. NAME: breakaway steel post concepts_18	DATE: 7/28/09 DRAWN BY: EMA/PJT REV. BY: JAF/SMA
SCALE: 1:4 UNITS: Inches		

Figure 18. Steel Tube In Steel Tube Part Details



 Midwest Roadside Safety	Universal Breakaway Steel Post Concept 1 Post Details	SHEET: 4 of 17 DATE: 7/28/09 DRAWN BY: EMA/PJT REV. BY: JAF/SMA
	DWG. NAME: breakaway steel post concepts_1b5	SCALE: 1:12 UNITS: Inches

**Figure 19. Steel Tube In Steel Tube Post Details**

### **5.3.2 Steel Tube in Steel Tube With Thru Bolt**

This concept was nearly identical to the steel tube in steel tube concept. The only difference was the upper tube was connected to the lower foundation tube with a thru bolt. Instead of sitting on top of a support bolt, the bolt passed through the upper tube, as shown in Figures 20 through 22. This concept relied on the bolt tearing out as the upper tube pulled up and out of the lower foundation tube. The thru bolt only passed through the upper tube on the traffic side. The non-traffic side was slotted; since, it is in compression during a strong-axis impact and would not tear out. In order to be consistent, this concept was also tested with a 6-in. (152-mm) embedment depth and a 1/8 in. (3.2 mm) clearance. This concept was believed to be most sensitive to weak-axis impacts. Under weak-axis loading, the post rotation would initially place very low tension on the retaining bolt. Thus, in order to explore the worst case situation, the thru-bolt design was tested in the weak axis.

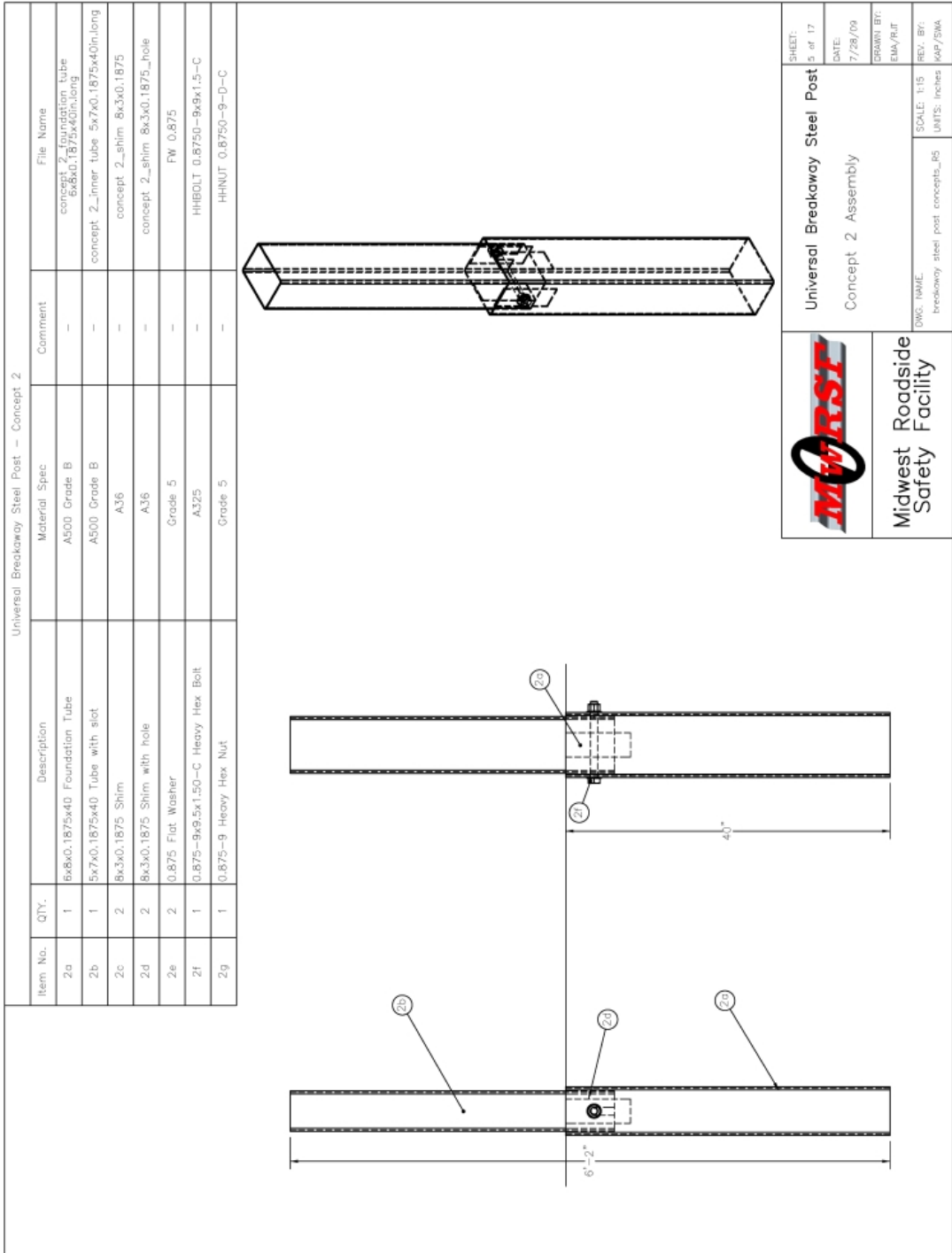
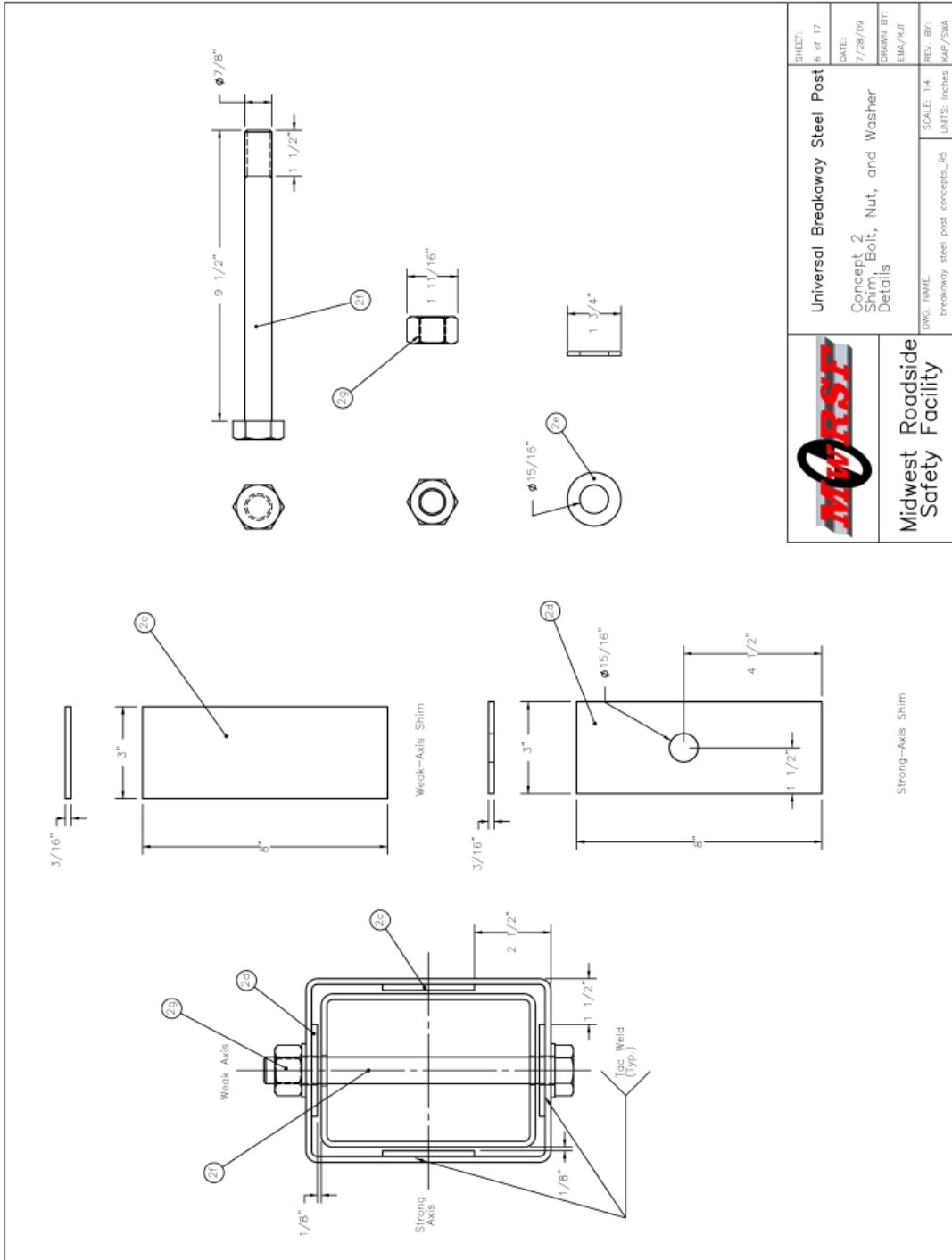
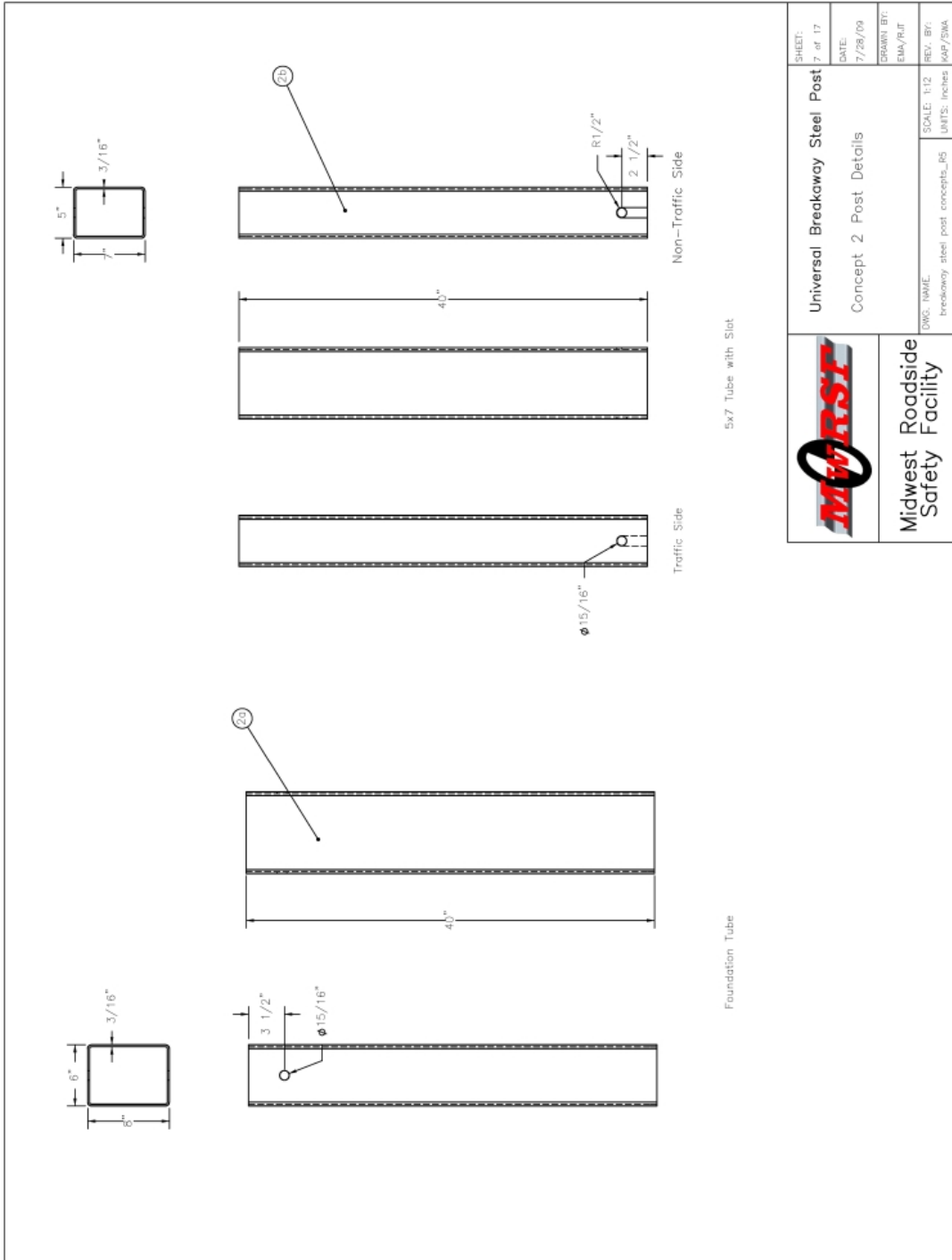


Figure 20. Steel Tube In Steel Tube With Thru Bolt Assembly Details



**Figure 21. Steel Tube In Steel Tube With Thru Bolt Part Details**




	SHEET: 7 of 17
	DATE: 7/28/09
DRAWN BY: EMA/PJT	REV. BY: JAF/SMA
DWG. NAME: breakaway steel post concepts_R5	SCALE: 1:12 UNITS: Inches
Universal Breakaway Steel Post Concept 2 Post Details	
Midwest Roadside Safety Facility	

Figure 22. Steel Tube In Steel Tube With Thru Bolt Post Details



### **5.3.3 Upper FRP Post**

This FRP concept relied on the same pop out failure mechanism as the first two concepts. However, this concept involved replacing the upper steel tube with a fiber reinforced plastic (FRP) tube. Similar to the first concept, the upper FRP post sat on top of a thru bolt to allow it to easily pop up and out of the lower foundation tube after some displacement.

FRP tubing is produced by numerous companies in standard shapes and sizes. The goal was to find the best available size of FRP tubing to fit in and form a 6 in. (152 mm) long “socket” with the lower 6-in. x 8-in. (152-mm x 203-mm) foundation tube. After researching numerous standard sizes, the 4-in. x 6-in. x 3/8-in. (102-mm x 152-mm x 9.5-mm) tubing provided by Advanced Fiber Products was chosen the best option available [15]. This FRP tubing had UV inhibitor and had ample strength for both strong- and weak-axis impacts. Thick shims were used to accommodate the size difference between the FRP tube and the lower foundation tube. For the first round of bogie testing, a wood/steel shim was utilized. These make-shift shims could be replaced if the FRP option proved to have promising potential for use as the universal breakaway post. The details of the upper FRP concept are presented in Figures 23 through 25.

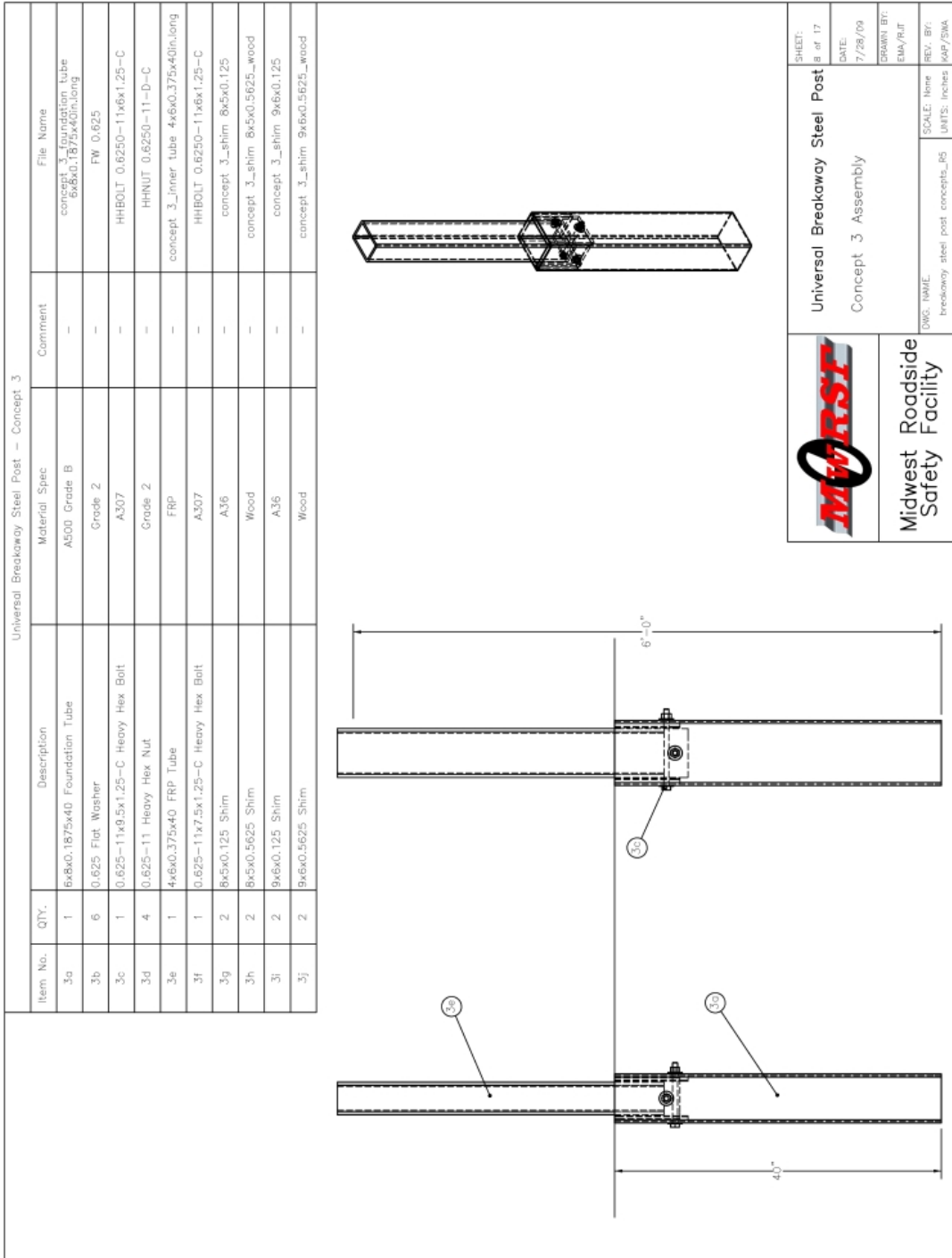


Figure 23. Upper FRP Post Assembly Details

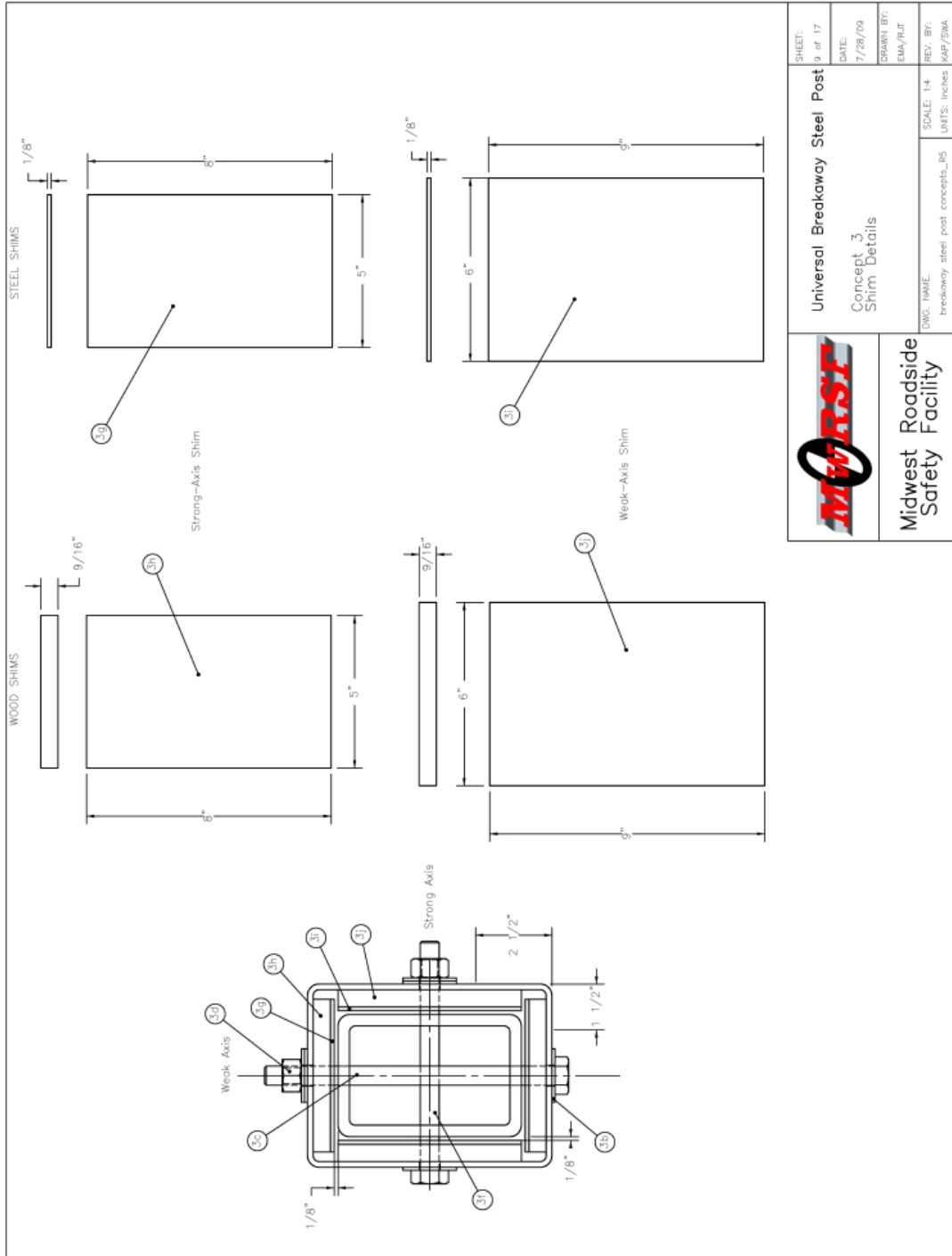
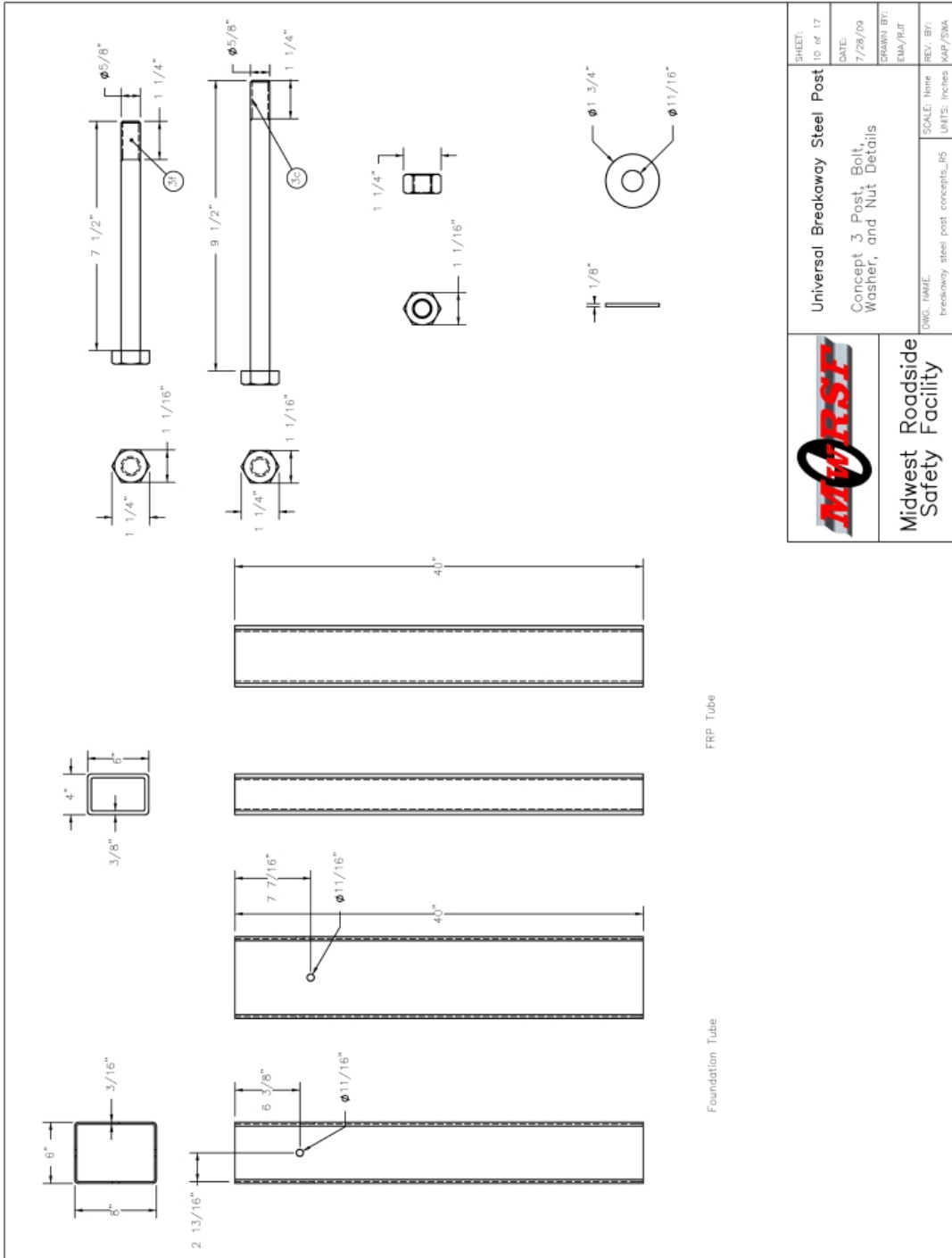


Figure 24. Upper FRP Post Shim Details



	Universal Breakaway Steel Post	SHEET: 10 of 17
	Concept 3 Post, Bolt, Washer, and Nut Details	DATE: 7/28/09
Midwest Roadside Safety Facility	DWG. NAME: breakaway steel post concepts_05	DRAWN BY: EMA/PLT
	SCALE: None UNITS: Inches	REV. BY: MAF/SMA

Figure 25. Upper FRP Post Part Details

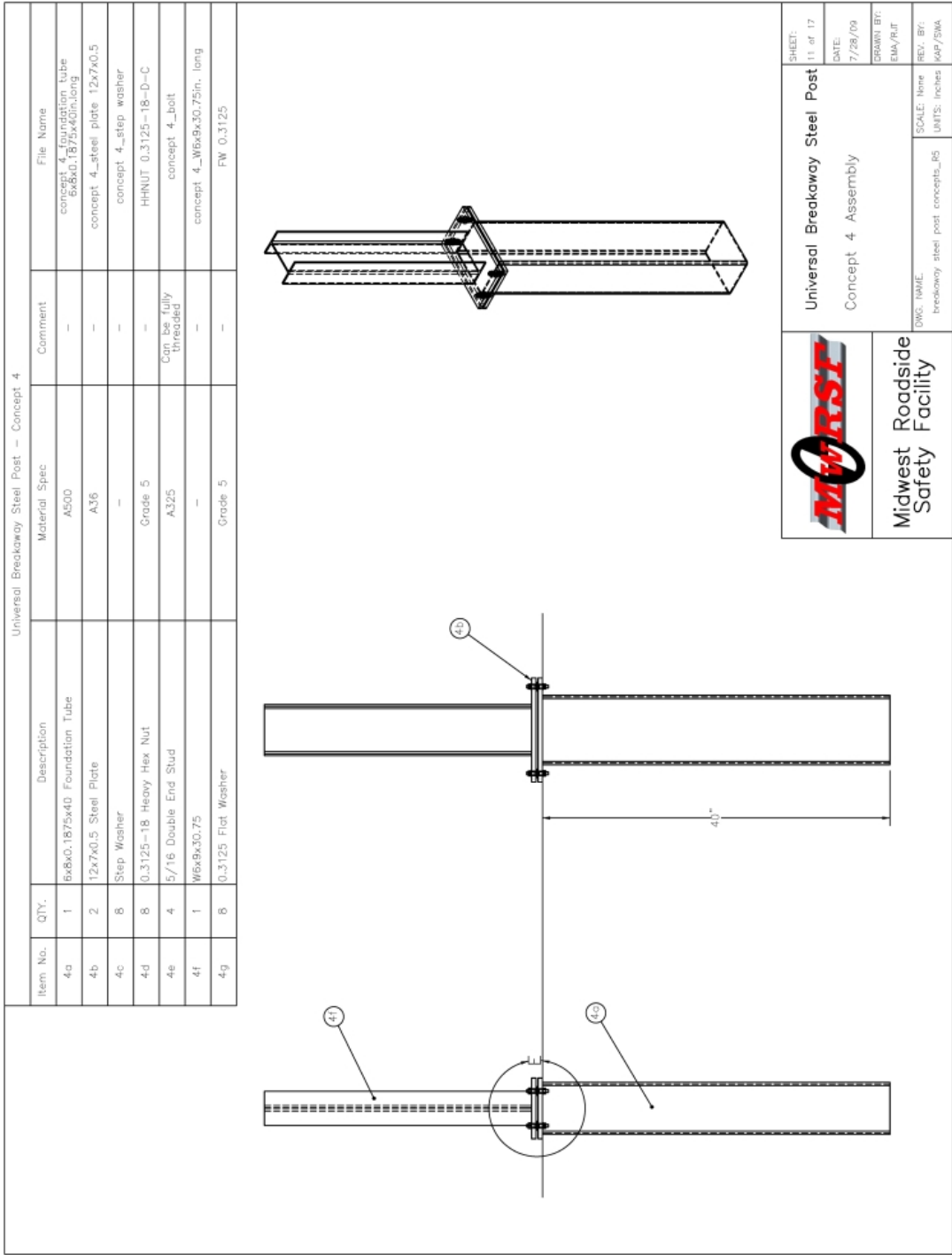
### 5.3.4 Fracturing Bolt (Slipbase)

The fracturing bolt (slipbase) concept relied on fracturing and shearing bolts to control the post strength. The lower foundation tube was connected to an upper W6x9 (W152x13.4) beam through a base plate and four breakaway bolts, as shown in Figures 26 through 30. Two 1/2-in. (12.7-mm) thick steel plates were rigidly welded to the bottom of the W6x9 (W152x13.4) beam and to the top of the foundation tube.

When impacted, the bolts were expected to break in tension on the impact side and to break in shear on the back side. Step washers were utilized to create a shear plane for the bolts. The size and location of the breakaway bolts control the post fracture load for this concept. The peak post load should be close to the point when a simple bending analysis predicts that the front bolts reach their rated tensile strength. In this manner, the size and locations of the splice bolts were initially selected. This analysis led to the selection of 5/16 in. (7.94 mm) diameter grade 5, fully-threaded rods for the fracturing bolts. The threaded rods were spaced apart 10 in. (254 mm) in the strong axis and 4 in. (102 mm) in the weak axis. A close-up view of the assembled fracturing bolt concept can be seen in Figure 26.



**Figure 26. Assembled Fracturing Bolt (Slipbase) Design**



**Figure 27. Fracturing Bolt (Slipbase) Assembly Details**

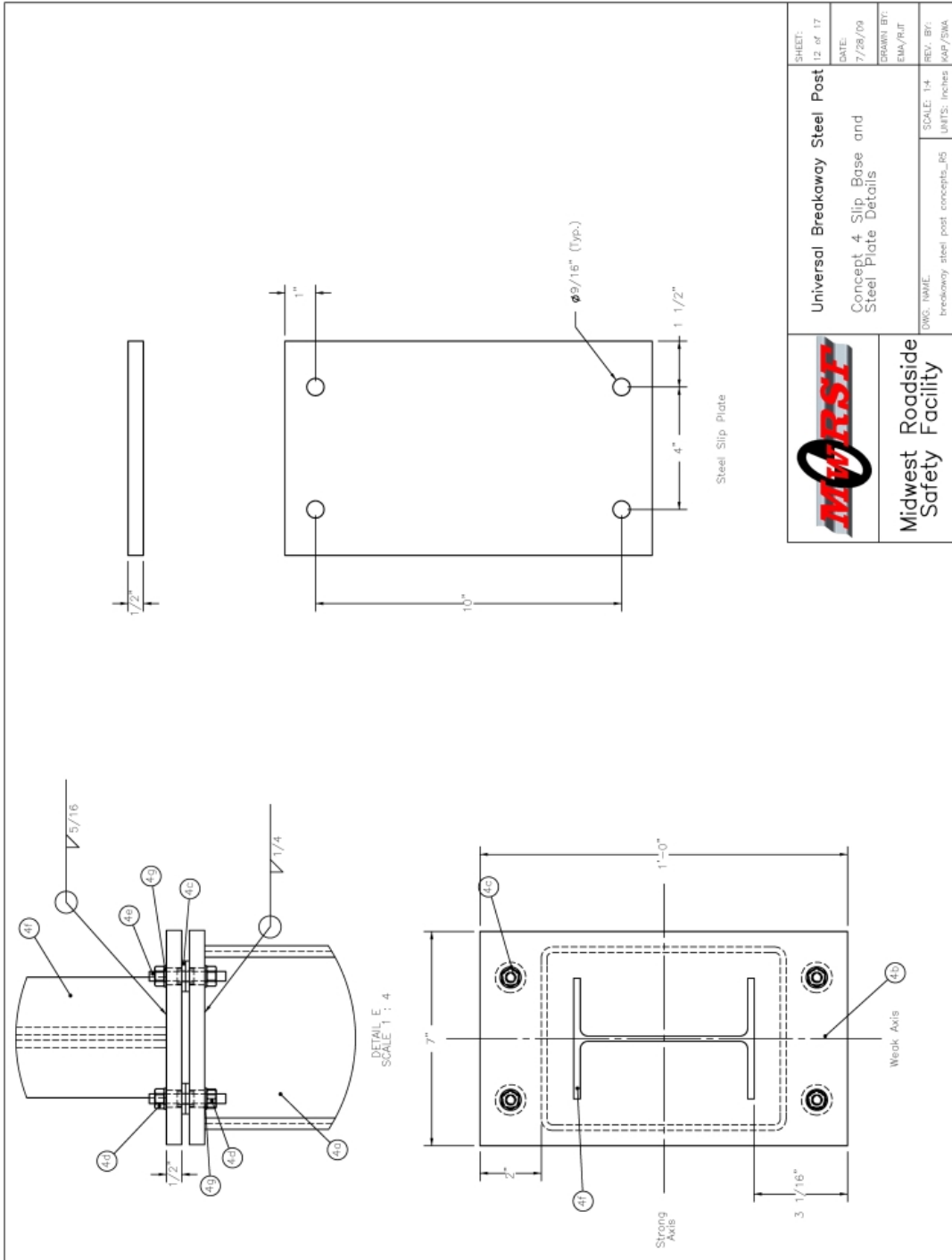


Figure 28. Fracturing Bolt (Slipbase) Steel Plate Details





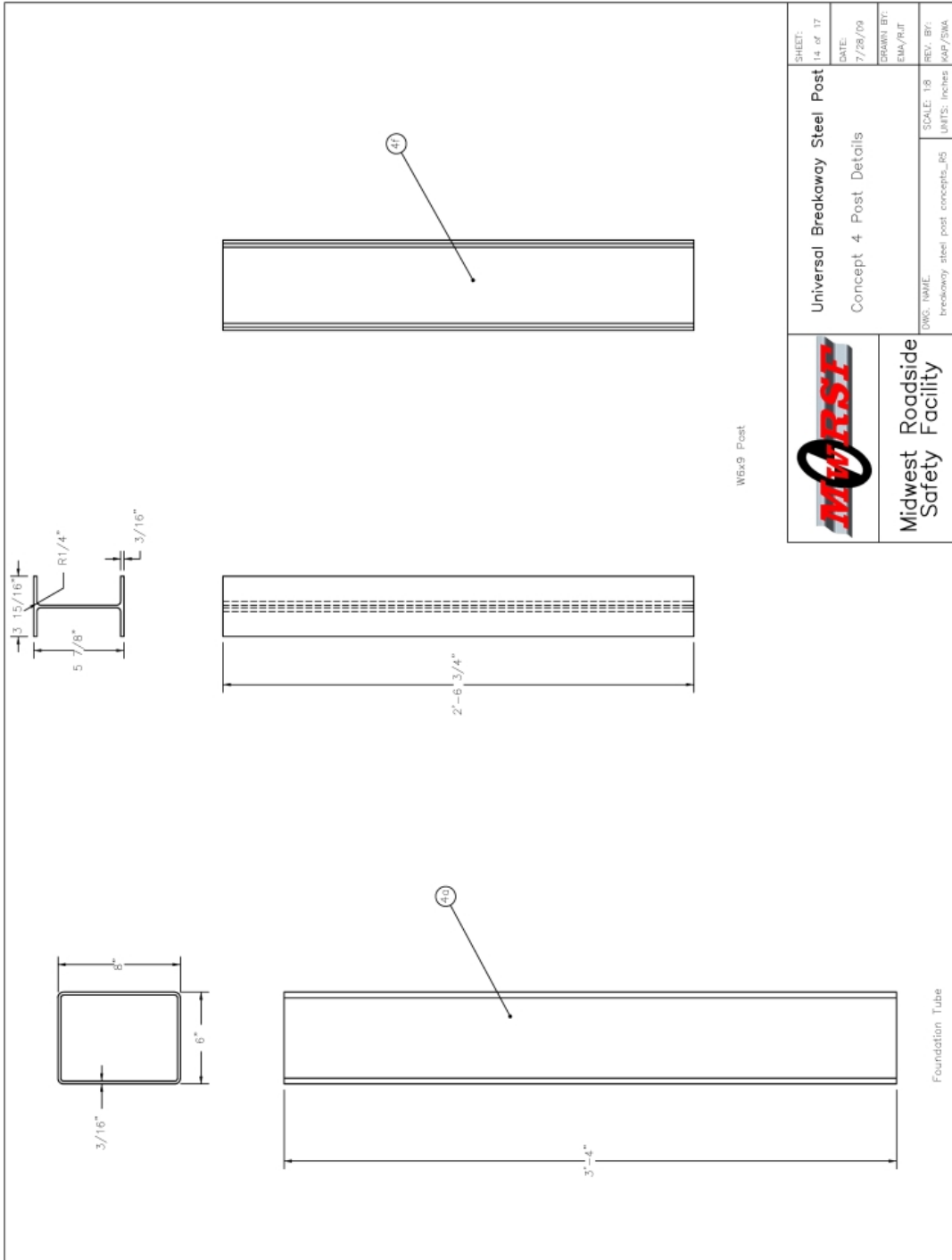
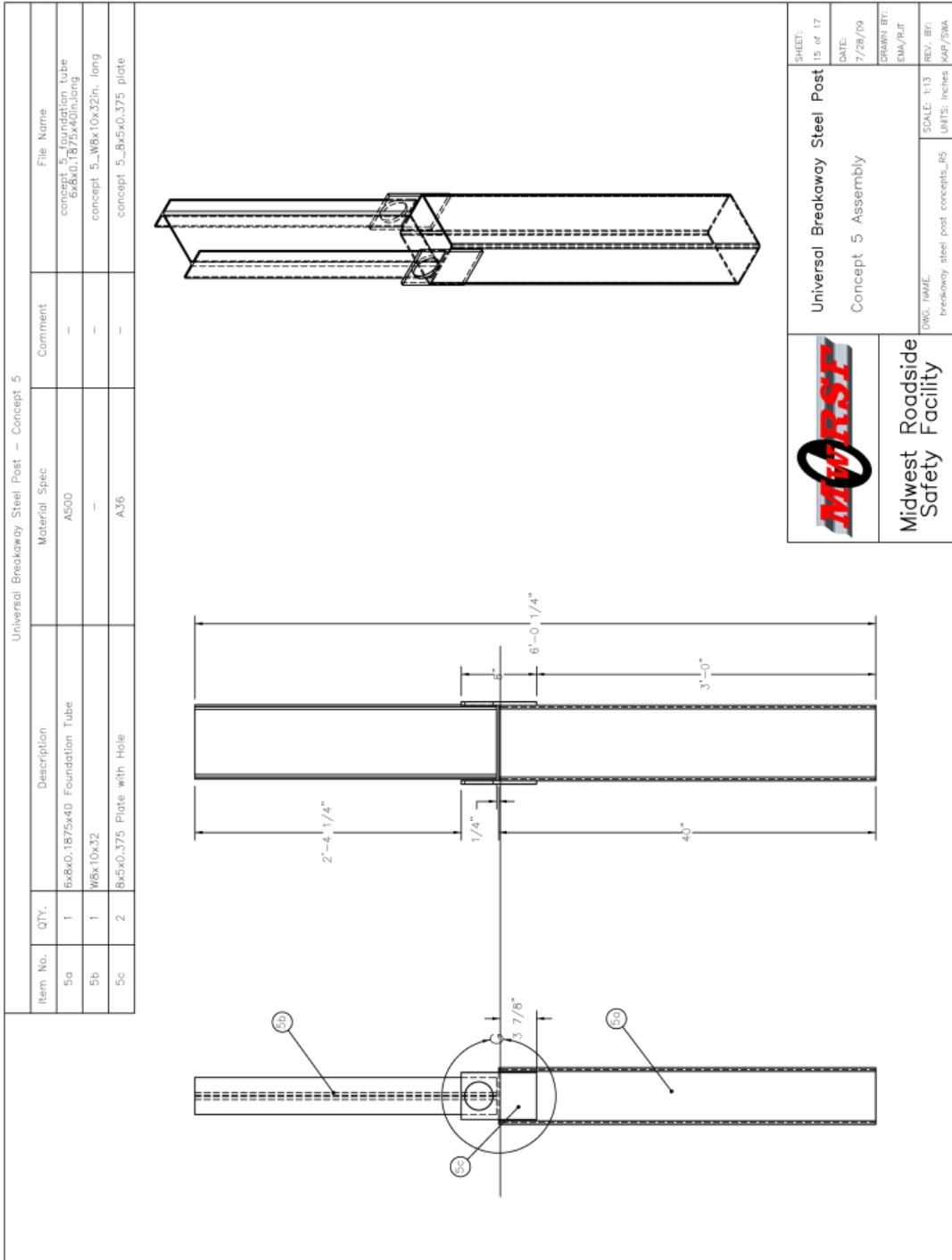


Figure 30. Fracturing Bolt (Slipbase) Post Details

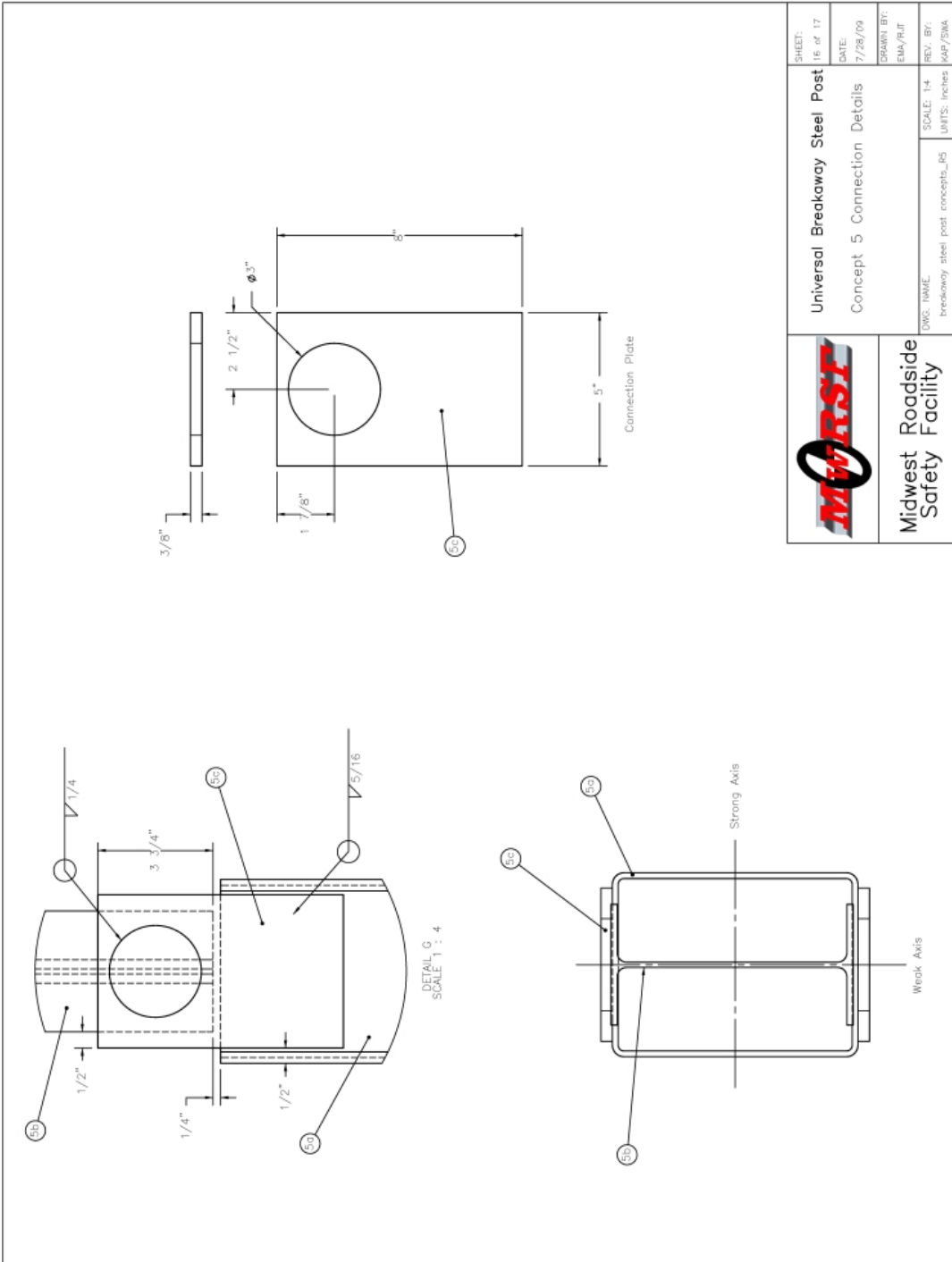
### **5.3.5 Circular Fillet Weld**

The circular fillet weld concept incorporated a splice plate with circular holes on the front and back of the post. The splice plates were welded to the upper post with a fillet weld around these holes. This concept relied on failure of these fillet welds to control the strength of the post. The two steel splice plates connected an upper W8x10 (W203x14.9) wide-flange section with the lower 6-in. x 8-in. x 3/16-in. (152 mm x 203 mm x 4.8 mm) foundation tube, as shown in Figures 31 through 33.

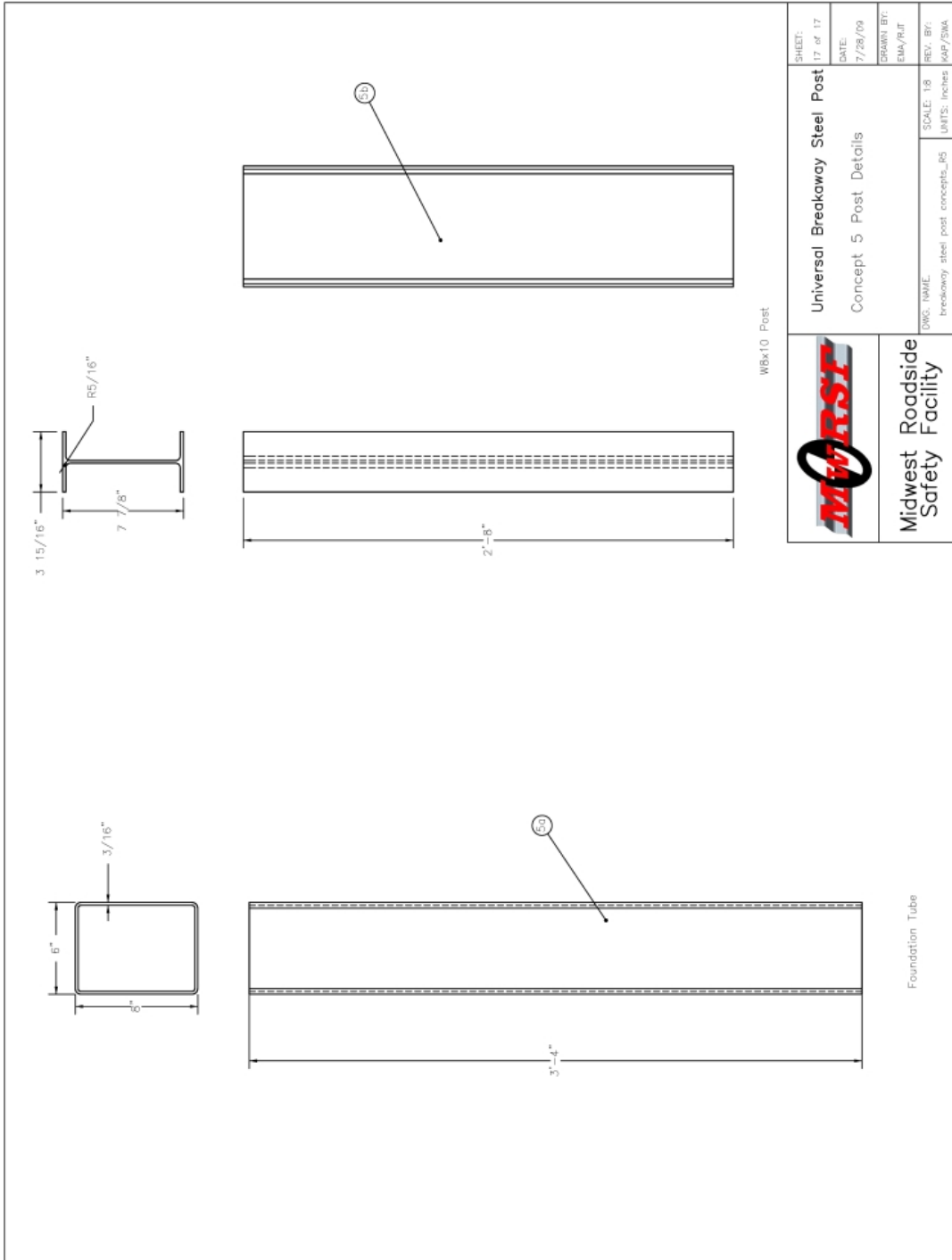
The circular breakaway welds were expected to rupture due to shear in both the strong and weak axis. In the strong axis, the welds break in transverse shear. In the weak axis, the welds break in shear from torsional loading induced into the circular welds. As seen in Figure 34, calculations were performed to estimate the area of weld needed to obtain the desired strength levels. It was decided to use a circular fillet weld, since this shape allows for the most consistent weld. As a result, this design is very similar to the breakaway steel post in patent number 5,988,598 and described in the “Design and Development of Steel Breakaway Posts” [16]. The difference is this circular fillet concept uses a fillet weld instead of a plug weld.



**Figure 31. Circular Fillet Weld Assembly Details**



**Figure 32. Circular Fillet Weld Connection Details**



**Figure 33. Circular Fillet Weld Post Details**

## Weak Axis

$$F_{resistance} = \frac{1.15 * F_w * A * r}{h}$$

Where:

$A = \text{Area of Single Weld} = t_e * L$

$t_e = \text{Weld Throat Thickness}$

$L = \text{Length of Weld}$

$r = \text{Radius of Circular Weld}$

$F_w = \text{Strength of Weld Or Base Material}$

$h = \text{Impact Height Above Weld}$

## - Strong Axis

$$F_{resistance} = \frac{0.577 * F_w * A * d}{h}$$

Where:

$A = \text{Area of Weld} = t_e * L$

$t_e = \text{Weld Throat Thickness}$

$L = \text{Length of Weld}$

$F_w = \text{Strength of Weld Or Base Material}$

$h = \text{Impact Height Above Weld}$

$d = \text{Distance between Circular Fillet Welds}$

**Figure 34. Circular Fillet Weld Calculations**

## 5.4 Equipment and Instrumentation

A variety of equipment and instrumentation was used to record and collect data.

Equipment and instruments utilized in this testing included:

- Bogie
- Accelerometer
- Pressure Tape Switches
- Digital Photographic Cameras

### 5.4.1 Bogie

A rigid frame bogie was used to impact the posts. The bogie impact head was constructed of 8-in. (203-mm) diameter, 1/2-in. (12.5-mm) thick, standard steel pipe, with 3/4-in. (19-mm) thick, neoprene belting wrapped around the pipe to prevent local damage to the post from the impact. The bogie with the impact head is shown on the guidance track in Figure 35. The weight (mass) of the bogie with the addition of the mountable impact head was 1,841 lbs (835 kg). The impact height contacted the test specimen at 24 7/8 in. (632 mm) above the ground. The target speed for the tests was 20 mph (32 km/h).

In all tests, a pickup truck with a reverse cable tow and guide rail system was used to propel and direct the bogie. The bogie was accelerated toward the post along the guidance system, which consisted of a steel pipe anchored above the tarmac. In all of the tests, the bogie wheels were aligned for caster and toe-in values of zero so that the bogie would track properly. When the bogie reached the end of the guidance system, it was released from the tow cable, allowing it to be free rolling when it struck the post. A remote braking system was installed on the bogie, to provide for safe deceleration of the bogie after the test.



**Figure 35. Rigid Frame Bogie on Guidance Track**

#### **5.4.2 Accelerometer**

One tri-axial piezoresistive accelerometer system, Model EDR-3, with a range of  $\pm 200$  g's, was developed by Instrumented Sensor Technology (IST) of Okemos, Michigan, and was mounted on the frame on the bogie near its center of gravity. Data sampling was at 3,200 Hz with a 1,120 Hz Butterworth low-pass filter with a -3dB cut-off. Computer software, "DynaMax 1.75" and a customized "Microsoft Excel" worksheet were used to analyze and plot the accelerometer data [17].

An additional accelerometer system, model DTS manufactured by Diversified Technical Systems, Inc. (DTS) of Seal Beach, CA, was used to measure the acceleration in the longitudinal, lateral, and vertical directions at a sample rate of 10,000 Hz. The environmental shock and vibration sensor/recorder system, a two-Arm piezoresistive accelerometer, was developed by Endevco of San Juan Capistrano, CA. Three accelerometers were used to measure each of the longitudinal, lateral, and vertical accelerations independently. Data was collected using a Sensor Input Module (SIM), Model TDAS3-SIM-16M. The SIM was configured with 16 MB SRAM



memory and 8 sensor input channels with 250 kB SRAM/channel. The SIM was mounted on a TDAS3-R4 module rack. The module rack is configured with isolated power/event/communications, 10BaseT Ethernet and RS232 communication, and an internal back-up battery. Both the SIM and module rack are crashworthy. “DTS TDAS Control” and “DADiSP” computer software programs, and a customized “Microsoft Excel” worksheet were used to analyze and plot the accelerometer data [18].

#### **5.4.3 Pressure Tape Switches**

Three pressure tape switches, spaced at 1.5-ft (0.457-m) intervals and placed near the end of the bogie track, were used to determine the speed of the bogie before the impact. As the front right tire of the bogie passed over each tape switch, a strobe light was fired sending an electronic timing signal to the data acquisition system. Test speeds were determined by dividing the measured distance between the switches by the time between these signals.

#### **5.4.4 Photography Cameras**

One high-speed AOS VIT cam digital video camera, with a Sigma 24-70 mm lens and an operating speed of 500 frames/sec, was located perpendicular to the post impact direction. Two JVC digital video cameras, each with an operating speed of 29.97 frames/sec, were also used to film the bogie tests.

### **5.5 Methodology of Testing**

A total of eight bogie tests were performed on posts about the strong and weak axes of bending. The tests were configured with posts embedded 40 in. (1,016 mm) in a testing pit. For the tests, holes measuring 24 in. (610 mm) in diameter and approximately 44 in. (1,118 mm) deep were augured in the soil. These holes were then filled with soil meeting AASHTO standard

specification for “Materials for Aggregate and Soil Aggregate Sub-base, Base, and Surface Courses,” designation M 147-65 (1990) Grading B. Standard compaction procedures with the pneumatic tamper were followed. The test parameters are shown in Table 9 and Figure 36.

**Table 9. Test Parameters**

<b>UBSP Test Parameters</b>
UBSP: Universal Breakaway Steel Post Concepts
Test: Strong Axis Impact at 0 degrees and Weak Axis Impact at 90 degrees
Accelerometer: EDR-3 and DTS Data
Bogie Weight (Mass): 1,841 lbs (835.1 kg)
Bumper Height: 24 7/8 in. (632 mm)
Post Length: 72 in. (1,829 mm)
Soil: 135 lb/ft <sup>3</sup> (2163 kg/m <sup>3</sup> ) NCHRP 350 (AASHTO 147-65 (1990) Grade B)

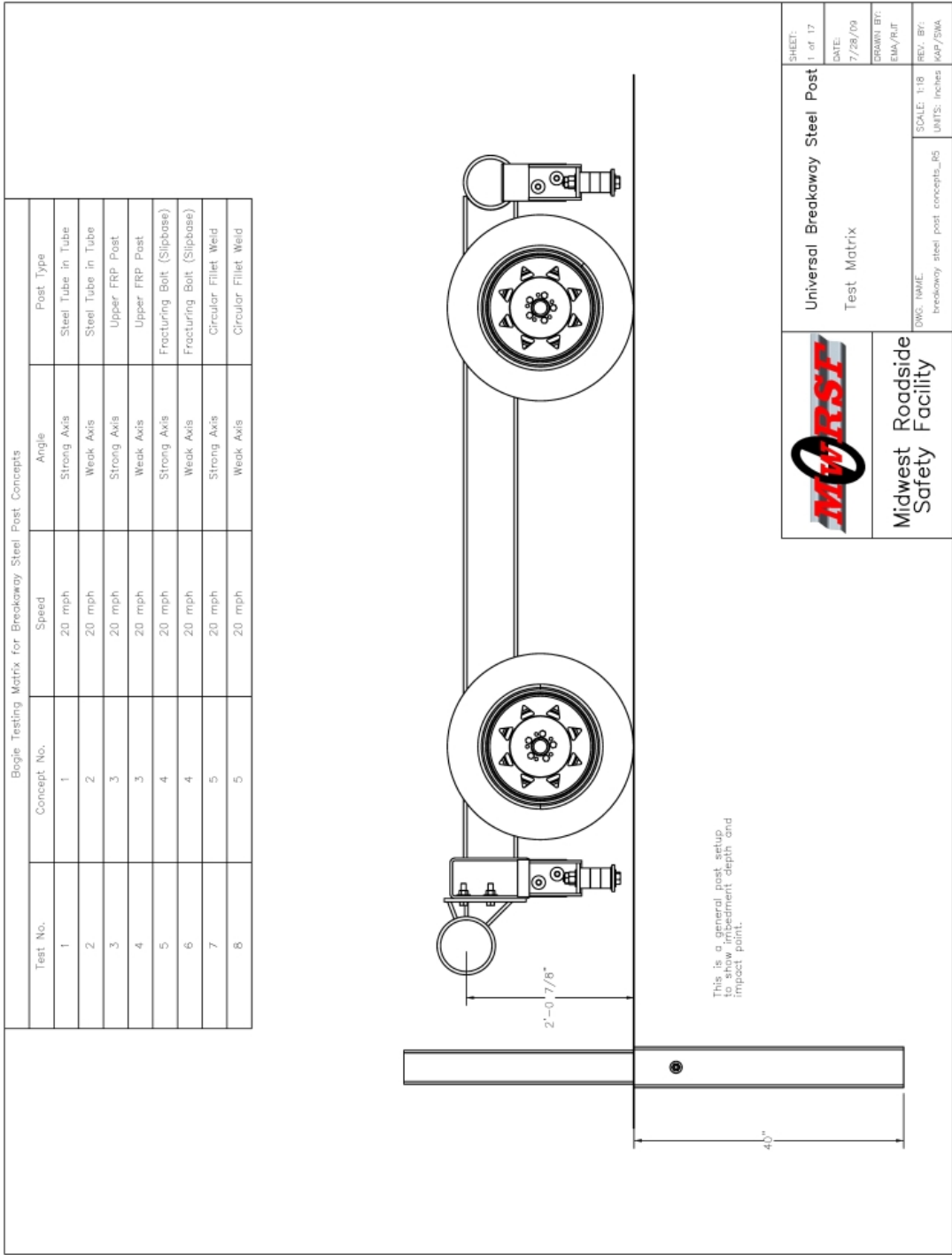
### **5.6 End of Test Determination**

During an impact, the data acquisition system continuously records the bogie accelerations after it is triggered. These recorded accelerations include vibrations in the bogie vehicle, impact head, and accelerometer mounting assembly. A consistent method for identifying the end of the test needed to be defined in order to assure that the post fracture performance could be compared.

The event time was identified as the time that the peak vibration in the acceleration trace subsided back toward zero, and no more high loads were measured. When the acceleration trace subsided toward zero, the force levels would also subside toward zero, and the energy levels would level off, clearly showing that the continuation of vibrations were not caused by interaction with the post. Also, each test was limited by the bogie-post contact time, so there were no unreasonably long test durations. For each test, the high-speed video was used to establish the length of time the bogie was actually in contact with the post. This time was then used to define maximum possible test length.

## 5.7 Data Processing

Initially, the data was filtered using a SAE Class 60 Butterworth filter conforming to the SAE J211/1 specifications [19]. The processed acceleration data was then multiplied by the mass of the bogie to obtain the impact force based upon Newton's Second Law. Next, the acceleration trace was integrated to find the change in velocity. The initial velocity of the bogie, calculated using the data from the pressure tape switches, was then used to determine the actual bogie velocity versus time. The calculated actual velocity trace versus time was then integrated to find the displacement versus time trace. Thus, the force versus time and the displacement versus time data could be combined to produce the force versus deflection curve for each test. Finally, integration of the force versus deflection curve provided the energy versus displacement curve for each test.



**Figure 36. General Bogie Test Setup**

## **5.8 Round 1 Bogie Testing Results**

The accelerometer data was processed for each test in order to obtain acceleration, velocity, and displacement curves, as well as force versus deflection and energy versus deflection curves. This section discusses those results for the EDR-3 accelerometer. Although both the EDR-3 and DTS data recorders were used for the tests, the current EDR-3 triggered and provided accurate results for every test, while the DTS did not trigger for every test. However, the accelerometers did provide similar results when both units had valid data. Also, using the EDR-3 was consistent with the previous bogie testing of the wood CRT posts. Individual test results are provided in Appendix A.

The following sections discuss the dynamic behavior and results for test nos. UBSP-1 through UBSP-8. Conclusions regarding the performance comparison of the different post concepts are discussed in a subsequent section in this report.

### 5.8.1 Test UBSP-1 – Steel Tube in Steel Tube

Test UBSP-1 was a strong-axis impact at 0 degrees on the steel tube in steel tube concept embedded in standard strong soil. The force and energy data are shown in Figures 37 and Figure , respectively. Time-sequential photographs of this test are shown in Figure 39. Upon impact, the upper steel tube began to rotate immediately and lost contact with the bogie head at 6 ms. The 1/8 in. (3.2 mm) clearance in the “socket” area between the foundation tube and upper tube allowed the upper post initially rotate freely in the socket. The upper post quickly reached the limits of free rotation, and at approximately 24 ms, the bogie regained contact with the upper steel tube. Thereafter, the bogie remained in contact with the upper post until 100 ms after impact. During this period, the upper tube popped out and 1 in. (25.4 mm) and 1 1/4 in. (31.75 mm) cracks formed on or near the downstream corners of the foundation tube. Also, the impact side of the upper tube experienced some deformation along the bottom. The lower foundation tube rotated 2 in. (50.8 mm) in the soil before the upper tube popped out. Post-impact images of the steel tubes can be seen in Figure 40.

The force versus deflection curve, as provided in Figure 37, indicated an initial peak in the force level, due to the inertial effects of the upper steel tube. After this initial peak, the force level subsided toward zero, while the post rotated freely in the socket area. The force levels increased rapidly when the upper post reached the limits of free rotation. Although the peak force levels were near the desired 12 kips (53 kN), the average force levels were lower than desired from when the post rotated freely. However, there were desirable energy levels for this breakaway post, as shown in energy versus deflection curve in Figure . The post broke away and did not rotate thru the soil absorbing large amounts of energy.

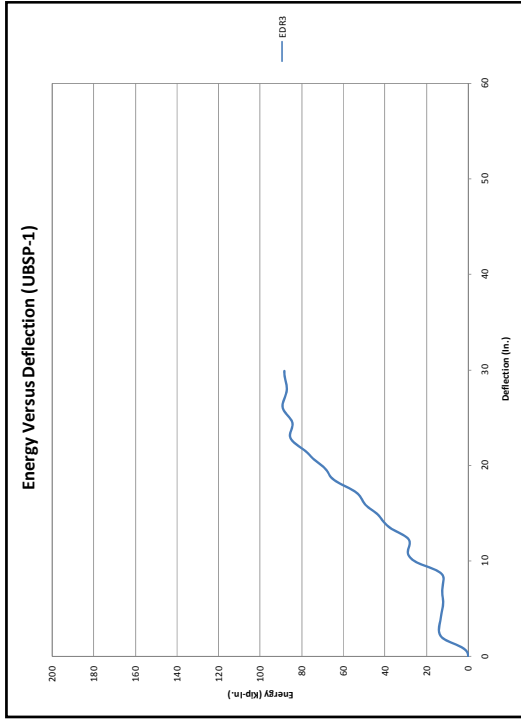


Figure 38a. Energy versus Deflection Curve for UBSP-1 - English

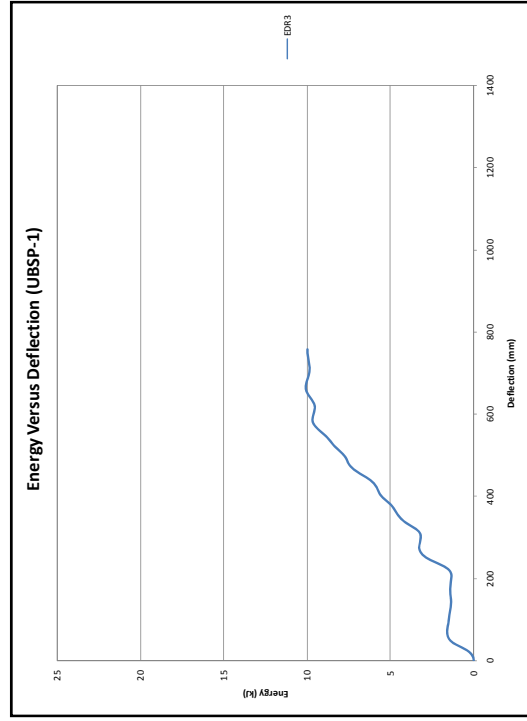


Figure 38b. Energy versus Deflection Curve for UBSP-1 - Metric

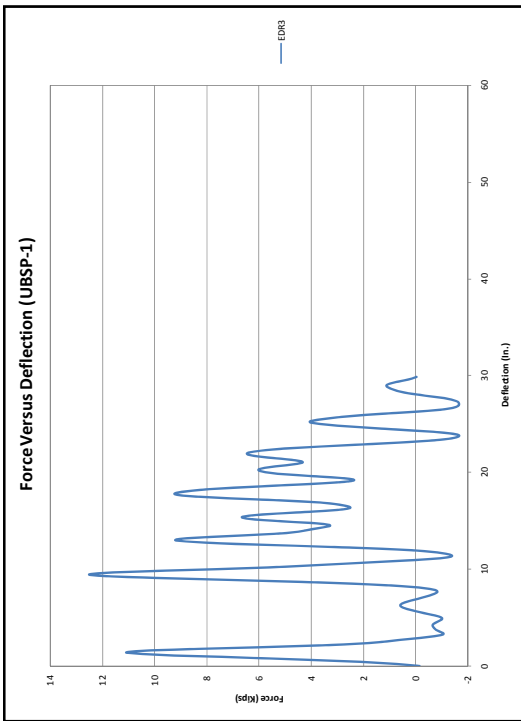


Figure 37a. Force versus Deflection Curve for UBSP-1 - English

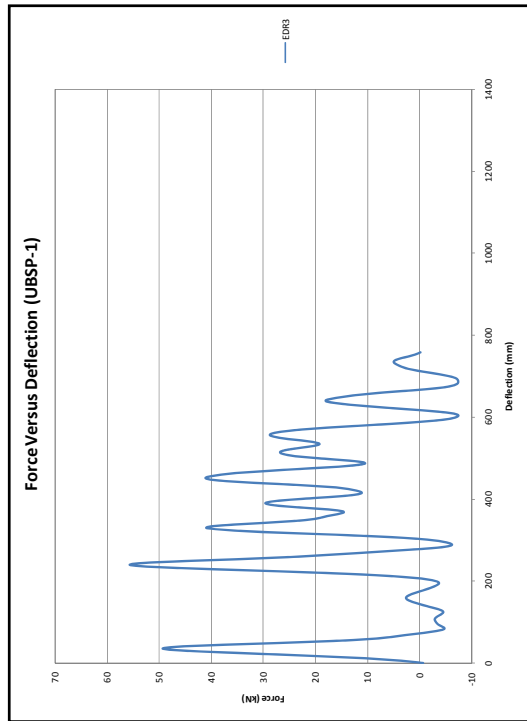


Figure 37b. Force versus Deflection Curve for UBSP-1 - Metric

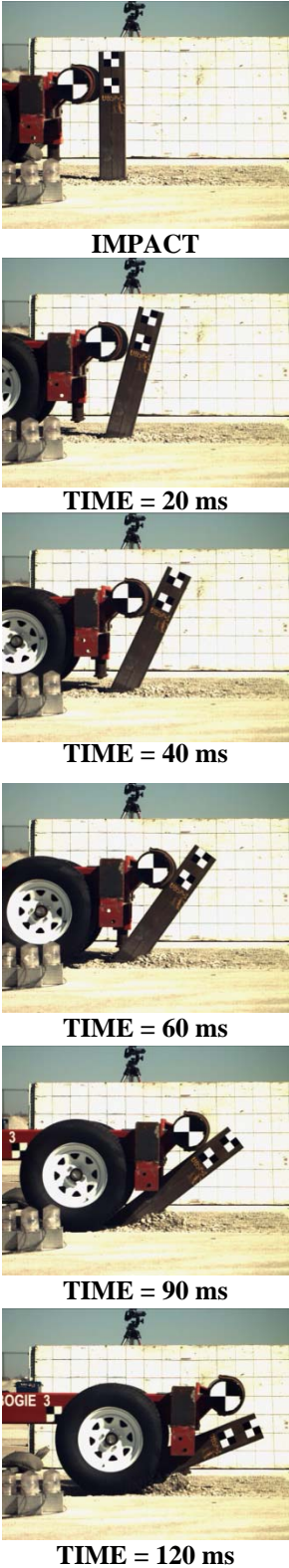


Figure 40. Post Impact Images of Test UBSP-1

Figure 39. Time Sequential Photographs, Test UBSP-1



### **5.8.2 Test UBSP-2 – Steel Tube in Steel Tube with Thru Bolt**

Test UBSP-2 was a weak-axis impact at 90 degrees on the steel tube in steel tube with a thru bolt concept. The force and energy data are shown in Figures 41 and 42, respectively. Time-sequential photographs are shown in Figure 43. When impacted by the bogie, the upper tube began to rotate immediately and lost contact with the bogie head at approximately 6 ms. At approximately 22 ms, the bogie regained contact with the post, and 4 1/2 in. (114.3 mm) and 4 3/8 in. (111.1 mm) cracks were formed near the downstream corners of the lower foundation tube. These cracks allowed the upper post to bend over and the bogie to eventually override the post and lose contact at approximately 148 ms. The upper tube also experienced minor deformation, but there was no sign of bolt tear out. As a result, this concept did not perform as desired. The upper tube did not pop up and break away from the lower foundation tube. Post-impact images can be seen in Figure 44.

The force versus deflection curve, provided in Figure 41, indicated an initial peak in the force level, due to the inertial effects of the upper steel tube. After this initial peak, the force level subsided towards zero as the post rotated due to the gap between the two tubes. Then, the force levels increased rapidly to undesired levels as the upper tube rotated over and did not break away cleanly. Also, the energy versus deflection curve is shown in Figure 42. By not breaking away cleanly and easily, both the force and energy levels were higher than desired.

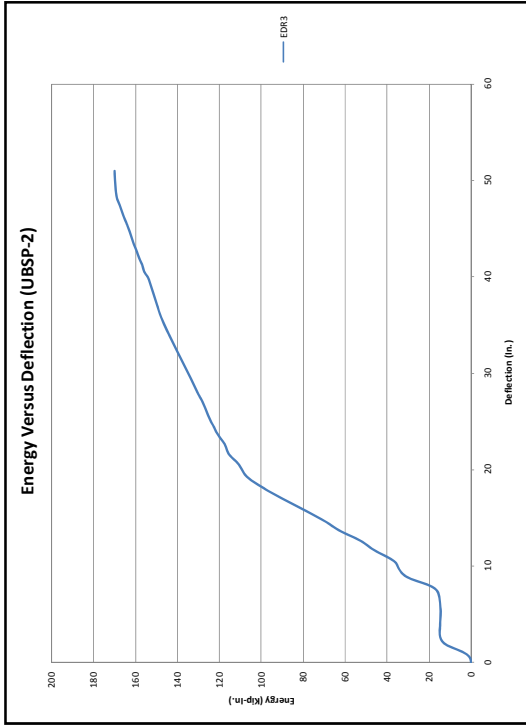


Figure 42a. Energy versus Deflection Curve for UBSP-2 - English

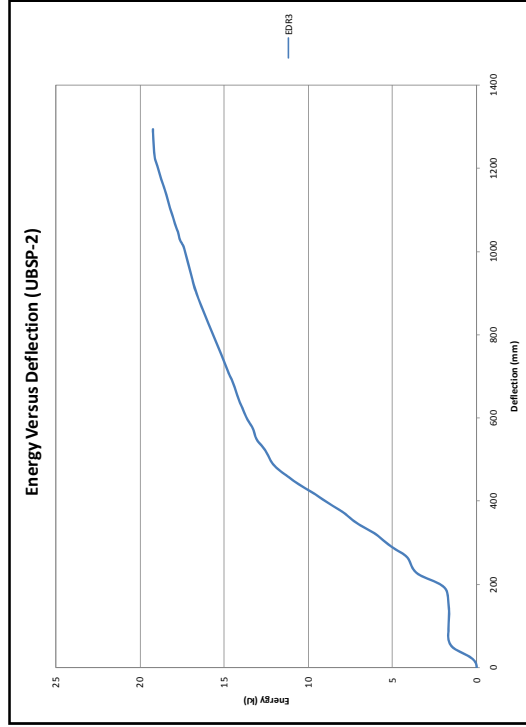


Figure 42b. Energy versus Deflection Curve for UBSP-2 - Metric

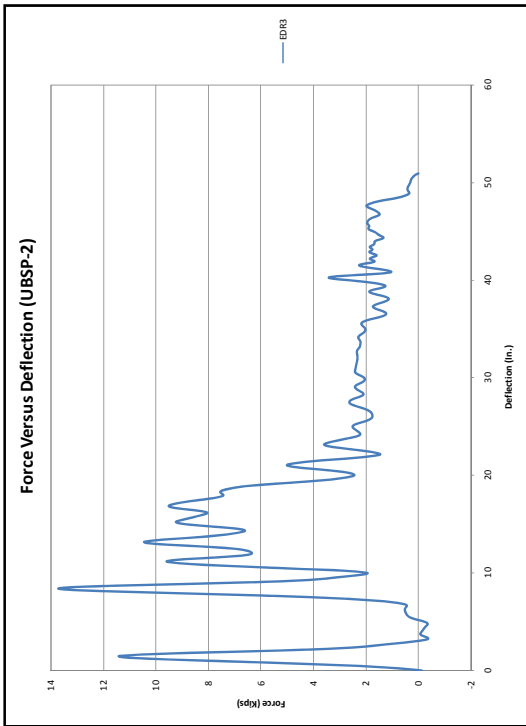


Figure 41a. Force versus Deflection Curve for UBSP-2 - English

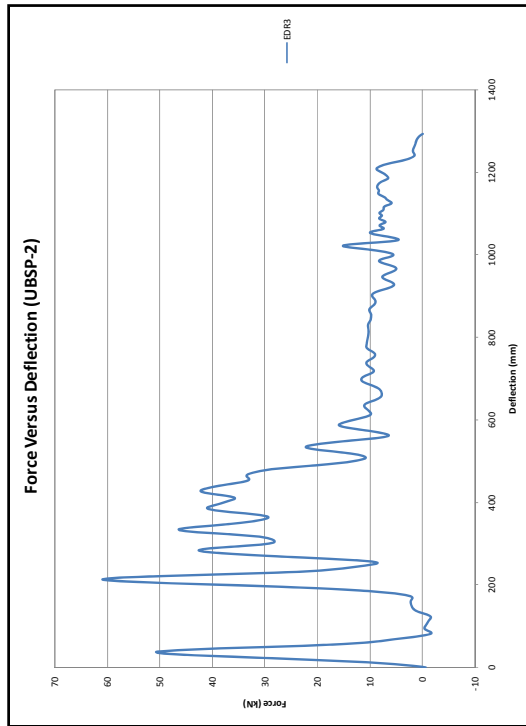


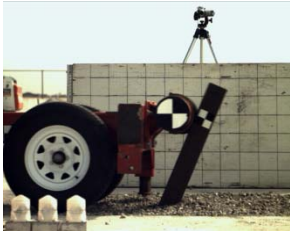
Figure 41b. Force versus Deflection Curve for UBSP-2 - Metric



**IMPACT**



**TIME = 20 ms**



**TIME = 40 ms**



**TIME = 60 ms**



**TIME = 90 ms**



**TIME = 120 ms**

**Figure 43. Time Sequential Images, Test UBSP-2**



**Figure 44. Post-Impact Images of Test UBSP-2**

### **5.8.3 Test UBSP-3 – Upper FRP Tube**

Test UBSP-3 was a strong-axis impact at 0 degrees on the fiber reinforced plastic (FRP) tube concept embedded in standard strong soil. The force and energy data are shown in Figures 45 and 46, respectively. Time-sequential photographs of this test are shown in Figure 47. Upon impact, the FRP tube began to rotate immediately and lost contact with the bogie head at approximately 6 ms. At approximately 14 ms, the bogie regained contact, and the lower foundation tube began rotating in the soil. The lower foundation tube rotated 1 in. (25 mm) in the soil and also experienced some yielding along the downstream side. The steel/wood shims suffered some damage as the wood crushed along the downstream side. The upper FRP post also showed brittle characteristics as there was some cracking and crushing on the upstream face, as shown in Figure 48. Finally at 68 ms, the FRP post popped out of the lower foundation tube and then remained in contact with the bogie head until approximately 92 ms, even though there was little resistance after the post had broken away.

The force versus deflection curve, as provided in Figure 45, indicated an initial peak in the force level due to the inertial effects of the upper FRP tube. After this initial peak, the force level subsided towards zero as the post rotated due to the clearance between the two tubes. Finally, the force levels climbed back up as the upper FRP tube rotated, deformed, and popped out of the lower foundation tube. Although the force levels did increase until the FRP popped out, the force levels were lower than the desired 12 kips (53 kN). Also, the energy versus deflection curve, as shown in Figure 46, reveals the low energy levels absorbed by this post.

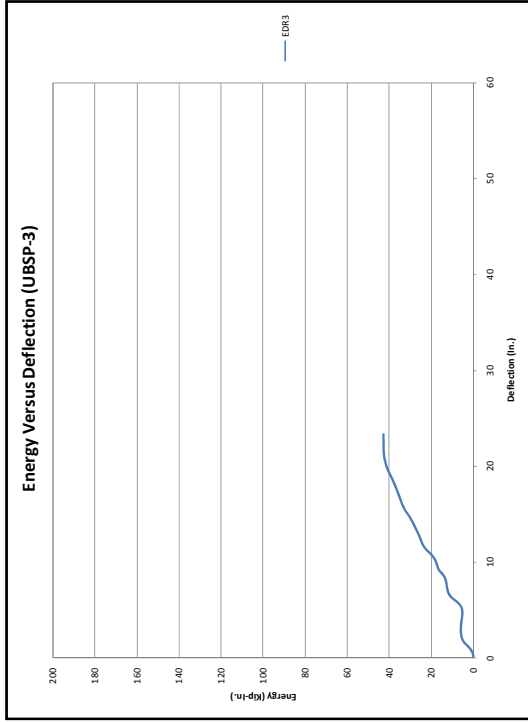


Figure 46a. Energy versus Deflection Curve for UBSP-3 - English

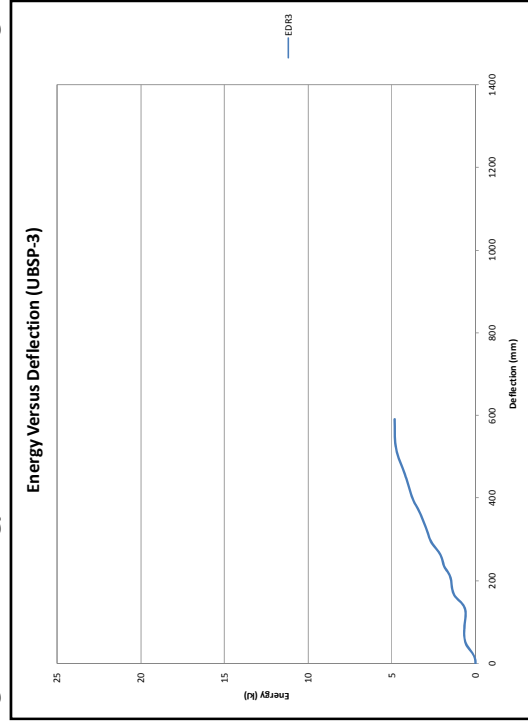


Figure 46b. Energy versus Deflection Curve for UBSP-3 - Metric

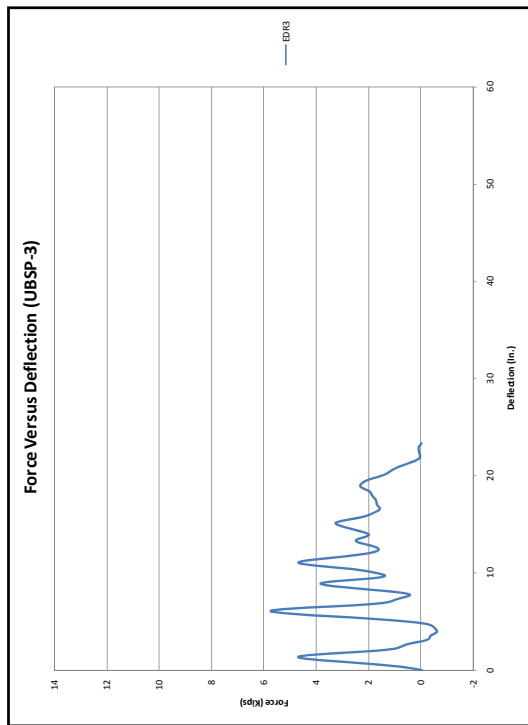


Figure 45a. Force versus Deflection Curve for UBSP-3 - English

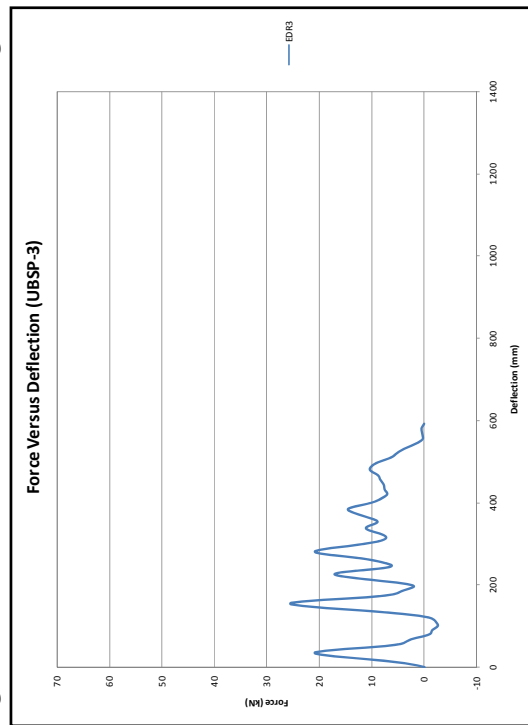
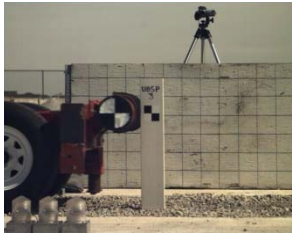


Figure 45b. Force versus Deflection Curve for UBSP-3 - Metric



**IMPACT**



**TIME = 20 ms**



**TIME = 40 ms**



**TIME = 60 ms**



**TIME = 90 ms**



**TIME = 120 ms**

**Figure 47. Time Sequential Photographs, Test UBSP-3**



**Figure 48. Post-Impact Images of UBSP-3**

#### **5.8.4 Test UBSP-4 – Upper FRP Tube**

Test UBSP-4 was a weak-axis impact at 90 degrees on the fiber reinforced plastic tube concept embedded in standard strong soil. The force and energy data are shown in Figures 49 and 50 respectively. Time-sequential photographs are shown in Figure 51. The FRP tube began to rotate immediately and lost contact with the bogie head at approximately 6 ms until 18 ms. After 18 ms, the FRP tube began to crush and rotated over until approximately 122 ms when the bogie ramped up and overrode the tube. Also, the lower foundation tube and the wood/steel shims yielded, which allowed the FRP post to bend over. However, there was not enough deformation to allow the FRP post to break away. After the bogie overrode the FRP tube, the tube sprung back and popped out backwards from the foundation tube, as seen in Figure 52.

As evidenced by the force and energy levels in the force versus deflection and energy versus deflection curves provided in Figures 49 and 50, respectively, the FRP post did not behave as desired. The upper FRP post did not pop out and break away from lower foundation tube. Even though the FRP post popped out as desired in the strong-axis impact in test UBSP-3, this weak-axis test exhibited a different behavior, as the FRP material was not brittle enough and did not crush enough to allow separation of the upper FRP tube. In weak-axis impacts, the upper FRP post needs to crush farther due to the shorter distance between the upstream and downstream faces of the post. This shorter distance decreases the rotation that occurs, and thus, increases the deformation needed to get the upper FRP tube to break away, which helped lead to the undesired behavior in this weak-axis impact.

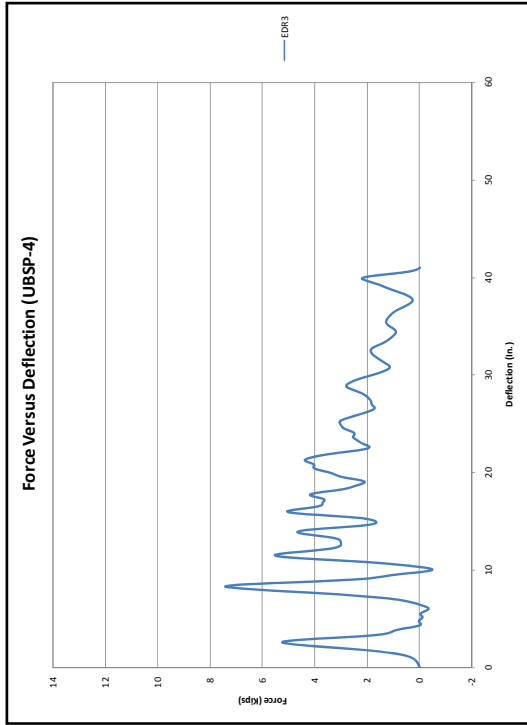


Figure 49a. Force versus Deflection Curve for UBSP-4 - English

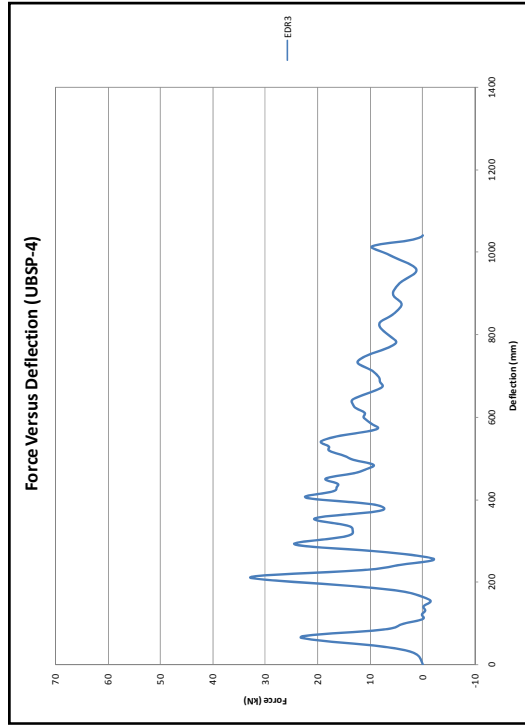


Figure 49b. Force versus Deflection Curve for UBSP-4 - Metric

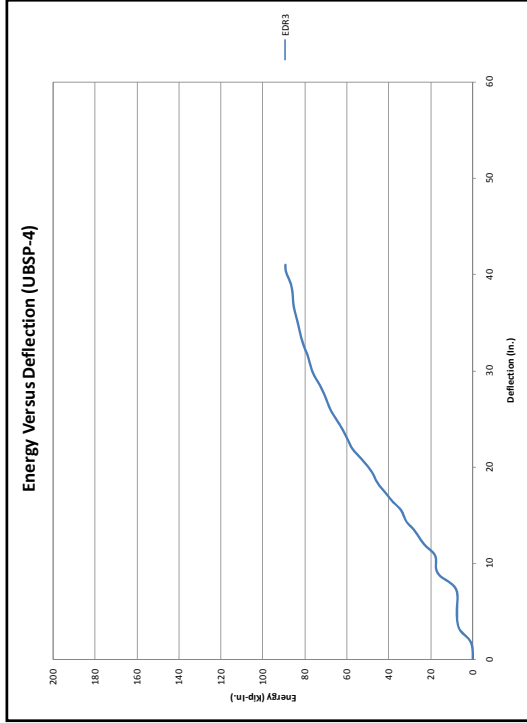


Figure 50a. Energy versus Deflection Curve for UBSP-4 - English

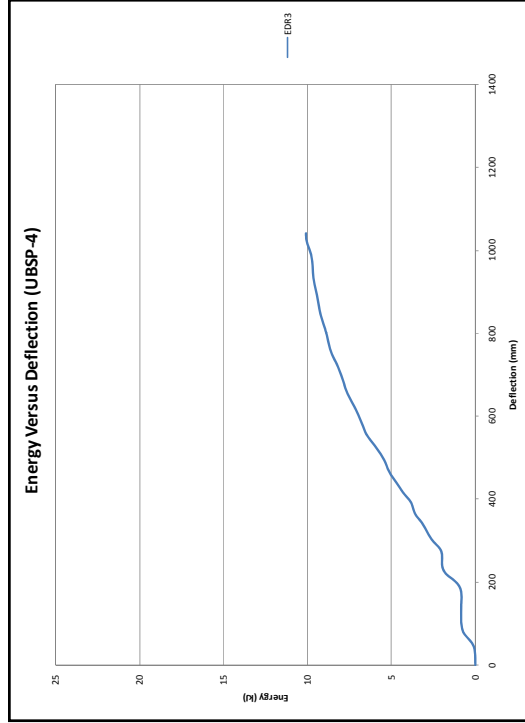
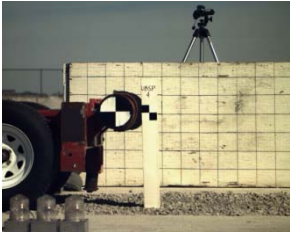


Figure 50b. Energy versus Deflection Curve for UBSP-4 - Metric





**IMPACT**



**TIME = 20 ms**



**TIME = 40 ms**



**TIME = 60 ms**



**TIME = 90 ms**



**TIME = 120 ms**

**Figure 51. Time Sequential Photographs, Test UBSP-4**



**Figure 52. Post-Impact Images of UBSP-4**

### **5.8.5 Test UBSP-5 – Fracturing Bolt (Slipbase)**

Test UBSP-5 was a strong-axis impact at 0 degrees on the fracturing bolt (slipbase) concept embedded in standard strong soil. The force and energy data are shown in Figures 53 and 54, respectively. Time-sequential photographs are shown in Figure 55. Upon impact, the post began to rotate immediately in the soil until the impact-side bolts broke in tension at approximately 16 ms. After the impact-side bolts broke, there was little resistance left from the post. The upper W6x9 (W152x13.4) post rotated around the non-impact side bolts, until these bolts eventually bent and broke away, thus leading to the post losing contact with the bogie head at approximately 70 ms. The only deformation in the post occurred to the bolts and washers. The bolts tended to break in either a level or 45 degree plane, and the washers were deformed from compression between the nuts, bolt heads, and the base plates. Post-impact images of the posts and fractured bolts can be seen in Figure 56.

As seen in the force versus deflection curve in Figure 53 and the energy versus deflection curve in Figure 54, the fracturing bolt concept adequately absorbed energy, but the magnitude of the force levels was too low. Even though the impact-side bolts broke in tension as expected, the non-impact side bolts did not affect the peak force levels and did not break due to shearing. The shear load did affect the failure, but the tensile load was the controlling force in the failure of the bolts.

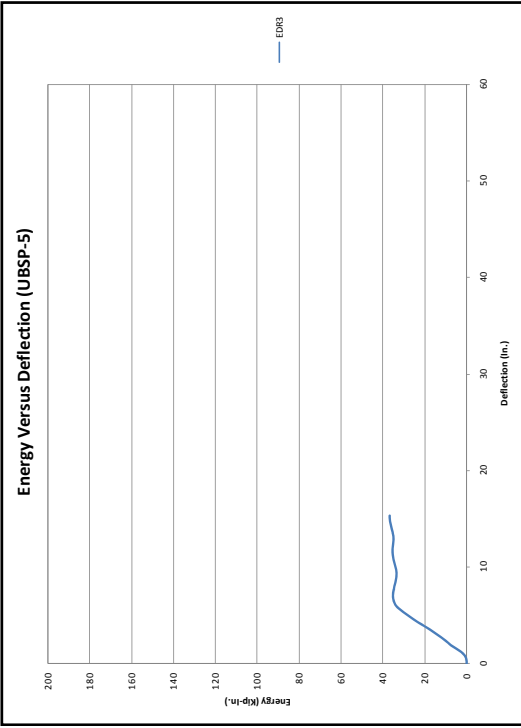


Figure 54a. Energy versus Deflection Curve for UBSP-5 - English

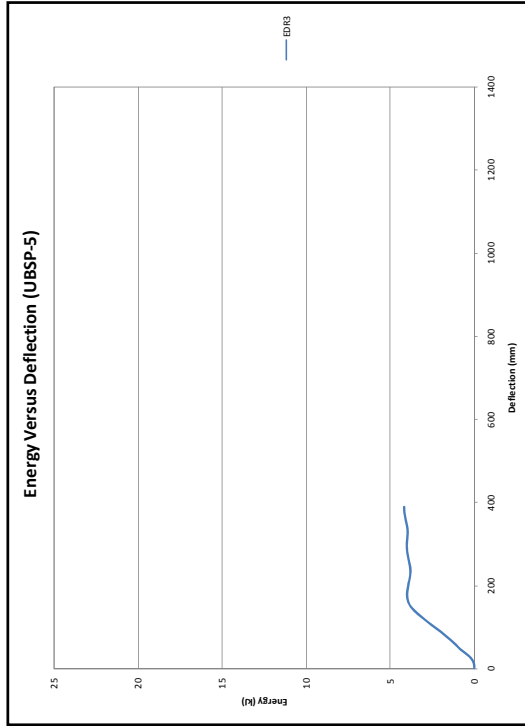


Figure 54b. Energy versus Deflection Curve for UBSP-5 - Metric

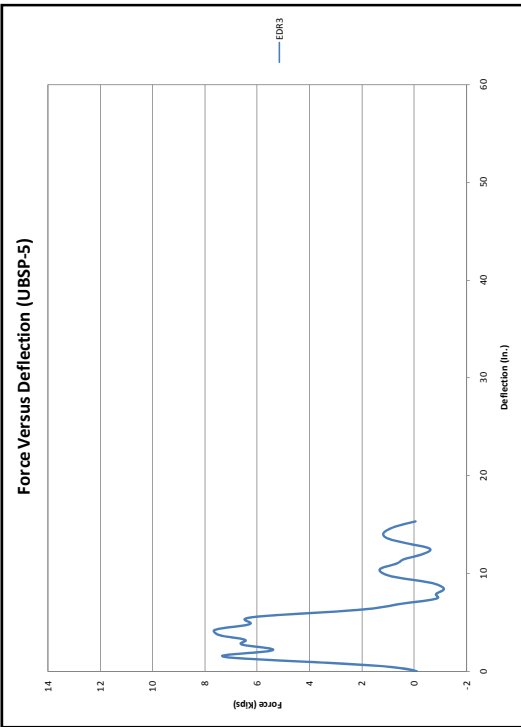


Figure 53a. Force versus Deflection Curve for UBSP-5 - English

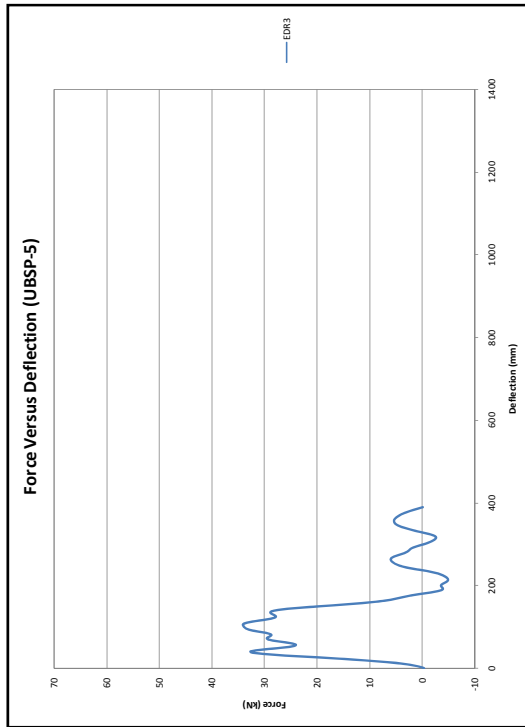


Figure 53b. Force versus Deflection Curve for UBSP-5 - Metric

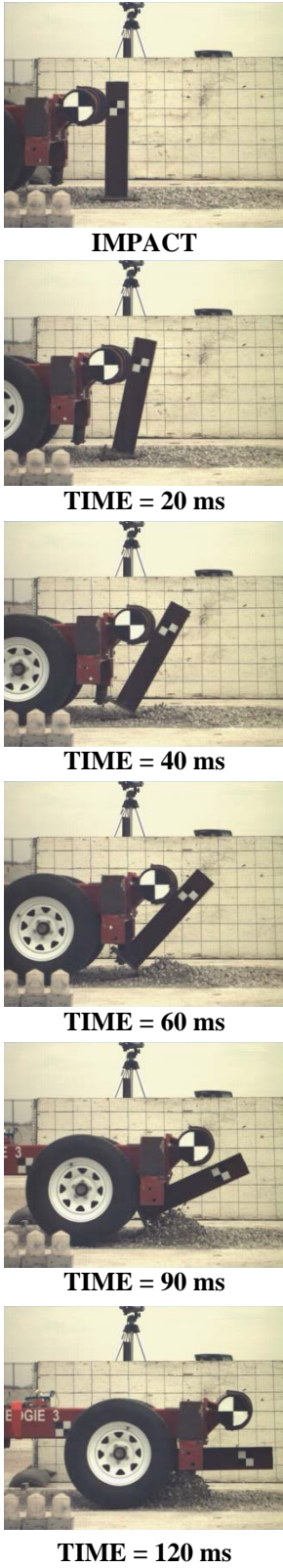


Figure 55. Time Sequential Photographs, Test UBSP-5



Figure 56. Post-Impact Images of UBSP-5

### **5.8.6 Test UBSP-6 – Fracturing Bolt (Slipbase)**

Test UBSP-6 was a weak-axis impact at 90 degrees on the fracturing bolt (slipbase) concept embedded in standard strong soil. The force and energy data are shown in Figures 57 and 58, respectively. Time-sequential photographs are shown in Figure 59. Upon impact, the post began to rotate immediately, and the impact-side bolts broke in tension at approximately 10 ms. After the impact-side bolts broke, the post rotated over with little resistance until the non-impact-side bolts broke away, and the post lost contact with the bogie head at approximately 46 ms. Similar to the strong-axis impact in test UBSP-5, the fracturing bolt concept broke away as desired.

As seen in the force versus deflection curve and the energy versus deflection curve in Figures 57 and 58, the fracturing bolt concept in a weak-axis impact had desirable strength and behavior. The impact-side bolts broke away at a peak load of 5.34 kips (23.8 kN) near the desired 6 kips (26.7 kN). Also, the post broke away quickly and absorbed a small amount of energy as desired. Similar to test UBSP-5, the only deformation in the post occurred to the bolts and washers. The bolts tended to break in either a level or 45 degree plane, and the washers were deformed from compression between the nuts, bolt heads, and the base plates. Post-impact images of the posts and fractured bolts can be seen in Figure 60.

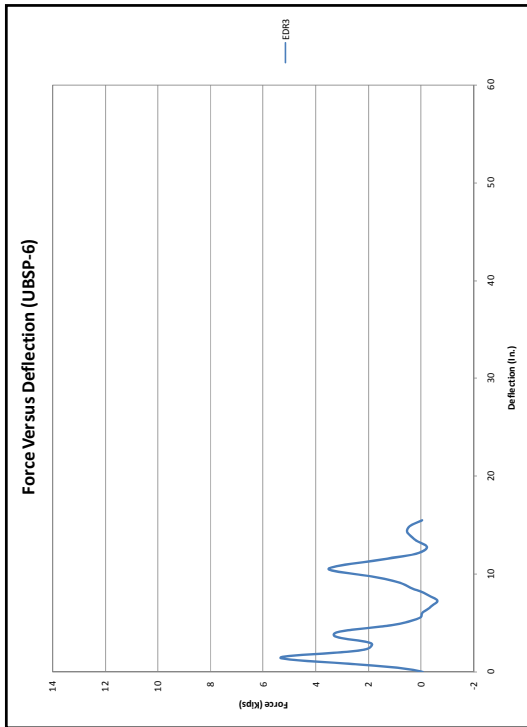


Figure 57a. Force versus Deflection Curve for UBSP-6 - English

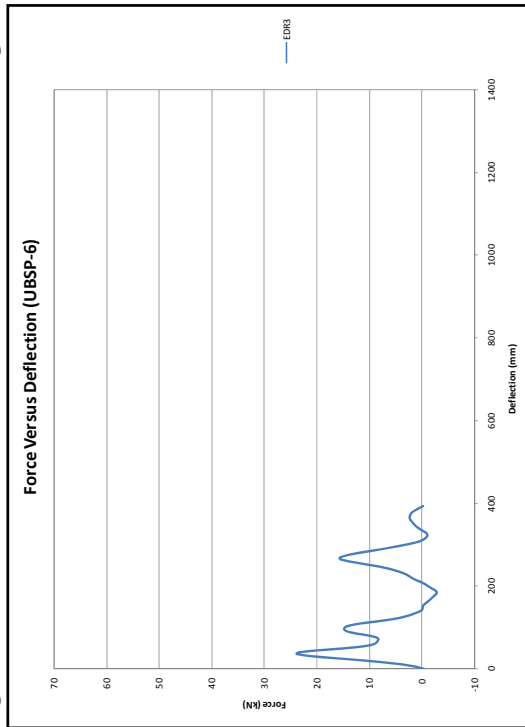


Figure 57b. Force versus Deflection Curve for UBSP-6 - Metric

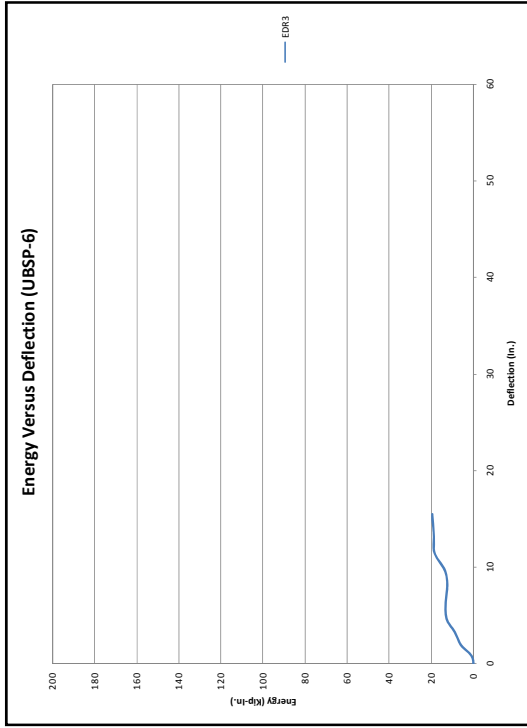


Figure 58a. Energy versus Deflection Curve for UBSP-6 - English

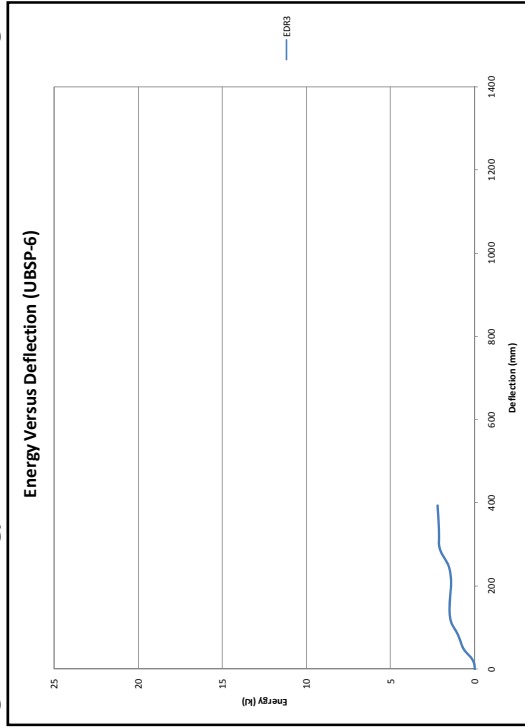


Figure 58b. Energy versus Deflection Curve for UBSP-6 - Metric



**IMPACT**



**TIME = 20 ms**



**TIME = 40 ms**



**TIME = 60 ms**



**TIME = 90 ms**



**TIME = 120 ms**

**Figure 59. Time Sequential Photographs, Test UBSP-6**



**Figure 60. Post-Impact Images of UBSP-6**

### **5.8.7 Test UBSP-7 – Circular Fillet Weld**

Test UBSP-7 was a strong-axis impact at 0 degrees on the circular fillet weld concept embedded in standard strong soil. Time-sequential photographs are shown in Figure 61. The post began to rotate immediately but did not break away as intended. As a result, the bogie never lost contact with the post and came to rest on top of the post, as seen in Figure 62. For this test, the acceleration transducers did not work, but this was not an issue since the post did not break away. The only deformation that occurred during the test was some slight yielding below ground level on the impact side of the lower foundation tube. This deformation could be a sign of frozen soil, which hindered any rotation of the tube.

The breakaway welds did not fail as expected due to error in judging the weld strength. The strength of the base steel material, 36 ksi (248 MPa), was used as the controlling strength of the weld. However, the strength of the actual weld material, 70 ksi (483 MPa), should have been used in the calculations for this concept. The strength of the actual weld material controls in this case with the weld acting as the failure mechanism.





**IMPACT**



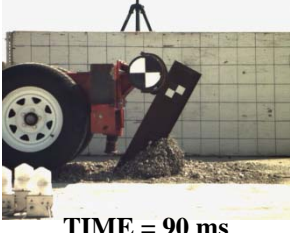
**TIME = 20 ms**



**TIME = 40 ms**



**TIME = 60 ms**



**TIME = 90 ms**



**TIME = 120 ms**

**Figure 61. Time Sequential Photographs, Test UBSP-7**



**Figure 62. Post-Impact Images of UBSP-7**

### **5.8.8 Test UBSP-8 – Circular Fillet Weld**

Test UBSP-8 was a weak-axis impact at 90 degrees on the circular fillet weld concept embedded in standard strong soil. The force and energy data are shown in Figures 63 and 64, respectively. Time-sequential photographs are shown in Figure 65. Upon impact, the post began to immediately rotate in the soil. At approximately 30 ms, the upper W8x10 (W203x14.9) post began to yield and buckle over the steel plates. Like in test UBSP-7, the post did not break away as desired, and the bogie continued to rotate and yield the circular fillet weld post until eventually overriding the post and losing contact at approximately 112 ms. The only deformation in the test occurred to the upper W8x10 (W203x14.9) post as it deformed and bent over the steel plates. There was no evidence of the weld failing, which again was due to an error in judging the strength of the weld. The post-impact images can be seen in Figure 66.

The force and energy versus deflection curves can be seen in Figures 63 and 64. These graphs also show the undesired behavior of this design. Although the peak force level of 7.45 kips (33.1 kN) was only slightly higher than the 6 kips (26.7 kN) desired, the high force levels continued through a large displacement. Thus, the post absorbed much more energy than desired by not breaking away.

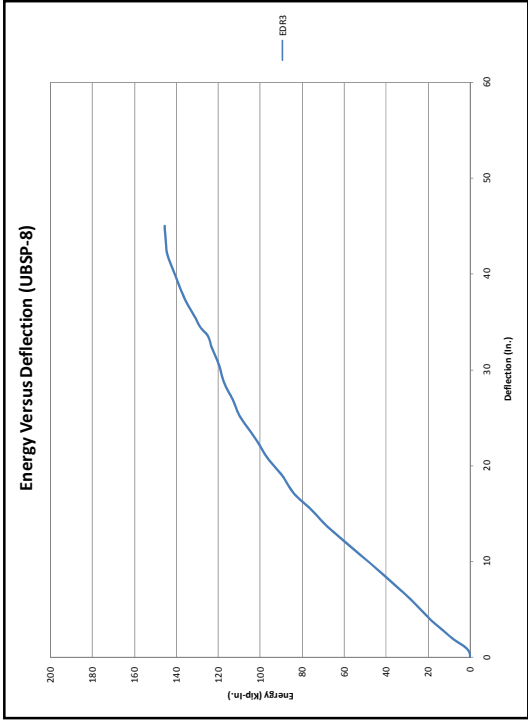


Figure 64a. Energy versus Deflection Curve for UBSP-8 - English

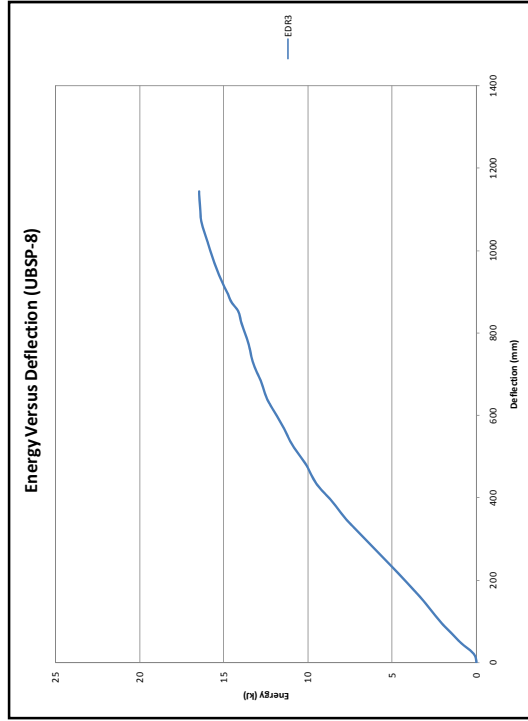


Figure 64b. Energy versus Deflection Curve for UBSP-8 - Metric

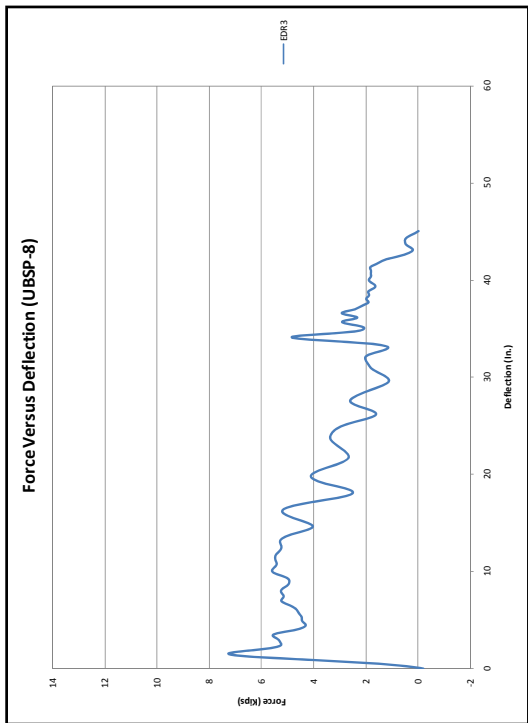


Figure 63a. Force versus Deflection Curve for UBSP-8 - English

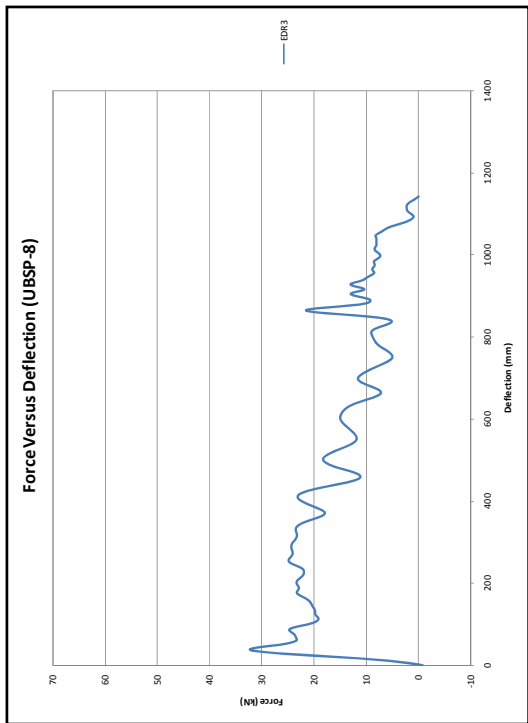


Figure 63b. Force versus Deflection Curve for UBSP-8 - Metric

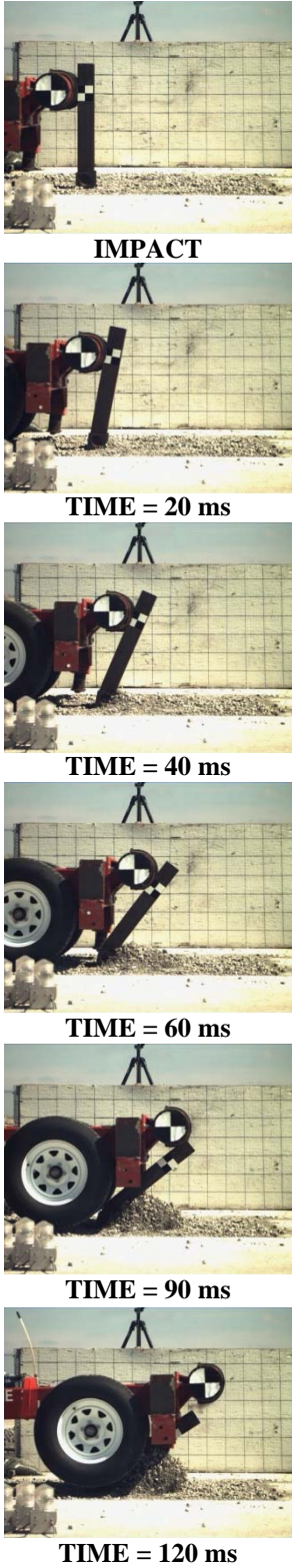


Figure 66. Post-Impact Images of UBSP-8

Figure 65. Time Sequential Photographs, Test UBSP-8

## 5.9 Round 1 Summary and Conclusions

The behavior of each post was evaluated with regard to its potential for matching CRT wood posts. A summary of the first round of bogie testing can be seen in Table 10.

For the first concept in test UBSP-1, the steel tube in steel tube broke away as desired. Even though this concept showed some promise, it was determined that there were too many factors controlling the post's strength and behavior to continue with this concept. In order to refine the results on this concept, there would need to be numerous bogie tests to get the desired behavior and results. Although simulation work with LS-DYNA [20] could be performed to help analyze different factors in the design, the fracture seen in the bogie test would be very difficult to predict and simulate after making design modifications. Thus, this concept was dropped from consideration for the Universal Breakaway Steel Post.

In test UBSP-2, the steel tube in steel tube with a thru bolt did not perform as desired. The bolt did not tear out, and thus, the upper tube did not break away. Therefore, the steel tube in steel tube with a thru bolt concept was dropped from consideration. Also, tests UBSP-3 and UBSP-4 with upper fiber reinforced plastic (FRP) tubes did not perform as desired. The FRP tube broke away too easily in the strong-axis impact and did not break away in the weak-axis impact in test UBSP-4. Similar to the steel tube in steel tube concept, the FRP tube concept could probably be made to work but had too many variables controlling its strength and behavior. Also, the crushing and deformation in the FRP would be very difficult to predict and simulate in LS-DYNA simulation work. As a result, the FRP tube concept was also dropped from consideration as the Universal Breakaway Steel Post.

The fracturing bolt (slipbase) concept tested in UBSP-5 and UBSP-6 performed sufficiently by breaking away cleanly in both the strong and weak axes. Even though all of the bolts broke away in tension instead of shear, the post showed great potential. The only issue was that the measured fracture loads were lower than those from CRT testing. As a result, the fracturing bolt concept was selected for inclusion in the second round of bogie testing.

Finally, the circular fillet weld concept did not break away in either test UBSP-7 or UBSP-8. However, this undesired behavior was due to the error in calculating of the weld fracture strength. From previous testing, it was known that this concept had desirable behavior with correct calculations, and it was decided to revise the design and include this concept in the second round of bogie testing.

Although most the concepts in the first round of bogie testing showed some potential for use as an Universal Breakaway Steel Post, the number of concepts was narrowed down to the two most promising designs. Both the fracturing bolt and circular fillet weld concepts demonstrated good potential for use as the Universal Breakaway Steel Post. As a result, these two concepts were modified and included in the second round of bogie testing to identify the design with the best potential for matching properties of the CRT.

**Table 10a. Summary of Round 1 Bogie Testing Results – English**

Test No.	Impact Velocity (mph)	Failure Type	Initial Peak Force		Initial Stiffness (kips/in.)	Peak Force		Total Energy	
			Displacement (in.)	Force (kips)		Displacement (in.)	Force (kips)	Displacement (in.)	Energy (kip-in.)
UBSP-1	19.4	Post Failure	1.39	11.1	8.00	9.43	12.5	29.8	89.2
UBSP-2	19.3	Post Yielded	1.37	11.2	8.14	8.30	13.5	51.3	161.2
UBSP-3	19.7	Post Failure	1.41	4.67	3.32	6.02	5.71	23.3	42.6
UBSP-4	19.6	Post Yielded	2.58	5.22	2.02	8.32	7.39	41.0	89.1
UBSP-5	19.4	Post Failure	1.60	7.34	4.60	4.10	7.66	15.3	36.8
UBSP-6	18.5	Post Failure	1.42	5.34	3.76	1.42	5.34	15.4	19.3
UBSP-7	19.4	Bogie Stopped	**	**	**	**	**	**	**
UBSP-8	20.2	Post Yielded	1.55	7.45	4.81	1.55	7.45	44.8	153.4

\* No data for UBSP-7

**Table 10b. Summary of Round 1 Bogie Testing Results – Metric**

Test No.	Impact Velocity (km/h)	Failure Type	Initial Peak Force		Initial Stiffness (kN/mm)	Peak Force		Total Energy	
			Displacement (mm)	Force (kN)		Displacement (mm)	Force (kN)	Displacement (mm)	Energy (kJ)
UBSP-1	31.2	Post Failure	31.2	49.4	1.40	240	55.6	757	10.1
UBSP-2	31.1	Post Yielded	34.8	49.8	1.43	211	60.0	1303	18.2
UBSP-3	31.7	Post Failure	35.8	20.8	0.58	153	25.4	592	4.81
UBSP-4	31.5	Post Yielded	65.5	23.2	0.35	211	32.9	1041	10.1
UBSP-5	31.2	Post Failure	40.6	32.6	0.81	104	34.1	389	4.16
UBSP-6	29.8	Post Failure	36.1	23.8	0.66	36.1	23.8	391	2.18
UBSP-7	31.2	Bogie Stopped	**	**	**	**	**	**	**
UBSP-8	32.5	Post Yielded	39.4	33.1	0.84	39.4	33.1	1138	17.3

## 6 BREAKAWAY POST BOGIE TESTING – ROUND 2

### 6.1 Purpose

The second round of bogie testing was performed to evaluate the design modifications of the fracturing bolt and circular fillet weld breakaway concepts. These tests were used to help determine which breakaway steel concept would be the best option for the Universal Breakaway Steel Post.

### 6.2 Scope

The second round of bogie testing was conducted on two different concepts, as detailed in Section 6.3. The test setup was identical to the previous setup used in the first round of bogie testing. All posts were embedded 40 in. (1,016 mm) in standard strong soil. The target impact condition for the tests was 20 mph (32 km/h) with the impact occurring at the centerline of the bogie, and at a height of 24 7/8 in. (632 mm) above the ground. For tests UBSP-9 and UBSP-11, technical difficulties were encountered with the speed trap system so the actual speed was not known, but the velocity of the tow truck was used to determine the speed for these two tests. Five tests were performed on the two concepts, and the scope of the second round of bogie testing is shown in Table 11.

**Table 11. Test Matrix for Round 2 Bogie Testing**

Test No.	Test Date	Post Concept	Speed		Impact Axis
			mph (km/h)	ft/s (m/s)	
UBSP-9	05-29-2008	Fracturing Bolt	19.9 (32.0)	29.2 (8.90)	Strong
UBSP-10	05-29-2008	Fracturing Bolt	19.1 (30.7)	28.0 (8.53)	Weak
UBSP-11	05-29-2008	Circular Fillet Weld	19.7 (31.7)	28.9 (8.81)	Weak
UBSP-12	06-04-2008	Circular Fillet Weld	18.7 (30.1)	27.4 (8.35)	Strong
UBSP-13	06-04-2008	Fracturing Bolt	18.7 (30.1)	27.4 (8.35)	Strong



## 6.3 Post Details

### 6.3.1 Fracturing Bolt

The fracturing bolt concept used in the second round of bogie testing only had minor changes from the first round of bogie testing. The post still utilized a lower foundation tube connected to an upper W6x9 (W152x13.4) beam and attached with four breakaway bolts. In the first round of bogie testing, this concept performed sufficiently but broke away at a lower peak force level than the desired 12 kips (53 kN) in the strong axis.

The first design revision included the use of standard washers and no step washers. This change was made after observing the behavior in the first round of bogie testing where the bolts broke away in tension versus in shear. As a result, there were no longer any patent concerns with using this concept.

Upon review, it was noticed that the non-impact-side bolts had minimal effect on the ultimate strength of the post. Thus, calculations were performed to help determine the spacing and size of the breakaway bolts, as seen in Figure 67. From these calculations, the diameter of the breakaway bolts was changed from 5/16 in. (7.9 mm) to 3/8 in. (9.5 mm) to increase the post strength about the strong axis of bending. Also, the bolts were moved closer together with respect to the weak axis to keep the force levels low enough for weak-axis impacts. The bolts were spaced apart 2 1/2 in. (64 mm) in the weak axis and 10 in. (254 mm) in the strong axis.

In the middle of the second round of bogie testing, there was a change in the breakaway connector used to attach the post segments. For tests UBSP-9 and UBSP-10, a 3/8 in. (9.5 mm) diameter, grade 5, double end stud was tested. However, in test UBSP-13, a 3/8 in. (9.5 mm) diameter, grade 5, hex head bolt was tested. Since the bolt and double end stud were the same

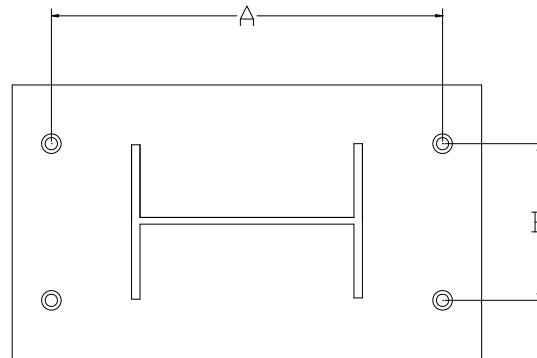
size and grade, they were believed to provide identical behavior and strength. The reason for the change was that the hex head bolt option contained fewer pieces and would be a simpler design to install. The switch from a rod to a bolt was the only design modification for tests UBSP-9, UBSP-10, and UBSP-13. The drawings shown in Figures 68 through 71 provide details for the hex head bolt configuration.

- **Strong Axis**

$$F_{resistance} = \frac{2(A)(F_u)(A_b)}{h}$$

Where:

- $A$  = Distance Between Fracturing Bolts
- $F_u$  = Ultimate Strength of Fracturing Bolt
- $A_b$  = Effective Area of Fracturing Bolt
- $h$  = Height of Impact Above Fracturing Bolt



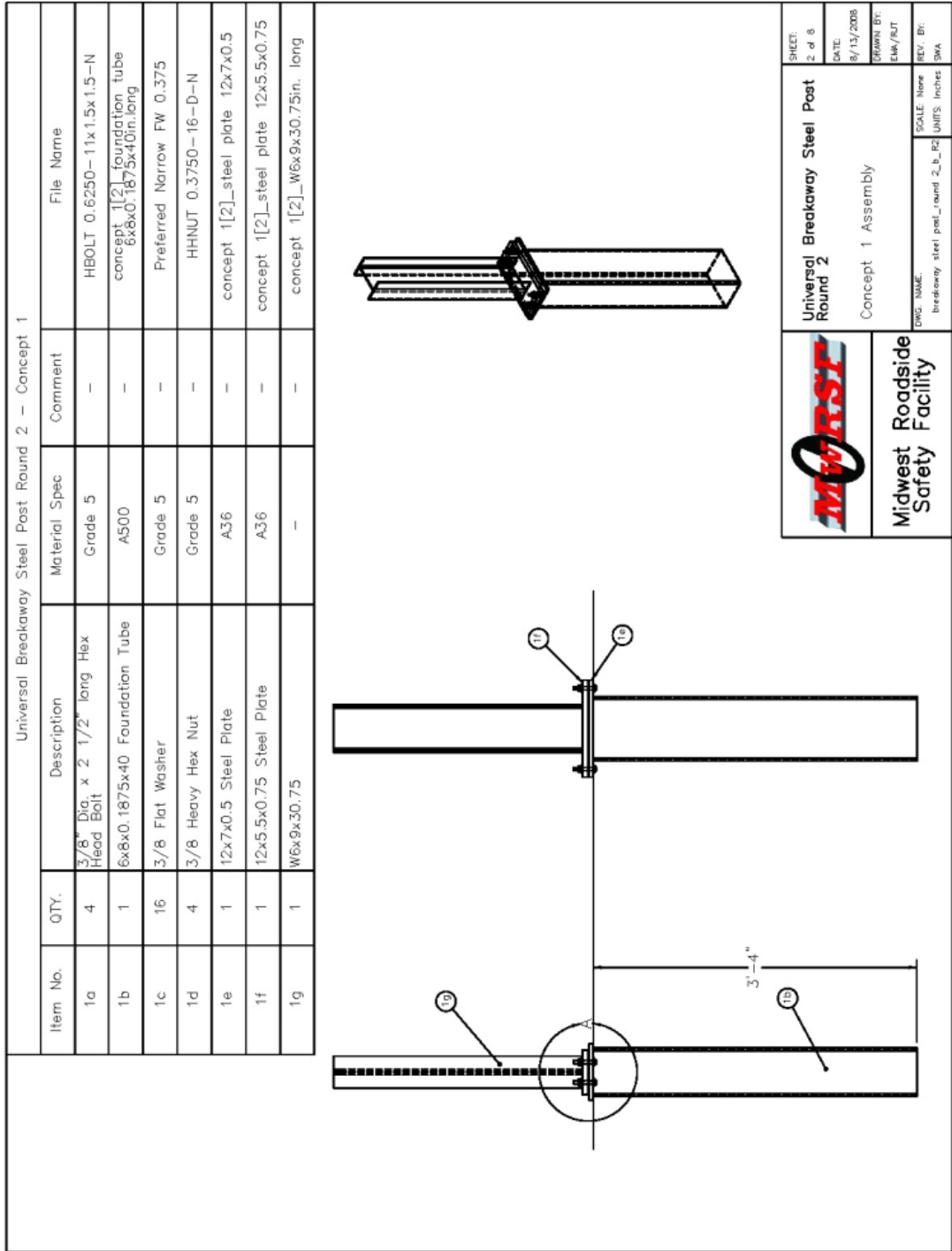
- **Weak Axis**

$$F_{resistance} = \frac{(2)(B)(F_u)(A_b)}{h}$$

Where:

- $B$  = Distance Between Fracturing Bolts
- $F_u$  = Ultimate Strength of Fracturing Bolt
- $A_b$  = Effective Area of Fracturing Bolt
- $h$  = Height of Impact Above Fracturing Bolt

**Figure 67. Fracturing Bolt Calculations**



**Figure 68. Revised Fracturing Bolt Design Details**

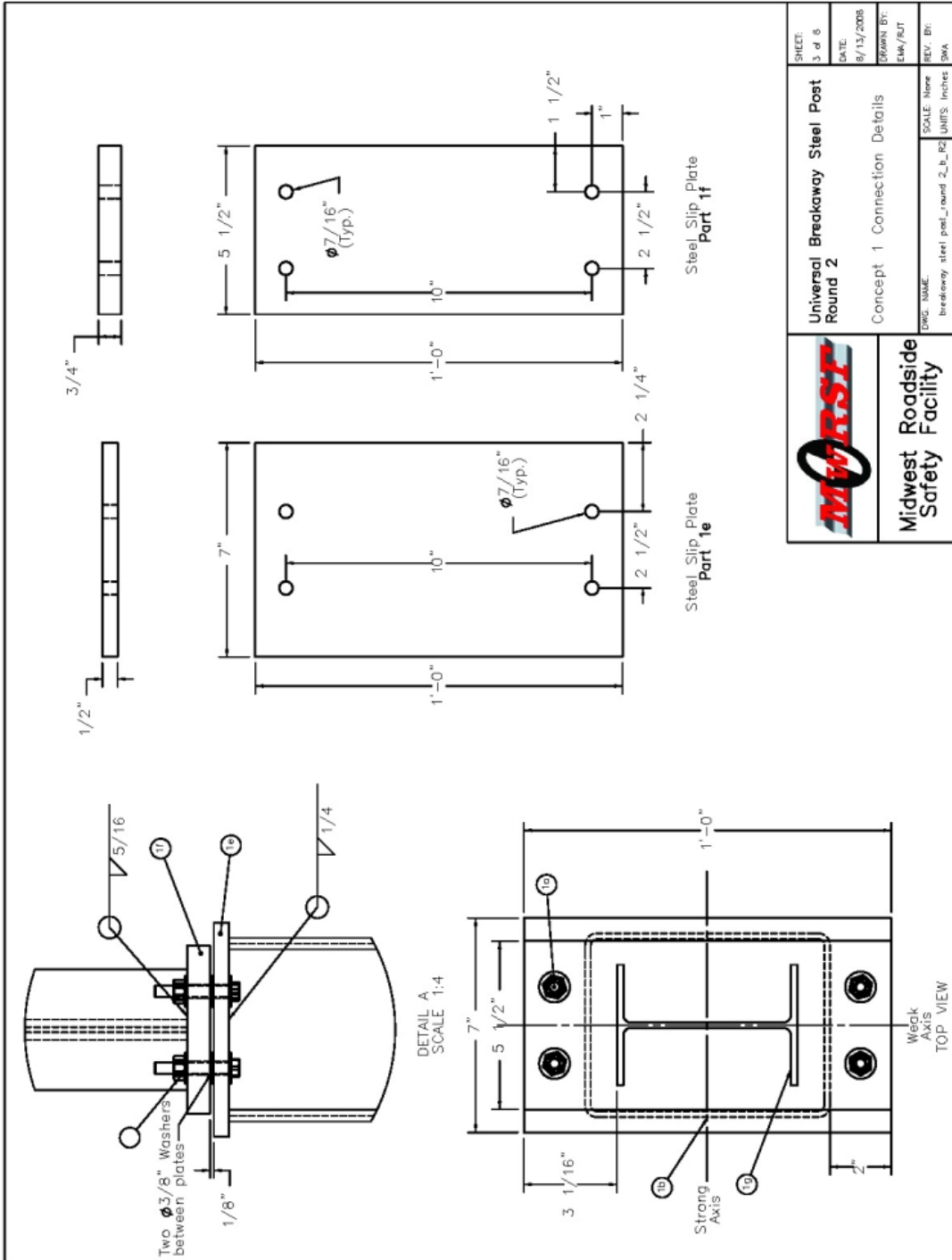


Figure 69. Revised Fracturing Bolt Design Details

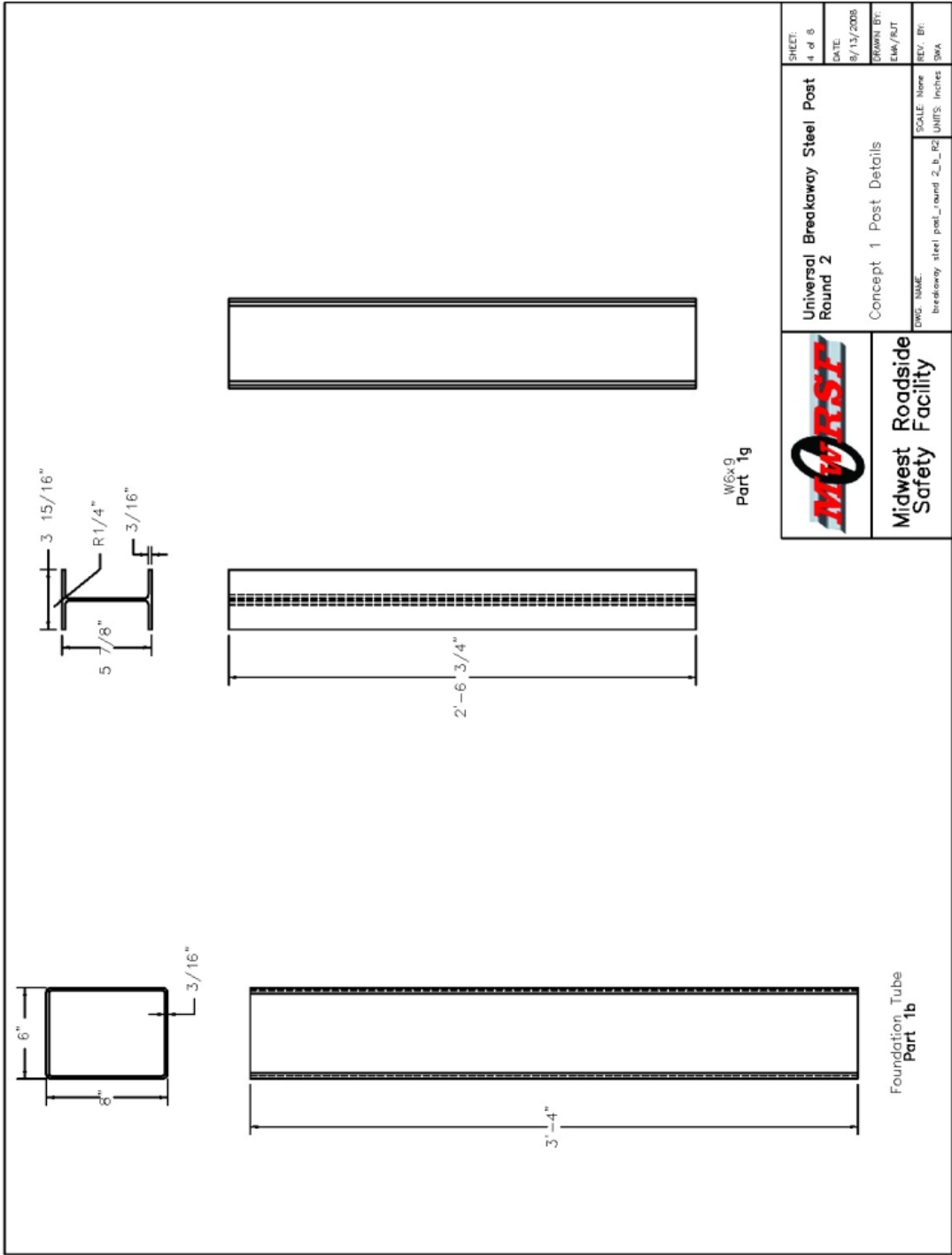


Figure 70. Revised Fracturing Bolt Design Details

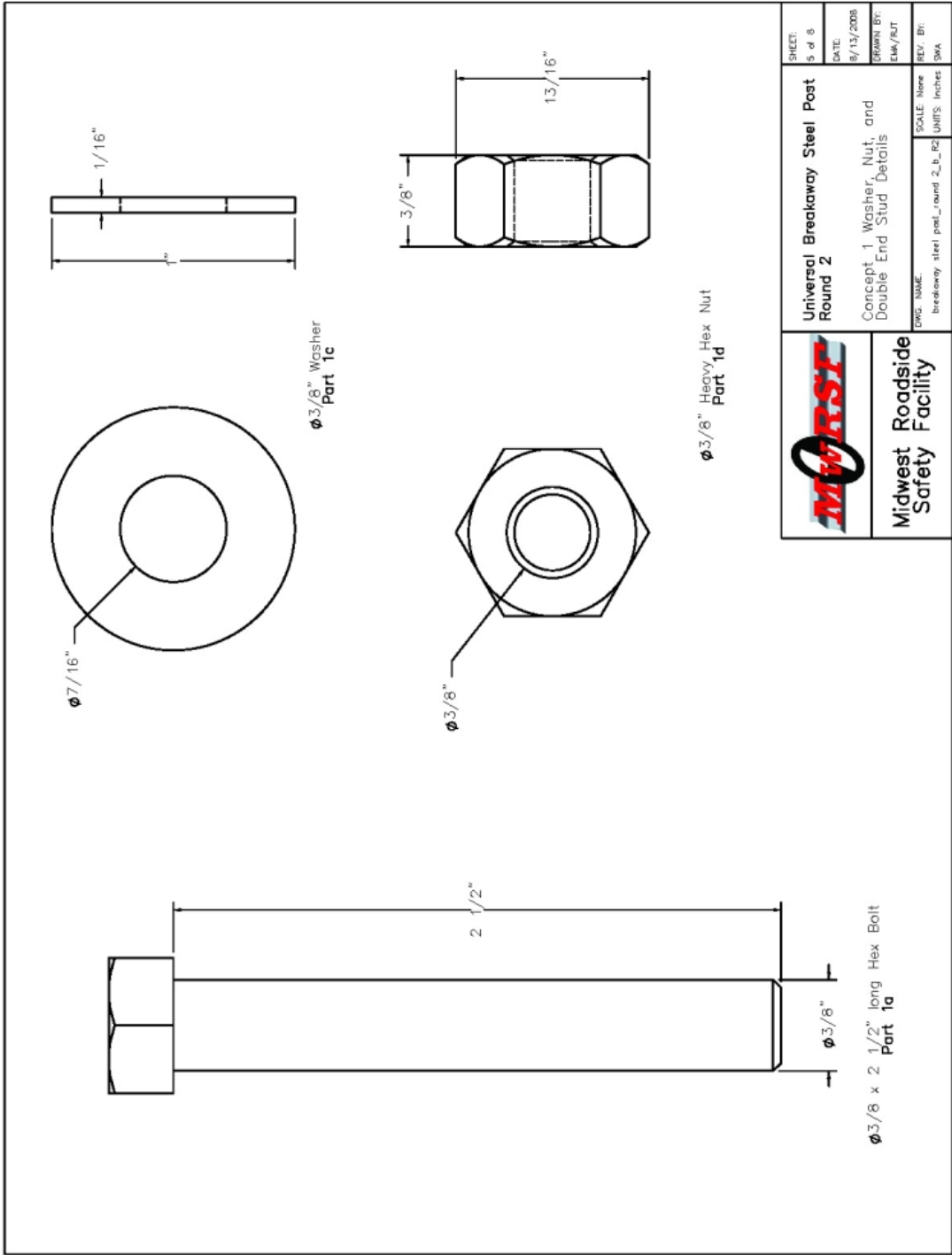


Figure 71. Revised Fracturing Bolt Design Details

### 6.3.2 Circular Fillet Weld

The circular fillet weld concept was also similar to the design evaluated in the first round of bogie testing. Once again, two steel splice plates were used to connect an upper W8x10 (W203x14.9) wide-flange section to the lower 6-in. x 8-in. x 3/16-in. (152-mm x 203-mm x 4.8-mm) foundation tube. However, the major difference was a reduction in the size of the circular breakaway weld.

In the first round of bogie testing, a 1/4-in. (6.4-mm) fillet weld was used around the circumference of a 3-in. (76-mm) diameter circle. This weld was reduced to a 3/16-in. (4.8-mm) weld used around a 1 1/2-in. (38-mm) diameter circle for the second round of bogie testing. Similar design calculations were used as in the first round of bogie testing, as shown previously in Figure 34. However, the yield strength of the 36 ksi (248 MPa) base steel was replaced with the 70 ksi (483 MPa) tensile strength of the weld material for calculating the fracture strength of the weld.

Another change in the design was the reduction in thickness of the two steel splice plates connecting the lower foundation tube to the upper wide flange section. For strong-axis impacts, the weld can shear out of the top of the splice plate in case the breakaway weld is made too strong. This alteration was performed to get two different failure modes in order to ensure the post breaks away as desired in the strong axis. Calculations on this splice plate tear out, as seen in Figure 72, were carried out to determine the edge distance of the weld and the thickness of the splice plate to ensure that the post breaks away even if a weld is too strong. All of the design changes are shown in Figures 73 through 75.

## Strong Axis

$$F_{resistance} = \frac{((\pi)(r)(t)(F_w) + 1.15(F_u)(t)(A))(d)}{h}$$

Where:

*A* = Edge Distance of Circular Fillet Weld

*F<sub>u</sub>* = Ultimate Strength of Splice Plate Steel

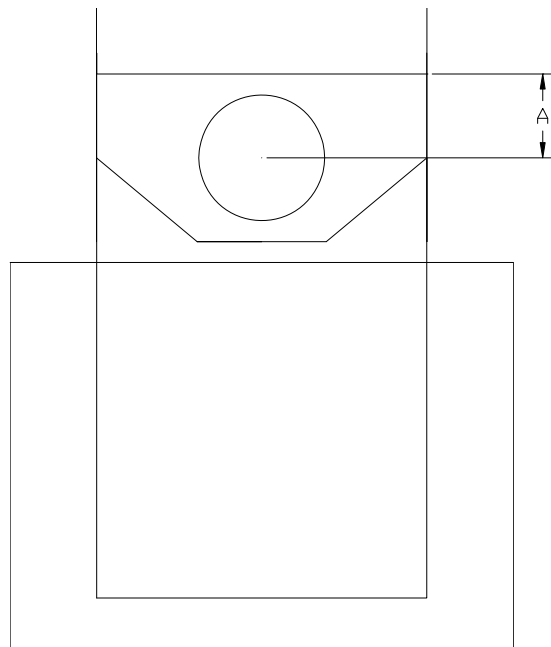
*r* = Radius of Circular Fillet Weld

*t* = Thickness of Splice Plate

*F<sub>w</sub>* = Tensile Strength of Weld Material

*d* = Distance between Circular Fillet Welds

*h* = Impact Height Above Weld



**Figure 72. Circular Fillet Weld Tear Out Calculations**



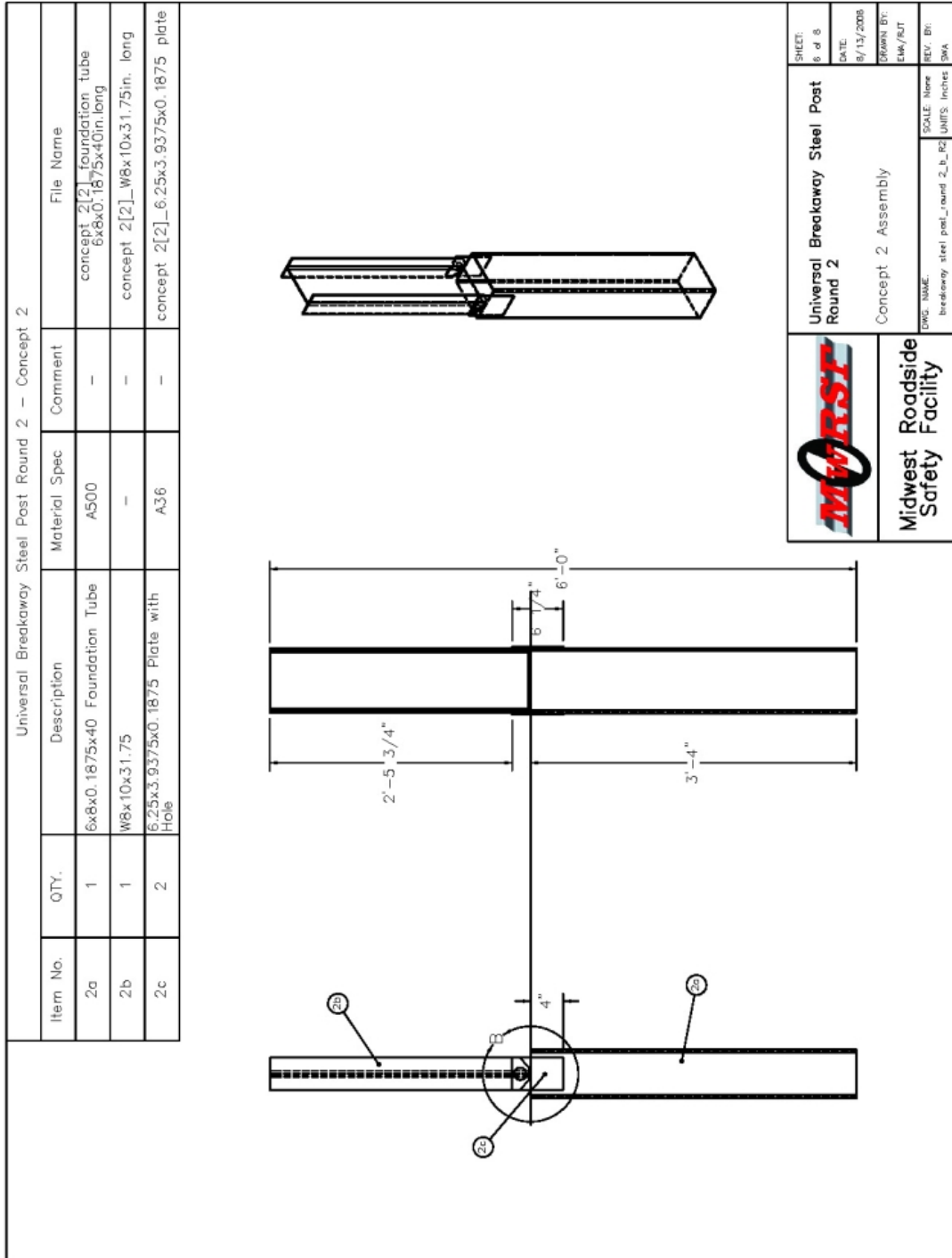
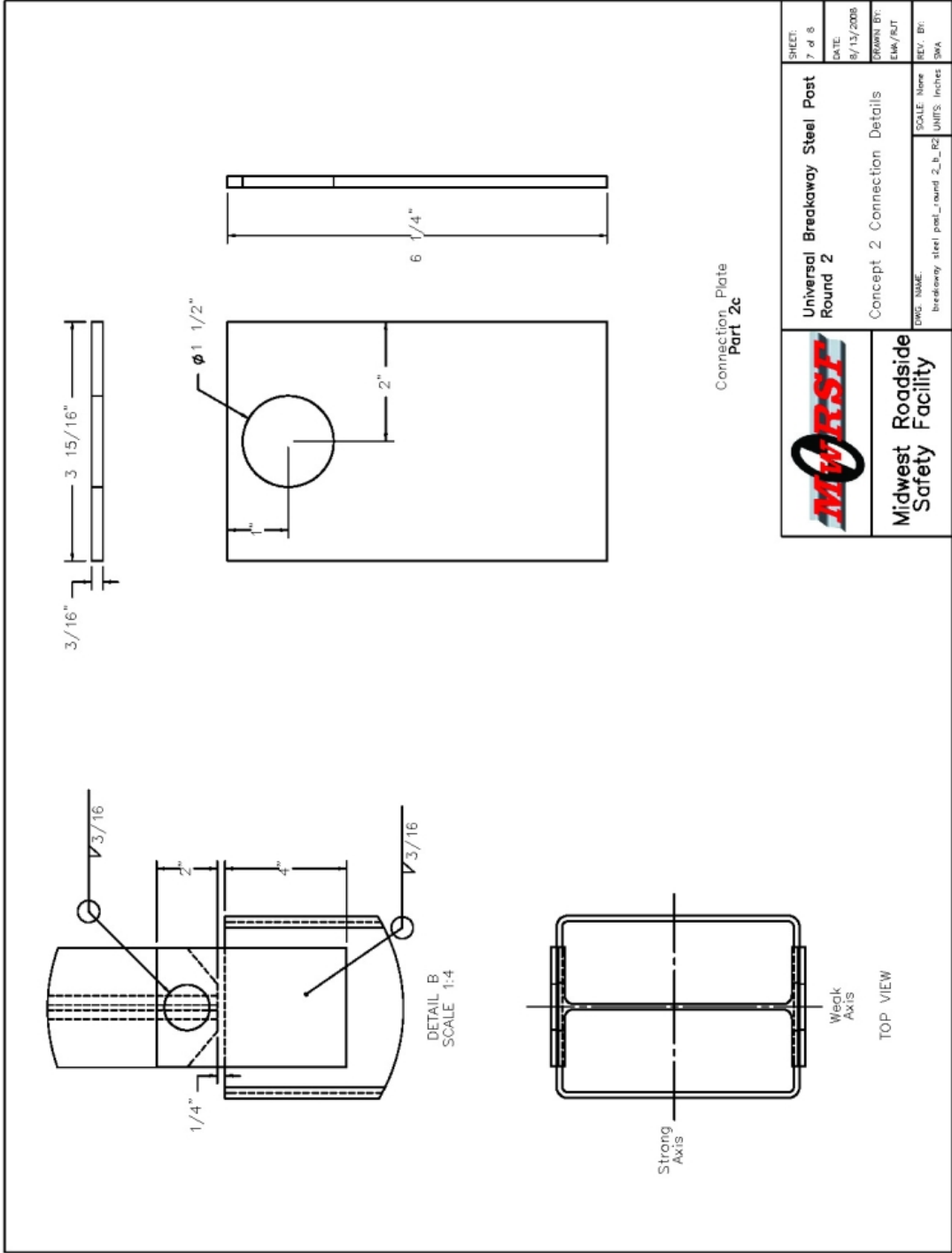
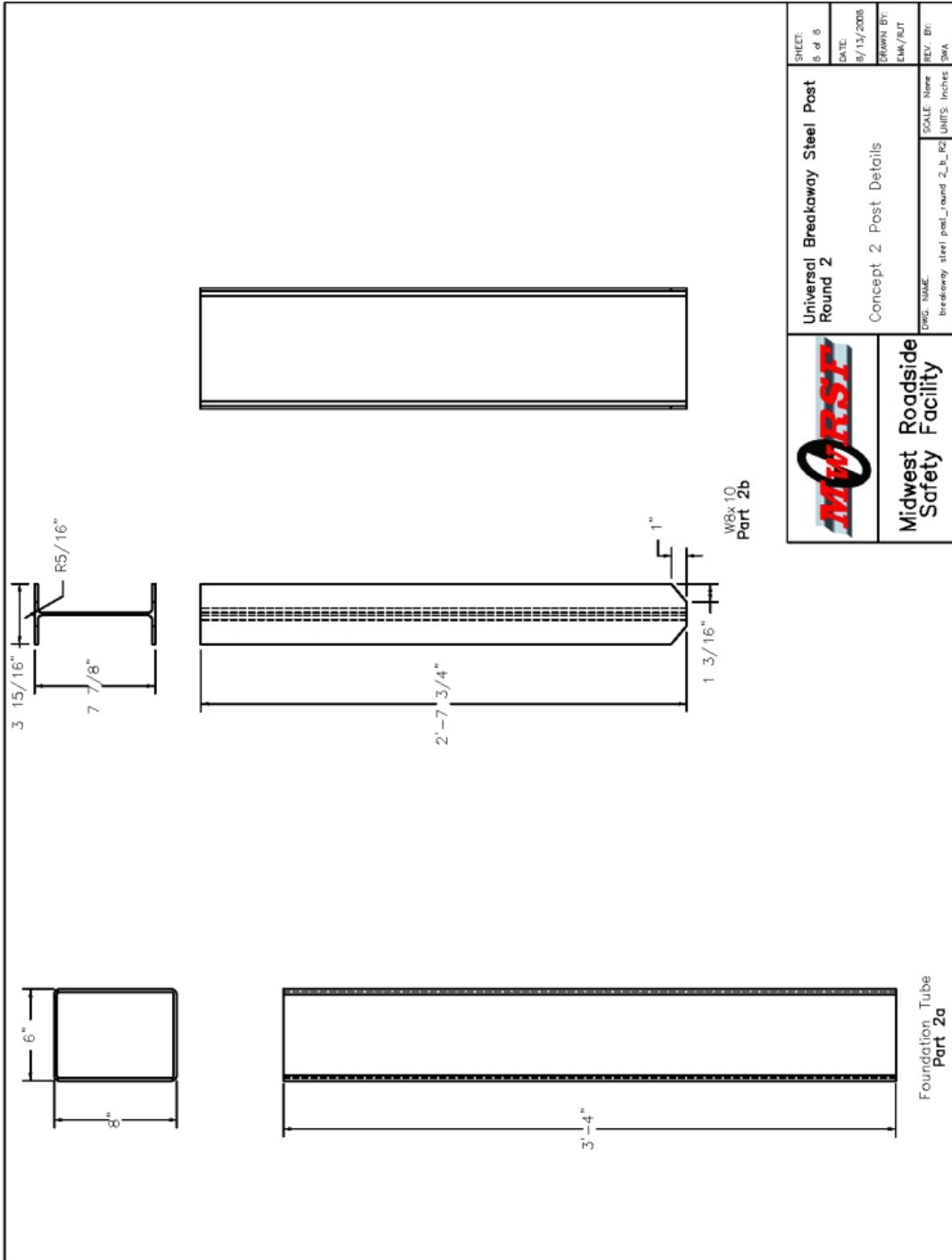


Figure 73. Revised Circular Fillet Weld Design Details



**Figure 74. Revised Circular Fillet Weld Design Details**




	Universal Breakaway Steel Post Round 2	SHEET: 8 of 8
	Concept 2 Post Details	DATE: 8/13/2008
Midwest Roadside Safety Facility	DWG. NAME: breakaway_steel_post_round_2_b.rvt	DRAWN BY: ELW/PJT
	SCALE: None	REV. BY: BWA
	UNITS: Inches	

Figure 75. Revised Circular Fillet Weld Design Details

## 6.4 Equipment and Instrumentation

The equipment and instrumentation used in the second round of bogie tests was largely the same as that used in the first round. The only differences were in the accelerometers used and in the methodology of auguring holes in the standard strong soil.

Similar to tests UBSP-1 through UBSP-8, the EDR-3 accelerometer was used for every test, provided accurate results, and was used for the results reported. For tests UBSP-9 through 11, the data acquisition system used the DTS accelerometer system, similar to the first round of bogie testing. The difference was in tests UBSP-12 and UBSP-13, where an EDR-4 accelerometer replaced the DTS unit. The tri-axial, piezoresistive, accelerometer system Model EDR-4M6 with a range of  $\pm 200$  g's was developed by Instrumented Sensor Technology (IST) of Okemos, Michigan and was mounted on the frame of the bogie near its center of gravity. Data sampling occurred at 10,000 Hz with a Butterworth low-pass filter with a -3dB cut-off frequency and a 1,500 Hz anti-aliasing filter.

The other equipment difference involved the hole size augured out of the soil testing pit. In tests UBSP-12 and UBSP-13, holes measuring 36 in. (914 mm) in diameter and deep enough to accommodate the 40 in. (1,016 mm) embedment depth were augured into the test pit. A 24-in. (610-mm) diameter hole was used previously in tests UBSP-1 through UBSP-11. The reason for the change was to reduce inconsistencies in the soil strength observed in the previous bogie testing.

The end of the test was determined in the same manner as used in the first round of bogie testing. The recorded acceleration data was also processed in the same manner as that recorded in the first round of bogie testing.

## **6.5 Round 2 Bogie Testing Results**

The accelerometer data was processed for each test in order to obtain acceleration, velocity, and displacement curves, as well as force versus deflection and energy versus deflection curves. This section discusses those results for the EDR-3 accelerometer. Using EDR-3 data was consistent with the first round of bogie testing. Individual test results are provided in Appendix A.

The following sections discuss the dynamic behaviors and results for test nos. UBSP-9 through UBSP-13. Conclusions regarding the performance of the different post concepts are discussed in Section 6.7.

### **6.5.1 Test UBSP-9 – Fracturing Bolt**

Test UBSP-9 was a strong-axis impact at 0 degrees on the fracturing bolt concept embedded in standard strong soil. The force and energy data are shown in Figures 76 and 77, respectively. Time-sequential photographs for this test are shown in Figure 78. Upon impact, the post began to rotate in the soil until the impact-side bolts broke in tension at approximately 30 ms. After the bolts broke, the post offered little resistance, and thus, the bogie head lost contact with the post from approximately 34 ms until 58 ms. The bogie regained contact with the post from 58 ms until 70 ms, when the non-impact-side bolts fractured and broke away. However, there was little resistance, and the post was pushed over to the ground. The only deformation in the post occurred to the bolts and washers. The bolts tended in break with either a level or 45 degree plane, and some impact-side washers were deformed from compression between the nuts, bolt heads, and the base plates. Post-impact images can be seen in Figure 79.

As seen in the force versus deflection curve in Figure 76 and the energy versus deflection curve in Figure 77, the fracturing bolt concept performed sufficiently by breaking at a peak load of 11.0 kips (48.9 kN) and absorbing energy up until the peak load was reached. The only issue was one of the impact-side nuts stripped off of the bolt instead of the bolt fracturing. This behavior was unexpected and may have caused premature failure at the 11.0 kips (48.9 kN) peak load. It was decided to rerun this strong-axis test on the fracturing bolt concept to ensure that the nut failure did not cause any unrealistic behavior. The results from this second test can be seen in test UBSP-13, as shown in Section 6.5.5. Even with the nut stripping, the post did break away as desired.

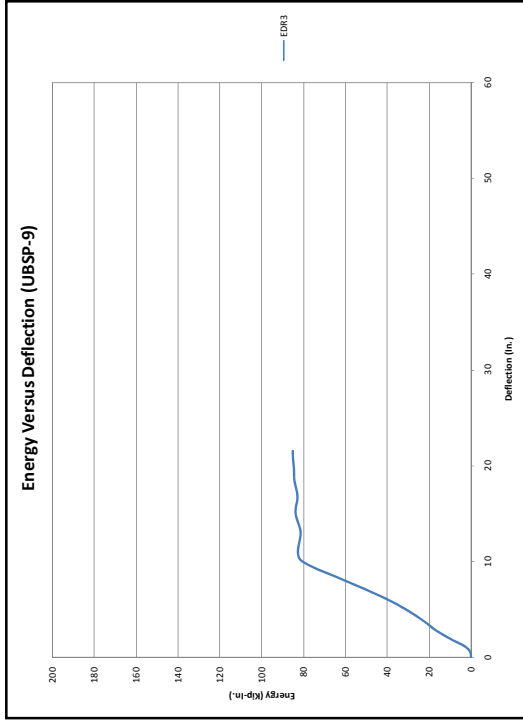


Figure 77a. Energy versus Deflection Curve for UBSP-9 - English

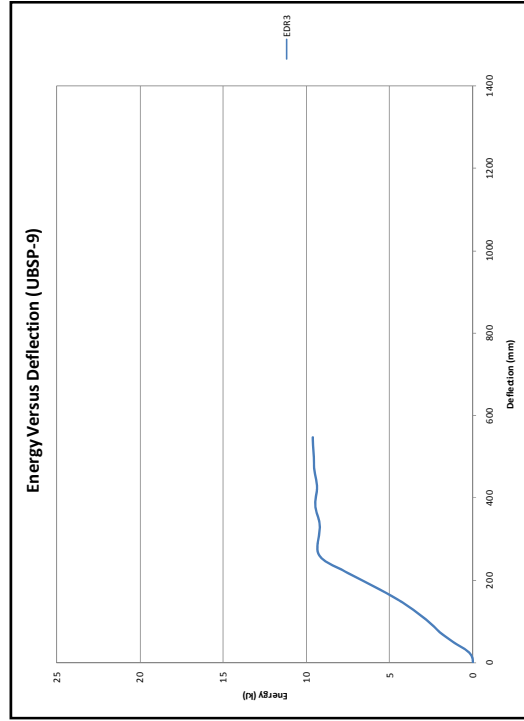


Figure 77b. Energy versus Deflection Curve for UBSP-9 - Metric

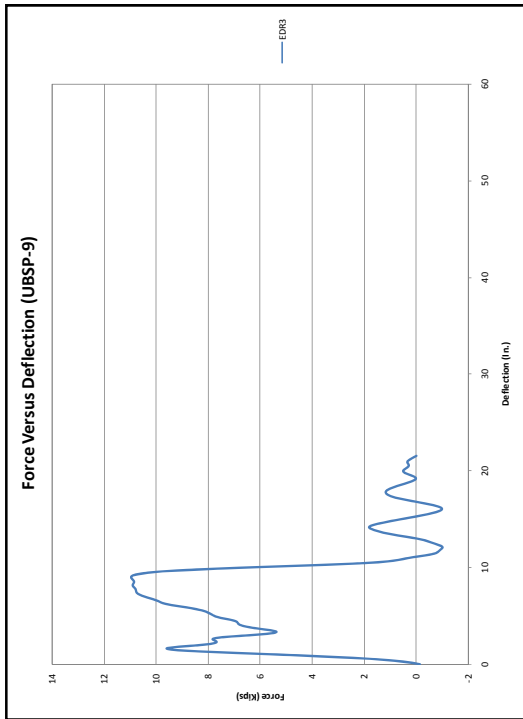


Figure 76a. Force versus Deflection Curve for UBSP-9 - English

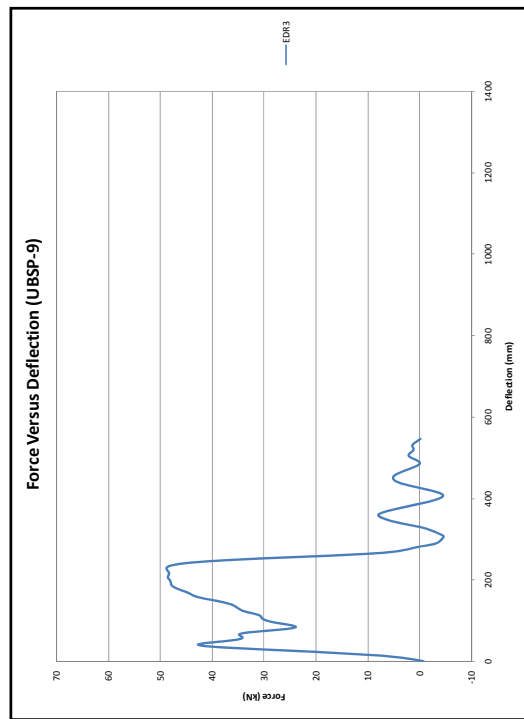


Figure 76b. Force versus Deflection Curve for UBSP-9 - Metric

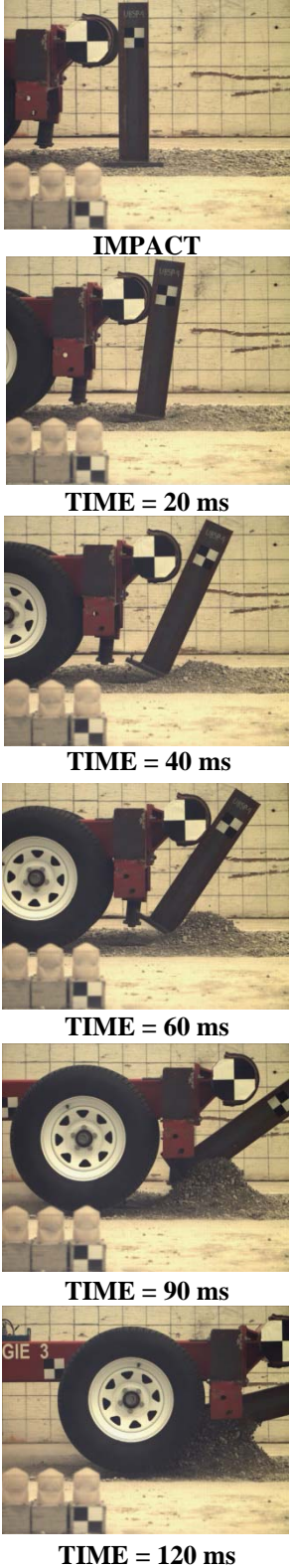


Figure 79. Post-Impact Images of UBSP-9

Figure 78. Time Sequential Photographs, Test UBSP-9



### **6.5.2 Test UBSP-10 – Fracturing Bolt**

Test UBSP-10 was a weak-axis impact at 90 degrees on the fracturing bolt concept embedded in standard strong soil. The force and energy data are shown in Figures 80 and 81, respectively. Time-sequential photographs are shown in Figure 82. The post began to immediately rotate in the soil until the impact-side bolts fractured in tension at approximately 14 ms. Next, the non-impact-side bolts broke at approximately 24 ms, thus causing the post to lose its resistance and contact with the bogie at 32 ms.

As seen in the force versus deflection curve provided in Figure 80, the fracturing bolt broke with a peak force level of 6.42 kips (28.6 kN), close to the 6 kips (26.7 kN) targeted in a weak-axis direction. As desired, the post did not absorb significant energy, as shown in Figure 81. The only post deformation occurred to the bolts and washers. The bolts again tended to break in either a level or 45 degree plane, and some washers were deformed from compression between the nuts, bolt heads, and the base plates. Post-impact images can be seen in Figure 83.

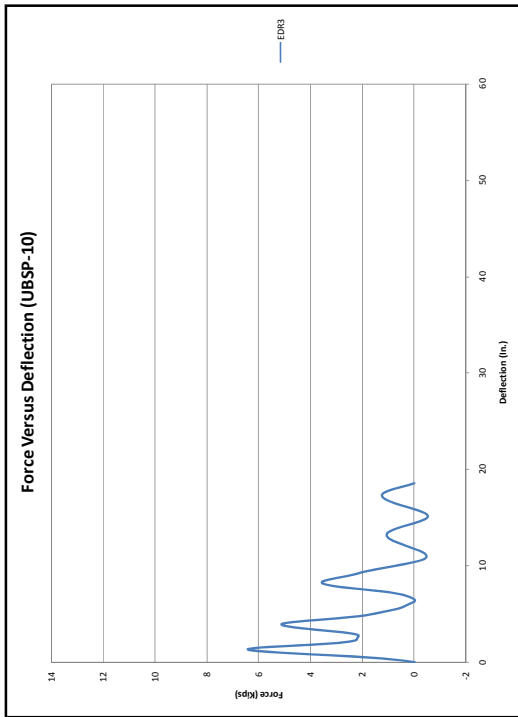


Figure 80a. Force versus Deflection Curve for UBSP-10 - English

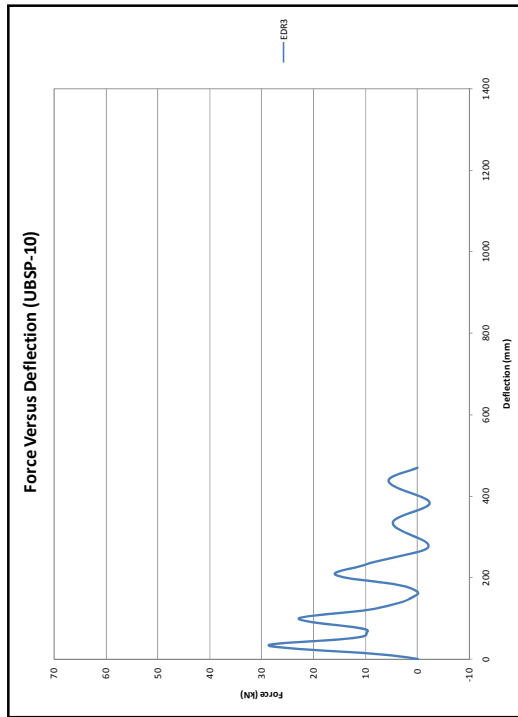


Figure 80b. Force versus Deflection Curve for UBSP-10 - Metric

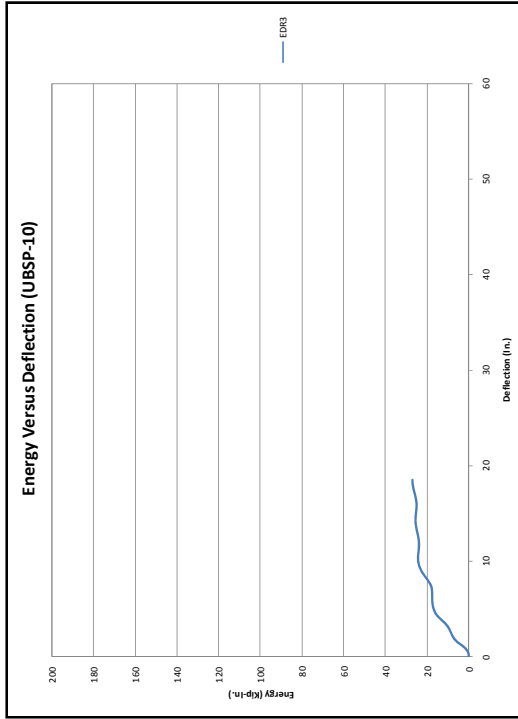


Figure 81a. Energy versus Deflection Curve for UBSP-10 - English

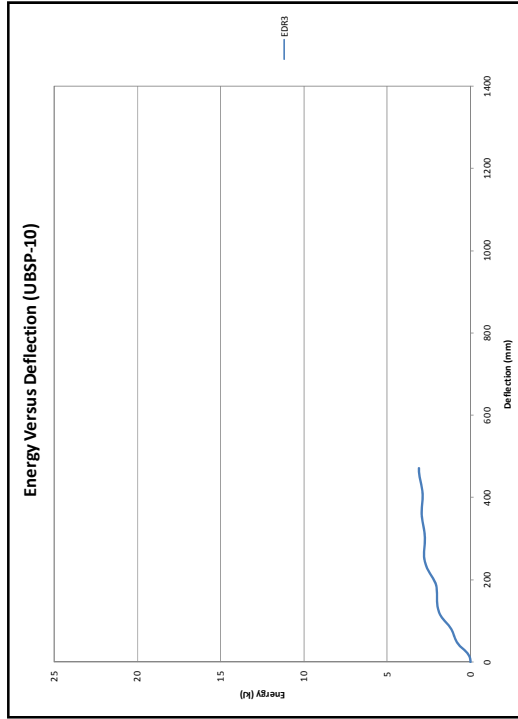


Figure 81b. Energy versus Deflection Curve for UBSP-10 - Metric



**IMPACT**



**TIME = 20 ms**



**TIME = 40 ms**



**TIME = 60 ms**



**TIME = 90 ms**



**TIME = 120 ms**

**Figure 82. Time Sequential Photographs, Test UBSP-10**



**Figure 83. Post-Impact Images of UBSP-10**

### **6.5.3 Test UBSP-11 – Circular Fillet Weld**

Test UBSP-11 was a weak-axis impact at 90 degrees on the circular fillet weld concept embedded in standard strong soil. The force and energy data are shown in Figures 84 and 85, respectively. Time-sequential photographs are shown in Figure 86. Upon impact, the post began to rotate immediately in soil. At approximately 32 ms, the circular fillet welds began to fracture, and the post began to rotate over to the ground. Eventually, the post lost contact with the bogie head at approximately 100 ms when the bogie overrode the post. Although both fillet welds did fracture, the post got caught up on one of the welds and did not break away cleanly, as desired. The welds were the only visible post damage, as seen in the post-impact images in Figure 87.

Similar to the fracturing bolt concept evaluated in test UBSP-10 using a weak-axis impact, this weak-axis test revealed that the circular fillet weld broke at low peak force level and did not absorb significant energy, as desired. The force versus deflection curve and energy versus deflection curve for test UBSP-11 are provided in Figures 84 and 85, respectively. The only undesired behavior was that the post did not break away cleanly.

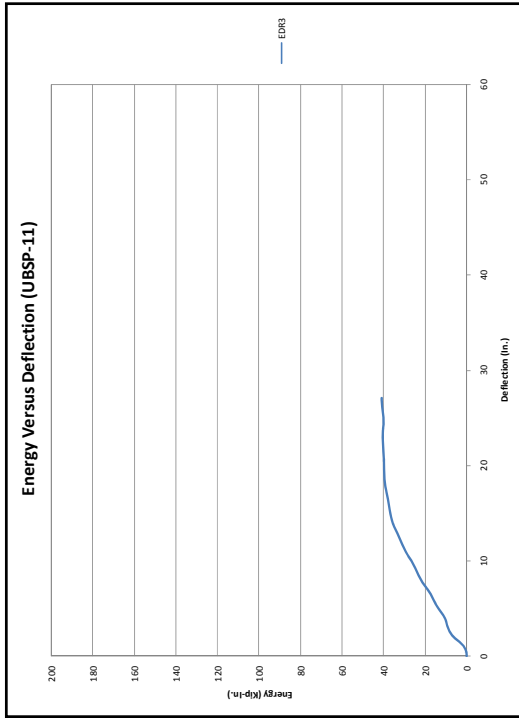


Figure 85a. Energy versus Deflection Curve for UBSP-11 - English

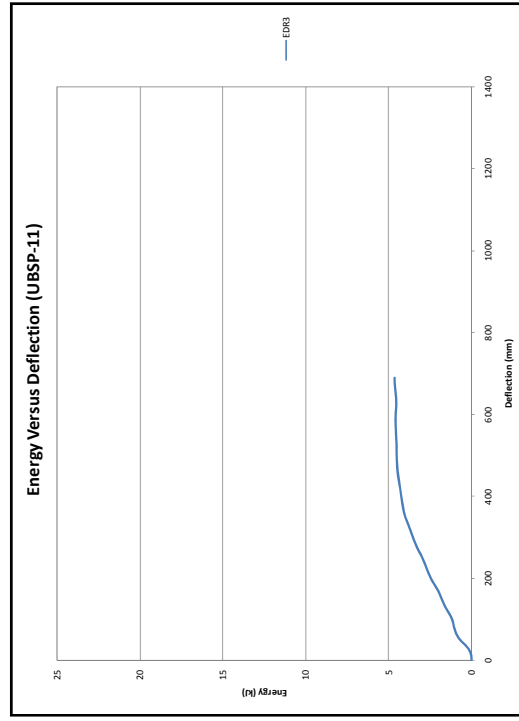


Figure 85b. Energy versus Deflection Curve for UBSP-11 - Metric

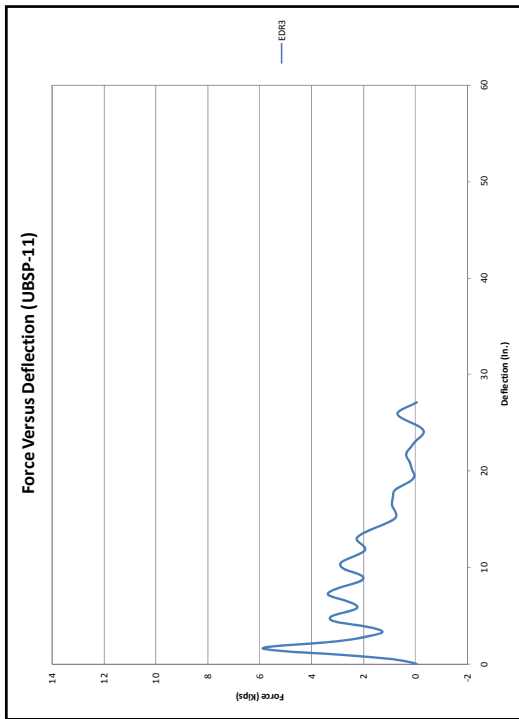


Figure 84a. Force versus Deflection Curve for UBSP-11 - English

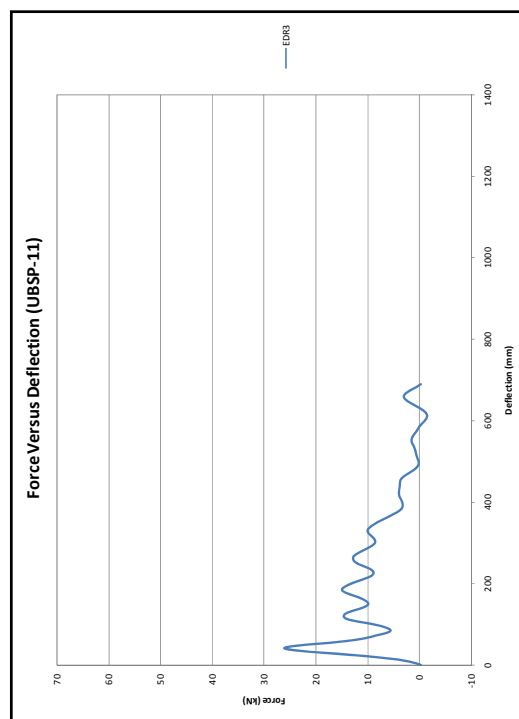


Figure 84b. Force versus Deflection Curve for UBSP-11 - Metric



**IMPACT**



**TIME = 20 ms**



**TIME = 40 ms**



**TIME = 60 ms**



**TIME = 90 ms**



**TIME = 120 ms**

**Figure 86. Time Sequential Photographs, Test UBSP-11**



**Figure 87. Post-Impact Images of UBSP-11**

#### **6.5.4 Test UBSP-12 – Circular Fillet Weld**

Test UBSP-12 was a strong-axis impact at 0 degrees on the circular fillet weld concept embedded in standard strong soil. The force and energy data are shown in Figures 88 and 89, respectively. Time-sequential photographs for this test are shown in Figure 90. Upon impact, the post began to rotate immediately and continued to rotate through the soil until approximately 200 ms when the bogie ramped and rode over the post. There was no sign of the circular fillet weld breaking away, but the splice plates yielded, as seen in post-impact images in Figure 91. It could not be determined when the splice plates began yielding due to the soil interfering with the camera views.

This bogie test demonstrated the behavioral inconsistencies of posts embedded in standard strong soil. As seen in the energy versus deflection curve in Figure 89, the circular fillet weld did not break away; instead, it rotated through the soil and absorbed a large amount of energy. Although this behavior was not expected, the post actually performed as desired for this soil strength. The post was designed to break away at a peak load of 12 kips (53 kN). As seen in Figure 88, the post rotated through the soil at an average force level of 6 kips (27 kN). Since the soil was weaker than expected, the post rotated through the soil as desired, although the force levels never came close to the 12 kip (53 kN) range. The unexpected reduction in the soil strength can be attributed to inconsistencies in the soil compaction and variations in the standard strong soil.

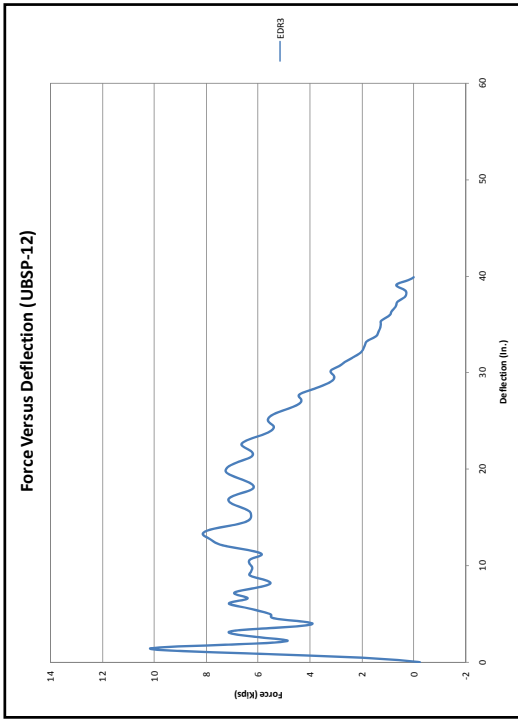


Figure 88a. Force versus Deflection Curve for UBSP-12 - English

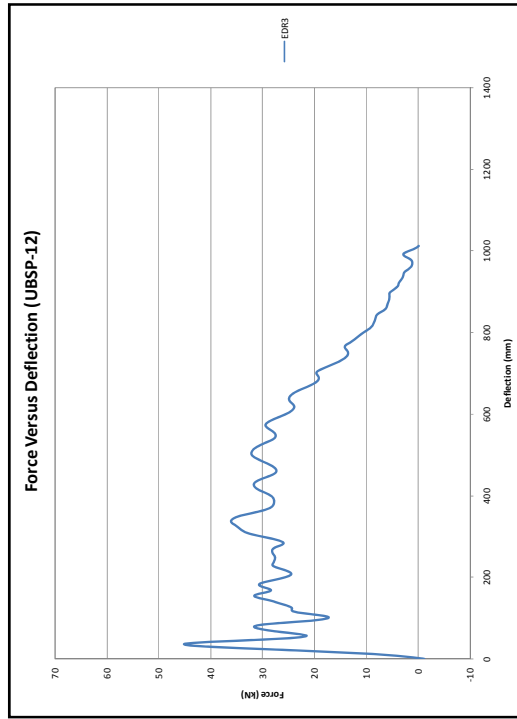


Figure 88b. Force versus Deflection Curve for UBSP-12 - Metric

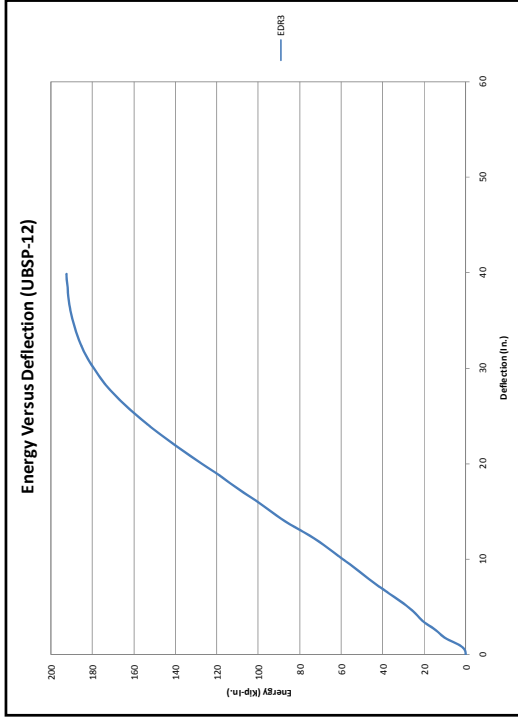


Figure 89a. Energy versus Deflection Curve for UBSP-12 - English

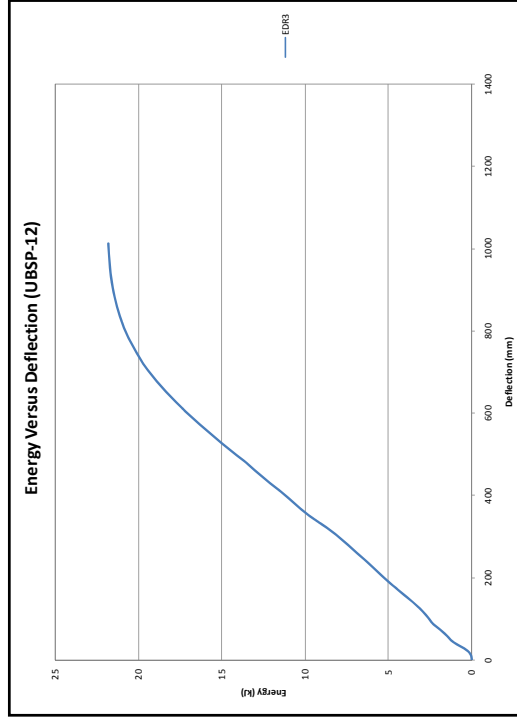
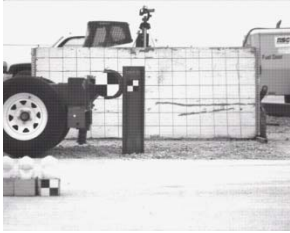
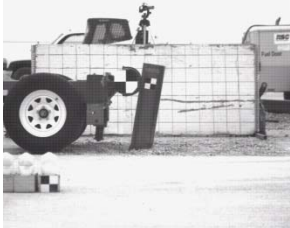


Figure 89b. Energy versus Deflection Curve for UBSP-12 - Metric

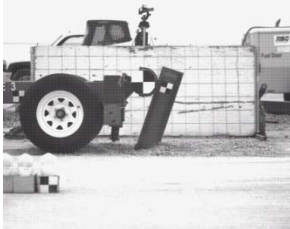




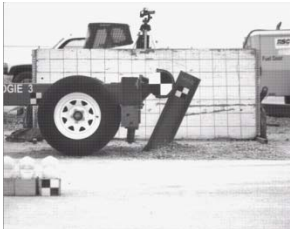
**IMPACT**



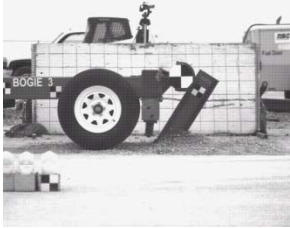
**TIME = 20 ms**



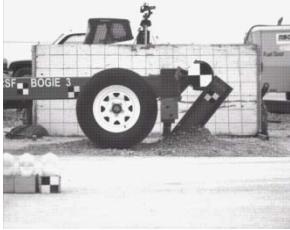
**TIME = 40 ms**



**TIME = 60 ms**



**TIME = 90 ms**



**TIME = 120 ms**

**Figure 90. Time Sequential Photographs, Test UBSP-12**



**Figure 91. Post-Impact Images of UBSP-12**

### **6.5.5 Test UBSP-13 – Fracturing Bolt**

Test UBSP-13 was a strong-axis impact at 0 degrees on the fracturing bolt concept embedded in standard strong soil. The force and energy data are shown in Figures Figure and Figure , respectively. As stated earlier, this test was a repeat of test UBSP-9 to ensure that the nut failure in UBSP-9 did not cause any unrealistic behavior. A comparison of tests UBSP-9 and UBSP-13 is provided in Section 6.6. Time-sequential photographs of test UBSP-13 are shown in Figure 94. Upon impact, the post began to rotate immediately through the soil. As the post continued to rotate in the soil, there was no sign of any fracture or deformation to the bolts or post, and the post remained in contact with the bogie head until approximately 198 ms when the bogie rode over the post.

Similar to test UBSP-12, this test showed the behavioral inconsistency of posts embedded in strong soil. As seen in the force versus deflection curve provided in Figure , the post rotated through the soil at approximately 5 kips (22 kN) and did not come close to the desired breakaway force level of 12 kips (53 kN). The post did absorb significant energy, as seen in Figure . Again, the unexpected reduction in soil strength can be attributed to inconsistencies in the compaction of the standard strong soil. The post did not break away, but it did perform as desired for this soil strength. Post-impact images of the undamaged post rotated over in the soil can be seen in Figure 95.

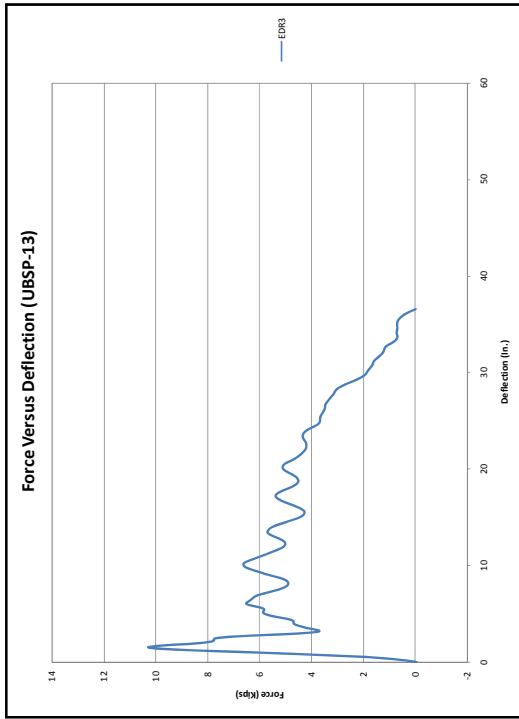


Figure 92a. Force versus Deflection Curve for UBSP-13 - English

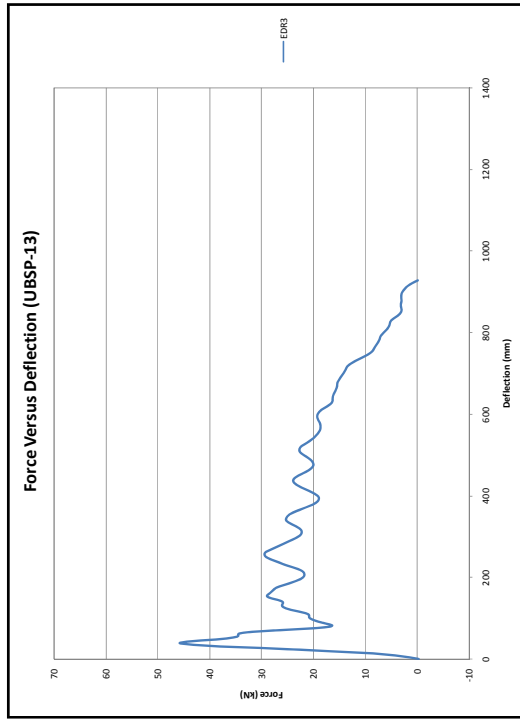


Figure 92b. Force versus Deflection Curve for UBSP-13 - Metric

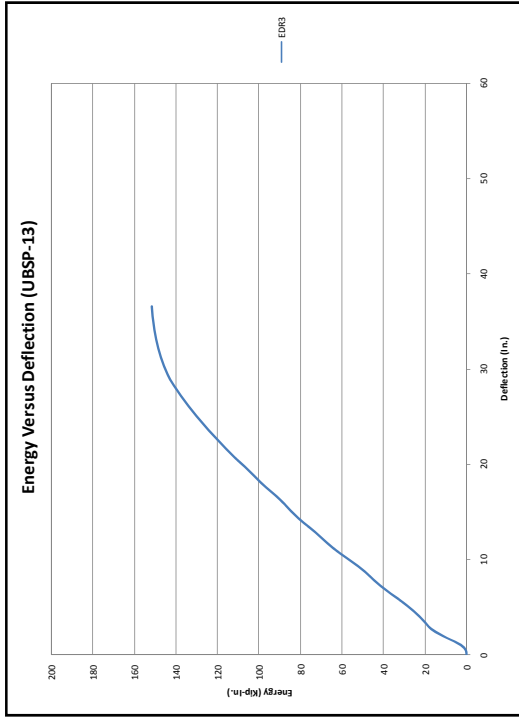


Figure 93a. Energy versus Deflection Curve for UBSP-13 - English

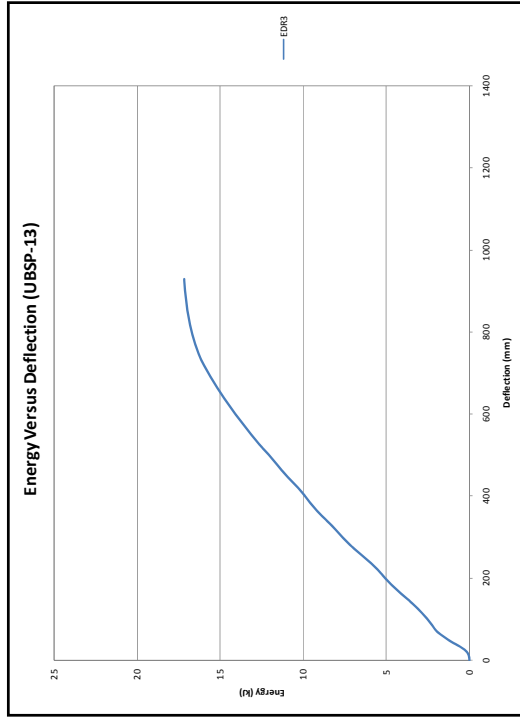
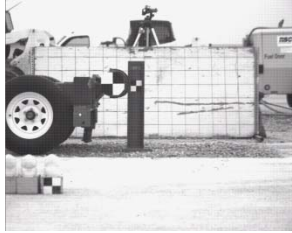
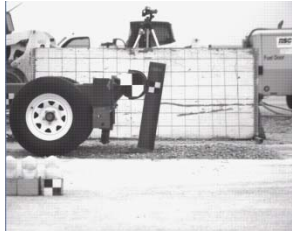


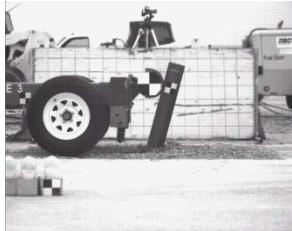
Figure 93b. Energy versus Deflection Curve for UBSP-13 - Metric



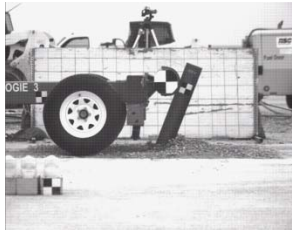
**IMPACT**



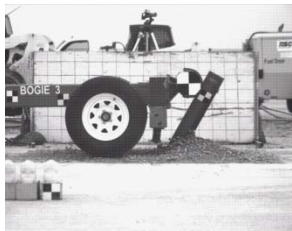
**TIME = 20 ms**



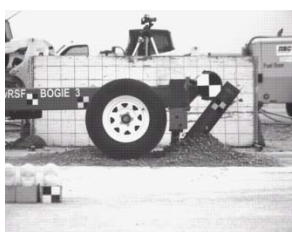
**TIME = 40 ms**



**TIME = 60 ms**



**TIME = 90 ms**



**TIME = 120 ms**

**Figure 94. Time Sequential Photographs, Test UBSP-13**



**Figure 95. Post-Impact Images of UBSP-13**

## **6.6 Test UBSP-9 versus Test UBSP-13**

Both tests UBSP-9 and UBSP-13 consisted of a strong-axis impact at 0 degrees on the fracturing bolt concept. After the nut stripped off of the double end stud in test UBSP-9, it was decided to rerun the test in order to ensure there was no undesired behavior from this nut failure. As stated previously, the only difference between the two tests pertained to the type of fastener used. In test UBSP-9, a 3/8-in. (9.5-mm) diameter, grade 5, double end stud was used. In test UBSP-13, a 3/8-in. (9.5-mm) diameter, grade 5, hex head bolt was used. Since the bolt and double end stud were the same size and grade, both fasteners should have identical behavior and strength. As noted previously, the change was made in order to reduce the number of pieces and provide a simpler design to install.

From the force and energy versus deflection curves shown in Figures 96 and 97, respectively, the two nearly identical tests had totally different behavior. In test UBSP-9, the fracturing bolt post rotated through the soil at approximately 11 kips (49 kN). However, in test UBSP-13, the post rotated through the soil at approximately 5 kips (22 kN). Although there were inconsistencies with the soil compaction, the fracturing bolt post performed as desired in both tests. The post broke away when the strong soil had more compaction, and it absorbed energy and rotated through the less compacted soil, as desired. The difference in these tests clearly shows the inconsistency when dealing with soil and also illustrates the attention that needs to be given to the compaction and potential variability of the standard strong soil.

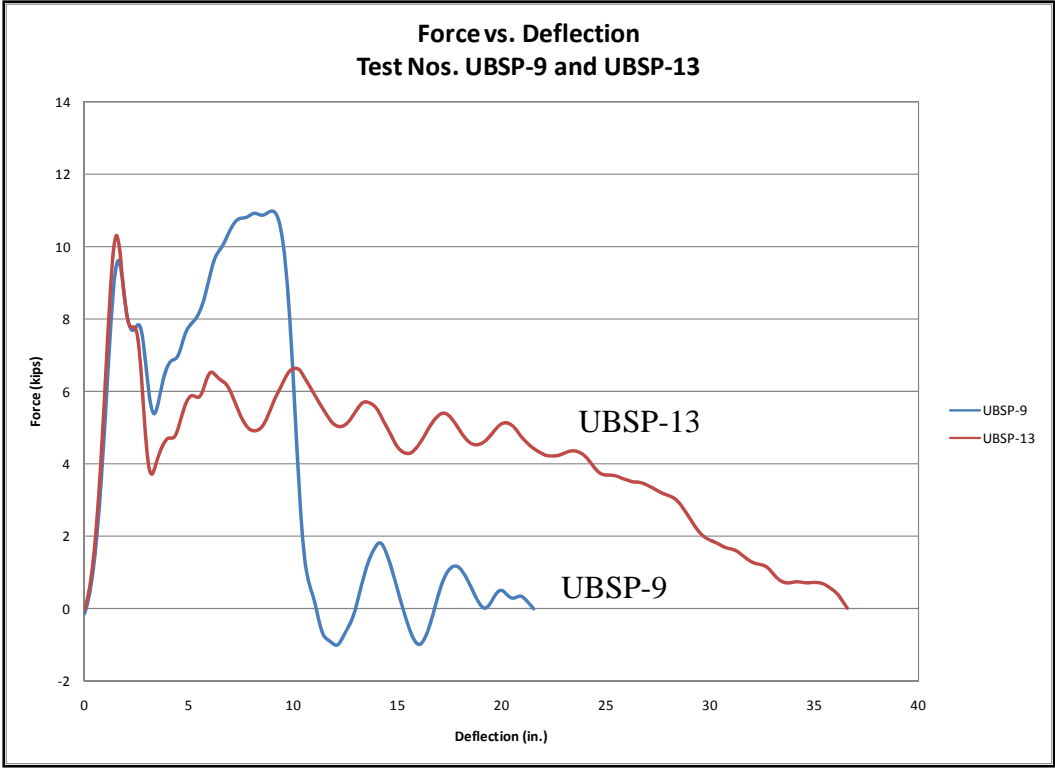


Figure 96a. Force versus Deflection Curves for UBSP-9 and 13 – English

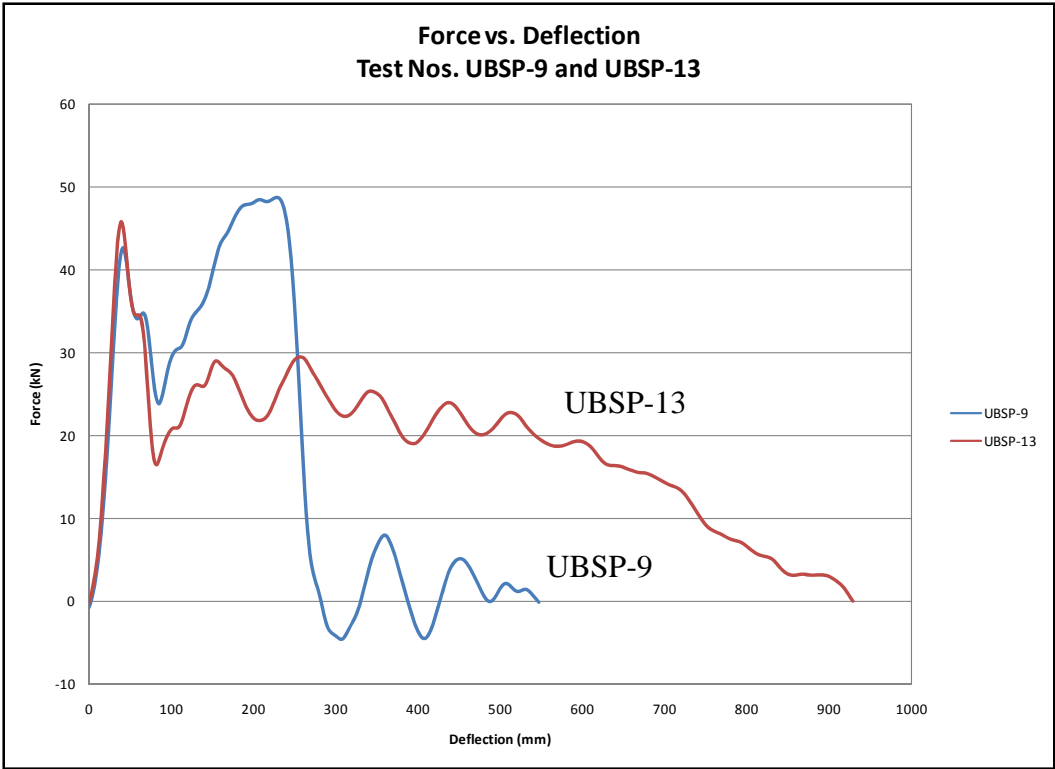


Figure 96b. Force versus Deflection Curves for UBSP-9 and 13 – Metric

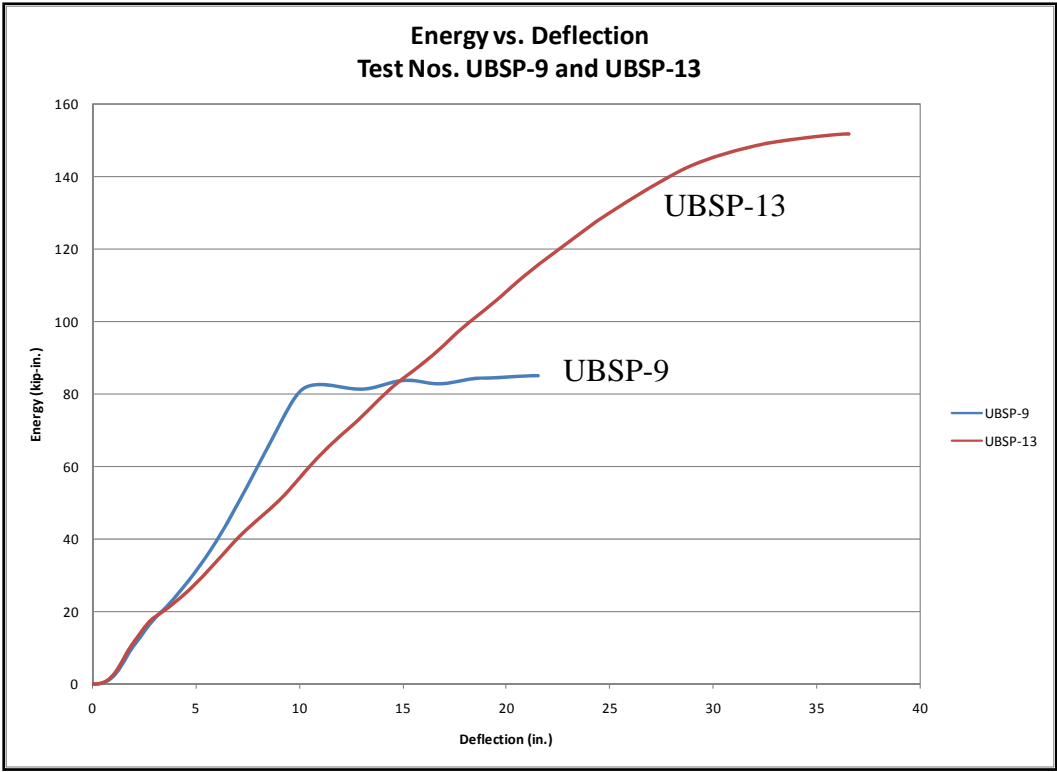


Figure 97a. Energy versus Deflection for UBSP-9 and 13 – English

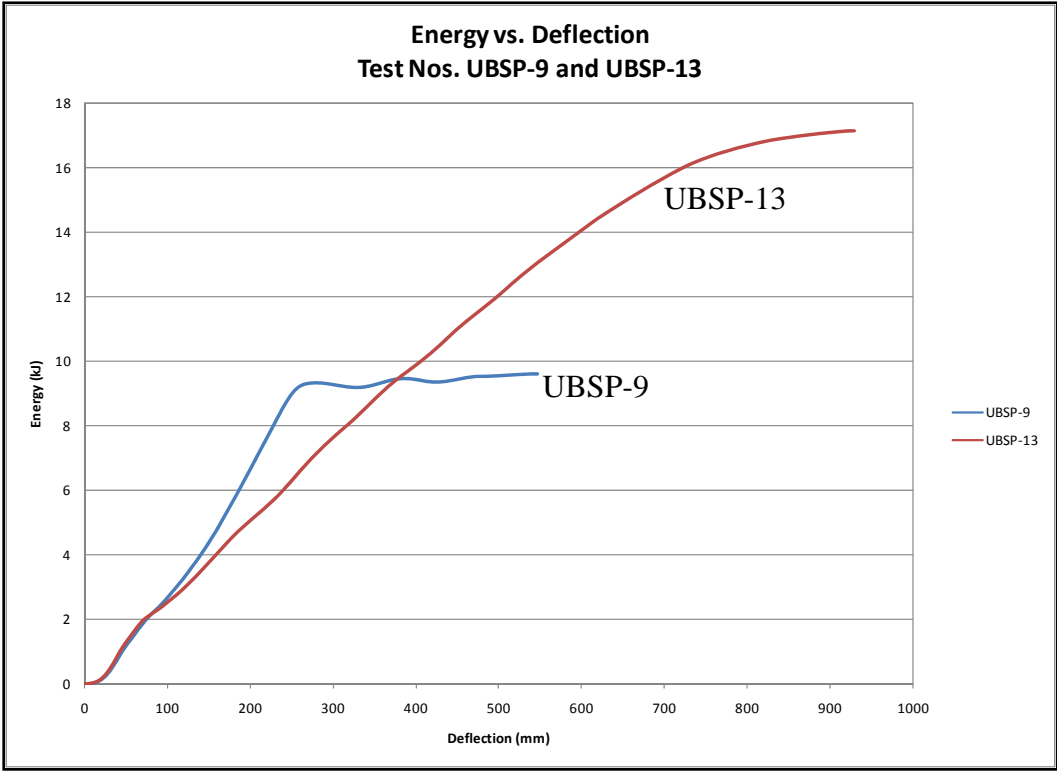


Figure 97b. Energy versus Deflection for UBSP-9 and 13 – Metric

## 6.7 Round 2 Summary and Conclusions

The second round of bogie testing consisted of five tests on two different breakaway concepts. After reviewing the results from all of the tests, the preferred concept was determined for the Universal Breakaway Steel Post. A summary of the second round of bogie testing is provided in Table 12.

First, all three tests on the fracturing bolt concept showed encouraging results. In test UBSP-9, the fracturing bolt performed as desired in a strong axis impact by breaking away at a peak load of 11.0 kips (49 kN). The only issue was that one nut stripped off instead of allowing the bolt to fracture. As a result, the evaluation was rerun in test UBSP-13, which was also a strong-axis impact test that showed desirable but unexpected behavior. There was an issue with the compaction of the soil, so the post just rotated through the soil at a low force level. However, the post performed as desired by not breaking away in the weaker soil. For test UBSP-10, the fracturing bolt concept was impacted in the weak axis and also performed as desired. The post had a peak force of 6.42 kips (28.6 kN), which is close to the desired 6 kip (26.7 kN) level.

There were two tests on the circular fillet weld that both performed adequately. In test UBSP-11, the circular fillet weld was impacted using the weak axis of bending, and the weld broke as desired. Even though the welds broke at 5.87 kips (26.1 kN) near the desired 6 kip (26.7 kN) level, one weld did not break away cleanly as it got hung up on the steel plates. For test UBSP-12, the circular fillet weld was impacted using the strong axis of bending, but this test showed the inconsistency and variation with standard strong soil. The post did perform as desired by rotating through the soil, but only since the strength of the soil was weaker than



expected. As a result, the actual breaking strength of the circular fillet weld concept in the strong axis was still an unknown.

After reviewing the results from the five tests on the two different concepts, it was decided that the fracturing bolt concept was the best option for the Universal Breakaway Steel Post, even though the circular fillet weld design did show some promise. The decision was based on several factors, including that the fracturing bolt post had already proven that it could break away cleanly in both impact directions. Also, there was a concern with the consistency of weld failures in the circular fillet weld concept. Another factor was that the fracturing bolt concept no longer had patent issues, while the circular fillet weld has possible patent concerns.

Once the fracturing bolt concept was selected for use as the Universal Breakaway Steel Post, it was necessary to demonstrate that this concept accurately represents the CRT wood post embedded in soil. As a result, CRT wood post testing in standard strong soil was deemed necessary for comparing to fracturing bolt concept that was previously tested in the strong soil. No previous research was found regarding the testing of CRT wood posts in soil. Thus, six bogie tests were later performed to assure that the fracturing bolt behavior matched that of the CRT wood posts placed in soil.

**Table 12a. Summary of Round 2 Bogie Testing Results – English**

Test No.	Impact Velocity (mph)	Failure Type	Initial Peak Force		Initial Stiffness (kips/in.)	Peak Force		Total Energy	
			Displacement (in.)	Force (kips)		Displacement (in.)	Force (kips)	Displacement (in.)	Energy (kip-in.)
UBSP-9	19.9	Post Failure	1.63	9.60	5.9	9.01	11.0	21.5	85.1
UBSP-10	19.1	Post Failure	1.36	6.42	4.7	1.36	6.42	18.5	27.3
UBSP-11	19.7	Post Failure	1.62	5.87	3.3	1.62	5.87	27.1	40.9
UBSP-12	18.7	Post Rotation	1.43	10.1	7.1	1.43	10.1	39.8	192.7
UBSP-13	18.7	Post Rotation	1.54	10.3	6.7	1.54	10.3	36.6	151.7

**Table 12b. Summary of Round 2 Bogie Testing Results – Metric**

Test No.	Impact Velocity (km/h)	Failure Type	Initial Peak Force		Initial Stiffness (kN/mm)	Peak Force		Total Energy	
			Displacement (mm)	Force (kN)		Displacement (mm)	Force (kN)	Displacement (mm)	Energy (kJ)
UBSP-9	19.9	Post Failure	41.4	42.7	1.0	228	48.9	546	9.61
UBSP-10	19.1	Post Failure	34.5	28.6	0.82	34.5	28.6	470	3.08
UBSP-11	19.7	Post Failure	41.1	26.1	0.58	41.1	26.1	688	4.62
UBSP-12	18.7	Post Rotation	36.3	44.9	1.2	36.3	44.9	1011	21.8
UBSP-13	18.7	Post Rotation	39.1	45.8	1.2	39.1	45.8	930	17.1

## **7 WOOD CRT POST BOGIE TESTING IN SOIL**

### **7.1 Purpose**

In this round of bogie testing, six tests were run on CRT wood posts embedded in standard strong soil. Previously, bogie testing was performed on CRT posts placed in a rigid sleeve to determine the wood post properties. However, these tests were performed with the CRT wood posts embedded 40 in. (1,016 mm) in standard strong soil to determine post-soil behavior. The results from this testing will be compared to those obtained for the fracturing bolt concept that also was tested in the standard strong soil.

### **7.2 Scope**

For this round of bogie testing, the wood posts were embedded 40 in. (1,016 mm) in standard strong soil. The test setup was identical to both the first and second round of bogie testing. The target test condition consisted of a 20 mph (32 km/h) impact speed occurring at the centerline of the bogie and at 24 7/8 in. (632 mm) above the ground. For tests UBSP-18 and UBSP-19, technical difficulties were encountered with the speed traps so the actual speed was not known. Thus, the target speed of 20 mph (32 km/h) was used for the analyses of tests UBSP-18 and UBSP-19. As shown in Table 13, a total of six tests were performed with two tests about the strong axis, weak axis, and at a diagonal angle at 45 degrees.

The 45-degree impact angle was chosen to be consistent with the previous CRT post testing in the rigid sleeve. This angle allowed for the evaluation of wood posts subjected to a biaxial loading condition. For vehicular impacts into the nose of the bullnose median barrier system, the posts in the curved section may be loaded at some oblique angle. As such, this testing

served to broaden the knowledge for wood post fracture and post-soil behavior due to a non-typical loading.

**Table 13. Test Matrix for Wood CRT Post Bogie Testing In Soil**

Test No.	Test Date	Speed		Impact Axis
		mph (km/h)	ft/s (m/s)	
UBSP-14	06-17-2008	19.1 (30.7)	28.0 (8.54)	Strong
UBSP-15	06-17-2008	20.5 (33.0)	30.1 (9.16)	Strong
UBSP-16	06-18-2008	20.2 (32.5)	29.6 (9.03)	Weak
UBSP-17	06-18-2008	20.6 (33.2)	30.2 (9.21)	Weak
UBSP-18	06-18-2008	20.0 (32.3)	29.3 (8.94)	45 Degrees
UBSP-19	06-19-2008	20.0 (32.3)	29.3 (8.94)	45 Degrees

### 7.3 Post Details

The posts evaluated in this round of bogie testing were identical to the CRT wood posts tested in the rigid sleeve and detailed in Chapter 3. Since wood is a highly variable material, all of the CRT wood posts were carefully documented. As shown in Table 14, the post dimensions, moisture content, mass (weight), ring density, and knots were all recorded. The post dimensions were measured at the top of the post. The moisture content was tested at 16 in. (406 mm) above ground line, at ground line, and at 20 in. (508 mm) below ground line with a pin type moisture meter [21]. It should be noted that the post used in test UBSP-14 had a considerable knot in a critical location.

### 7.4 Equipment and Instrumentation

The equipment and instrumentation used in this bogie testing was nearly identical to that used in the second round of bogie testing. The only difference was that tests UBSP-16 through UBSP-19 only used the EDR-3 accelerometer. In tests UBSP-14 and UBSP-15, both the EDR-3 and EDR-4 accelerometers were used, similar to the second round of bogie testing. Still, the

EDR-3 was used for all of the tests and for the results that are reported. Also, the test setup, end of test determination, and data processing were the same as that used in the first and second rounds of the bogie testing.

**Table 14a. CRT Wood Post Details – English**

Test No.	Post Dimensions (in.)		Moisture Content (%)			Weight (lbs)	Ring Density (rings/in.)	Knots
	@ Top	@ Bottom	16 in. Above Ground Line	Ground Line	20 in. Below Ground Line			
UBSP-14	5-7/8" x 7-7/8"	5-7/8" x 8-1/4"	9	11	12	70.2	4.5-5	Bad
UBSP-15	5-5/8" x 7-11/16"	5-3/4" x 7-3/4"	13	13	16	77.4	6.5-7	OK
UBSP-16	5-5/8" x 7-3/4"	5-3/4" x 7-3/4"	16	16	17	74.8	10	OK
UBSP-17	6-1/4" x 8-1/4"	6-1/4" x 8-1/4"	23	35	32	73.2	7	OK
UBSP-18	6-1/4" x 8-1/4"	6-3/8" x 8-3/8"	15	16	16	73.2	9	OK
UBSP-19	5-7/8" x 7-7/8"	5-3/8" x 7-7/8"	17	18	17	64.8	10	OK

**Table 14b. CRT Wood Post Details – Metric**

Test No.	Post Dimensions (mm)		Moisture Content (%)			Mass (kg)	Ring Density (rings/cm)	Knots
	@ Top	@ Bottom	406 mm Above Ground Line	Ground Line	508 mm Below Ground Line			
UBSP-14	149 x 200	149 x 210	9	11	12	31.8	1.8-2.0	Bad
UBSP-15	143 x 195	146 x 197	13	13	16	35.1	2.6-2.8	OK
UBSP-16	143 x 197	146 x 197	16	16	17	33.9	3.9	OK
UBSP-17	159 x 210	159 x 210	23	35	32	33.2	2.8	OK
UBSP-18	159 x 210	162 x 213	15	16	16	33.2	3.5	OK
UBSP-19	149 x 200	149 x 200	17	18	17	29.4	3.9	OK

## **7.5 Test Results for Wood CRT Posts in Soil**

The accelerometer data was processed for each test in order to obtain acceleration, velocity, and displacement curves, as well as force versus deflection and energy versus deflection curves. This section discusses those results for the EDR-3 accelerometer, which is consistent with the first and second rounds of the bogie testing. Individual test results are provided in Appendix A.

The following sections discuss the dynamic behaviors and results for test nos. UBSP-14 through UBSP-19. Also, the standard strong soil and a comparison to the results of the CRT wood posts in a rigid sleeve from Chapter 3 are both discussed in section 7.6.

### **7.5.1 Test UBSP-14 – Strong Axis (0 Degree) Impact on CRT Post**

Test UBSP-14 was a strong-axis impact at 0 degrees on the wood CRT post embedded in standard strong soil. The force and energy data are shown in Figures 98 and 99, respectively. Time-sequential photographs are shown in Figure 100. Approximately 10 ms after impact, the wood CRT post began to fracture on the tension side near the upper breakaway hole at ground level. The post continued to fracture as it was deflected by the bogie's impact head until the post lost all strength and lost contact with the bogie at 72 ms.

As shown in the post-impact images provided in Figure 101, the CRT wood post had a large knot located near the breakaway hole where the post fractured. This knot caused some unexpected results. As seen in Figure 98, this CRT wood post broke at a peak load of 8.3 kips (36.9 kN), which was less than the 12 kip (53.4 kN) load for which the post was predicted to break, as determined in rigid sleeve testing documented in Chapter 3. Also, the post broke away quite quickly, did not rotate through the soil, and did not absorb much energy, as provided in Figure 99. From the results, it is believed that the knot greatly affected the strength and behavior of the post, but it also showed the variability and inconsistency of wood material.



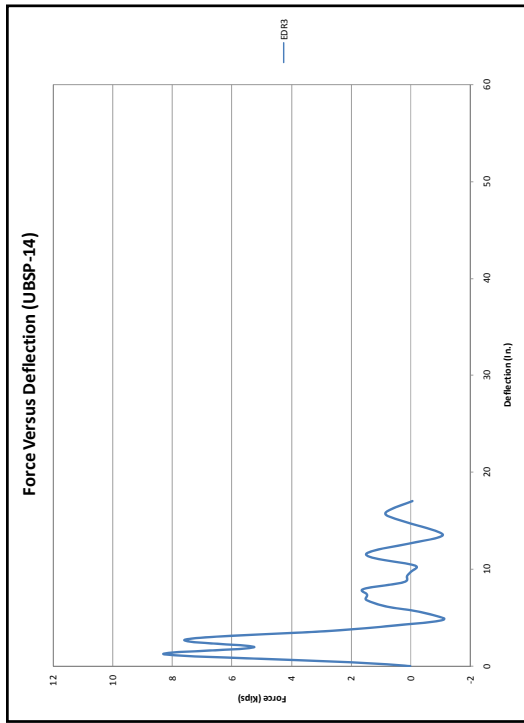


Figure 98a. Force versus Deflection Curve for UBSP-14 - English

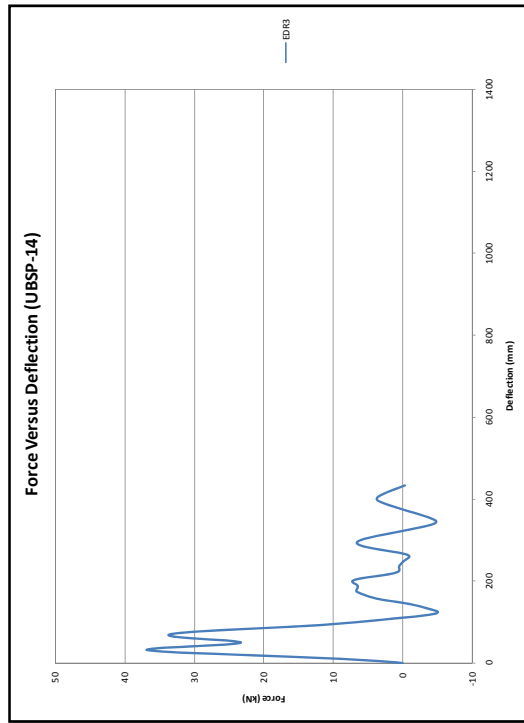


Figure 98b. Force versus Deflection Curve for UBSP-14 - Metric

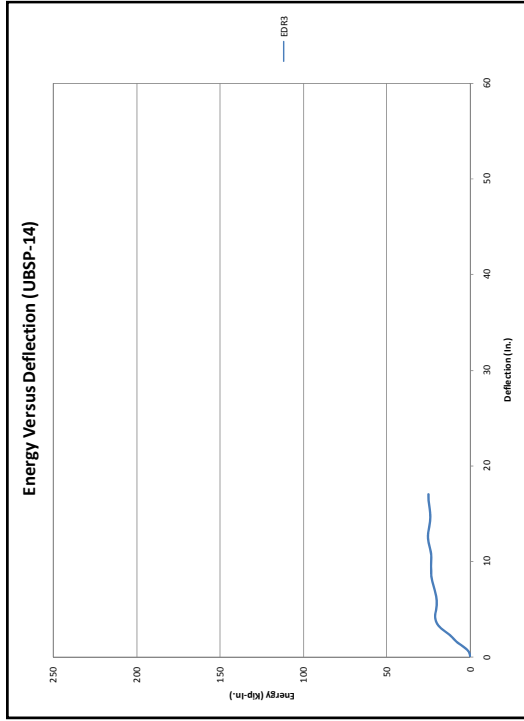


Figure 99a. Energy versus Deflection Curve for UBSP-14 - English

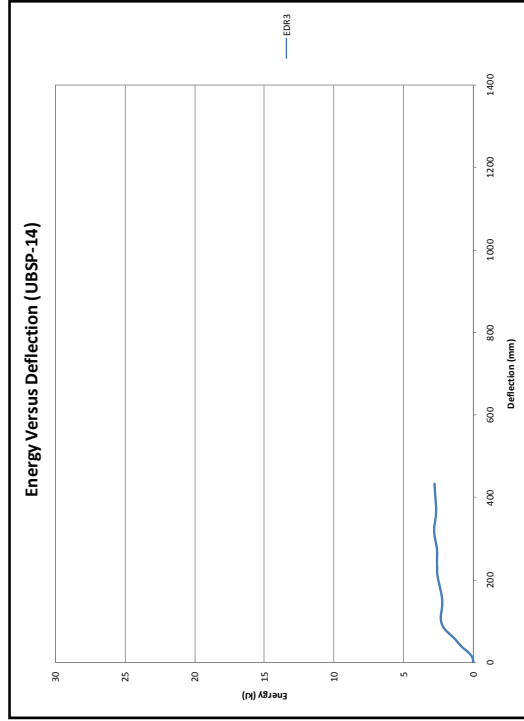
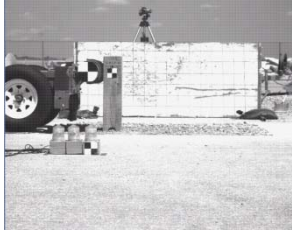
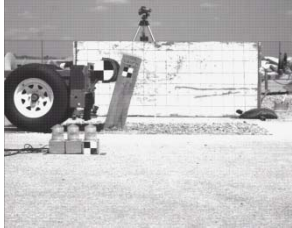


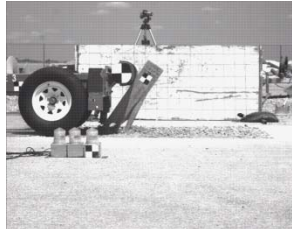
Figure 99b. Energy versus Deflection Curve for UBSP-14 - Metric



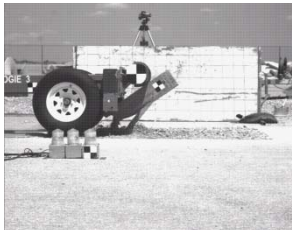
**IMPACT**



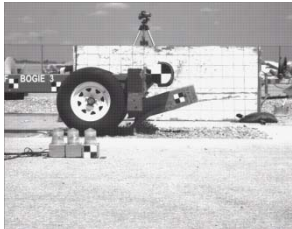
**TIME = 20 ms**



**TIME = 40 ms**



**TIME = 60 ms**



**TIME = 90 ms**



**TIME = 120 ms**

**Figure 100. Time Sequential Photographs, Test UBSP-14**



**Figure 101. Post-Impact Images of UBSP-14**

### **7.5.2 Test UBSP-15 – Strong-Axis (0 Degree) Impact on CRT Post**

Test UBSP-15 was also a strong-axis impact at 0 degrees on the wood CRT post embedded in standard strong soil. The force and energy data are shown in Figures 102 and 103, respectively. Time-sequential photographs are shown in Figure 104. Even though this test was a repeat of test UBSP-14, a different behavior was observed. Upon impact, the wood CRT post rotated through the soil instead of fracturing near the ground line. The bogie head remained in contact with the post until approximately 178 ms when the bogie ramped over the rotated post. The post showed no signs of fracturing, and the only damage was impact marks from the bogie head, as shown in the post-impact images of the post in Figure 105.

As depicted in Figures 102 and 103, the CRT wood post rotated through the soil, absorbed significant energy, and did not break away. When compared to test UBSP-14, the results demonstrated the affect that defects have on wood post properties as well as on post-soil behavior. In addition, this post rotated through the soil at approximately 5 kips (22 kN), which was lower than 12 kips (53.4 kN), where the post would not have been expected to break. Thus, the wood post performed as expected for this weaker soil strength. Based on this test and the second round of breakaway steel post testing, there were concerns regarding the inconsistent soil strength.

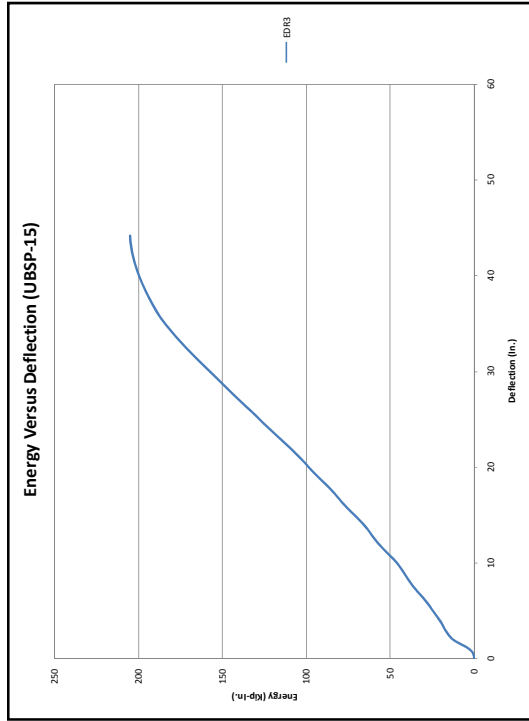


Figure 103a. Energy versus Deflection Curve for UBSP-15 - English

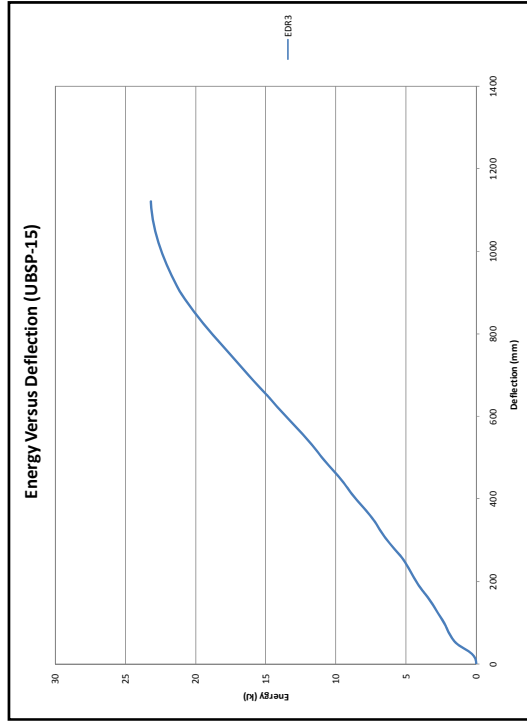


Figure 103b. Energy versus Deflection Curve for UBSP-15 - Metric

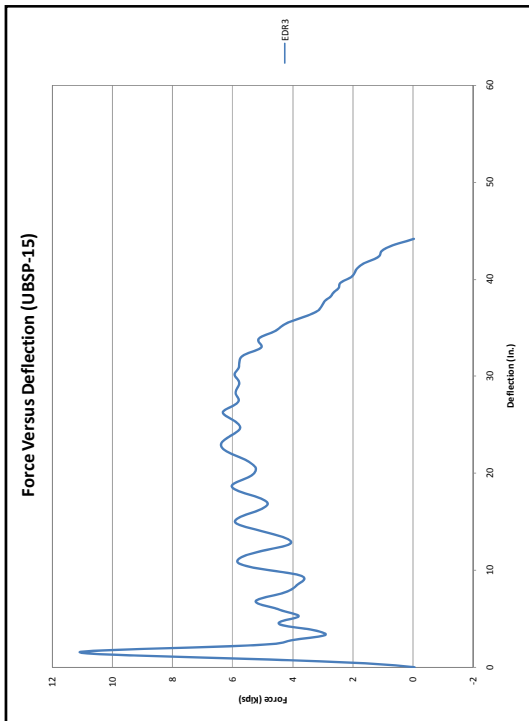


Figure 102a. Force versus Deflection Curve for UBSP-15 - English

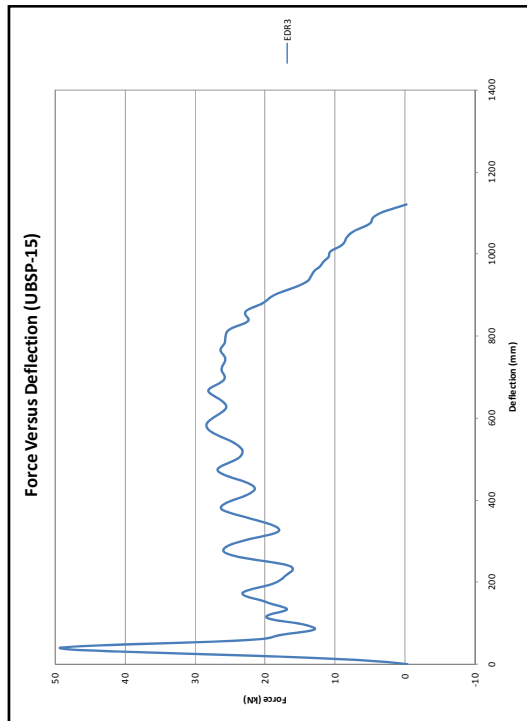
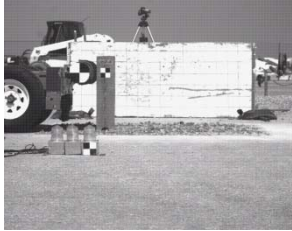
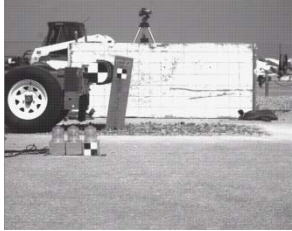


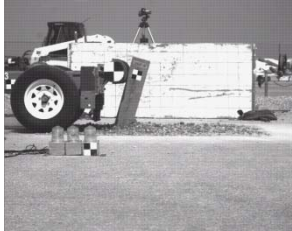
Figure 102b. Force versus Deflection Curve for UBSP-15 - Metric



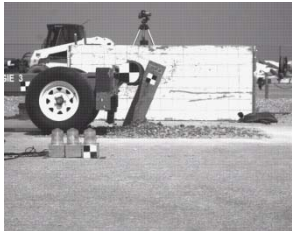
**IMPACT**



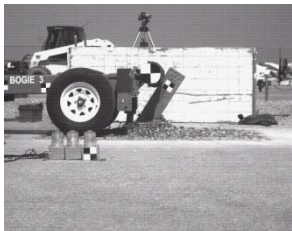
**TIME = 20 ms**



**TIME = 40 ms**



**TIME = 60 ms**



**TIME = 90 ms**



**TIME = 120 ms**

**Figure 104. Time Sequential Photographs, Test UBSP-15**



**Figure 105. Post-Impact Images of UBSP-15**

### **7.5.3 Test UBSP-16 – Weak-Axis (90 Degree) Impact on CRT Post**

Test UBSP-16 was a weak-axis impact at 90 degrees on the wood CRT post embedded in standard strong soil. Due to technical difficulties, no high-speed photography was available for this test. However, the post was observed to rotate through the soil. The post did not break away and was in contact with the bogie head until the bogie overrode the post.

As shown in Figures 106 and 107, the post rotated through the soil at approximately 4 kips (18 kN) and absorbed significant energy. This 4-kip force level was notably low when considering the CRT wood post with its 8-in. (203-mm) wide face had to move considerably more soil when impacted about the weak axis of bending. Once again, the test results revealed inconsistencies in the behavior of compacted, standard strong soil. However, the post performed as expected for this soil resistance, as the force levels did not reach the predicted fracture load of approximately 6 kips (27 kN) other than the inertial spike. Post-impact images of the undamaged post and displaced soil are shown in Figure 108.

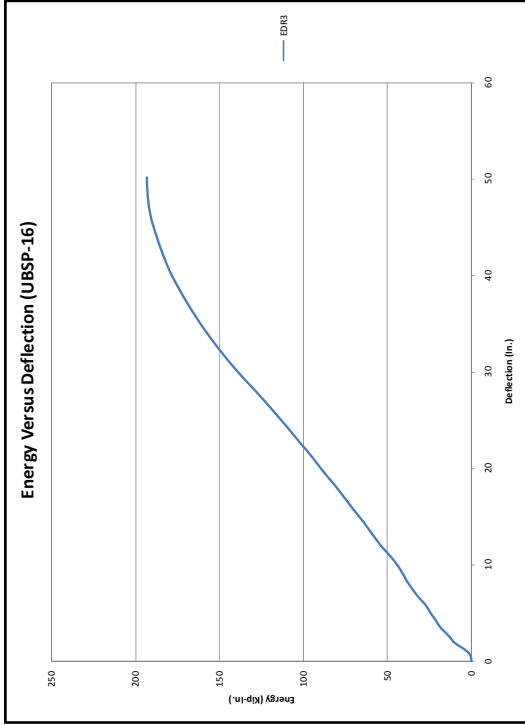


Figure 107a. Energy versus Deflection Curve for UBSP-16 - English

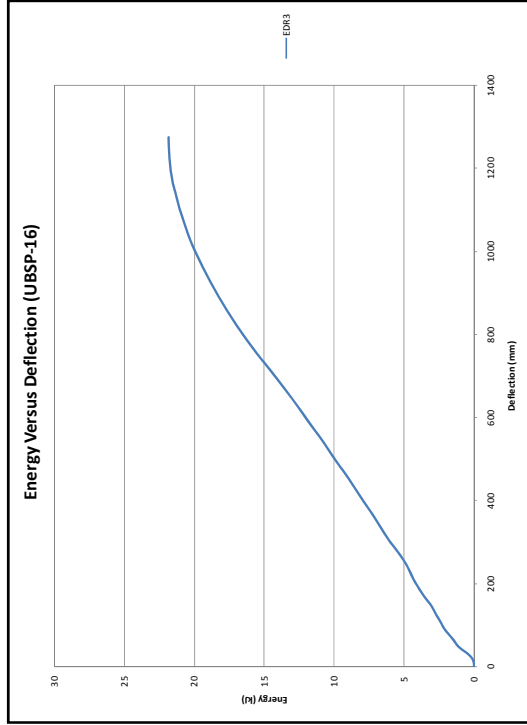


Figure 107b. Energy versus Deflection Curve for UBSP-16 - Metric

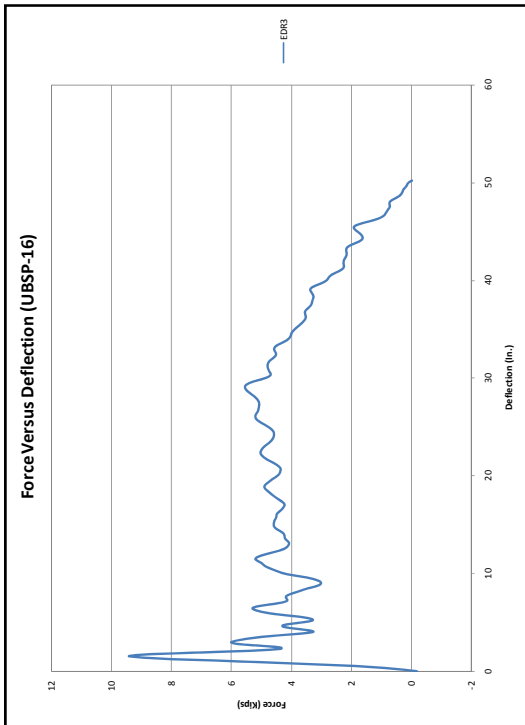


Figure 106a. Force versus Deflection Curve for UBSP-16 - English

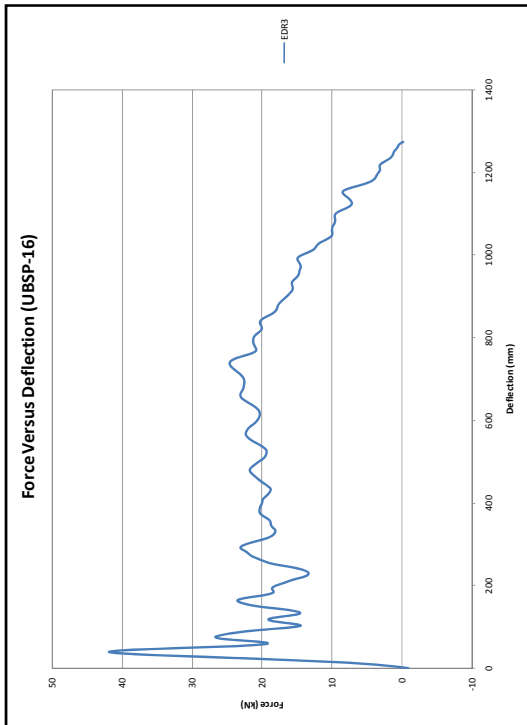
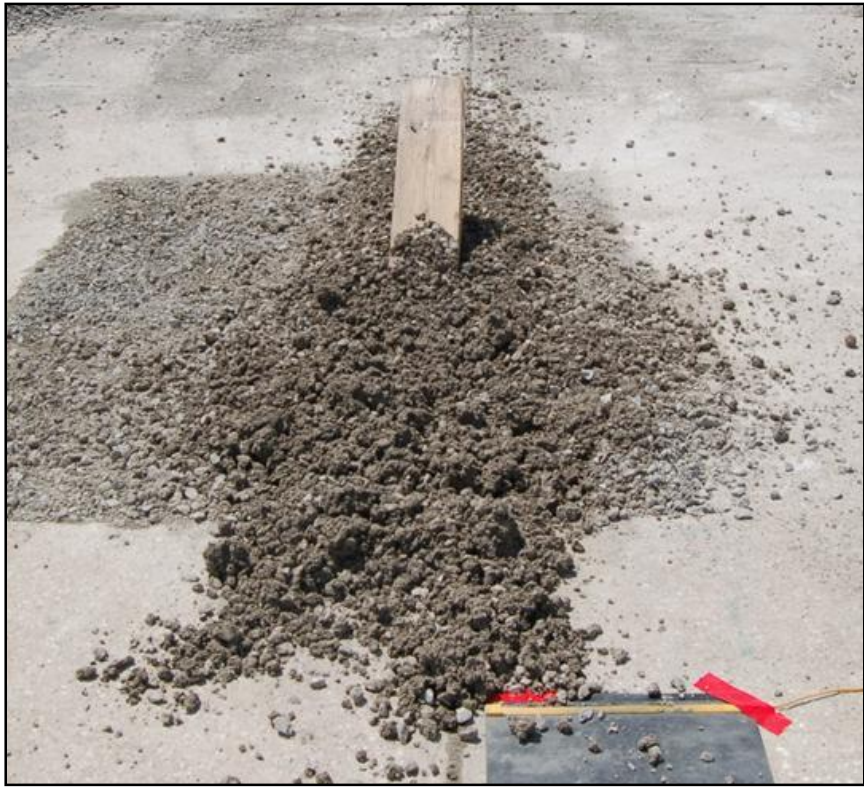


Figure 106b. Force versus Deflection Curve for UBSP-16 - Metric



**Figure 108. Post-Impact Images of UBSP-16**



#### **7.5.4 Test UBSP-17 – Weak-Axis (90 Degree) Impact on CRT Post**

Test UBSP-17 also consisted of a weak-axis impact at 90 degrees on the wood CRT post embedded in standard strong soil. The force and energy data are shown in Figures 109 and 110, respectively. Time-sequential photographs are shown in Figure 111. Upon impact, the post began to immediately rotate in the soil. Next, the post began to fracture, thus causing the post to lose its resistance to the bogie vehicle. The fracture occurred just below ground level and was not immediately visible. The post eventually lost contact with the bogie at 92 ms.

As shown in the force versus deflection and energy versus deflection curves in Figures 109 and 110 respectively, the post broke away at approximately 5 kips (22 kN) after rotating approximately 5 in. (127 mm). This post-soil behavior was close to what was expected, since the CRT post was predicted to break away at 6 kips (27 kN) for bending about the weak axis and embedment in a sleeve. The post broke just below ground level on the bottom side of the upper breakaway hole. Post-impact images for the displaced soil and fractured post are provided in Figure 112.

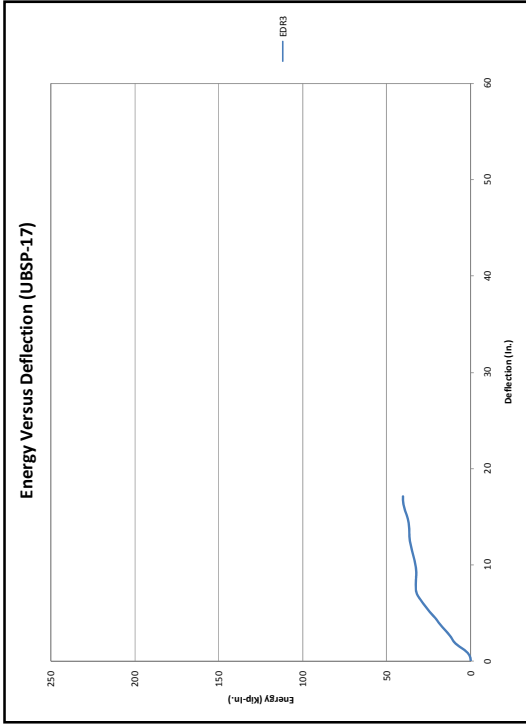


Figure 110a. Energy versus Deflection Curve for UBSP-17 - English

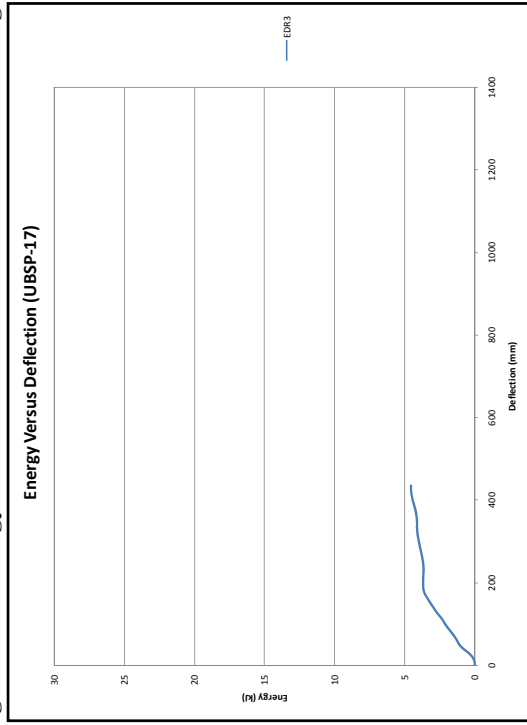


Figure 110b. Energy versus Deflection Curve for UBSP-17 - Metric

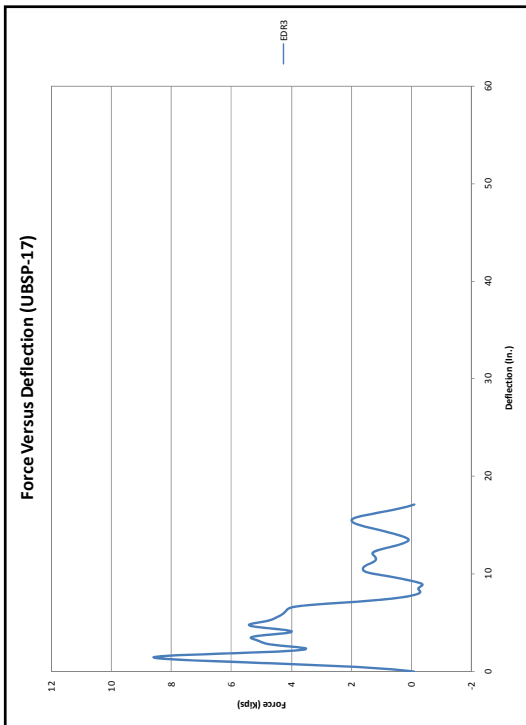


Figure 109a. Force versus Deflection Curve for UBSP-17 - English

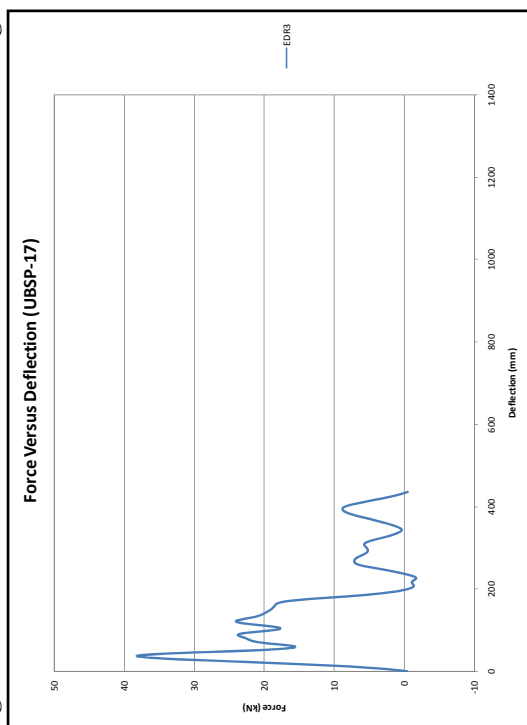


Figure 109b. Force versus Deflection Curve for UBSP-17 - Metric



**IMPACT**



**TIME = 20 ms**



**TIME = 40 ms**



**TIME = 60 ms**



**TIME = 90 ms**



**TIME = 120 ms**

**Figure 111. Time Sequential Photographs, Test UBSP-17**



**Figure 112. Post-Impact Images of UBSP-17**

### **7.5.5 Test UBSP-18 – Diagonal-Axis (45 Degree) Impact on CRT Post**

Test UBSP-18 was a 45-degree impact on a wood CRT post embedded in standard strong soil. The force and energy data are shown in Figures 113 and 114, respectively. Time-sequential photographs are shown in Figure 115. Upon impact, the post began to rotate immediately and continued to rotate through the soil until approximately 162 ms when the bogie ramped and overrode the post. There was no sign of wood fracture. Post-impact images of the standard strong soil and CRT wood post are provided in Figure 116.

As shown in the force versus deflection and energy versus deflection curves provided in Figures 113 and 114, the post rotated through the soil and absorbed considerable energy. Similar to the weak-axis impact condition, the CRT wood post had to move more soil as compared to the strong-axis impact condition. In this test, the post did rotate at a higher force level of 7 kips (31 kN), which was close to predicted fracture load of 8 kips (36 kN) for the diagonal impact condition. As would be expected for the observed force level, the post did not break away.

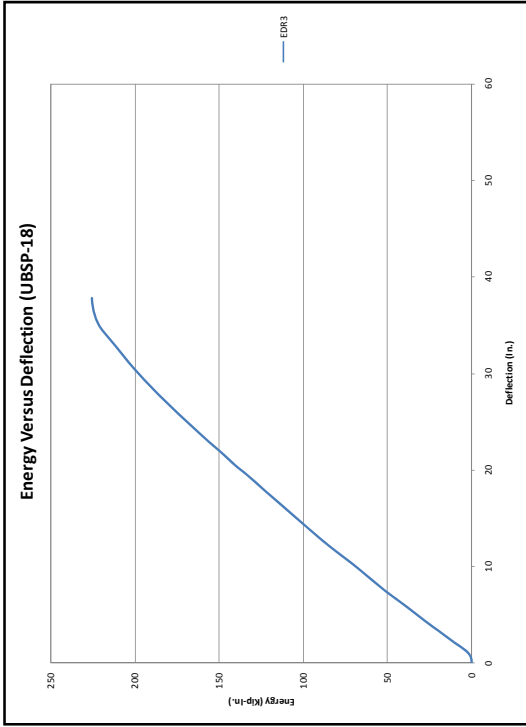


Figure 114a. Energy versus Deflection Curve for UBSP-18 - English

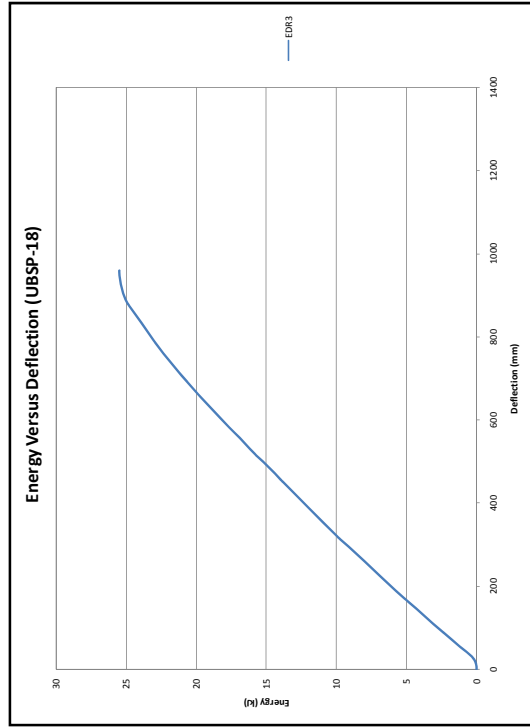


Figure 114b. Energy versus Deflection Curve for UBSP-18 - Metric

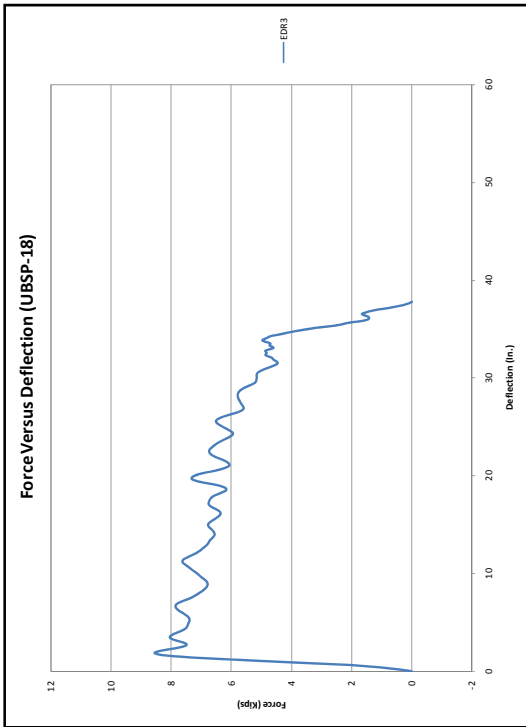


Figure 113a. Force versus Deflection Curve for UBSP-18 - English

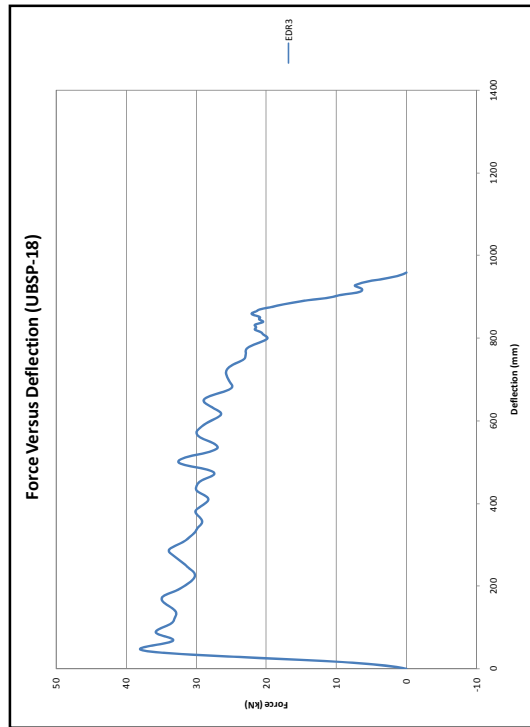


Figure 113b. Force versus Deflection Curve for UBSP-18 - Metric



**IMPACT**



**TIME = 20 ms**



**TIME = 40 ms**



**TIME = 60 ms**



**TIME = 90 ms**



**TIME = 120 ms**

**Figure 115. Time Sequential Photographs, Test UBSP-18**



**Figure 116. Post-Impact Images of UBSP-18**

### **7.5.6 Test UBSP-19 – Diagonal-Axis (45 Degree) Impact on CRT Post**

Test UBSP-19 was also a 45-degree impact on a wood CRT post embedded in standard strong soil. The force and energy data are shown in Figures 117 and 118, respectively. Time-sequential photographs are shown in Figure 119. The post began to rotate immediately upon impact and continued to rotate through the soil until the bogie ramped and overrode the post at approximately 154 ms. There was no sign of post fracture. Post-impact images from the test are provided in Figure 120. The only post damage occurred to the top region due to contact with bogie as it overrode the post.

Force versus deflection and energy versus deflection curves are provided in Figures 117 and 118. Even though the post rotated through the soil similar to that observed in test UBSP-18, the force level was 5 kips (22 kN) instead of the 7 kips (31 kN) observed in test UBSP-18. Thus, these two tests once again showed the effect that inconsistent, compacted, standard strong soil had on post-soil behavior.

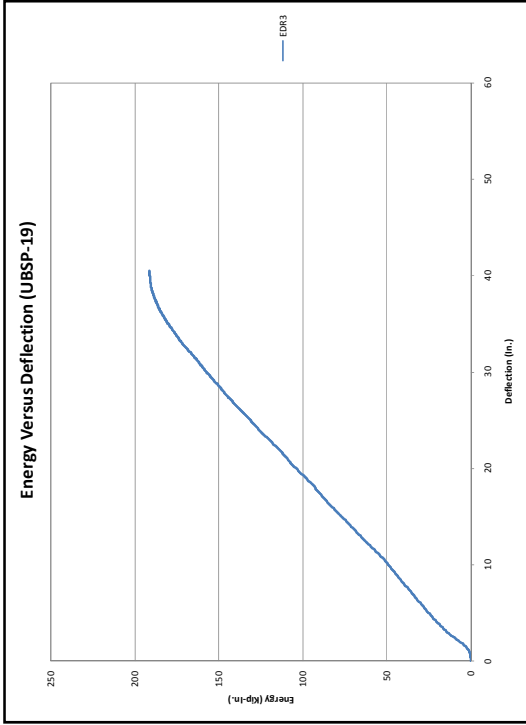


Figure 118a. Energy versus Deflection Curve for UBSP-19 - English

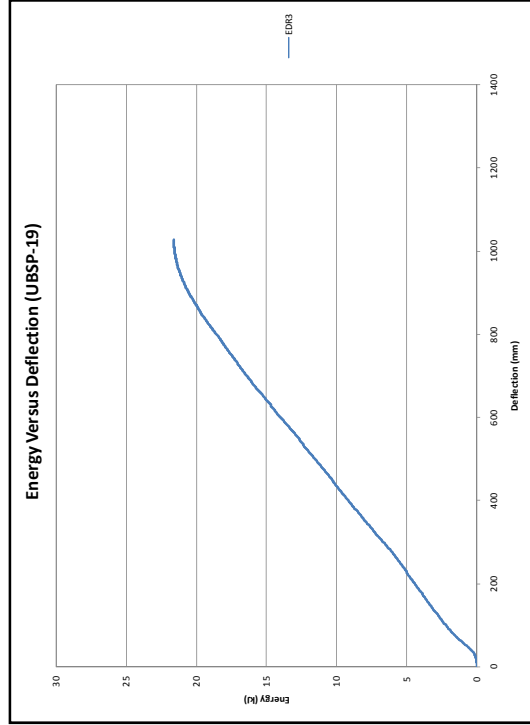


Figure 118b. Energy versus Deflection Curve for UBSP-19 - Metric

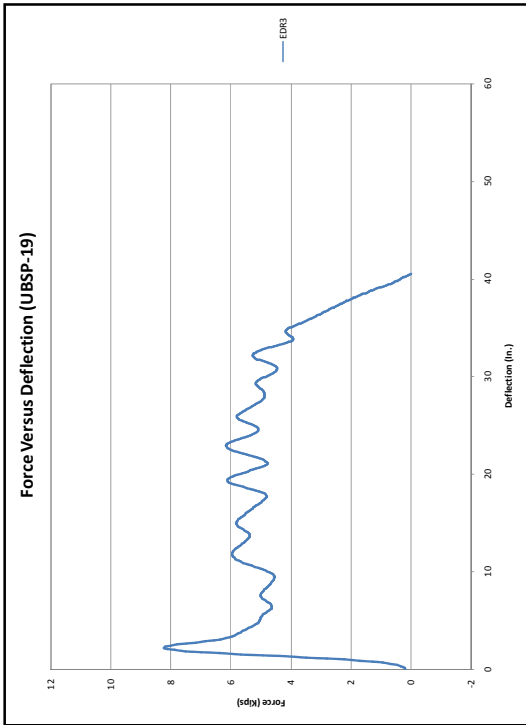


Figure 117a. Force versus Deflection Curve for UBSP-19 - English

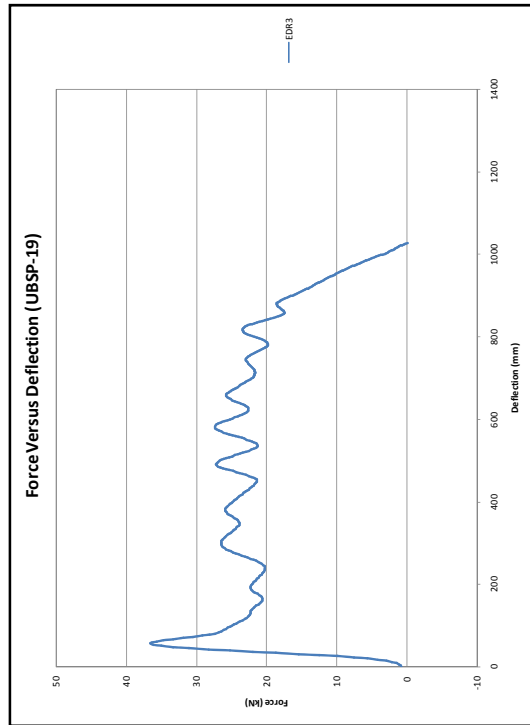
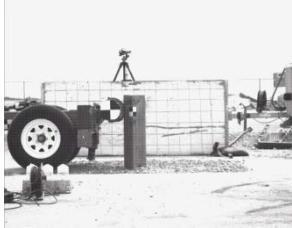
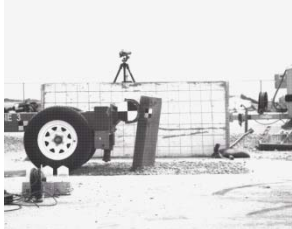


Figure 117b. Force versus Deflection Curve for UBSP-19 - Metric

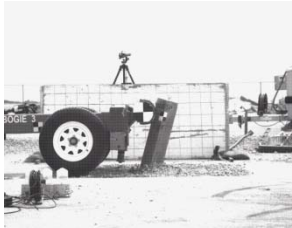




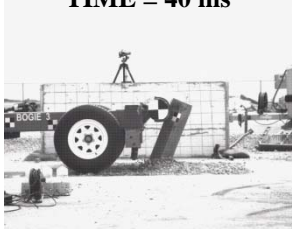
**IMPACT**



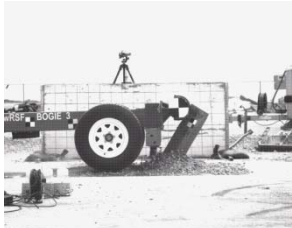
**TIME = 20 ms**



**TIME = 40 ms**



**TIME = 60 ms**



**TIME = 90 ms**



**TIME = 120 ms**

**Figure 119. Time Sequential Photographs, Test UBSP-19**



**Figure 120. Post-Impact Images of UBSP-19**

## 7.6 Summary and Conclusions

A summary of the results for the six CRT wood post, soil tests in this round of bogie testing is provided in Table 15. In a strong-axis impact in test UBSP-14, the wood CRT post had a knot near the breakaway hole, and the post broke away at a low peak force level. For another strong-axis impact in test UBSP-15, the post rotated through the soil at approximately 5 kips (22 kN), which was lower than the expected capacity of the post of 12 kips (53.4 kN) from the rigid sleeve testing. Test UBSP-16 was a weak-axis impact condition where the CRT wood post rotated through the soil at a low force level and did not break away as expected. In the second weak-axis test, test no. UBSP-17, the post broke away at approximately 5 kips (22 kN), which was close to the predicted fracture load of 6 kips (27 kN). For the two diagonal impact tests, test nos. UBSP-18 and UBSP-19, the posts rotated through the soil at force levels lower than the expected breaking force and did not break away.

As previously mentioned, there was concern that the post-soil behavior may have been influenced by inconsistencies in soil compaction and soil behavior. However, it was believed that the test results could still provide useful information for making comparisons to the results from the fracturing bolt concept.

Even with the inconsistency in the tests, there was no reason to doubt the fracturing bolt concept would have the same behavior as the CRT wood posts in soil. It had already been shown in test nos. UBSP-9 and UBSP-13 that the fracturing bolt would rotate through the soil in weaker soil and would break away with stronger soil. This behavior was similar with the CRT wood posts in soil, where the wood posts would also rotate through weaker soil and break away in stronger soil. Thus, even though comparisons between the fracturing bolt and CRT wood posts in

soil were difficult due inconsistent soil compaction and behavior, the fracturing bolt concept still had similar behavior as the CRT wood post tests in soil.

The only issue was that the fracturing bolt concept had never been tested at an oblique (diagonal) angle. As a result, the fracturing bolt needed to be tested at an oblique angle to make certain it matched the strength and behavior of the CRT wood post. Also, there were minor refinements to the fracturing bolt design, so the fracturing bolt was retested in a strong axis impact in addition to the oblique angle test for a third round of bogie testing on the fracturing bolt design.

**Table 15a. Test Results for CRT Wood Posts In Soil – English**

Test No.	Impact Velocity (mph)	Failure Type	Initial Peak Force		Initial Stiffness (kips/in.)	Average Force				Total Energy	
			Displacement (in.)	Force (kips)		@ 5" (kips)	@ 10" (kips)	@ 15" (kips)	@ 20" (kips)	Displacement (in.)	Energy (kip-in.)
UBSP-14	19.1	Post Failure	1.25	8.29	6.61	4.05	2.31	1.58	1.23	17.0	24.9
UBSP-15	20.5	Post Rotation	1.57	11.1	7.04	4.92	4.58	4.74	4.92	44.1	204.9
UBSP-16	20.2	Post Rotation	1.55	9.42	6.07	4.77	4.38	4.43	4.46	50.2	193.1
UBSP-17	20.6	Post Failure	1.47	8.58	5.83	4.68	3.28	2.52	2.02	17.1	40.4
UBSP-18	20.0	Post Rotation	1.86	8.55	4.59	6.43	6.86	6.91	6.87	37.8	225.7
UBSP-19	20.0	Post Rotation	2.19	8.21	3.75	4.99	4.86	5.12	5.18	40.5	191.0

**Table 15b. Test Results for CRT Wood Posts In Soil - Metric**

Test No.	Impact Velocity (km/h)	Failure Type	Initial Peak Force		Initial Stiffness (kN/mm)	Average Force				Total Energy	
			Displacement (mm)	Force (kN)		@ 127 mm (kN)	@ 254 mm (kN)	@ 381 mm (kN)	@ 508 mm (kN)	Displacement (mm)	Energy (kJ)
UBSP-14	30.7	Post Failure	31.8	36.9	1.16	18.0	10.3	7.03	5.47	432	2.81
UBSP-15	33.0	Post Rotation	39.9	49.4	1.23	21.9	20.4	21.1	21.9	1120	23.1
UBSP-16	32.5	Post Rotation	39.4	41.9	1.06	21.2	19.5	19.7	19.8	1275	21.8
UBSP-17	33.2	Post Failure	37.3	38.2	1.02	20.8	14.6	11.2	8.98	434	4.56
UBSP-18	32.2	Post Rotation	47.2	38.0	0.80	28.6	30.5	30.7	30.6	960	25.5
UBSP-19	32.2	Post Rotation	55.6	36.5	0.66	22.2	21.6	22.8	23.0	1029	21.6

## 8 BREAKAWAY POST BOGIE TESTING – ROUND 3

### 8.1 Purpose

The third round of bogie testing was performed to evaluate design refinements in fracturing bolt breakaway concept. Two bogie tests were performed to ensure that the fracturing bolt concept sufficiently matched the post-soil behavior and strength of the CRT wood post.

### 8.2 Scope

The third round of bogie testing was conducted on the fracturing bolt concept with minor refinements, as detailed in Section 8.3. The test setup was identical to the previous setup used for the bogie testing of CRT wood posts in soil. The posts were embedded 40 in. (1,016 mm) in standard strong soil. With the erratic results during the testing of CRT wood posts placed in soil, it was confirmed that the strong soil was compacted thoroughly using 6-in. (152-mm) lifts for the third round of tests. The target test condition consisted of a 20 mph (32 km/h) speed and an impact occurring at the centerline of the bogie vehicle, or at 24 7/8 in. (632 mm) above the ground. Two bogie tests were performed, as shown in Table 16. One test was planned for bending about the strong axis. For the second test, the oblique impact angle was set at 45 degrees to be consistent with previous testing. No changes were planned for the weak-axis load condition. Thus, a weak-axis impact was not performed. The behavior of the fracturing bolt concept would be expected to have the same response as that observed in the weak-axis condition in test UBSP-10.

**Table 16. Test Matrix for Round 3 Bogie Testing**

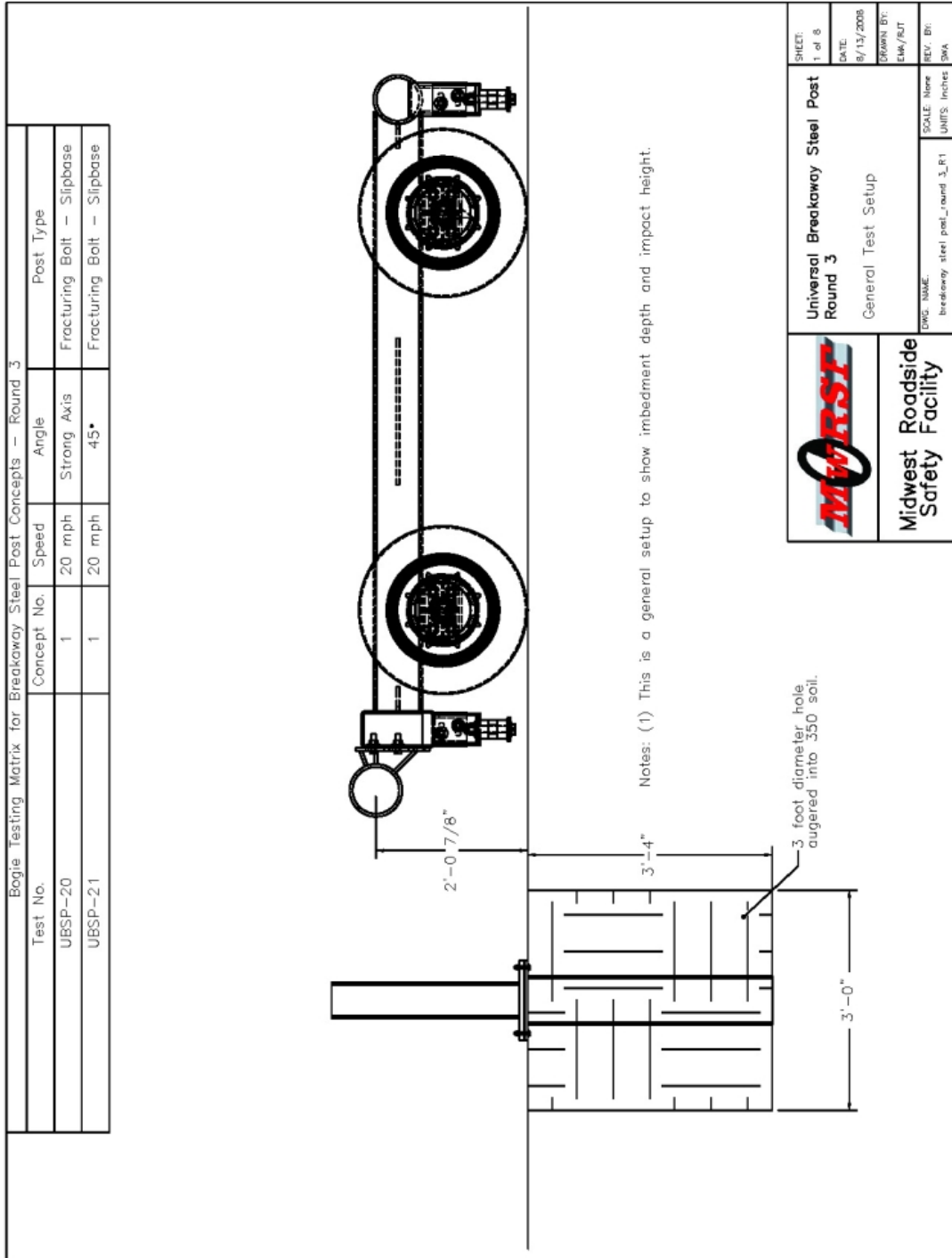
Test No.	Test Date	Post Concept	Speed		Impact Axis
			mph (km/h)	ft/s (m/s)	
UBSP-20	06-30-2008	Fracturing Bolt	19.0 (30.6)	27.9 (8.49)	Strong
UBSP-21	06-30-2008	Fracturing Bolt	19.6 (31.5)	28.7 (8.76)	45 Degrees

### **8.3 Post Details**

The fracturing bolt concept was the only post tested in this third round of bogie testing. The design was nearly identical to the fracturing bolt used in test UBSP-13 in the second round of bogie testing, except that the bolts were spaced out farther to strengthen the post for bending about the strong axis. The bolts were previously spaced 10 in. (254 mm) apart, but for third round testing, the bolts were spaced 10 13/16 in. (275 mm) apart in the strong-axis direction. This modification was performed to strengthen the post and have it deflect more before it rupturing. The bolt spacing for a weak-axis impact was not altered. Also, fully threaded hex bolts, or tap bolts, were used for the fracturing bolt concept. This change was incorporated to ensure that the bolts would consistently break away regardless of the installation. The design refinements are shown in Figures 121 through 124.

### **8.4 Equipment and Instrumentation**

The equipment and instrumentation was the same as that used in CRT wood post testing in soil. The EDR-3 was the only accelerometer system used for these two tests. Also, the test setup, end of test determination, and data processing were the same as that used in the first and second rounds of bogie testing.



	<b>Midwest Roadside Safety Facility</b>
<b>Universal Breakaway Steel Post Round 3</b>	General Test Setup
SHEET: 1 of 8	DATE: 8/13/2008
DRAWN BY: ELW/PLT	REV. BY: BWA
DWG. NAME: breakaway_steel_post_round_3_R1	SCALE: None UNITS: Inches

**Figure 121. Fracturing Bolt Details**

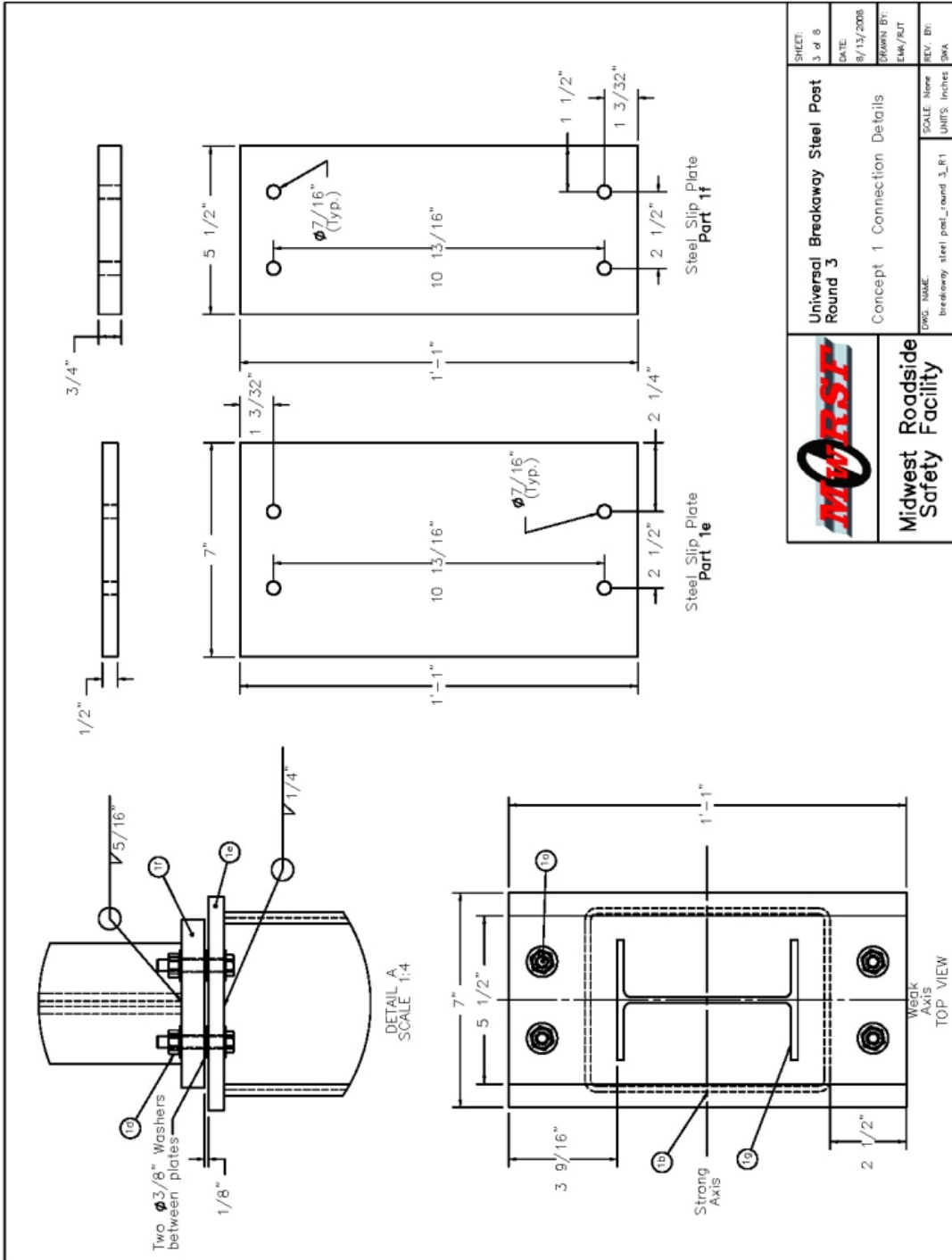


Figure 122. Fracturing Bolt Details



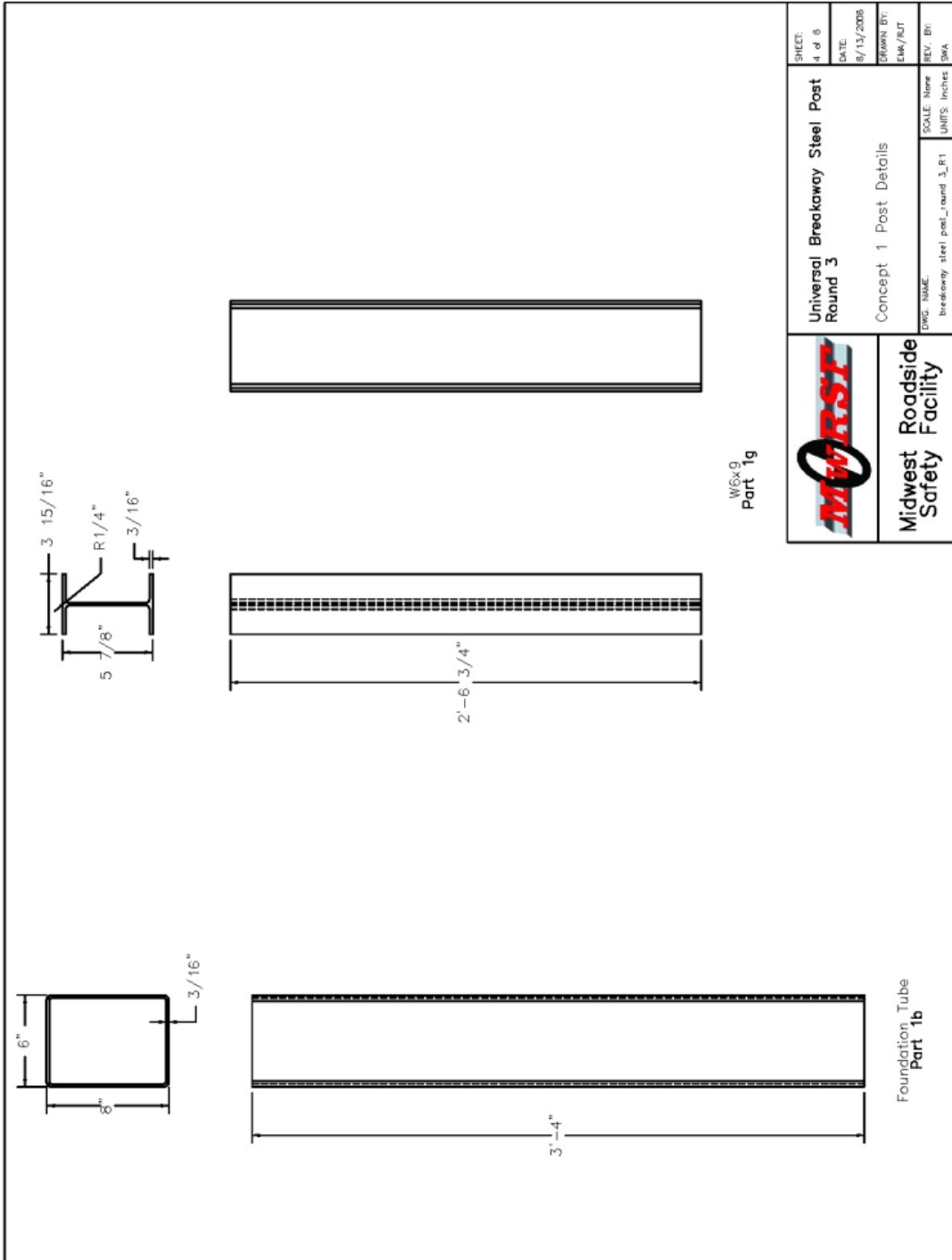


Figure 123. Fracturing Bolt Details

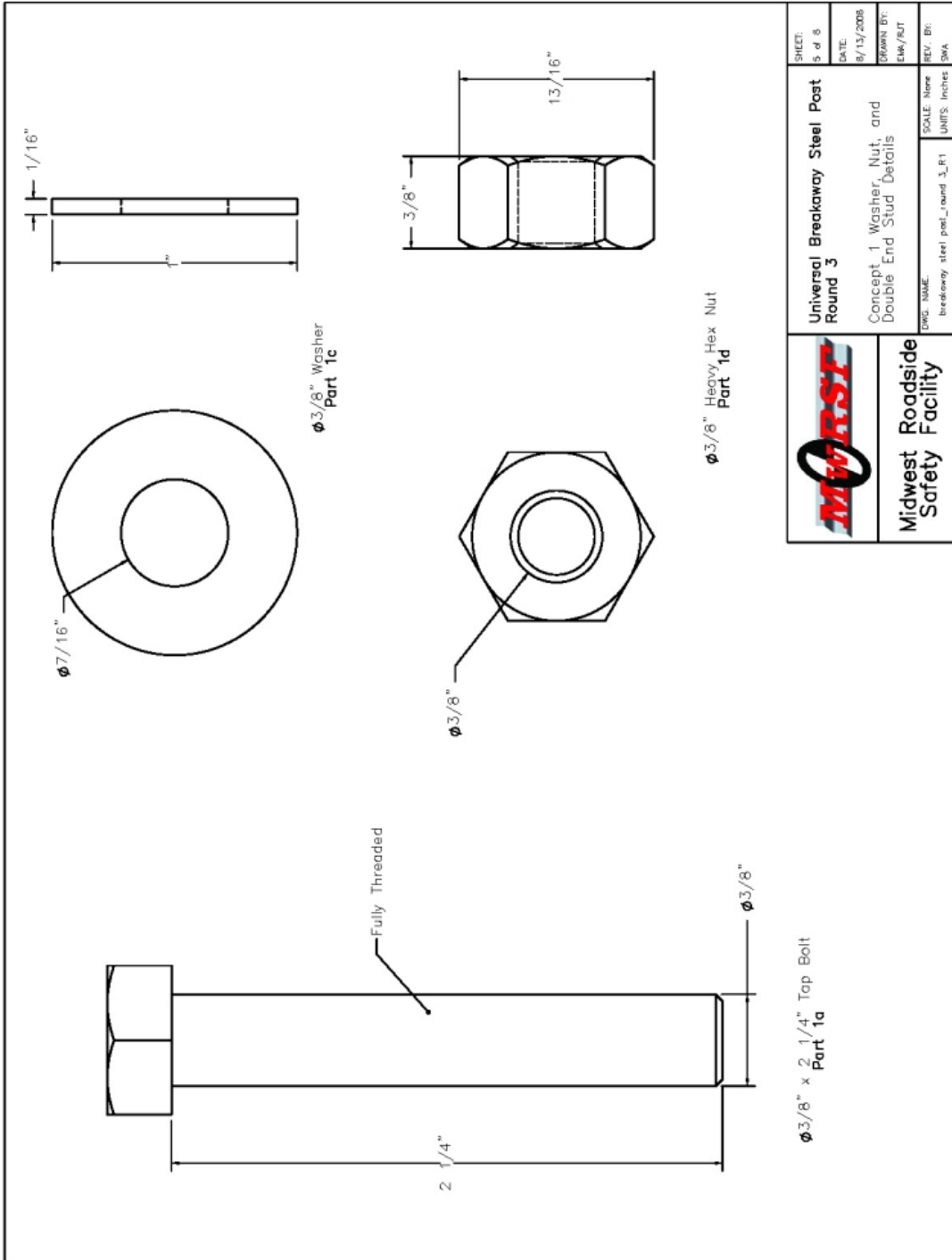


Figure 124. Fracturing Bolt Details

### **8.5 Test Results for Fracturing Bolt Concept – Round 3**

The accelerometer data was processed for each test in order to obtain acceleration, velocity, and displacement curves, as well as force versus deflection and energy versus deflection curves. This section discusses those results for the EDR-3 accelerometer. Individual test results are provided in Appendix A.

The following sections discuss the dynamic behaviors and results for test nos. UBSP-20 through UBSP-21. However, conclusions regarding a comparison in post performance for the different post concepts are discussed in a subsequent section.

### **8.5.1 Test UBSP-20 – Fracturing Bolt – Strong Axis**

Test UBSP-20 was a strong-axis impact at 0 degrees on the fracturing bolt concept embedded in standard strong soil. The force and energy data are shown in Figures 125 and 126, respectively. Time-sequential photographs are shown in Figure 127. The post began to rotate immediately and the impact-side bolts broke in tension at approximately 26 ms. As a result of the bolt fracture, the post offered little resistance, and thus, the bogie head lost contact with the post from approximately 30 ms until 54 ms. The bogie later regained contact with the post from 54 ms until 64 ms, but there was little resistance as the impact-side bolts had already failed, and the post was pushed to the ground.

As shown in the force versus deflection and energy versus deflection curves provided in Figures 125 and 126, the fracturing bolt concept performed sufficiently by breaking away cleanly at a peak load of 10.8 kips (48 kN) and absorbing energy up to that peak load. All of the bolts fractured as desired but at a slightly lower peak load than expected, which was probably due to the actual moment arm, or distance between the bolts being shorter than anticipated. However, the post strength was close to the 12-kip (53 kN) desired force level, and the post did break away cleanly, thus leaving a 2 1/4 in. (57 mm) gap in the soil. This test performed similar to test no. UBSP-9, when the soil was also well compacted. Post deformation was observed in the bolts and washers with some slight yielding noticed in the two steel plates. Post-impact images of the post, bolts, and soil are provided in Figure 128. Also, close-up images of the fractured bolts and damaged washers are shown in Figure 129.

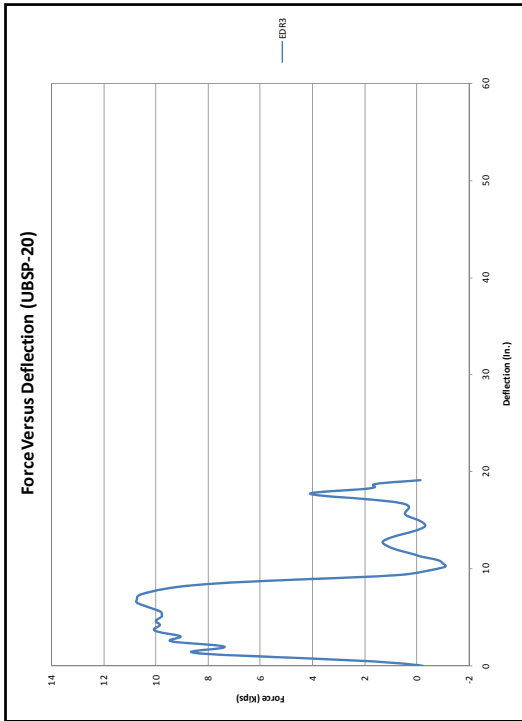


Figure 125a. Force versus Deflection Curve for UBSP-20 - English

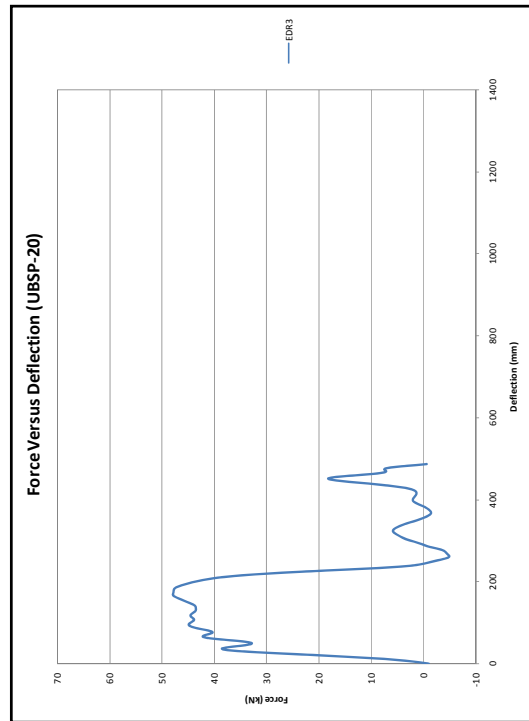


Figure 125b. Force versus Deflection Curve for UBSP-20 - Metric

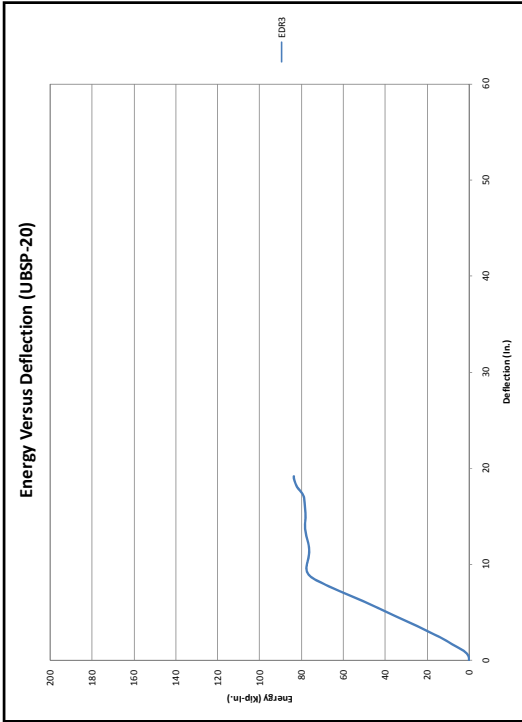


Figure 126a. Energy versus Deflection Curve for UBSP-20 - English

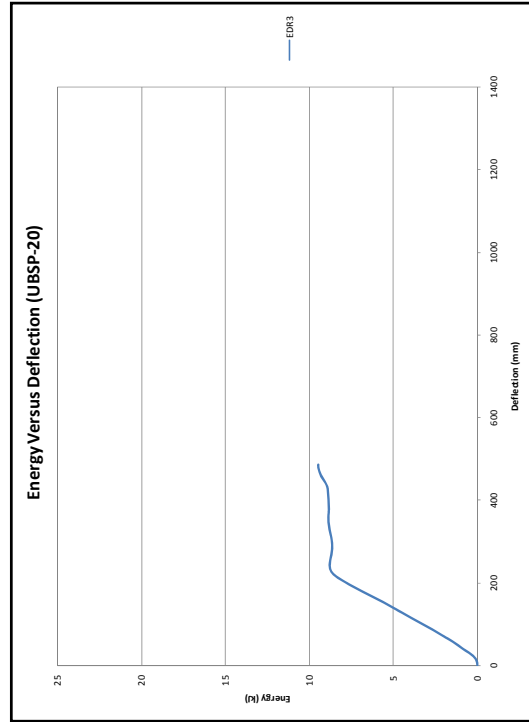


Figure 126b. Energy versus Deflection Curve for UBSP-20 - Metric

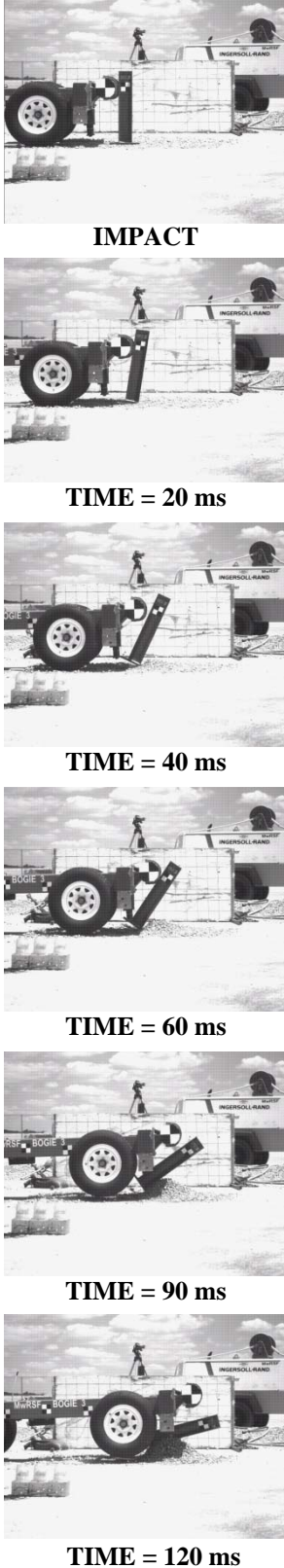


Figure 128. Post-Impact Images of UBSP-20

Figure 127. Time Sequential Photographs, Test UBSP-20



**Figure 129. Additional Images of Bolt and Washer Damage of UBSP-20**

### **8.5.2 Test UBSP-21 – Fracturing Bolt – 45-Degree Angle**

Test UBSP-21 was a 45-degree impact on the fracturing bolt concept embedded in standard strong soil. The force and energy data are shown in Figures 130 and 131, respectively. Time-sequential photographs are shown in Figure 132. The post immediately began to rotate in the soil and twist due the 45-degree oblique impact. At approximately 22 ms, the first bolt on the impact side fractured. The other three bolts fractured soon thereafter, but there is no clear indication of when fracture occurred. After all four bolts had fractured, the post was weakened and lost contact with the bogie's head at approximately 64 ms.

Upon review of the force versus deflection and energy versus deflection curves provided in Figures 130 and 131, it was clear that the test performed as desired. The post broke away cleanly at a peak force level of 8.3 kips (37 kN), which was close to the targeted load value of 8 kips (36 kN) for a 45-degree impact. For this oblique load condition, the fracturing bolt post was impacted on the flange of the upper W6x9 (W152x13.4) post segment. As a result, damage occurred to the flange near the impact location. Also, the 1/2-in. (13-mm) thick, bottom steel plate was bent down on the downstream corner. There was a 1/2-in. (13-mm) gap in the soil. Post-impact images of the post, bolts, and soil are shown in Figure 133. Additional close-up images of the fractured bolts and damaged washers are provided in Figure 134.



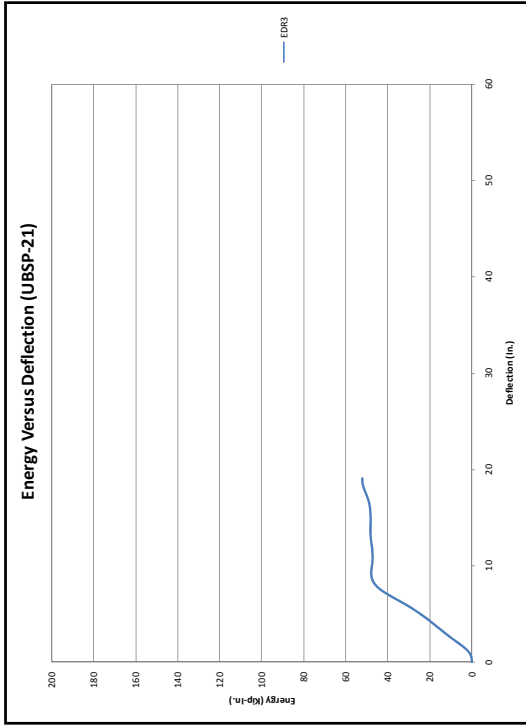


Figure 131a. Energy versus Deflection Curve for UBSP-21 - English

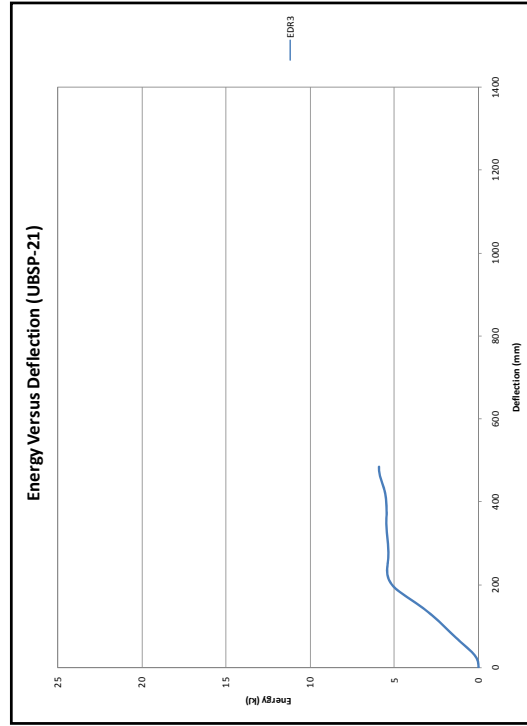


Figure 131b. Energy versus Deflection Curve for UBSP-21 - Metric

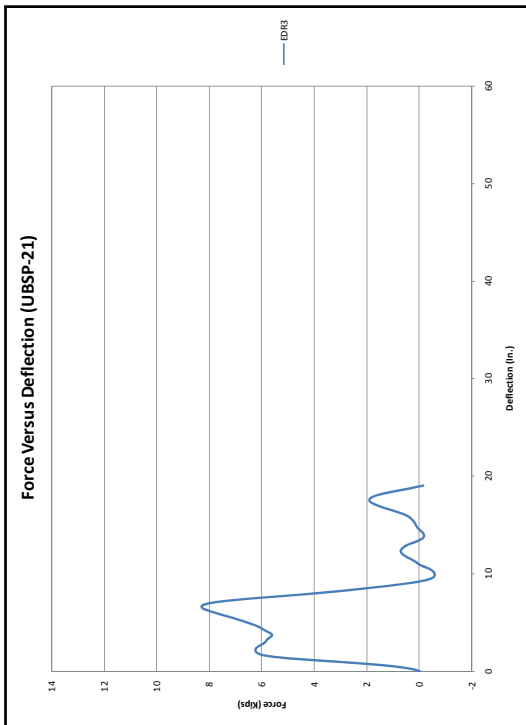


Figure 130a. Force versus Deflection Curve for UBSP-21 - English

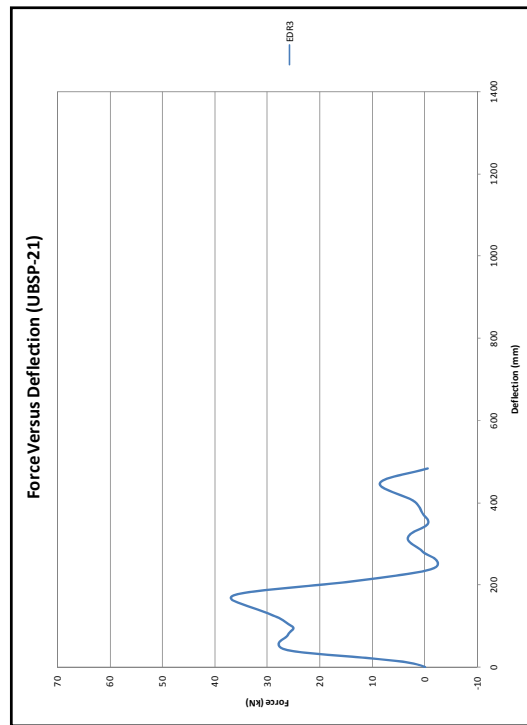
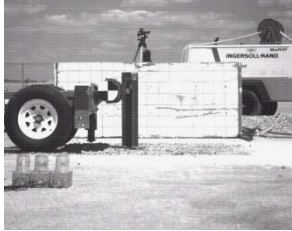


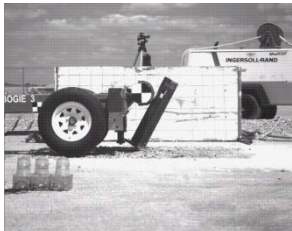
Figure 130b. Force versus Deflection Curve for UBSP-21 - Metric



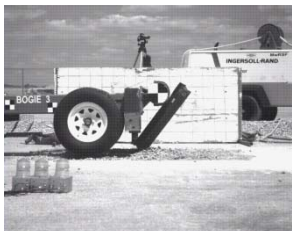
**IMPACT**



**TIME = 20 ms**



**TIME = 40 ms**



**TIME = 60 ms**



**TIME = 90 ms**



**TIME = 120 ms**

**Figure 132. Time Sequential Photographs, Test UBSP-21**



**Figure 133. Post-Impact Images of UBSP-21**



**Figure 134. Additional Images of Bolt and Washer Damage of UBSP-21**

## 8.6 Round 3 Summary and Conclusions

A summary of the round 3 bogie testing results is provided in Table 17. The final two bogie tests were performed to ensure that the fracturing bolt concept sufficiently matched the strength and post-soil behavior of the CRT wood post. Both a strong-axis impact and an oblique (45-degree) impact were performed on the fracturing bolt concept. No changes were planned that would affect the weak-axis impact condition. As such, a weak-axis bogie test was not performed.

First, the strong-axis load condition, test no. UBSP-20, provided desired results. The fracturing bolt concept broke away cleanly at a peak load of 10.8 kips (48 kN) and absorbed energy up to that peak load. All of the bolts fractured as desired but at a slightly lower peak load than expected, which was probably due to the actual moment arm or distance between the bolts being shorter than anticipated. However, the post strength was close to the 12-kip (53 kN) desired force level, and the post broke away cleanly in the well-compacted soil. The second test, test no. UBSP-21 consisted of a 45-degree, oblique angle impact on the fracturing bolt concept. During this test, the post performed very adequately and broke away cleanly at a peak load of 8.3 kips (37 kN), which is close to the targeted value of 8 kips (36 kN).

As proven by these last two bogie tests, the fracturing bolt closely matched the strength and post-soil behavior of the CRT wood post. The strength of the fracturing bolt was close to the targeted strength level for each impact angle, allowing the post to break away cleanly. Thus, the fracturing bolt post concept was deemed ready for full-scale crash testing and evaluation in the thrie-beam bullnose system.

**Table 17a. Summary of Round 3 Bogie Testing Results – English**

Test No.	Impact Velocity (mph)	Failure Type	Initial Peak Force		Initial Stiffness (kips/in.)	Peak Force		Total Energy	
			Displacement (in.)	Force (kips)		Displacement (in.)	Force (kips)	Displacement (in.)	Energy (kip-in.)
UBSP-20	19.0	Post Failure	1.45	8.65	5.9	6.65	10.8	19.1	83.6
UBSP-21	19.6	Post Failure	2.14	6.24	2.9	6.60	8.3	19.0	52.2

**Table 17b. Summary of Round 3 Bogie Testing Results – Metric**

Test No.	Impact Velocity (km/h)	Failure Type	Initial Peak Force		Initial Stiffness (kN/mm)	Peak Force		Total Energy	
			Displacement (mm)	Force (kN)		Displacement (mm)	Force (kN)	Displacement (mm)	Energy (kJ)
UBSP-20	30.6	Post Failure	36.8	38.5	1.0	169	48.0	485	9.45
UBSP-21	31.5	Post Failure	54.4	27.8	0.51	168	36.9	483	5.90

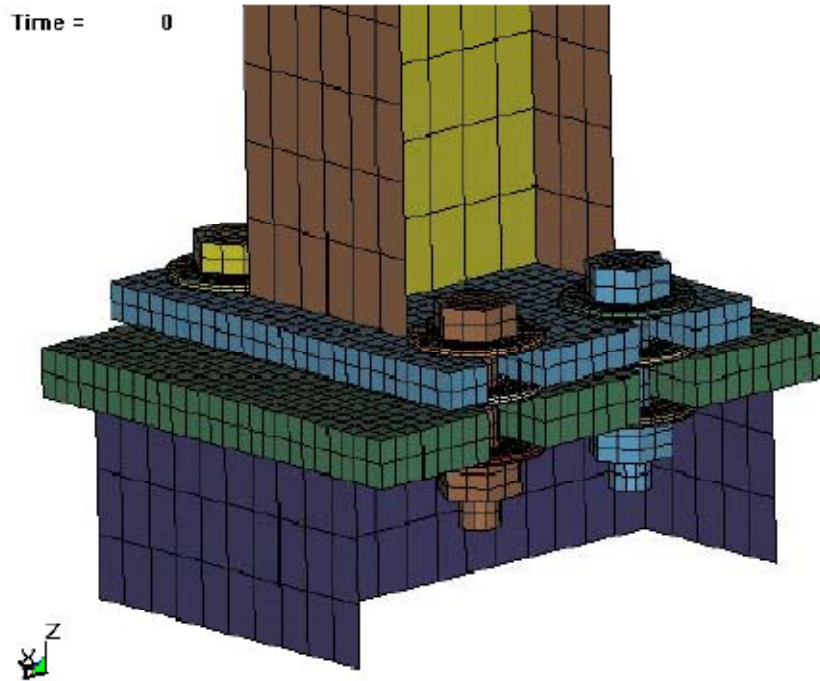
## **9 COMPUTER SIMULATION**

### **9.1 Introduction**

In addition to the dynamic bogie testing, preliminary computer simulation modeling using LS-DYNA [20] was performed to evaluate and analyze the fracturing bolt post. This nonlinear, finite element analysis (FEA) was planned in order to gain confidence and knowledge with modeling the fracturing bolt concept in the event that design modifications were needed in the future.

### **9.2 Previous LS-DYNA Modeling**

First, although this new breakaway steel post relies on fracturing bolts, the design still remains similar to existing slipbase designs. As a result, previous LS-DYNA slipbase simulation models were researched and investigated. Hiser [22] reviewed and summarized the previous slipbase simulation studies completed through 2003. Later, Hiser developed a slipbase model, as shown in Figure 135, which served as the basis for the simulation model of the fracturing bolt concept. However, more detail was added to include a more accurate model for predicting bolt failure, an improved bogie model, and soil to allow the post to rotate.



**Figure 135. Hiser Slipbase Model**

### **9.3 Fracturing Bolt Model Details**

The simulation model of the fracturing bolt post was developed and validated against results from a strong-axis bogie test, test no. UBSP-20, as described previously in Section 8.5.1. Later, the model was also validated using the results from test nos. UBSP-10 and UBSP-21, which were impacts in the weak- and 45-degree axes, respectively.

#### **9.3.1 Part Details**

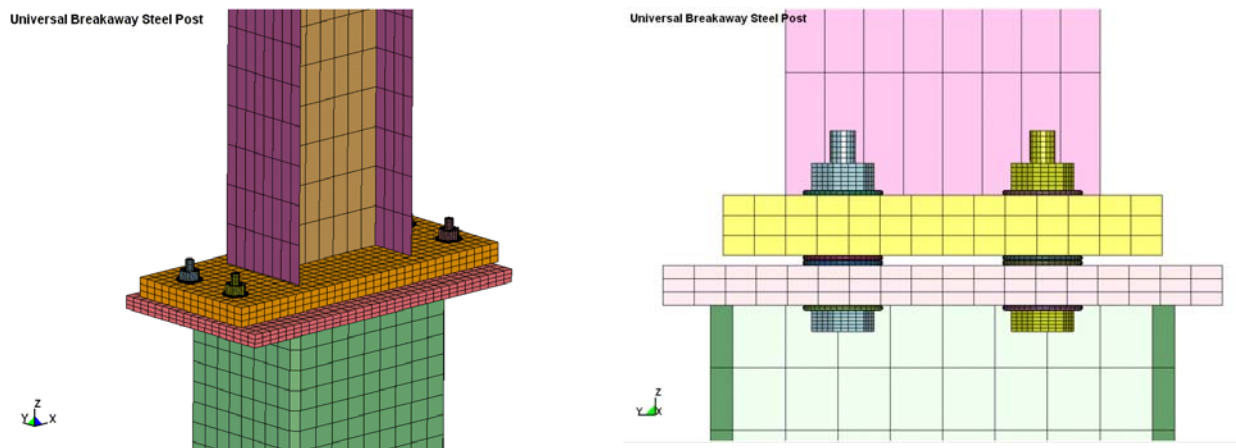
The first step for simulating the new fracturing bolt post was to develop an accurate mesh of the post geometry. The post consisted of many parts, as listed in Table 18. All of the parts, besides the bolt shafts, matched the actual geometry of the post. The bolt shafts were meshed to match the tensile area of the bolt.

The different parts were then assigned appropriate element types and material properties. The MAT\_024 material properties for the ASTM A36 steel were taken from a previous study [22], while the ASTM A325 bolt properties were initially estimated using the yield strength [95 ksi (0.655 GPa)] and the ultimate strength [125 ksi (0.862 GPa)]. Later, the ASTM A325 bolt material properties were altered to better match the actual bogie testing results, as discussed in Section 9.6.2. Different views of the mesh are provided in Figure 136.

**Table 18. Model Parts, Element Types, and Materials**

Parts	Element Type	Material
I-beam Web	Fully Integrated Shell Elements (Very Fast)	A36 Steel, MAT_024
I-beam Flange	Fully Integrated Shell Elements (Very Fast)	A36 Steel, MAT_024
Upper Steel Plate	Fully Integrated Selectively-Reduced Solid Elements	A36 Steel, MAT_024
Lower Steel Plates	Fully Integrated Selectively-Reduced Solid Elements	A36 Steel, MAT_024
Bottom Tube	Fully Integrated Shell Elements (Very Fast)	A36 Steel, MAT_024
Bolt Shaft #1	Fully Integrated Selectively-Reduced Solid Elements	A36 Steel, MAT_024
Bolt Head and Nut #1	Fully Integrated Selectively-Reduced Solid Elements	A325 Bolt Material, MAT_024
Bolt Shaft #2	Fully Integrated Selectively-Reduced Solid Elements	A325 Bolt Material, MAT_024
Bolt Head and Nut #2	Fully Integrated Selectively-Reduced Solid Elements	A325 Bolt Material, MAT_024
Bolt Shaft #3	Fully Integrated Selectively-Reduced Solid Elements	A325 Bolt Material, MAT_024
Bolt Head and Nut #3	Fully Integrated Selectively-Reduced Solid Elements	A325 Bolt Material, MAT_024
Bolt Shaft #4	Fully Integrated Selectively-Reduced Solid Elements	A325 Bolt Material, MAT_024
Bolt Head and Nut #4	Fully Integrated Selectively-Reduced Solid Solid Elements	A325 Bolt Material, MAT_024
Washer #1 through #16	Fully Integrated Selectively-Reduced Solid Elements	Rigid Material

\*The 16 Washers were defined in 16 separate parts



**Figure 136. Meshed Fracturing Bolt Post**

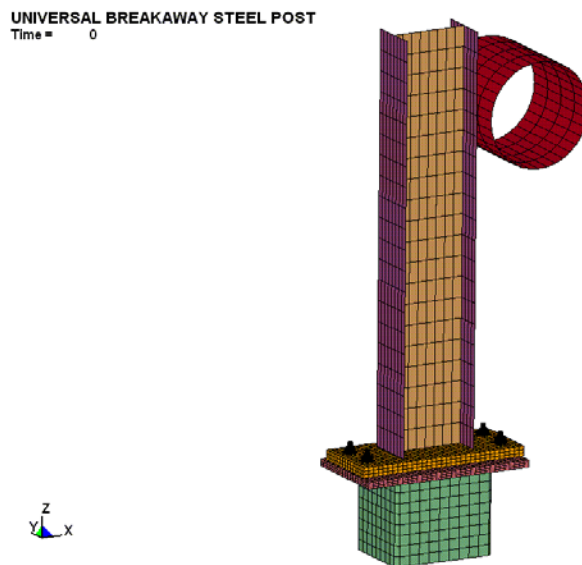


### 9.3.2 Connection Details

Various techniques were used to connect model parts together. For the I-beam flange and web, the nodes were merged. For each bolt, the nodes between the bolt head, nut part, and bolt shaft part were merged together. A contact tied nodes to surface command was used to connect both the I-beam to the upper steel plate as well as the lower steel plate to the bottom tube. \*CONTACT\_AUTOMATIC\_SINGLE\_SURFACE was used for contact between the bolts, washers, nuts, and steel plates.

### 9.4 Initial Simulation Results – Rigid Cylinder Impacts

After modeling the fracturing bolt post, initial simulations were run with a simple rigid cylinder impacting the fracturing bolt post about the strong axis of bending, as shown in Figure 137. Soil was excluded from these first simple models. The bottom tube was rigidly constrained just below the ground surface, and the rest of the embedded tube was ignored. These runs were performed to ensure that proper bolt prestress and post behavior was obtained before additional complexity was added to the model.



**Figure 137. Rigid Cylinder Impact**

#### **9.4.1 Contact and Prestressing Issues**

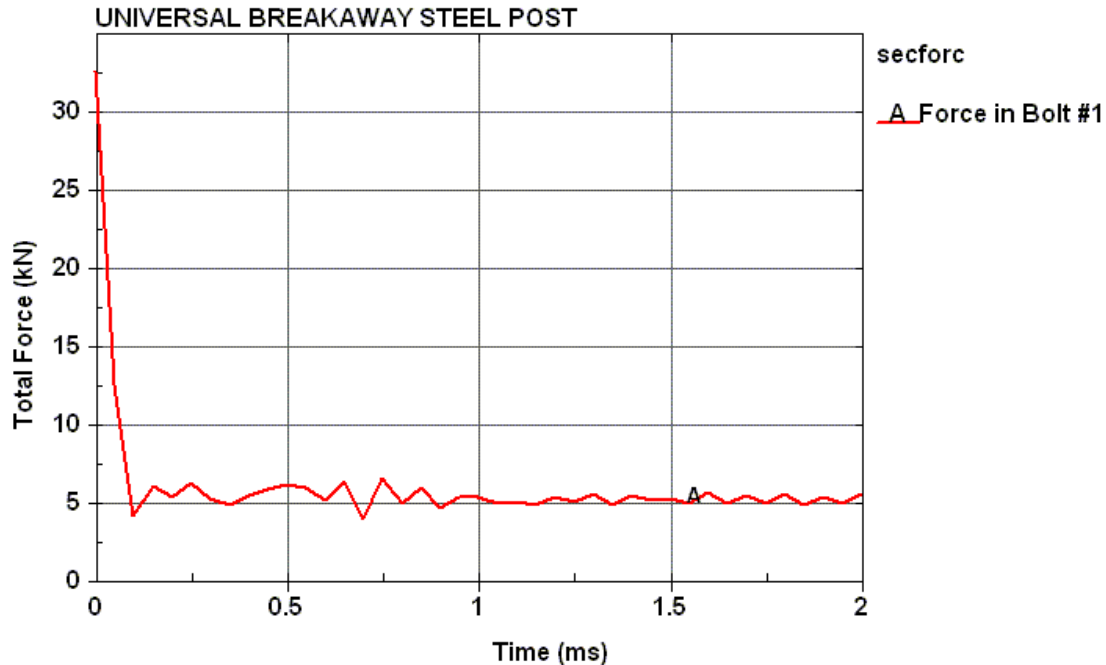
Numerous changes were made to this simple model in order to prestress the bolts and eliminate all contact issues. At first, no gaps were included between the different parts in the post, and the washers were meshed with sharp corners. However, the model did not work correctly with these features. Contact issues were observed that caused the washers to jump and slide around.

The first fix was to add gaps between the washers, bolts, nuts, and steel plates. After studying different gap sizes, a 0.000394 in. (0.01 mm gap) seemed to fix the contact issues. However, when bolt preload was added into the system, the contact issues reappeared. Thus, the second fix included the rounding of the corners of the washers in addition to the use of gaps in the model. Also, the I-beam and the bottom tube were dropped from the contact definitions. As a result of these changes, the contact feature was working correctly, and the bolts were able to be prestressed.

#### **9.4.2 Prestressing Results**

The prestress in the bolt shafts was assigned using the \*INITIAL\_STRESS\_SOLID command, similar to that used in the Hiser research study. An excel spreadsheet using the CONCATENATE command was set up to prestress every integration point for all of the elements in the bolt shafts.

The preload in the bolts required approximately 2 ms to reach equilibrium, as seen in Figure 138. The prestress stabilized as the initial gaps in the model disappeared and the deformable parts compressed.



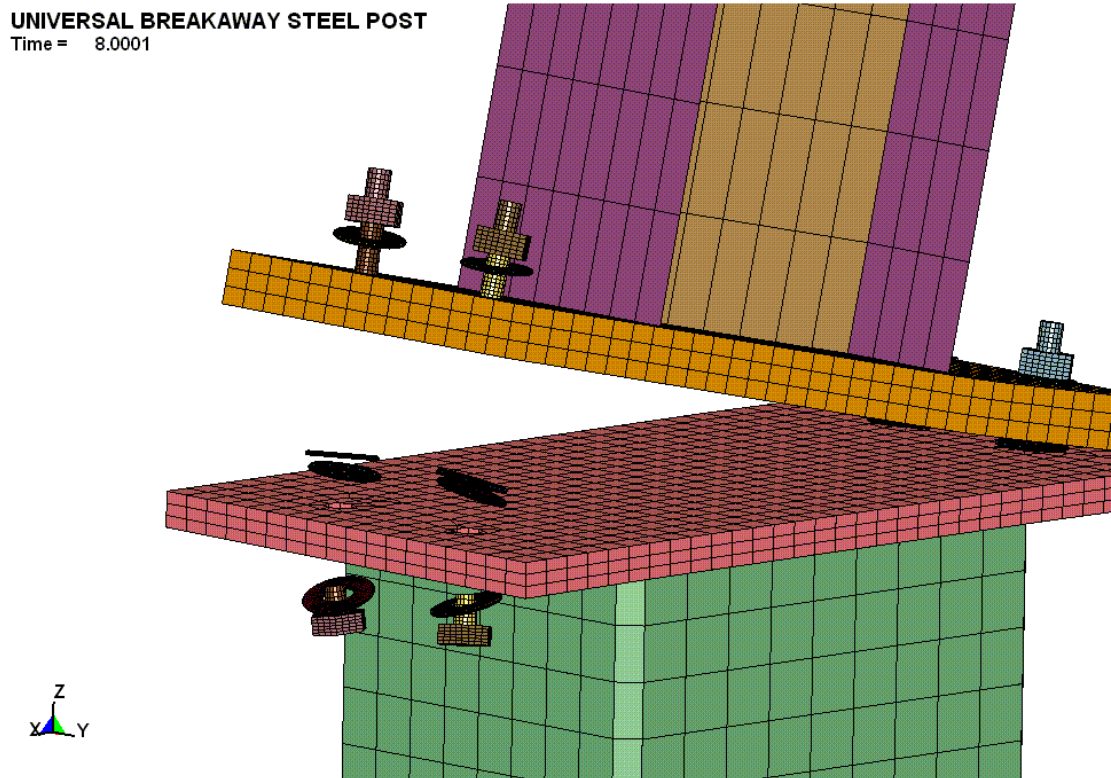
**Figure 138. Prestress Levels in One Bolt Shaft**

A prestress of 94 ksi (0.65 GPa) was assigned to the bolt shafts. This value was just below the yield stress of the bolts and resulted in a final bolt preload of approximately 1.12 kips (5 kN). In the actual bogie test, there was no torque value specified for the bolts, and the pre-load in the bolts was unknown. All that was known was that the bolts were tightened up “snugly”. Thus, it was decided to move forward using a bolt prestress of 94 ksi (0.65 GPa), since there was at least some pre-load in the bolt and no known pre-load levels for which to compare against.

#### **9.4.3 Rigid Cylinder Impact Results**

After allowing the prestressing in the bolts to stabilize, the rigid cylinder impacted the fracturing bolt post. This impact was run to ensure proper post behavior before adding more complexity to the model. In the actual bogie test, the bolts broke without much deformation to the remainder of the post. This behavior was also observed in the initial simulations, as shown in Figure 139. Thus, it seemed as though this simulation with the simple cylindrical impactor was

working properly, and focus of the simulation effort shifted toward adding more detail and accuracy to the model.

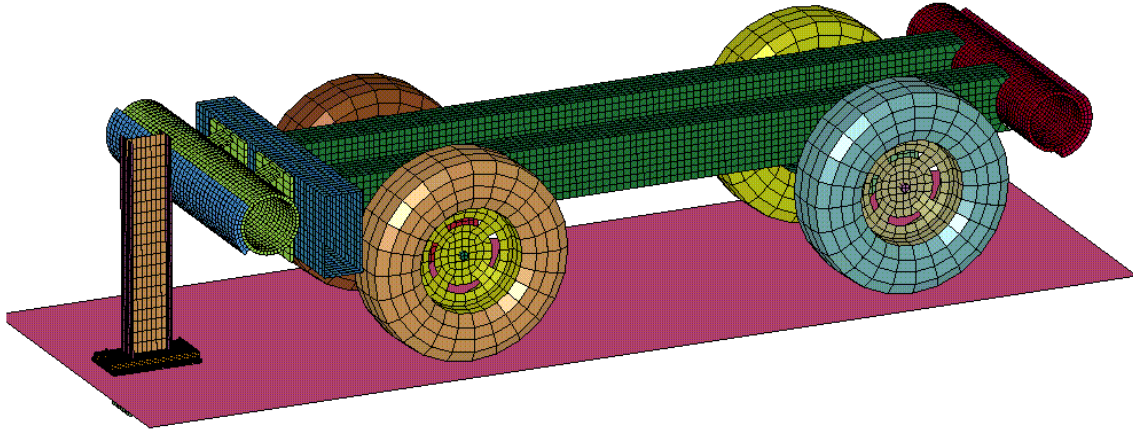


**Figure 139. Rigid Cylinder Impact Results**

## **9.5 Bogie and Soil Model Details**

### **9.5.1 Bogie Model**

Next, a previously developed bogie model was added to the fracturing bolt model, as shown in Figure 140. For modeling impacts into the fracturing bolt concept, changes included the deletion of the rigid cylinder impactor, moving the fracturing bolt post to the correct position, and adding a more accurate bogie model. At first, the post experienced more contact issues even before being impacted. However, when the soft option in the \*CONTACT\_AUTOMATIC\_SINGLE\_SURFACE was changed to a value equal to 2, the post model worked fine with the bogie model.



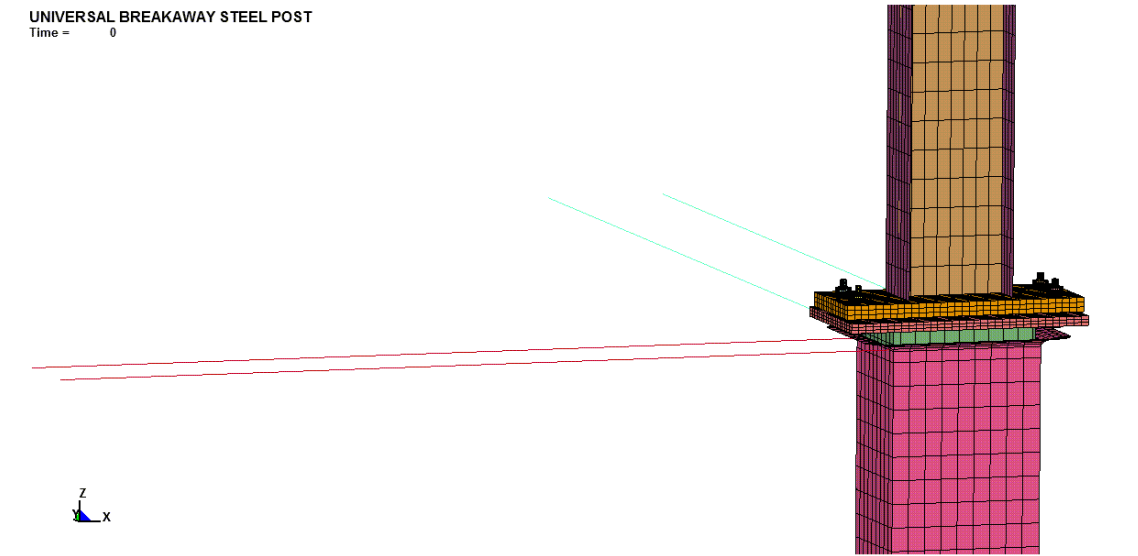
**Figure 140. Fracturing Bolt Model with the Bogie Model Before Impact**

The bogie model was given an initial velocity to match the velocity in the actual bogie testing. Also, an \*ELEMENT\_MASS command was added to give the bogie the correct weight (mass) to that measured in the actual bogie testing. A \*CONTACT\_ AUTOMATIC\_GENERAL command was used for the contact between the bogie head and the fracturing bolt post.

### **9.5.2 Soil Model**

The last addition to the simulation model was a previously developed soil model. This soil model used springs, \*MAT\_SPRING\_GENERAL\_NONLINEAR, to simulate the soil behavior, as shown in Figure 141. Two springs were used to mimic the soil resistance in both the strong and weak axis of the fracturing bolt post. The springs were attached to a rigid tube, which were scaled and placed around the full length of the bottom foundation tube of the fracturing bolt post. The rigid tube had fixed translation and fixed rotation in the vertical Z-axis about its center of gravity. Thus, this rigid tube only allowed the post to rotate against the soil springs.

UNIVERSAL BREAKAWAY STEEL POST  
Time = 0



**Figure 141. Soil Springs and Rigid Soil Tube**

The loading of the soil springs seemed to working correctly, but after the bolts broke, the unloading of soil springs caused the post to quickly spring back to zero displacement. In order to fix this incorrect behavior, the springs' unloading curves were changed to only have 0.04 in. (1 mm) of displacement, while having a high force, 1,799 kips (8,000 kN), to not allow any reverse rotation. Also, an initial yield force was specified for the soil springs to ensure that the unloading curve would be used. With the unloading curve of the soil springs fixed, the soil seemed to work properly. Thus, the focus was shifted to accurately match the behavior the real bogie testing.

## **9.6 Final Simulation Results**

Once all of the components in the simulation model were working correctly, numerous simulations were performed in order to match the simulation results with those obtained from the bogie testing program. Different soil loading curves and different bolt material properties were the primary variables that were altered to better match the results from the actual bogie testing.

For this effort, the goal for the simulation was to be able to accurately match the physical behavior observed in the bogie testing, including the force and energy versus deflection curves.

At first, only the strong-axis impact condition (test UBSP-20) was validated in order to obtain the appropriate soil loading curves and bolt material properties. Once the strong axis impact condition was validated, the model was also validated against the weak-axis impact condition (test UBSP-10) and the diagonal (45-degree) impact (test USBP-21).

### 9.6.1 Soil Loading Curve

First, numerous loading soil curves were investigated to match the actual bogie testing results from test UBSP-20. As previously stated, the soil gap in the actual test was measured to be approximately 2 1/4 in. (57 mm). The loading curve from the initial soil model, as shown in Table 19, showed promising results with a soil gap of approximately 2 in. (50 mm), but the force levels were higher than desired. As a result, lower soil strengths were tried, but it did not have much effect until the soil strength was significantly reduced. For significantly reduced soil strength, the post still bounced off of the bogie head too quickly, and the results were not accurate. Next, stronger soil strengths were simulated, and these tests only led to higher and more inaccurate force levels. Thus, it was determined to use the initial soil curve, as shown in Table 19, and investigate different bolt material properties.

**Table 19. Soil Loading Curve**

Displacement (mm)	Force (kN)*
-351	0
-263	-11.7
-210	-17
-70	-16.7
-15	-11.3
0	0
9	42.5
246	42.9

\* Negative Values for Compression of Springs

### 9.6.2 Final Bolt Material Properties

Initially, the bolt material properties were estimated using the yield and ultimate strength levels. The initial bolt failure occurred at an effective plastic strain of 0.30 and a corresponding effective plastic stress of 130 ksi (0.90 GPa). However, it was discovered that this failure made the bolts too weak, and thus, they fractured too quickly. Also, the simulated bolts behaved in a more ductile manner than what was observed in the actual physical testing.

As a result, simulations were performed to determine which stress and strain values should be used to match the strength and behavior for the actual testing. From this effort, the best results were obtained using the bolt material properties listed in Table 20, where failure was at a effective plastic strain of 0.25 and a effective plastic stress of 218 ksi (1.5 GPa).

**Table 20. Final ASTM A325 Bolt Material Properties – MAT\_024**

ro	e	pr	sigy	eppf
7.86*10-06	210	0.26	0.655	0.25

plastic stress/strain curve

0	0.25
0.655	1.5

\*Input for LS-DYNA Deck

### 9.6.3 Strong-Axis Impact Results

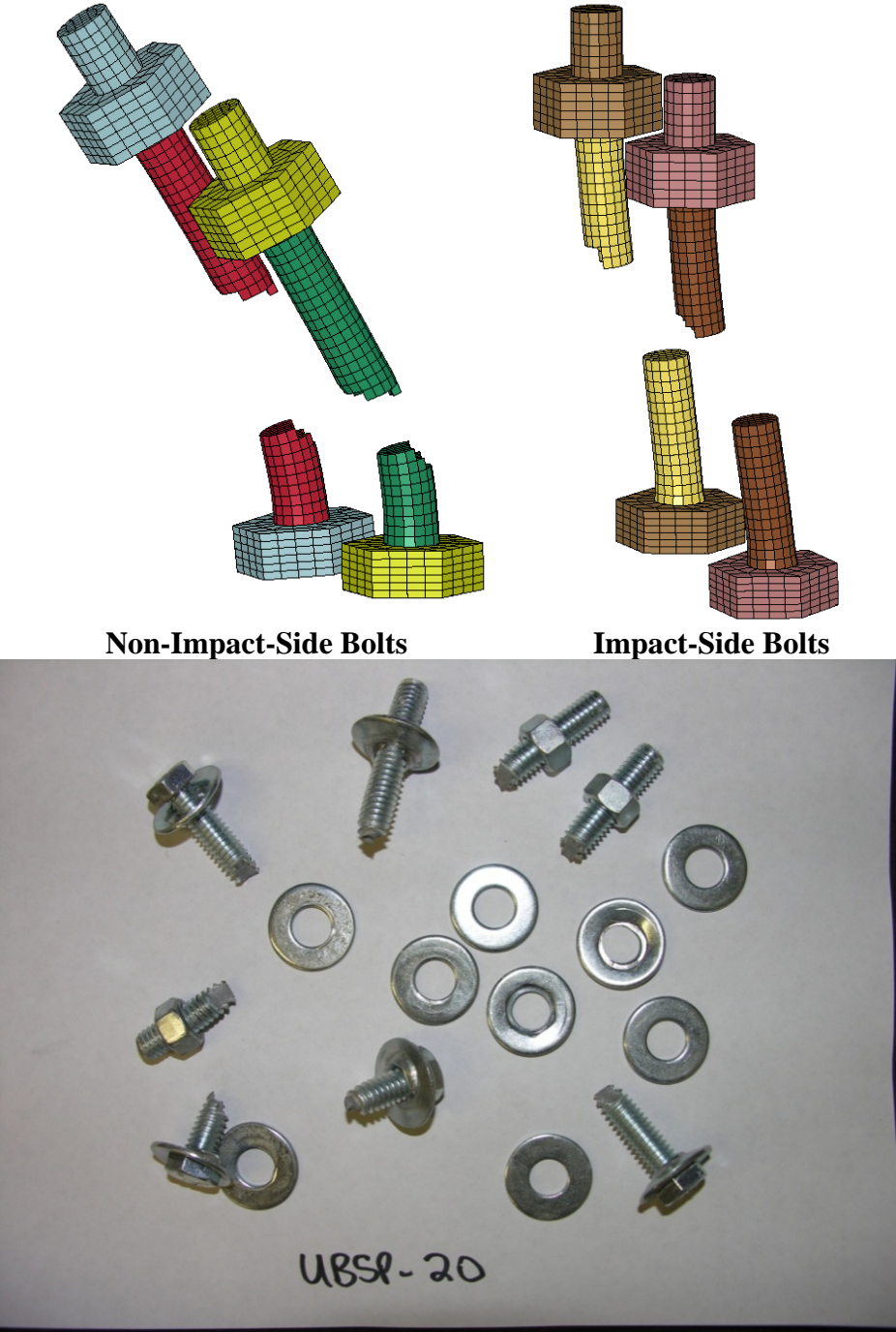
As outlined previously in Section 8.5.1 for bogie test UBSP-20, the bogie head impacted the post and stayed in contact until approximately 26 ms when the impact-side bolts broke in tension. Most the post deformation occurred to the bolts with some yielding and deformation in the lower steel plate, upper steel plate, and in a few of the washers.

The simulation results matched the general post behavior observed in the physical test closely. The bolt fracture behavior also closely matched the physical behavior, as shown in Figure 142, where the bolts either broke in a flat or a 45-degree plane. As provided in Figure

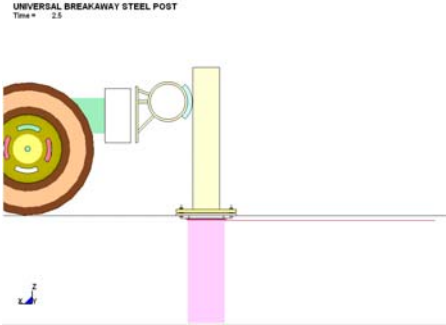
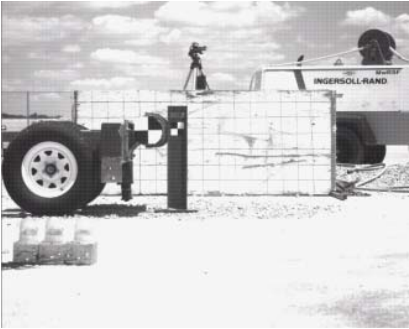


143, the time-sequential photographs showed the general simulated behavior followed the behavior in the actual test with the main difference being that the bolts broke quicker in the simulation.

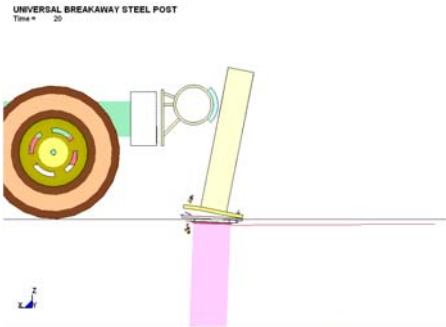
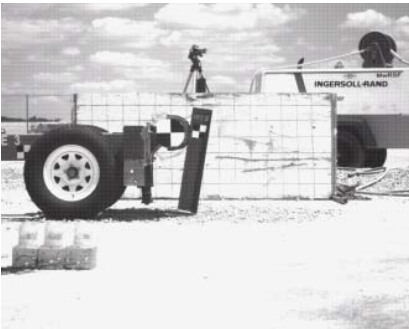
The force versus deflection and energy versus deflection curves for both the simulations and actual bogie tests are shown in Figures 144 and 145. The simulation results were very similar to the actual test results through approximately 4 in. (100 mm) of deflection. However, after this deflection, the simulated force levels jumped higher than observed in the actual testing, thus resulting in the premature bolt failure and reduced energy absorbed by the post. Numerous simulations were performed to prevent premature bolt failure. But, in every instance, the highest bolt stress occurred at around 20 ms or before. Possible reasons for the differences in the simulation results, such as from using rigid washers, are explained in Section 9.7. Still, the force levels and total energy of the simulation did tend to follow the general physical test with the notable difference being the timing for when the bolts broke.



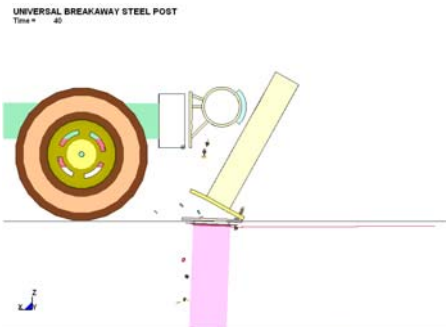
**Figure 142. Bolt Fracture Images of the Simulation and Actual Testing**



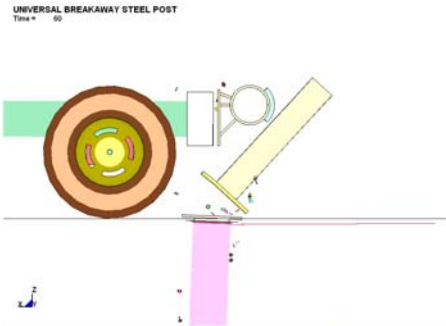
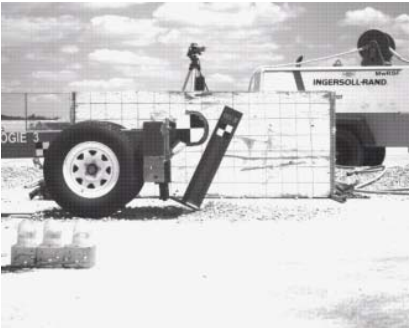
**IMPACT**



**TIME = 20 ms**



**TIME = 40 ms**



**TIME = 60 ms**

**Figure 143. Time Sequential Photographs – Strong-Axis Impact**

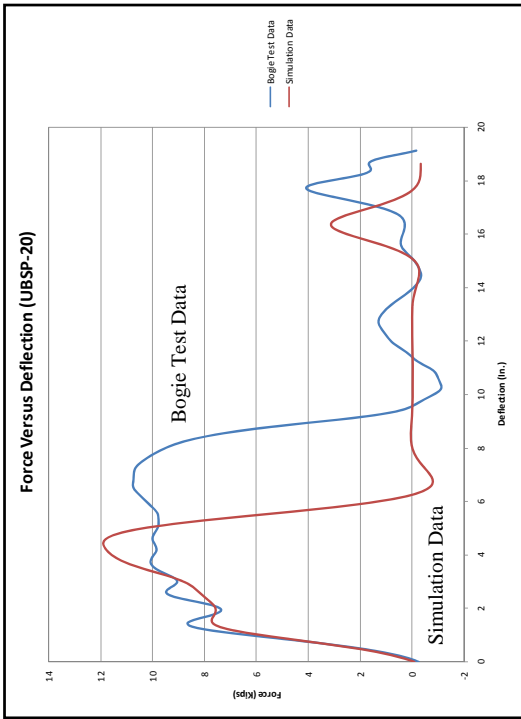


Figure 144a. Force vs. Deflection Curve, UBSP-20 Comparison - English

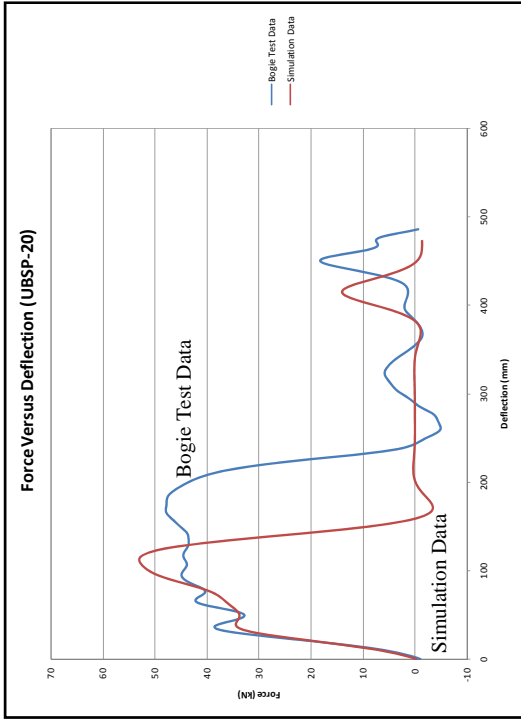


Figure 144b. Force vs. Deflection Curve, UBSP-20 Comparison - Metric

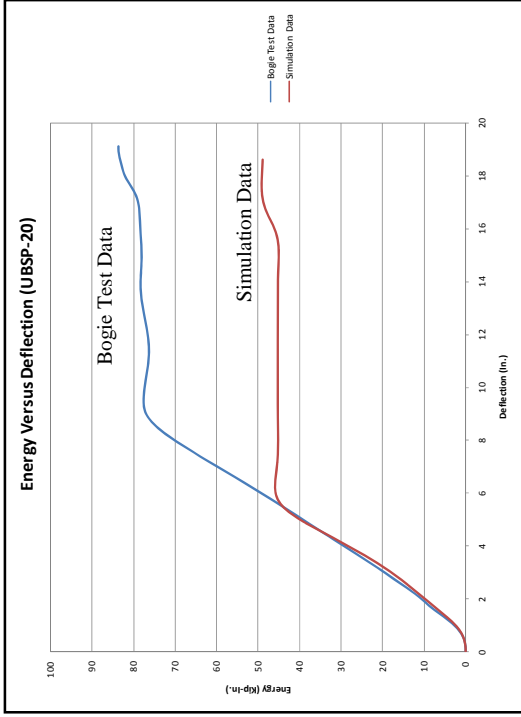


Figure 145a. Energy vs. Deflection Curve, UBSP-20 Comparison - English

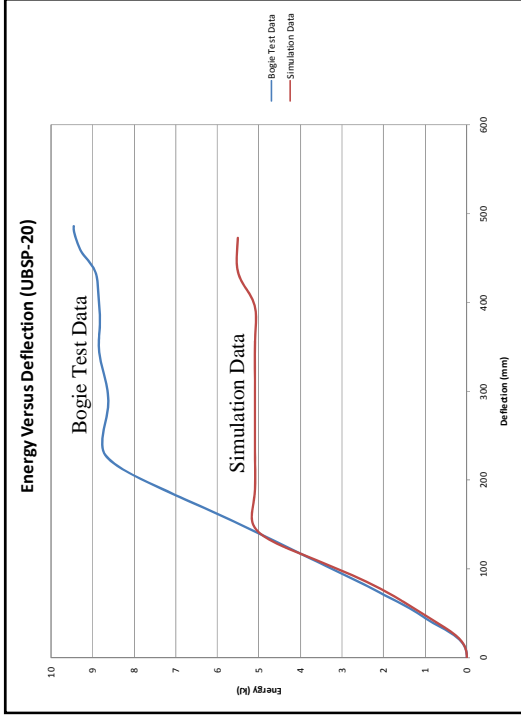


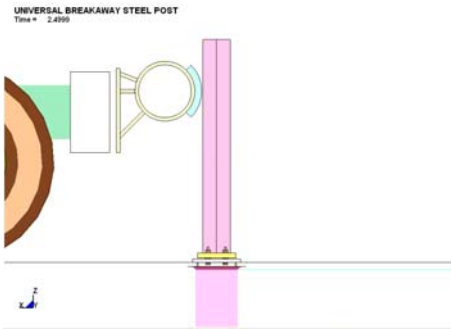
Figure 145b. Energy vs. Deflection Curve, UBSP-20 Comparison - Metric

#### **9.6.4 Weak-Axis Impact Results**

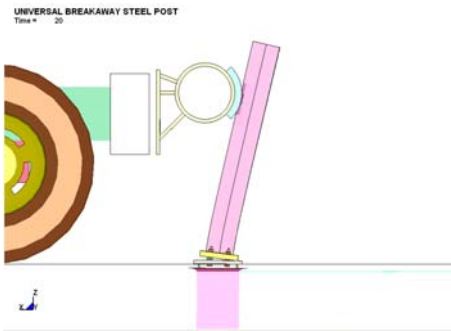
As outlined previously in Section 6.5.2 for bogie test UBSP-10, the post began to rotate immediately and the impact-side bolts fractured at approximately 14 ms. Next, the non-impact-side bolts broke at approximately 24 ms, causing the post to lose its resistance and lose contact with the bogie at 32 ms.

The simulation results were very similar to the general post behavior observed in the physical test. As shown in Figure 146, the time-sequential photographs revealed that the general simulated behavior followed the behavior in the actual test with the main difference being more damage to the upper W6x9 (W152x13.4) post in the simulation. There was more deformation where the bogie impacted the post in the simulation than observed in the actual testing. Also, the upper W6x9 (W152x13.4) post buckled slightly in the simulation, which was not observed in the actual bogie test.

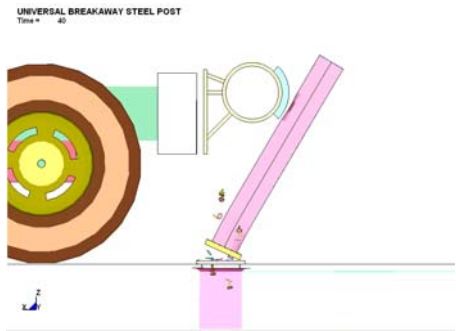
The force versus deflection and energy versus deflection curves for both the simulations and actual bogie tests are shown in Figures 147 and 148. As shown, the simulation did tend to follow the same general behavior, force levels, and energy levels observed in the actual bogie testing. The main difference was the simulated post held on slightly longer and absorbed more energy. Still, the force levels and total energy of the simulation tended to follow the general behavior of the actual testing closely.



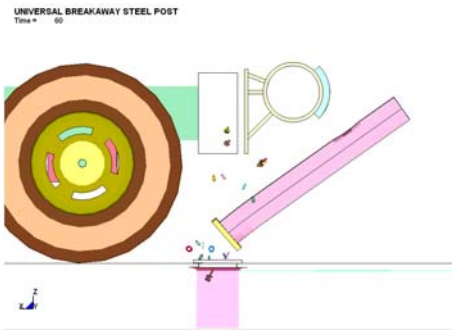
**IMPACT**



**TIME = 20 ms**



**TIME = 40 ms**



**TIME = 60 ms**

**Figure 146. Time Sequential Photographs – Weak Axis Impact**

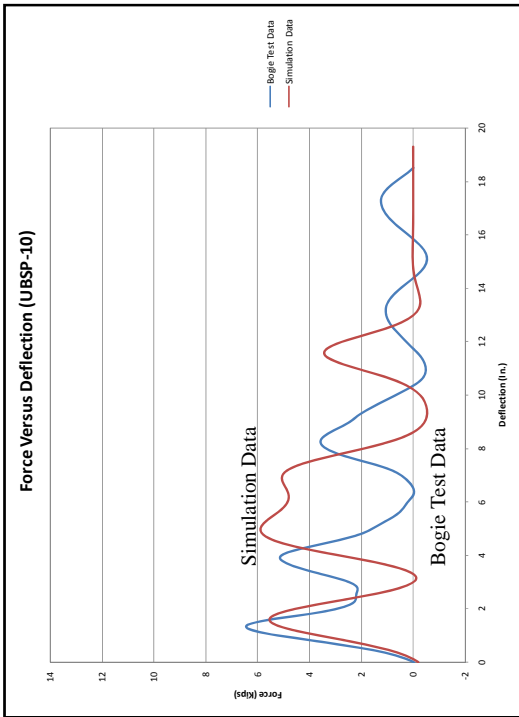


Figure 147a. Force vs. Deflection Curve, UBSP-10 Comparison - English

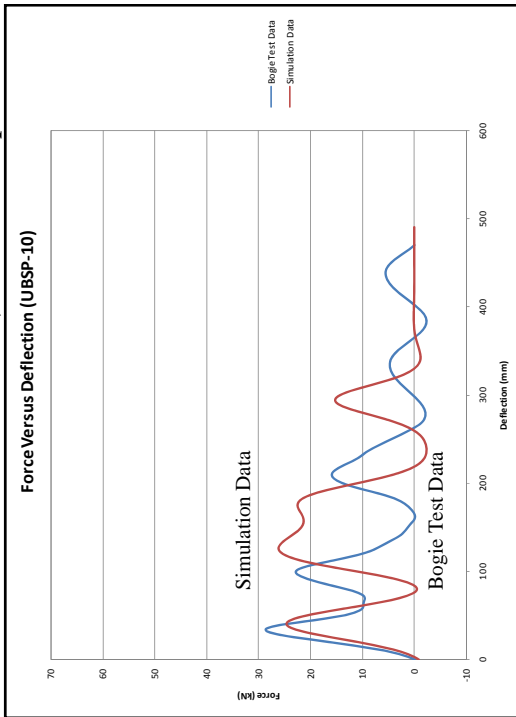


Figure 147b. Force vs. Deflection Curve, UBSP-10 Comparison - Metric

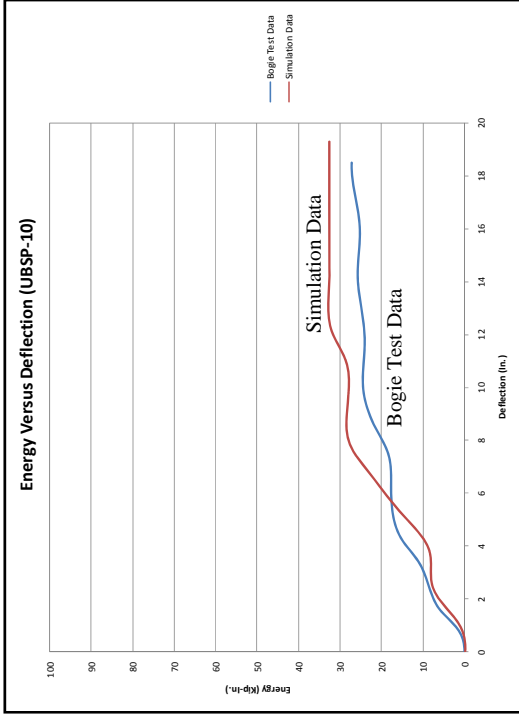


Figure 148a. Energy vs. Deflection Curve, UBSP-10 Comparison - English

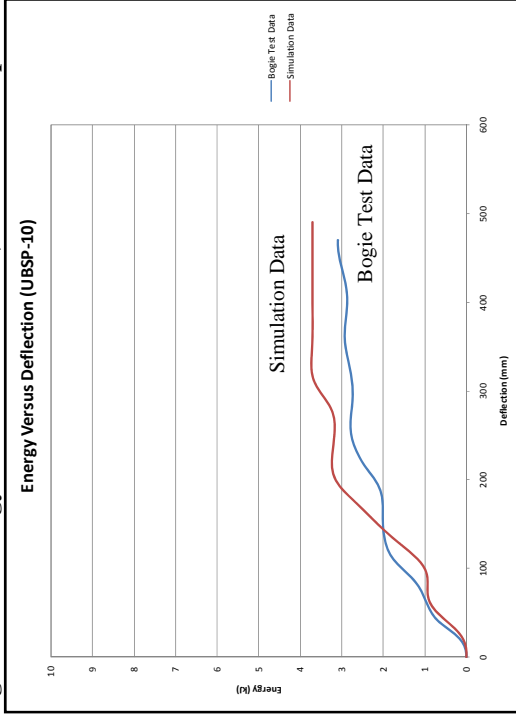


Figure 148b. Energy vs. Deflection Curve, UBSP-10 Comparison - Metric

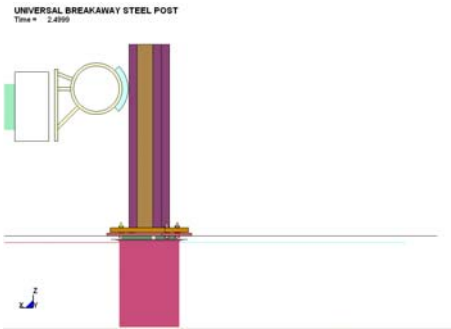
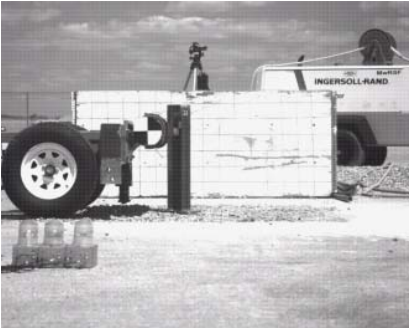
### **9.6.5 Diagonal (45-Degree) Axis Impact Results**

As outlined previously in Section 8.5.2 for bogie test UBSP-21, the bogie head impacted the post and stayed in contact until approximately 26 ms when the impact-side bolts broke in tension. Most of the post deformation occurred to the bolts with some yielding and deformation in the lower steel plate, upper steel plate, and in a few of the washers.

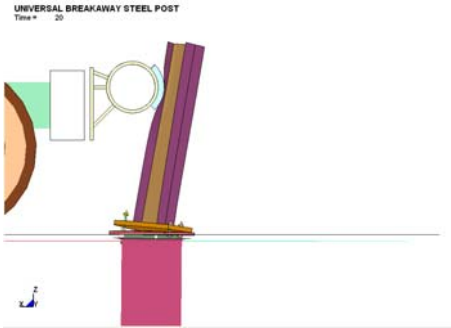
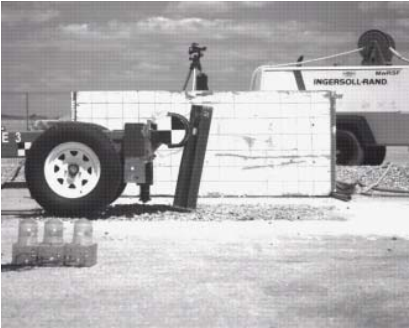
The simulation results matched the general behavior of this diagonal angle impact closely, as shown in the time-sequential photographs provided in Figure 149. One observed difference was that initial bolt fracture occurred earlier in the simulation as compared to the actual test. Other than this difference, both the general behavior and deformation pattern observed in the simulation seemed to match the bogie testing.

The force versus deflection and energy versus deflection curves for both the simulations and actual bogie tests are shown in Figures 150 and 151. The simulated force levels were very similar to the actual bogie testing results. The simulated energy levels were slightly lower than those observed in the actual testing. Still, overall, the force levels and total energy of the simulation tended to follow the same general behavior that was observed in the actual testing.

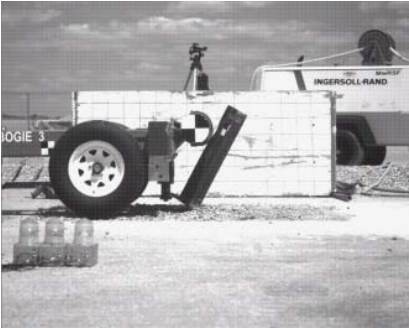




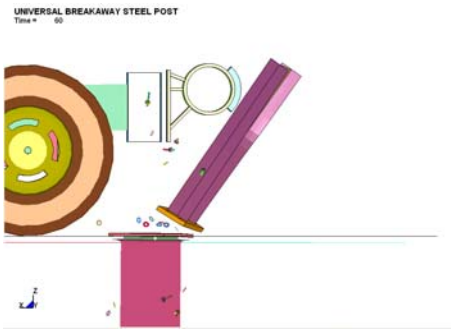
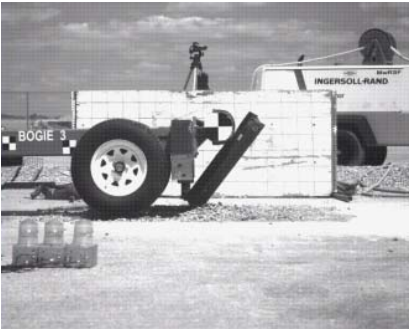
**IMPACT**



**TIME = 20 ms**



**TIME = 40 ms**



**TIME = 60 ms**

**Figure 149. Time Sequential Photographs – Diagonal Axis Impact**

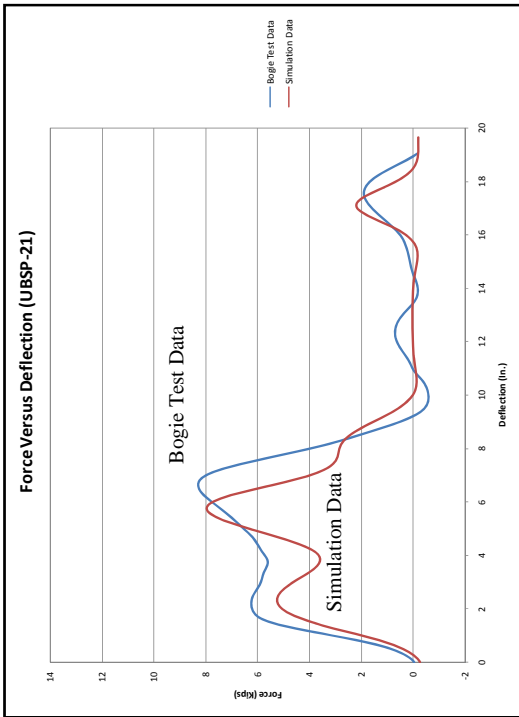


Figure 150a. Force vs. Deflection Curve, UBSP-21 Comparison - English

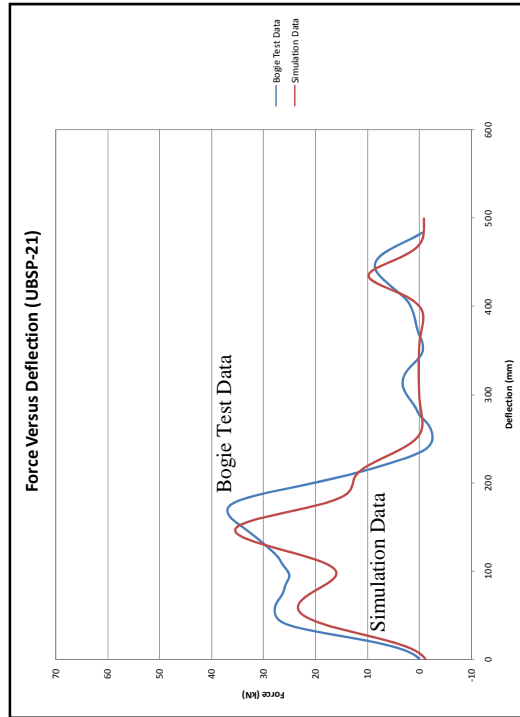


Figure 150b. Force vs. Deflection Curve, UBSP-21 Comparison - Metric

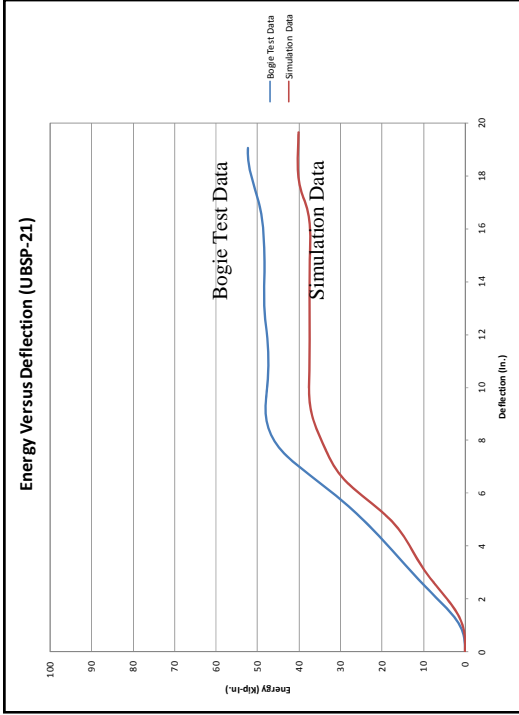


Figure 151a. Energy vs. Deflection Curve, UBSP-21 Comparison - English

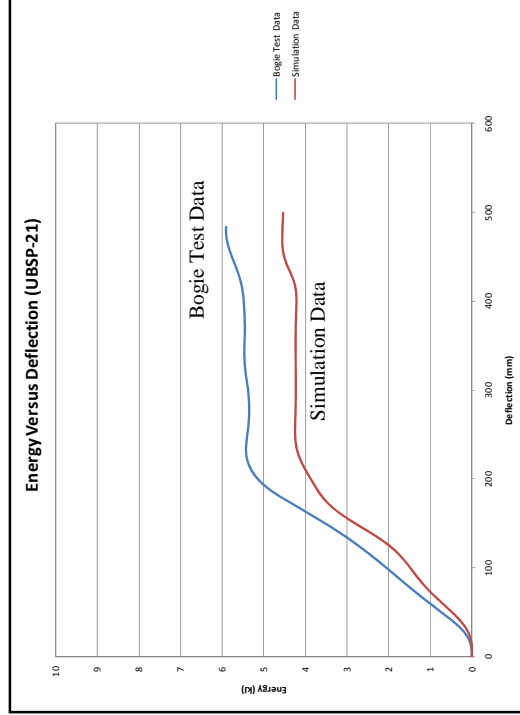


Figure 151b. Energy vs. Deflection Curve, UBSP-21 Comparison - Metric

## 9.7 Conclusions/Recommendations

Computer simulation of the fracturing bolt post was performed using three different axes of impact. For all three impact conditions, the fracturing bolt post broke away cleanly as observed in the actual bogie tests. Thus, this fracturing bolt post model may eventually be used in computer simulation of full-scale vehicle crash tests into three beam bullnose barriers in order to evaluate future design modifications. However, this post model would still require additional refinement to allow for improved comparisons between simulated and physical test results, especially for the energy versus deflection curve observed in strong-axis testing.

The differences between the simulation and physical test results may have occurred from multiple sources, including the soil model, the bolt material model, contact with the bogie, and potentially from using rigid material for the washers. A few simulations were run using deformable washers in an attempt to match the deformation observed in the actual testing. However, the fine mesh used for the washers caused the computational time to significantly increase. A simulation with deformable washers caused the computational time to increase from 4 hours 6 minutes with rigid washers to 16 hours 3 minutes. In addition, technical information in terms of material properties was unavailable for modeling small washers. Thus, further investigation is needed before deformable washers are used to improve the simulation results obtained for the fracturing bolt post. The simulations using deformable washers caused the posts to break away too quickly in strong-axis impacts.

Other future research should include refinements for improving the accuracy for the soil and bolt material models. Currently, these models were modified in an attempt to match results

observed in the the bogie testing, but the modifications to the soil model were not based on physical data. Also, the contact between the bogie and the post should be further investigated.

## 10 FULL-SCALE CRASH TEST PROGRAM

### 10.1 Test Requirements

Terminals and crash cushions, such as bullnose median barriers, must satisfy the requirements provided in NCHRP Report No. 350 [4] in order to be accepted for use on new construction projects or as a replacement for existing barriers not meeting current safety standards. From previous testing [3], the bullnose median barrier was defined as a non-gating barrier, and thus, must fulfill the requirements for a non-gating device. A non-gating device is designed to contain and either redirect or capture a vehicle when impacted downstream from the end of the device.

According to NCHRP Report No. 350, terminals and crash cushions must be subjected to eight full-scale vehicle crash tests, five using a pickup truck weighing approximately 2,000 kg (4,409 lbs) and three using a small car weighing approximately 820 kg (1,808 lbs), designated as 2000P and 820C, respectively. The required 2000P crash tests for a Test Level 3 (TL-3) device are: (1) Test 3-31, a 100 km/h impact at a nominal angle of 0 degrees on the tip of the barrier nose; (2) Test 3-33, a 100 km/h impact at a nominal angle of 15 degrees on the tip of the barrier nose; (3) Test 3-37, a 100 km/h impact at a nominal angle of 20 degrees on the beginning of the LON (Length-of-Need); (4) Test 3-38, a 100 km/h impact at a nominal angle of 20 degrees on the Critical Impact Point (CIP); and (5) Test 3-39, a 100 km/h reverse direction impact at an angle of 20 degrees at a location of one half of the distance to the LON from the end of the terminal. The required 820C crash tests for a TL-3 device are: (1) Test 3-30, a 100 km/h impact at a nominal angle of 0 degrees on the tip of the barrier nose with a 1/4-point offset; (2) Test 3-32, a 100 km/h impact at a nominal angle of 15 degrees on the tip of the barrier nose; and (3)

Test 3-36, a 100 km/h impact at a nominal impact angle of 15 degrees on the beginning of the LON. It is noted that the Critical Impact Point (CIP) mentioned above is defined for non-gating terminals as the point along the installation where it unknown whether the guardrail will capture the impacting vehicle or redirect it.

Previous testing in “Phase I, II, and III Development of a Bullnose Guardrail System for Median Applications” [1-3] successfully completed all of the required tests on the wood-post, thrie beam bullnose system. Based on the success of the previous testing, it was believed that the tests required for this project would be those tests that would be affected by the change from the wood CRT posts to the steel fracturing bolt posts. After considerable discussion, researchers determined that two full-scale crash tests, with a possible third test, would be required in this project:

- (1) Test Designation 3-38 (2000P at CIP);
- (2) Test Designation 3-30 (820C end-on, with 1/4-point offset); and possibly
- (3) Test Designation 3-31 (2000P end-on to evaluate penetration distance)

The full-scale vehicle crash test matrix is provided in Figure 152.

## **10.2 Evaluation Criteria**

Evaluation criteria for full-scale vehicle crash testing are based on three appraisal areas: (1) structural adequacy; (2) occupant risk; and (3) vehicle trajectory after collision. Criteria for structural adequacy are intended to evaluate the ability of the terminal to contain, redirect, or allow controlled vehicle penetration in a predictable manner. Occupant risk evaluates the degree of hazard to occupants in the impacting vehicle. Vehicle trajectory after collision is a measure of the potential for the post-impact trajectory of the vehicle to cause subsequent multi-vehicle

accidents, thereby subjecting occupants of other vehicles to undue hazard or to subject the occupants of the impacting vehicle to secondary collisions with other fixed objects. These three evaluation criteria are defined in Table 21. The full-scale vehicle crash testing program was conducted and reported in accordance with the evaluation procedures provided in NCHRP Report No. 350.

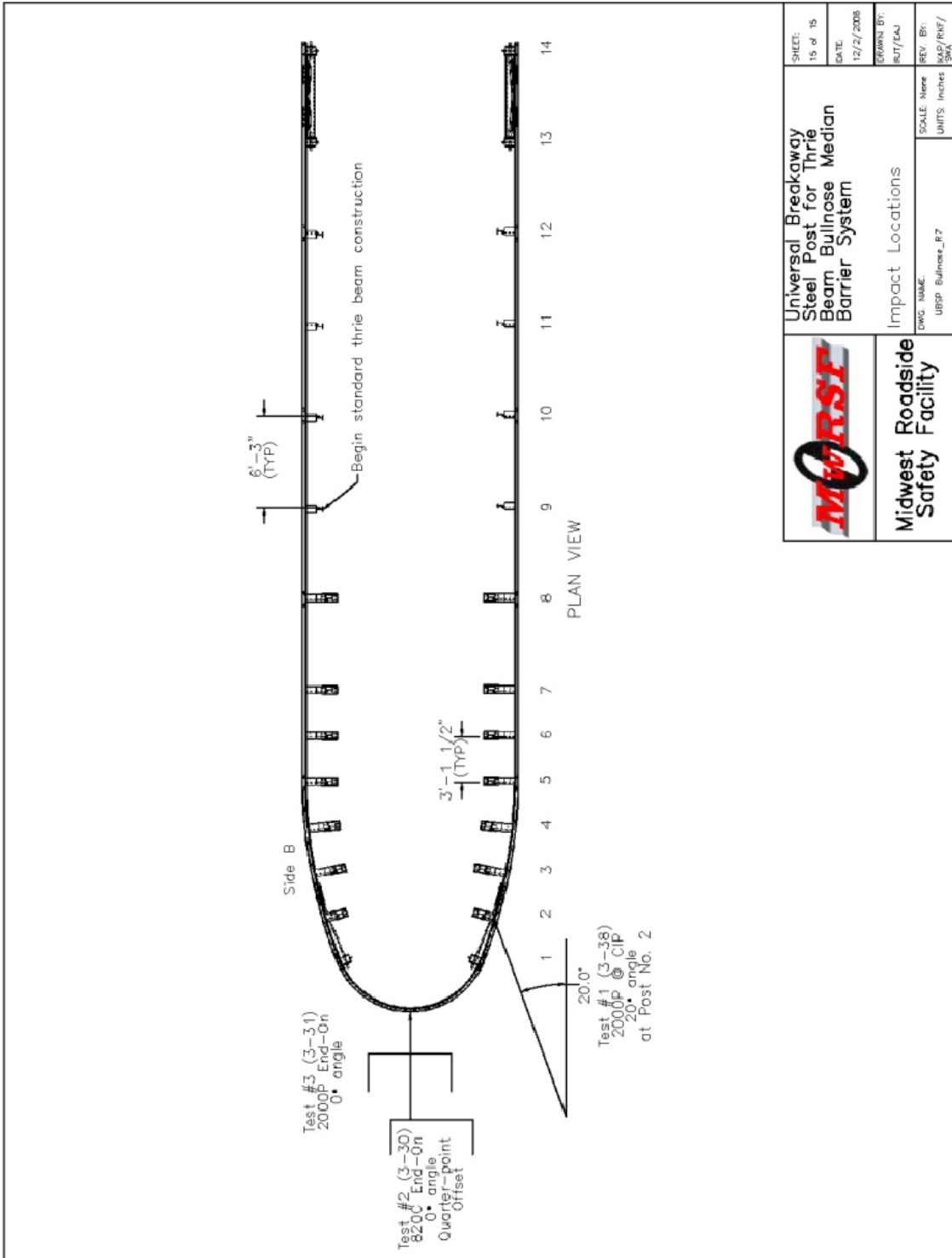


Figure 152. Full-Scale Crash Test Matrix



**Table 21. NCHRP Report No. 350 Evaluation Criteria for Crash Tests**

Evaluation Factors	Evaluation Criteria	Applicable Tests						
Structural Adequacy	A. Test article should contain and redirect the vehicle; the vehicle should not penetrate, underide, or override the installation although controlled lateral deflection of the test article is acceptable.	3-36 3-37 3-38						
	C. Acceptable test article performance may be by redirection, controlled penetration, or controlled stopping of the vehicle.	3-30 3-31 3-32 3-33 3-39						
Occupant Risk	D. Detached elements, fragments or other debris from the test article should not penetrate or show potential for penetrating the occupant compartment, or present an undue hazard to other traffic, pedestrians, or personnel in a work zone. Deformations of, or intrusions into, the occupant compartment that could cause serious injuries should not be permitted.	ALL						
	F. The vehicle should remain upright during and after collision although moderate roll, pitching, and yawing are acceptable.	ALL						
	H. Occupant impact velocities should satisfy the following: <b>Occupant Impact Velocity Limits (m/s)</b> <table border="1" data-bbox="548 961 1101 1045"> <thead> <tr> <th>Component</th> <th>Preferred</th> <th>Maximum</th> </tr> </thead> <tbody> <tr> <td>Longitudinal and Lateral</td> <td>9</td> <td>12</td> </tr> </tbody> </table>	Component	Preferred	Maximum	Longitudinal and Lateral	9	12	3-30 3-31 3-32 3-33 3-36
	Component	Preferred	Maximum					
Longitudinal and Lateral	9	12						
I. Occupant ridedown accelerations should satisfy the following: <b>Occupant Ridedown Acceleration Limits (G's)</b> <table border="1" data-bbox="548 1150 1101 1234"> <thead> <tr> <th>Component</th> <th>Preferred</th> <th>Maximum</th> </tr> </thead> <tbody> <tr> <td>Longitudinal and Lateral</td> <td>15</td> <td>20</td> </tr> </tbody> </table>	Component	Preferred	Maximum	Longitudinal and Lateral	15	20	3-30 3-31 3-32 3-33 3-36	
Component	Preferred	Maximum						
Longitudinal and Lateral	15	20						
Vehicle Trajectory	K. After collision it is preferable that the vehicle's trajectory not intrude into adjacent traffic lanes.	ALL						
	L. The occupant impact velocity in the longitudinal direction should not exceed 12 m/sec and the occupant ridedown acceleration in the longitudinal direction should not exceed 20 G's.	3-37 3-38 3-39						
	M. The exit angle from the test article preferably should be less than 60 percent of the test impact angle, measured at the time the vehicle lost contact with the device.	3-36 3-37 3-38 3-39						
	N. Vehicle trajectory behind the test article is acceptable.	3-30 3-31 3-32 3-33 3-39						

### **10.3 Bullnose Median Barrier Design Details**

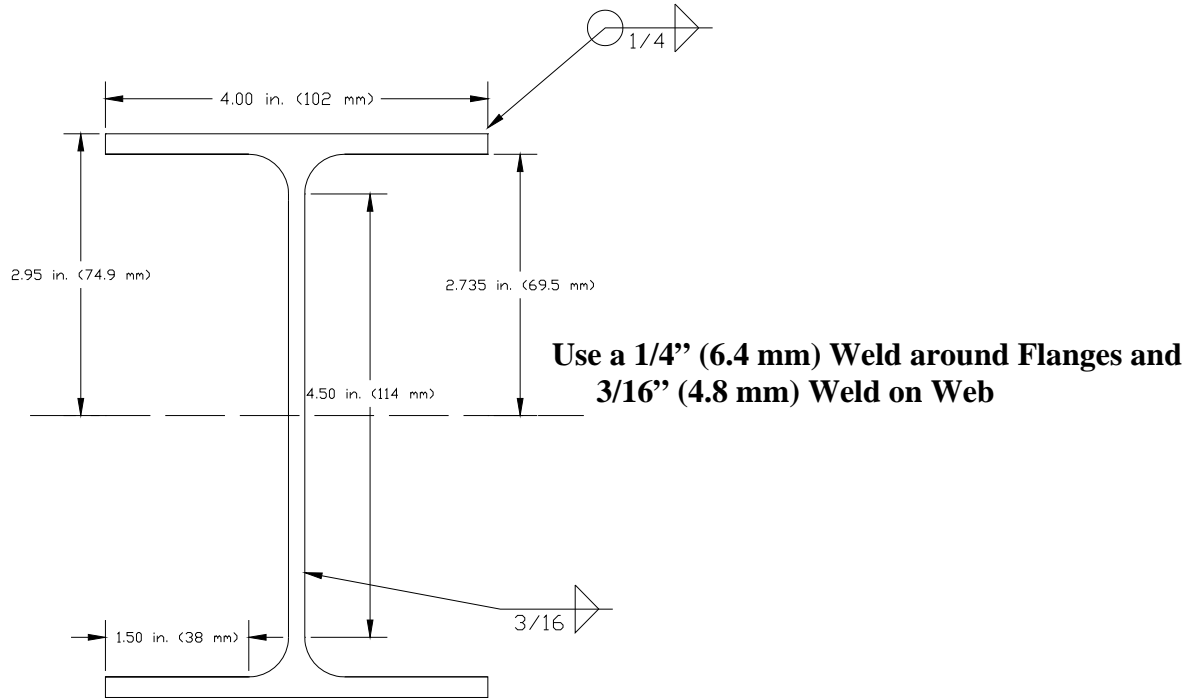
The complete layout of the three beam bullnose barrier system is shown in Figure 154 with details shown in Figures 155 through 167. Similar to previous testing, a one-half barrier system was utilized for the testing program in order to limit costs and construction time. The bullnose system was constructed with twenty-eight posts, with fourteen posts positioned on each side of the system. The first post on each side of the system was a three beam Breakaway Cable Terminal (BCT) wood post. Although the goal of this study was to develop an all-steel system, it was found in previous testing that using a BCT wood post in the anchorage system allowed for improved performance and the effective capture of the pickup truck [5]. Also, the objective for this study focused on the replacement of the wood CRT posts with steel posts, or other non-wood posts. Anchor posts are different and would require a different steel post design. The new fracturing bolt steel post used in the bullnose median barrier system was the same design previously used in the third round of bogie testing on the breakaway posts. Photographs of the system are provided in Figures 168 through 170.

All of the posts were placed in a compacted course, crushed limestone material meeting Grading B of AASHTO M 147-65 as found in NCHRP 350. The soil was placed using 6 in. (152 mm) lifts in 2-ft (610-mm) diameter augured holes. Also, the fracturing bolts in the breakaway posts were torqued to 35 ft-lbs (47.5 N-m) for the full-scale crash testing program.

#### **10.3.1 Revised Weld Details for Fracturing Bolt Post**

After completing full-scale crash testing program using the fracturing bolt post details described above, it was determined that the 5/16-in. (7.9-mm) weld that was tested as in Figure 160 and that was used to connect the upper W6x9 (W152x13.4) post to the upper steel plate was

overdesigned and could be made smaller for any future testing or use. As shown in Figure 153, calculations were made that demonstrated the welds could be reduced from 5/16 in. (7.9-mm) as tested to a 1/4-in. (6.4-mm) weld on the flanges and 3/16-in. (4.8-mm) weld on the web around the W6x9 (W152x13.4). The weld strength was checked for both strong- and weak-axis impacts, where the target loads were 12 kips (53 kN) and 6 kips (27 kN), respectively. Thus, this smaller weld could be used for any future testing.



**Strong-Axis Impact**

$$I_{outside\ flange} = (2) \left( \frac{1}{12} \right) (4)(0.707 * 0.25)^3 + (2)(0.707)(0.25)(4)(2.95)^2 = 12.31\ in^4$$

$$I_{inside\ flange} = (2) \left( \frac{1}{12} \right) (3)(0.707 * 0.25)^3 + (2)(0.707)(0.25)(3)(2.735)^2 = 7.94\ in^4$$

$$I_{web} = (2) \left( \frac{1}{12} \right) (0.707)(0.1875)(4.5)^3 = 2.01\ in^4$$

$$I_{total} = 22.26\ in^4$$

$$S = \frac{22.26}{2.95} = 7.55\ in^3$$

$$M_{capacity} = 7.55 (58\ ksi) = 437.67\ k * in.$$

$$Peak\ Force\ Capacity = \frac{437.67}{24.875} = 17.6\ kips > 12\ kips - OK$$

**Weak Axis-Impact**

$$I_{outside\ flange} = (2) \left( \frac{1}{12} \right) (0.25)(0.707)(4)^3 = 1.89\ in^4$$

$$I_{inside\ flange} = (4) \left( \frac{1}{12} \right) (0.25)(0.707)(1.5)^3 + (4)(0.707)(0.25)(1.5)(0.75 + 0.5)^2 = 1.86\ in^4$$

$$I_{end\ of\ flange} = (4) \left( \frac{1}{12} \right) (0.215)(0.707 * 0.25)^3 + (4)(0.707)(0.25)(0.215)(2 + 0.125)^2 = 0.69\ in^4$$

$$I_{web} = (2) \left( \frac{1}{12} \right) (4.5)(0.707 * 0.1875)^3 + (2)(0.707)(0.1875)(4.5)(0.085 + 0.09375)^2 = 0.79\ in^4$$

$$I_{total} = 5.23\ in^4$$

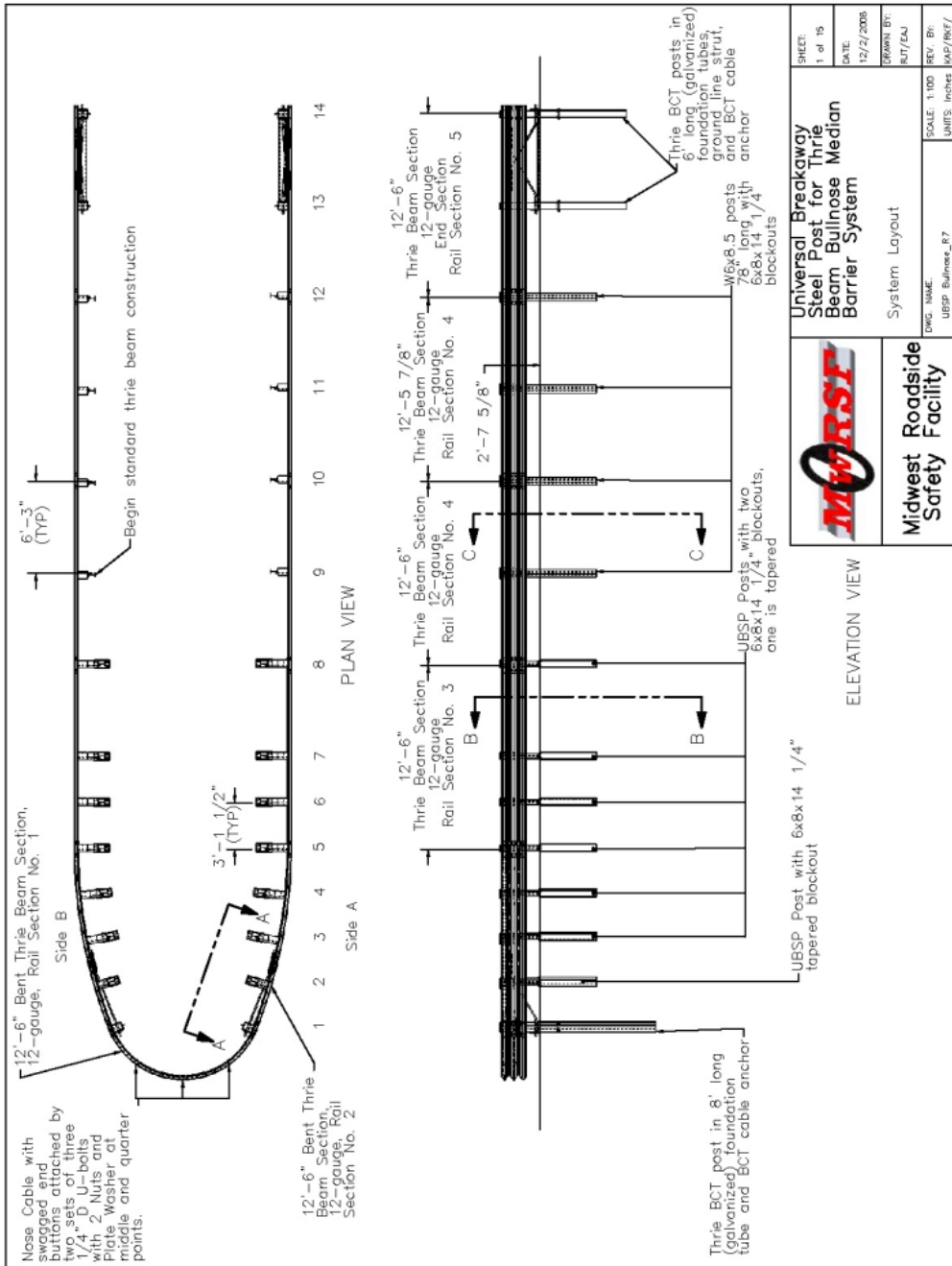
$$S = \frac{5.23}{2.00} = 2.615\ in^3$$

$$M_{capacity} = 2.615 (58\ ksi) = 151.7\ k * in.$$

$$Peak\ Force\ Capacity = \frac{151.7}{24.875} = 6.1\ kips > 6\ kips - OK$$

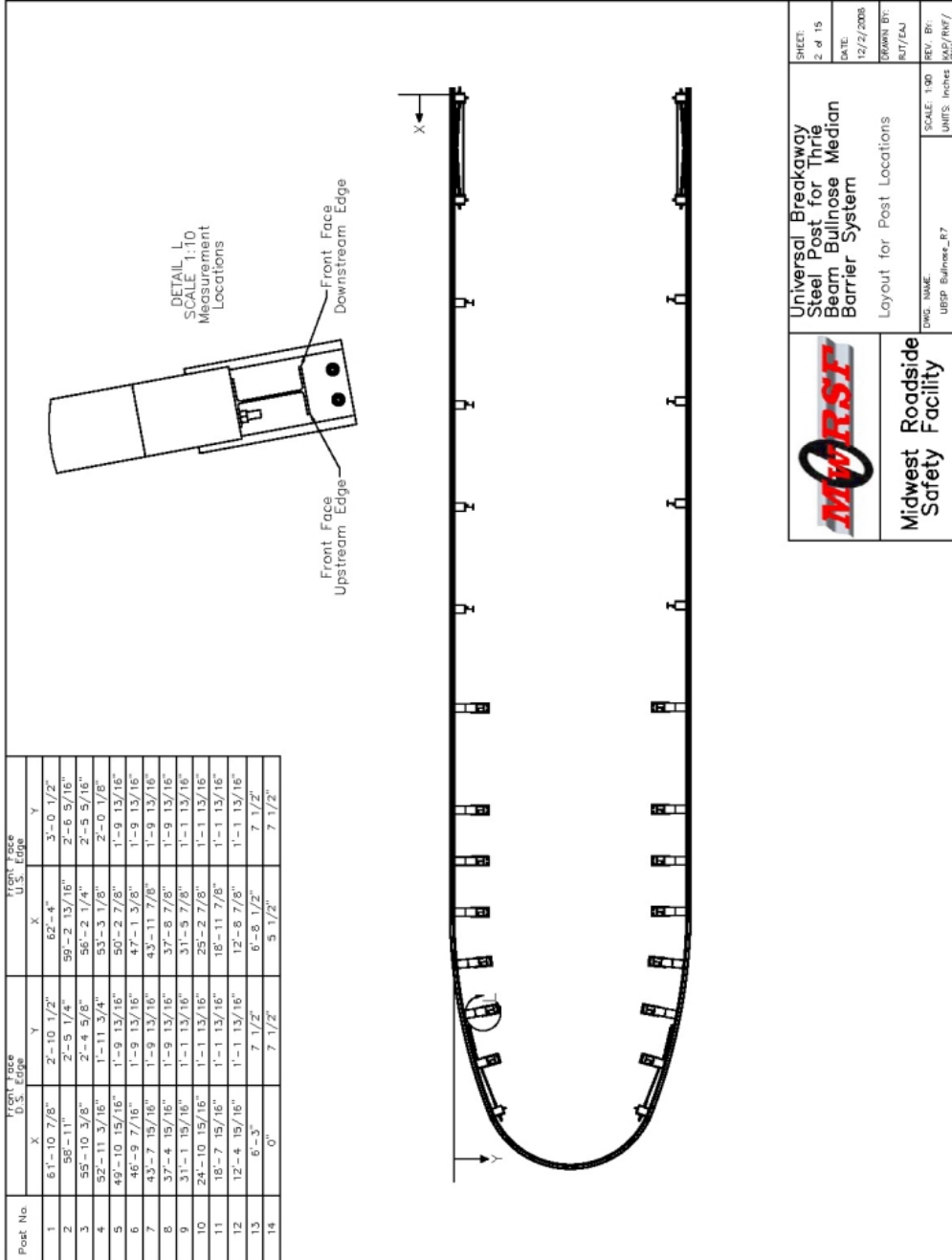
\*Include 1/4" (6.4 mm) weld completely around flange to ensure weld strength

**Figure 153. Fracturing Bolt Recommended Welds**



		<b>Universal Breakaway Steel Post for Thrie Beam Bullnose Median Barrier System</b>
<b>Midwest Safety Facility</b>		System Layout
DWG. NAME: UBSP Bullnose_B7		SCALE: 1/8" = 1'-0" UNITS: inches
SHEETS: 1 of 15	DATE: 12/2/2008	DRAWN BY: R/J/EAJ
		REV. BY: MGP/RKF/SAK

**Figure 154. UBSP Bullnose Median Barrier System Layout**



	Universal Breakaway Steel Post for Triple Beam Bullnose Median Barrier System Layout for Post Locations	SHEET: 2 of 15 DATE: 12/2/2008 DRAWN BY: BJT/EJW REV. BY: MAP/PNF/ SKA
	Midwest Roadside Safety Facility UBSP Bullnose_F7	SCALE: 1/80 UNITS: Inches

Figure 155. UBSP Bullnose Post Locations

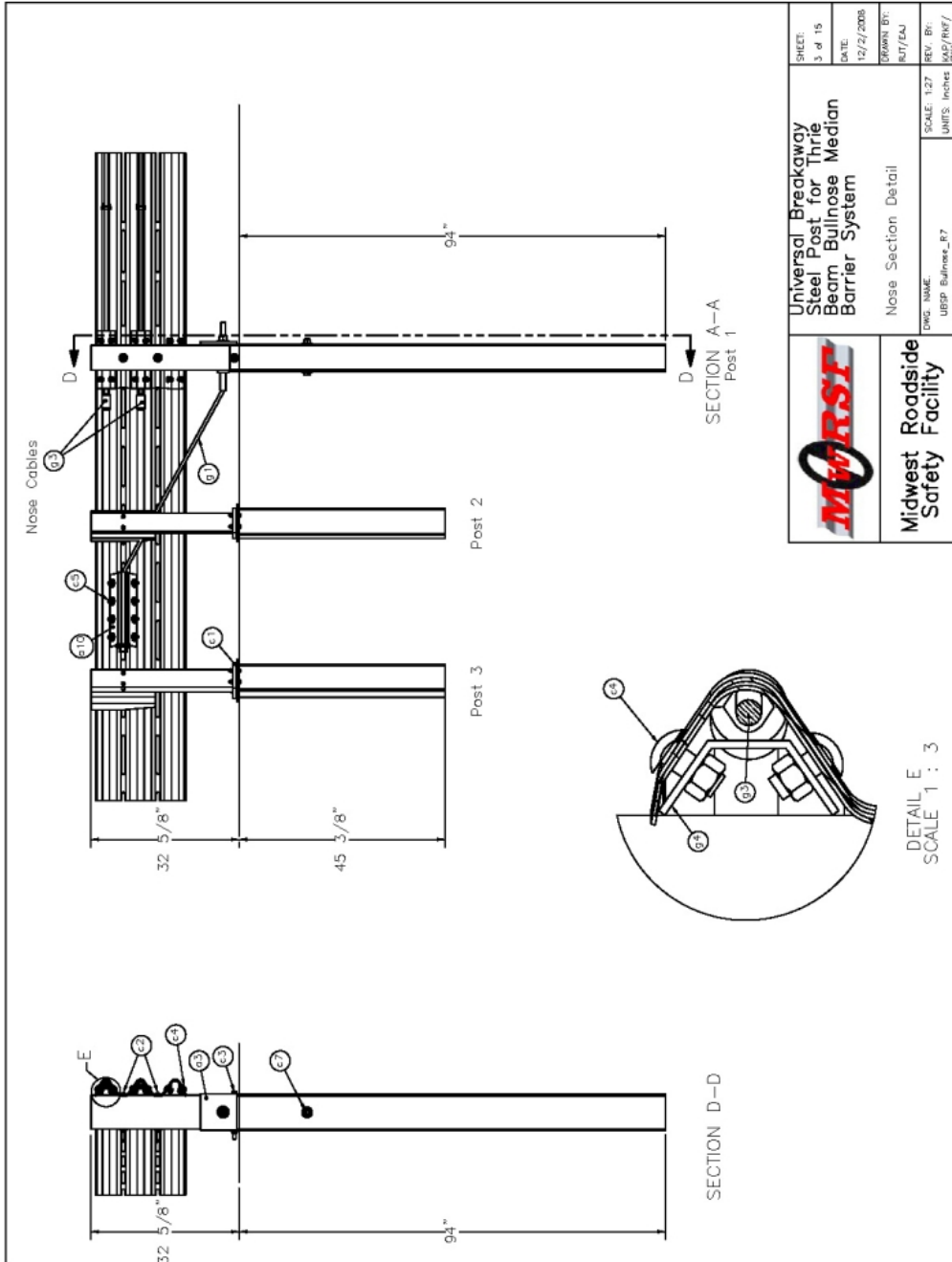


Figure 156. USBP Bullnose Nose Section Detail

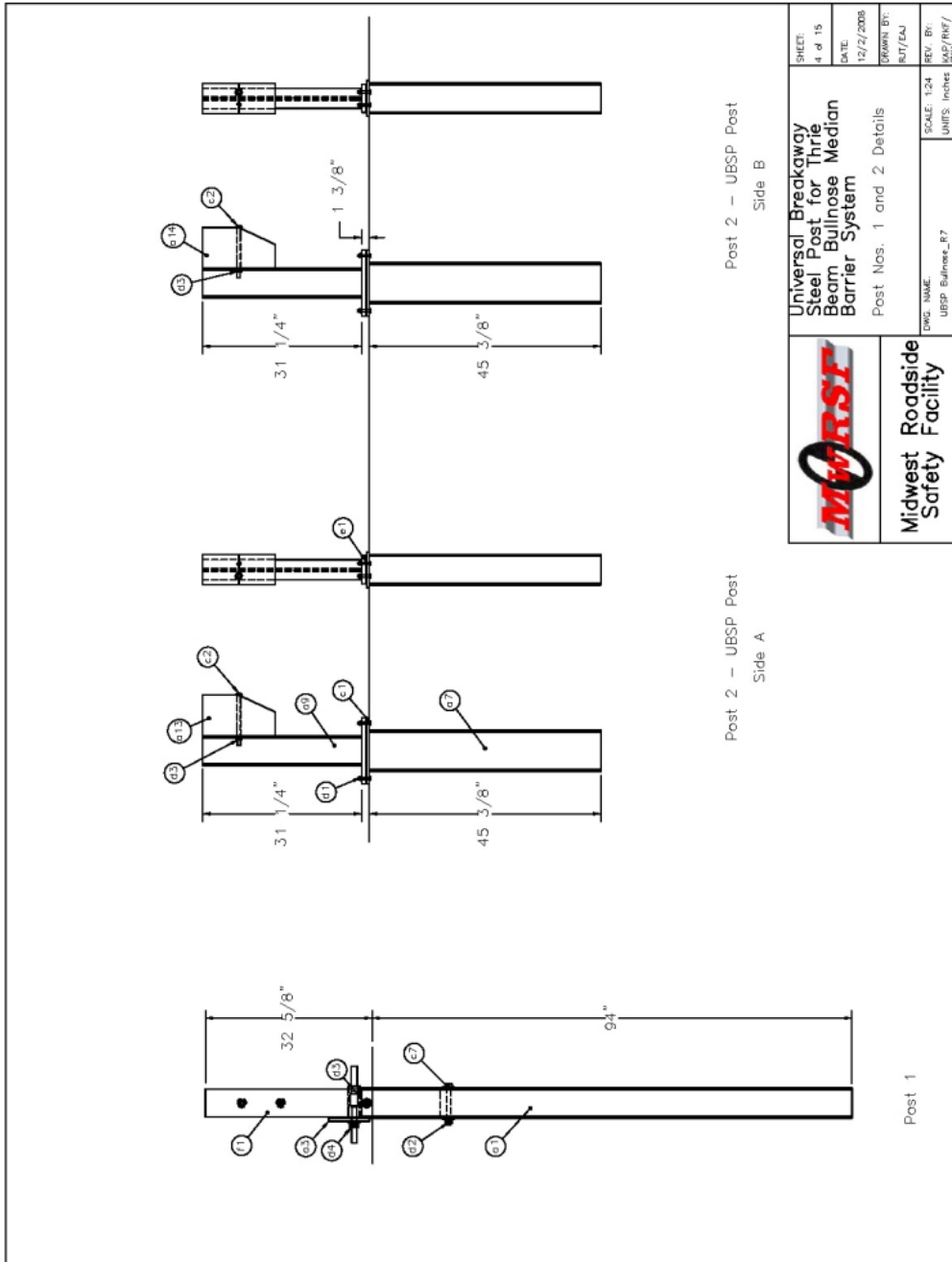
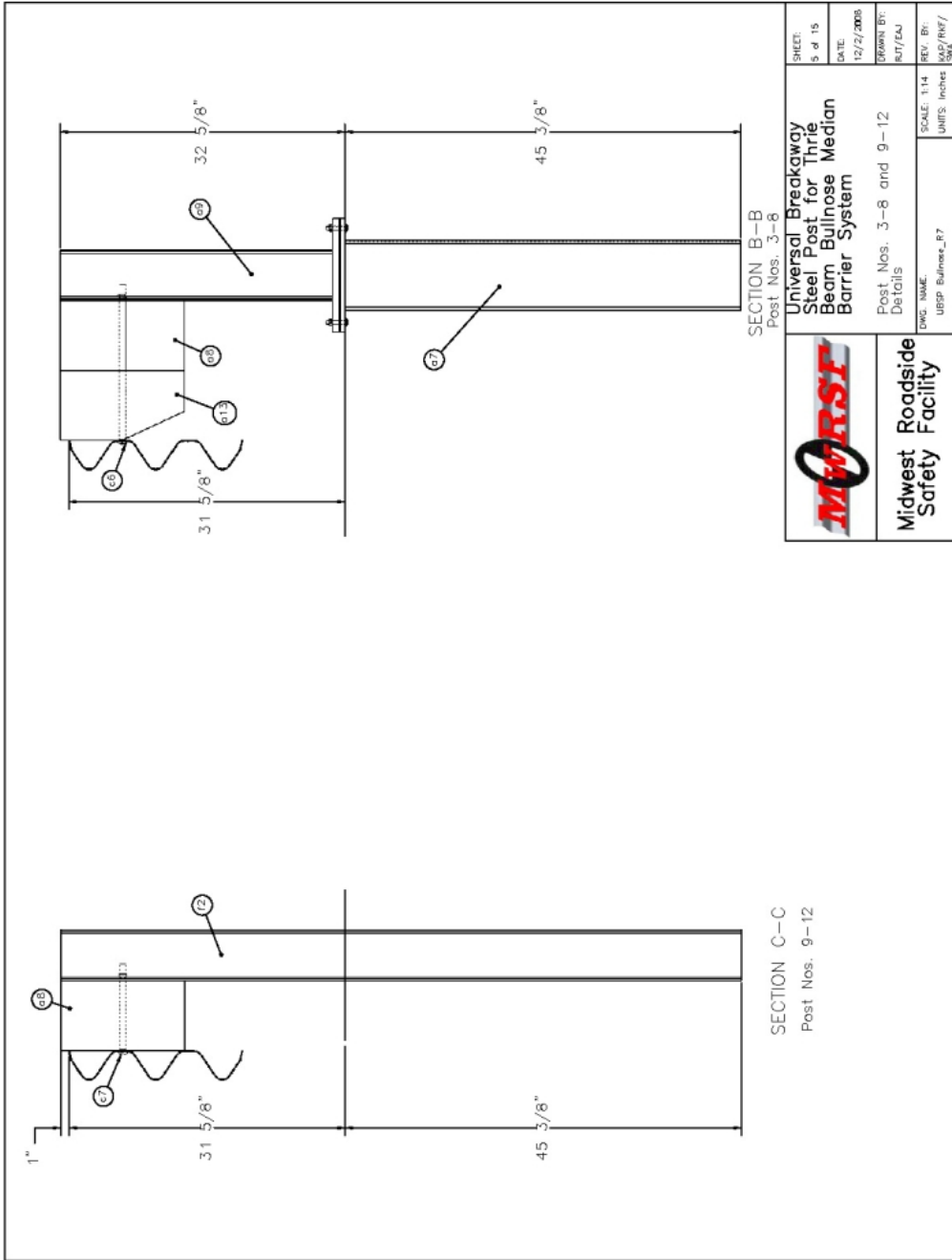
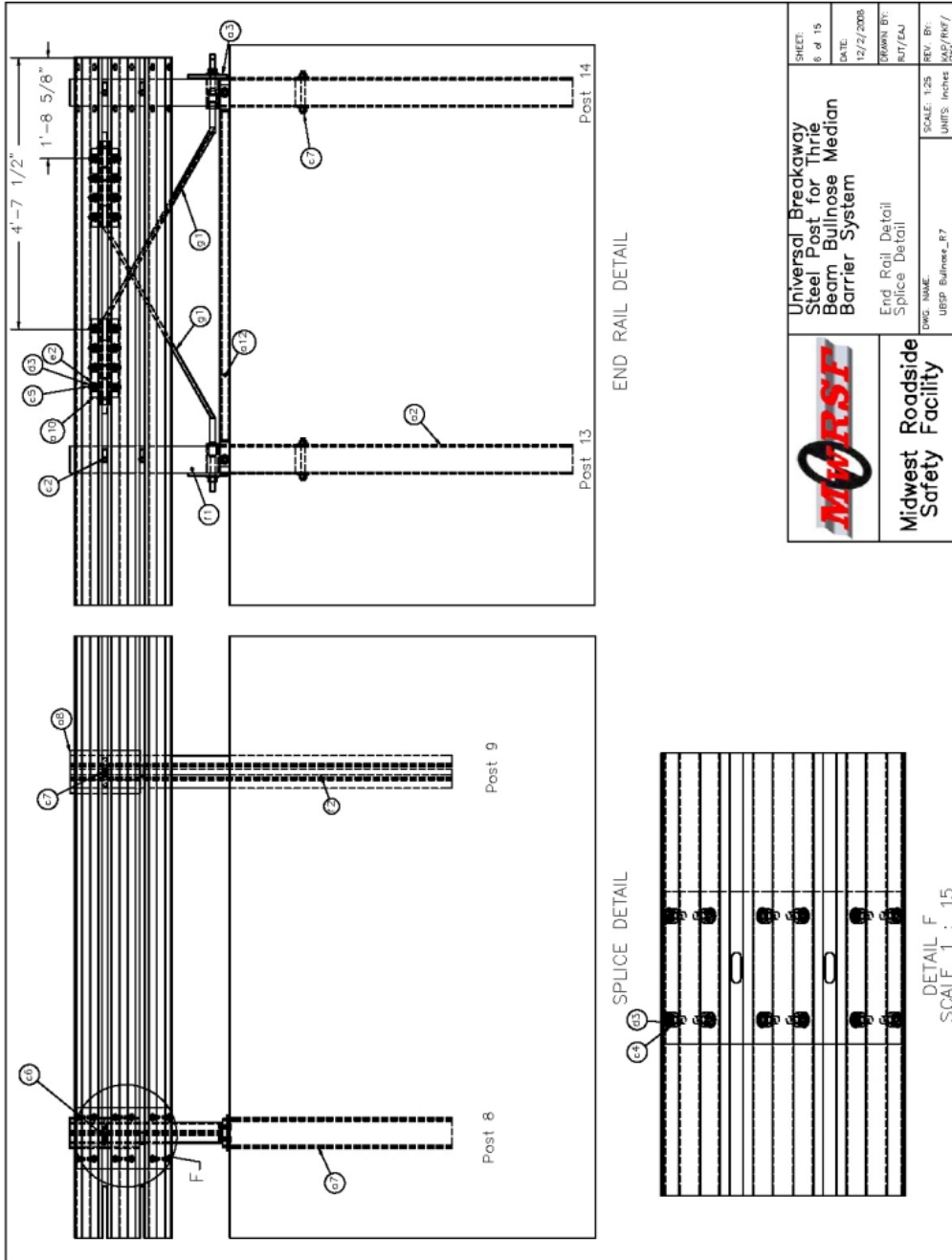


Figure 157. UBSP Bullnose Post Nos. 1 and 2 Details

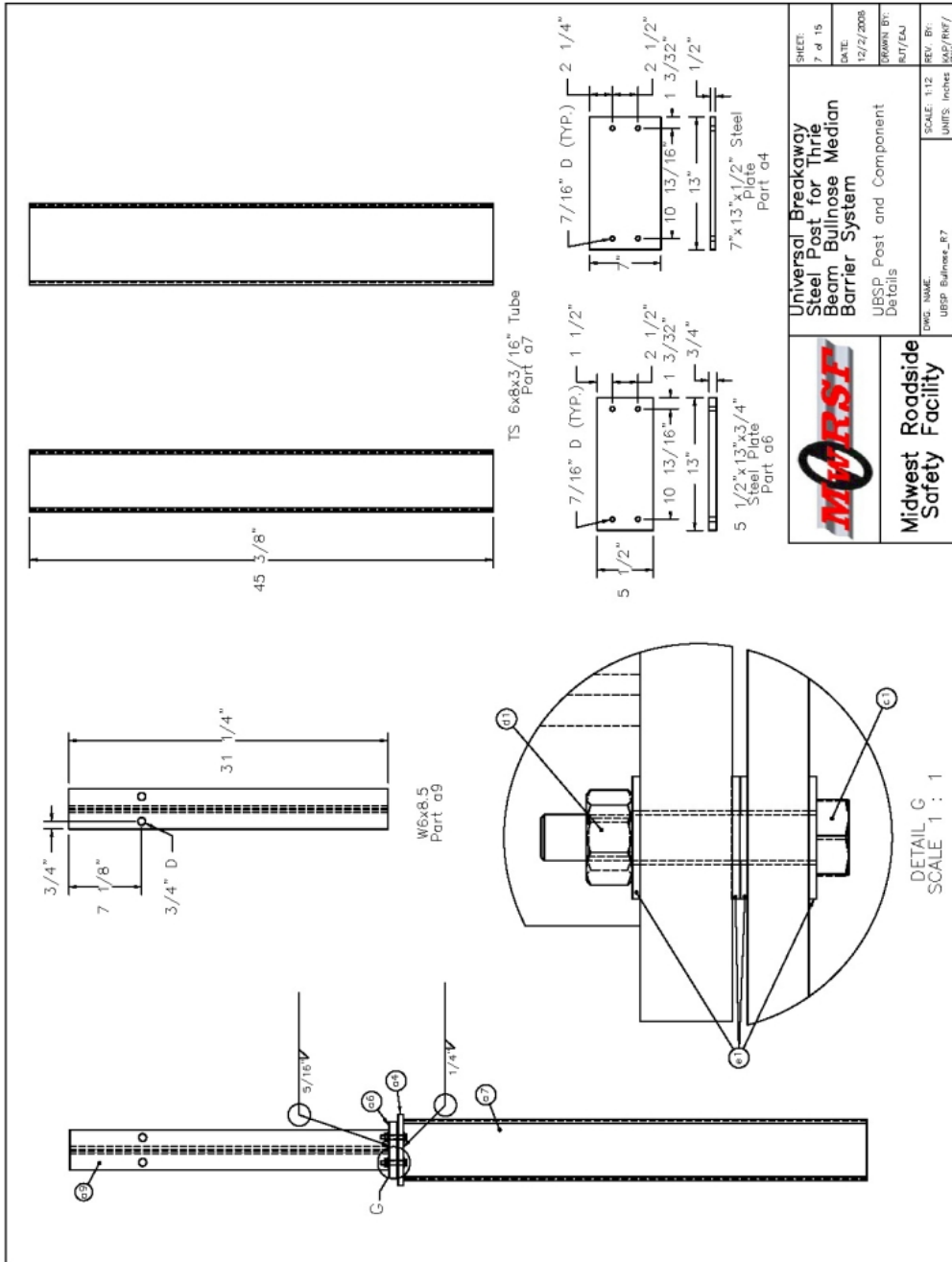




**Figure 158. UBSP Bullnose Post Nos. 3-8 and 9-12 Details**



**Figure 159. UBSP Bullnose End Rail Detail and Splice Detail**



\*\*See Section 14.2 For Weld Recommendations on Connecting W6x8.5 (Part a9) to Steel Plate (Part a6)

**Figure 160. UBSP Bullnose Fracturing Bolt Details – As Tested**

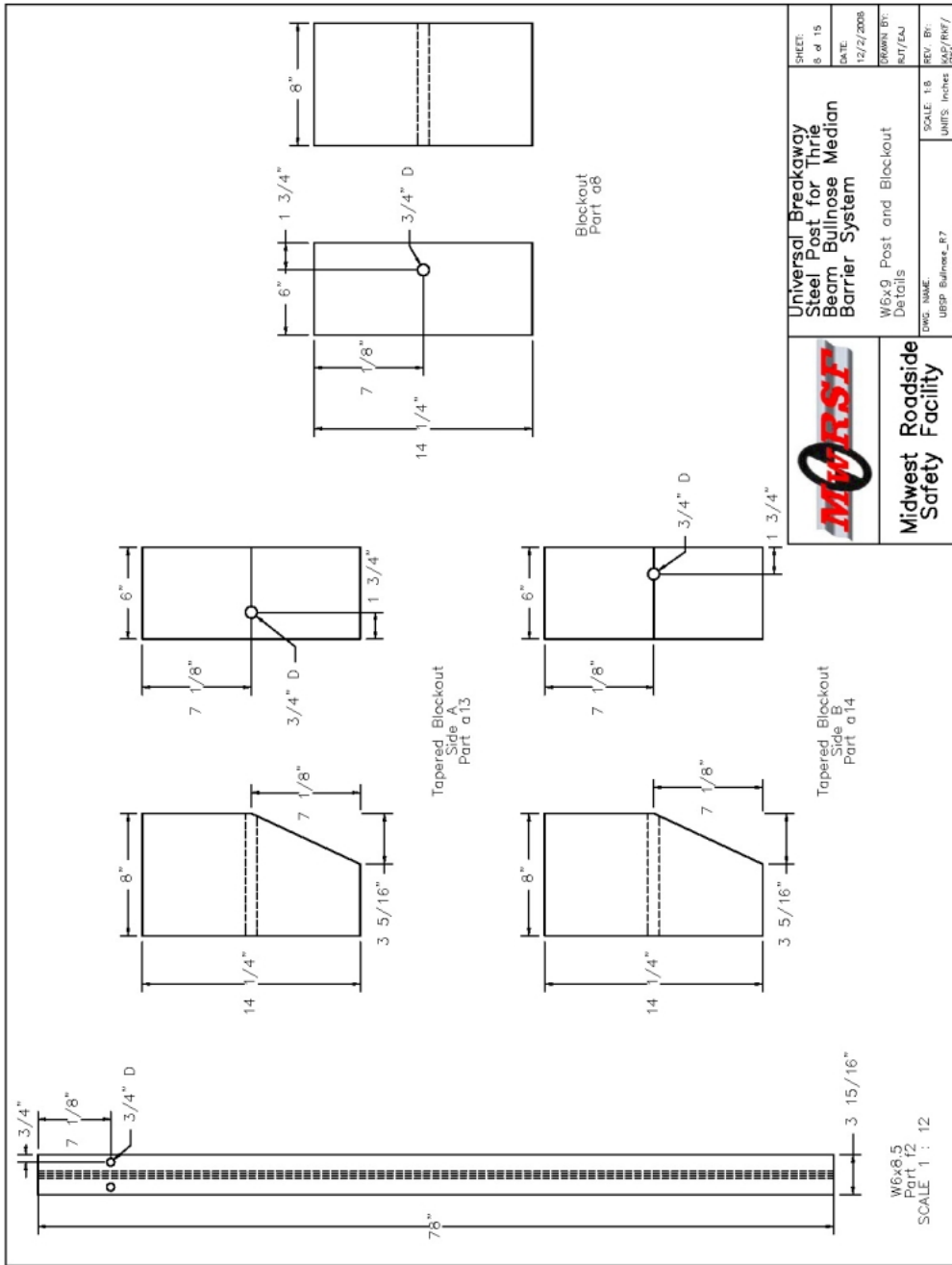
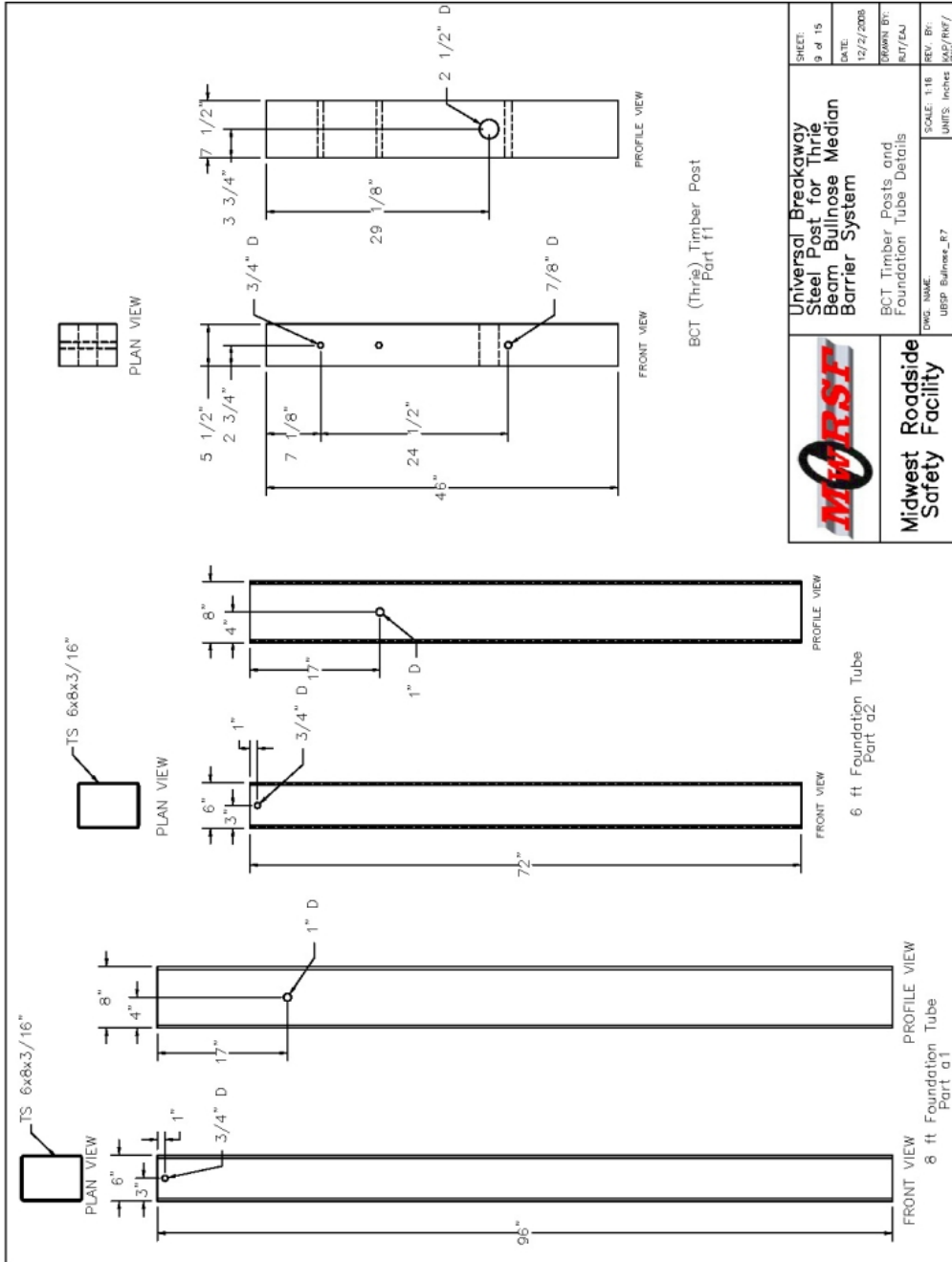



Figure 161. UBSP Bullnose W6x9 (W152x13.4) Post and Blockout Details



	Universal Breakaway Steel Post for Thrie Beam Bullnose Median Barrier System	SHEET: 9 of 15
	BCT Timber Posts and Foundation Tube Details	DATE: 12/2/2008
Midwest Safety Facility	DWG. NAME: UBSP_Ejurers_F7	DRAWN BY: BJT/EJ
	SCALE: 1/16 UNITS: Inches	REV. BY: MAP/PNF/ SKA

**Figure 162. UBSP Bullnose BCT Wood Post and Foundation Tube Details**



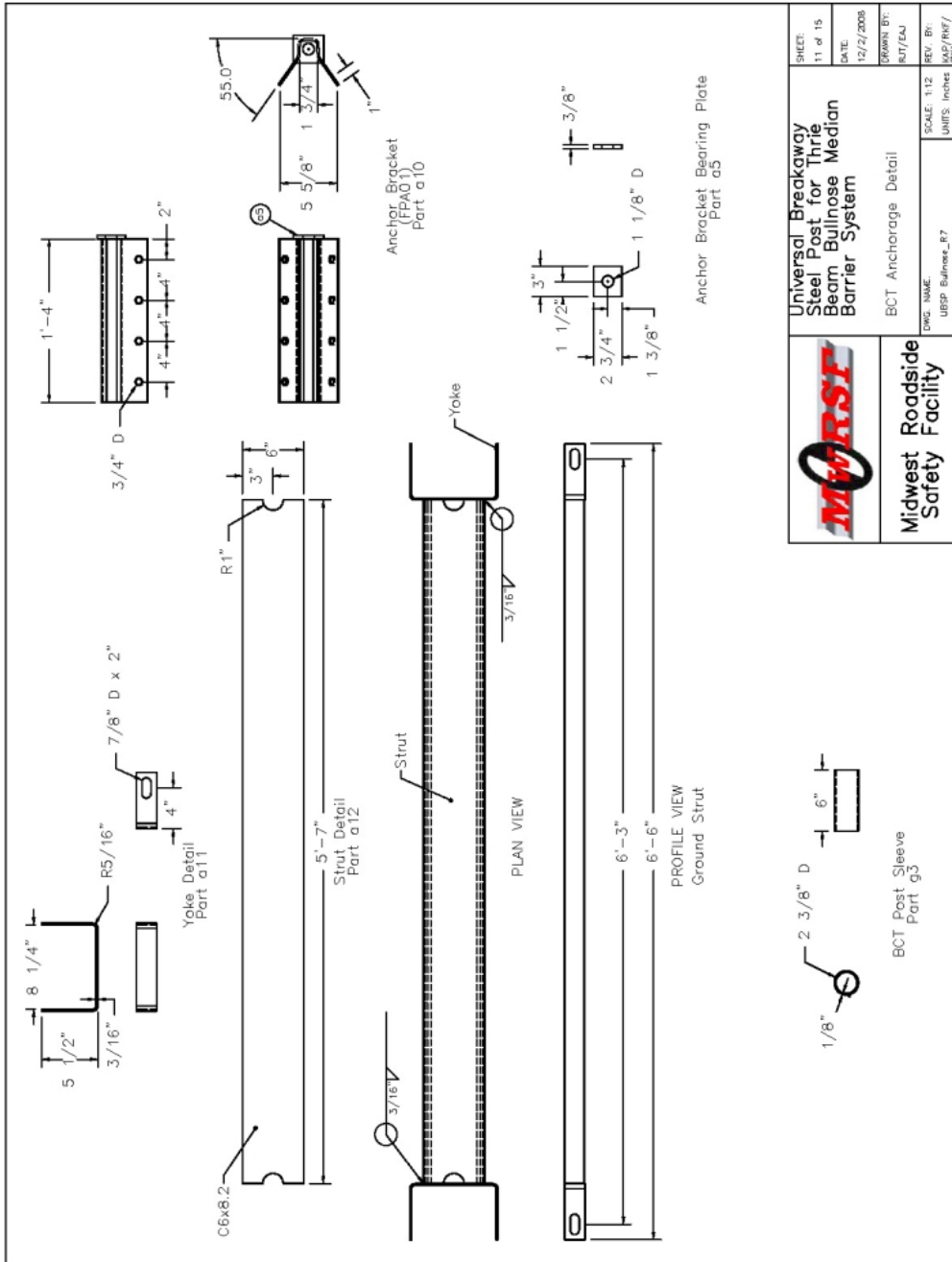


Figure 164. UBSP Bullnose BCT Anchoage Details

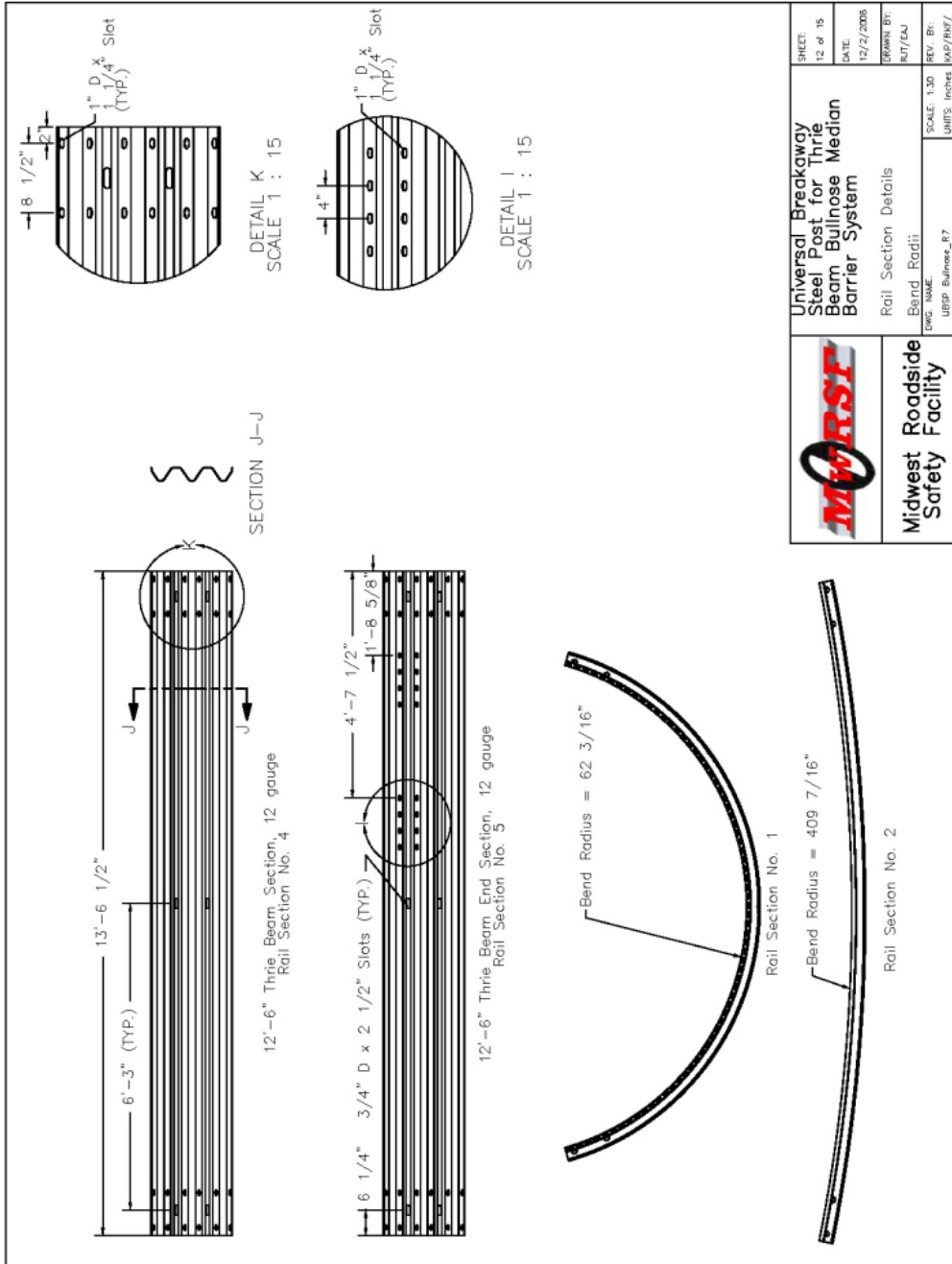


Figure 165. UBSP Bullnose Rail Section Details



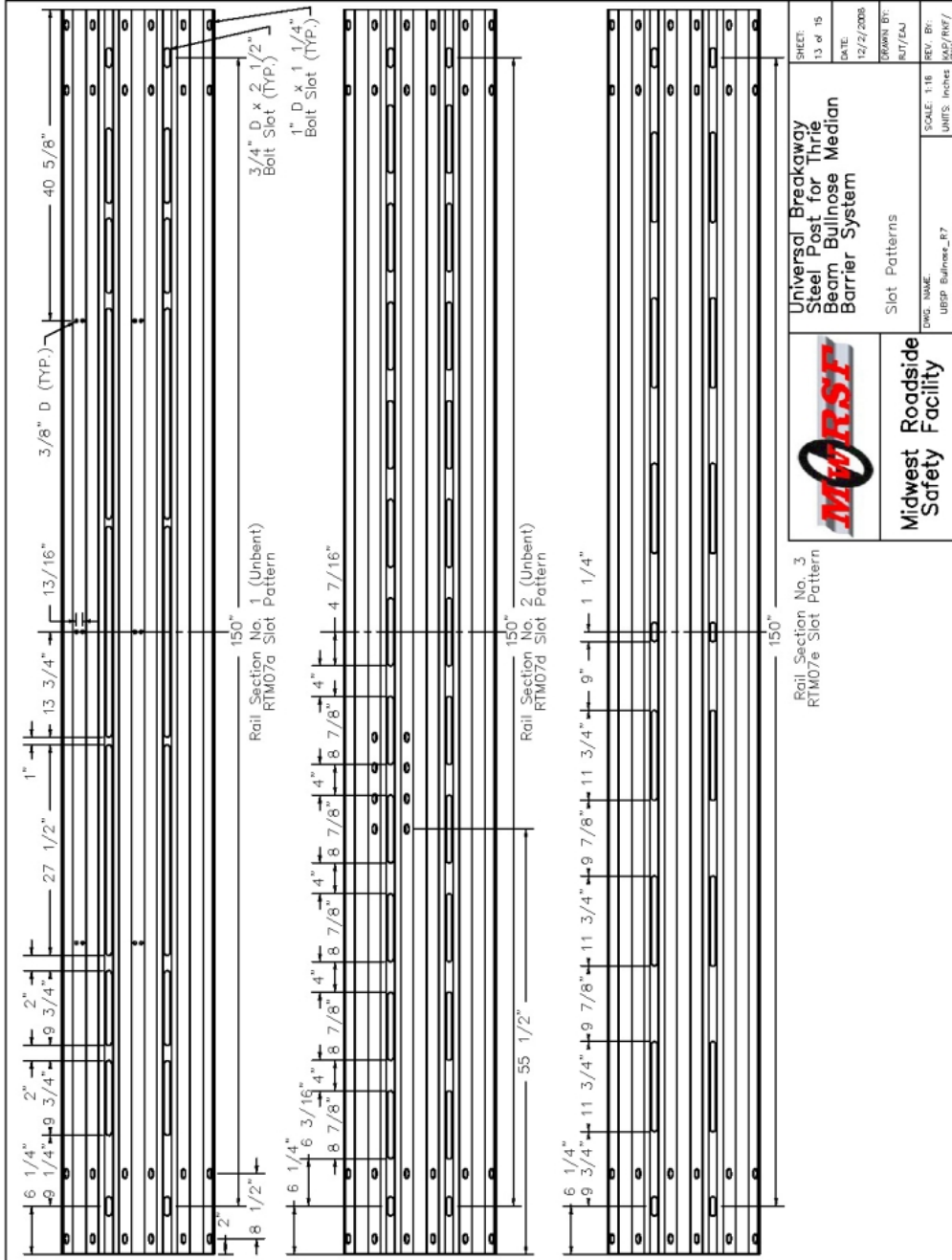



Figure 166. UBSP Bullnose Rail Slot Patterns

UBSP Bullnose				
Item No.	QTY	Description	Material Specification	Hardware Guide
a1	2	96" Foundation Tube	A500 Grade B	PTEO5
a2	4	72" Foundation Tube	A500 Grade B	PTEO5
a3	6	8 x 8 x 5/8" Anchor Bearing Plate	A36	FFB01
a4	14	13 x 7 x 1/2" Steel Plate	A36	FFB01
a5	6	Anchor Bracket End Plate	A36	FFA01
a6	14	13 x 5 1/2 x 3/4" Steel Plate	A36	FFA01
a7	14	6 x 8 x 3/16 x 45 3/8" long Foundation Tube	A500 Grade B	PD009
a8	20	6 x 8 x 14 1/4" Blockout	SYP Grade No.1 or better	FFA01
a9	14	W6x8.5 x 31 1/4" long (W6x9 can be substituted)	A36	FFA01
a10	6	Anchor Bracket	A36	FFA01
a11	4	Yoke	A36	FFA01
a12	2	Straight Ground Strut 67" long	C6x8.2 Channel Section A36 Steel	FFA01
a13	7	6 x 8 x 14 1/4" Tapered Blockout - Side A	SYP Grade No.1 or better	Blockout with Offset Hole
a14	7	6 x 8 x 14 1/4" Tapered Blockout - Side B	SYP Grade No.1 or better	Blockout with Offset Hole
b1	4	12'-6" Triple Beam Section	12 gauge AASHTO M180	RTM02a
b2	1	Bent 12'-6" Triple Beam Section - Radius 62.3/16"	12 gauge AASHTO M180	RTM07a
b3	2	12'-6" Triple Beam Section with Extra Slots	12 gauge AASHTO M180	RTM07e
b4	1	12'-6" Triple Beam End Section - Side A	12 gauge AASHTO M180	RTM07a
b5	1	12'-6" Triple Beam End Section - Side B	12 gauge AASHTO M180	RTM07a
b6	1	Bent 12'-6" Triple Beam Section - Radius 409 7/16" - Side A	12 gauge AASHTO M180	RTM07b
b7	1	Bent 12'-6" Triple Beam Section - Radius 409 7/16" - Side B	12 gauge AASHTO M180	RTM07b
c1	56	Hex Top Bolts 3/8" Dia x 2 1/4" long (Fully Threaded)	A325	FFB03
c2	14	5/8" Dia x 10" long Guardrail Bolt	A325	FFB03
c3	6	5/8" Dia x 10" long Hex Head Bolt	A325	FFB03
c4	120	5/8" Dia x 1 1/2" long Guardrail Bolt	A325	FFB01
c5	48	5/8" Dia x 1 1/2" long Hex Head Bolt	A325	FFB01
c6	12	5/8" Dia x 18" long Guardrail Bolt	A325	FFB04
c7	6	7/8" Dia x 7 1/2" long Hex Head Bolt	A325	FFB04
d1	56	3/8" Dia Hex Nut	A56.30H Galvanized	FFB02a
d2	6	7/8" Dia Hex Nut	A56.30H	FFB02a
d3	208	5/8" Dia Hex Nut	A56.30H	FFB02a
d4	12	1" Dia Hex Nut	A56.30H	FFB02a
e1	224	3/8" Dia Flat Washer	F436 Gr. 1 Galvanized	FFB02a
e2	112	5/8" Dia Flat Washer	F436 Gr. 1	FFB02a
e3	12	7/8" Dia Flat Washer	F436 Gr. 1	FFB02a
e4	12	1" Dia Flat Washer	F436 Gr. 1	FFB02a
f1	6	BCT Thrift Post	SYP Grade No. 1 or better (No knots, 1B" above or below ground tension face)	FFO04
f2	8	W6x8.5 x 78" long (W6x9 can be substituted)	A36	FFO04
g1	6	BCT Cable 6'-6" Long	6 x 19 Cable IWRC IPS	FFA01
g2	5	2 3/8" O.D. x 6" long BCT Post Sleeve	ASTM A53 Grade B Schedule 40	FFA02
g3	2	Bullnose Nose Cable ø625" x 14'-4" Long	Cable Top Button, S-109 Size No. 12 SB 2 7/8" Stock No. 1040395 for ø25 Dia. (ø25) wire rope (or any similarly sized swage-grip button ferules)	FFA02
g4	4	Nose Cable Anchor Plates 12 5/8" x 5 13/16"	A36	FFA02
g5	6	1/4" Dia U-Bolt Plate Washer	Galvanized A307	FFA02
g6	6	1/4" Dia U-Bolt	Galvanized A307	FFA02
g7	12	1/4" Dia Hex Nut	Galvanized A307	FFA02



**Midwest Safety Facility**

**Universal Breakaway Steel Post for Thrift Beam Bullnose Median Barrier System**

Bill of Materials

DWG. NAME: UBSP Bullnose\_F7

SHEET: 14 of 15  
DATE: 12/2/2008  
DRAWN BY: BJT/EJW  
REV. BY: MAP/PNF/SBA  
SCALE: None  
UNITS: Inches

Figure 167. UBSP Bullnose Bill of Materials



**Figure 168. UBSP Bullnose Barrier**



**Figure 169. UBSP Bullnose Barrier**



**Figure 170. UBSP Bullnose Barrier**

## **10.4 Test Facility**

The testing facility is located at the Lincoln Air-Park on the northwest side of the Lincoln Municipal Airport and is approximately 5 miles (8.0 km) northwest of the University of Nebraska-Lincoln.

## **10.5 Vehicle Tow and Guidance System**

A reverse cable tow system with a 1:2 mechanical advantage was used to propel the test vehicle. The distance traveled and the speed of the tow vehicle were one-half that of the test vehicle. The test vehicle was released from the tow cable before impact with the barrier system. A digital speedometer was located on the tow vehicle to increase the accuracy of the test vehicle impact speed.

A vehicle guidance system developed by Hinch [23] was used to steer the test vehicle. A guide-flag, attached to the front-right wheel and the guide cable, was sheared off before impact with the barrier system. This shearing action allowed the vehicle to be completely unrestrained at impact. The 3/8-in. (9.5-mm) diameter guide cable was tensioned to approximately 3000 lbs (13.3 kN), and supported laterally and vertically every 100 ft (30.48 m) by hinged stanchions. The hinged stanchions stood upright while holding up the guide cable, but as the vehicle was towed down the line, the guide-flag struck and knocked each stanchion to the ground. For test USPBN-1, the vehicle guidance system was 884 ft (269 m) long.

## **10.6 Test Vehicle**

For test no. USPBN-1, a 2000 GMC C2500 pickup truck was used as the test vehicle. The test inertial and gross static weights were 4,474 lbs (2,029 kg). The test vehicle is shown in Figure 171, with its dimensions shown in Figure 172.

Black and white, checkered targets were placed on the vehicle, as shown in Figure 173, to aid in the analysis of the high-speed digital video. One target was placed directly above each of the wheels, and another was placed at the vehicle's center of gravity on both the driver and passenger sides. In addition, targets were placed on the top of the vehicle. One was placed at the vehicle's center of gravity, two were placed on the windshield, one was placed on the hood of the vehicle, two were placed in the pickup box, and four targets were placed on the side walls of the box.

The front wheels of the test vehicle were aligned for camber, caster, and toe-in values of zero so the vehicle would track properly along the guide cable. A 5B flash bulb was mounted on the left quarter point of the vehicle's roof to pinpoint the time of impact with the test article on the high-speed video footage. The flash bulb was fired by a pressure tape switch mounted on the front-left corner of the bumper. A remote-controlled brake system was installed in the test vehicle so the vehicle could be brought safely to a stop after the test.

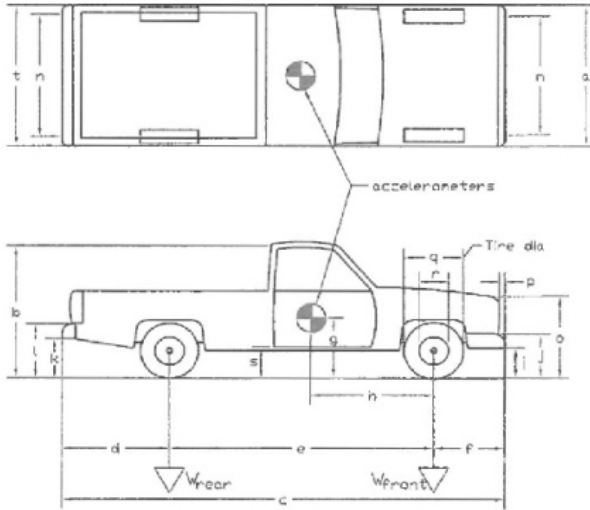


**Figure 171. Test Vehicle, Test USPBN-1**



Date: 11/26/2008 Test Number: USPBN-1 Model: 2000p/C 2500  
 Make: Chevrolet Vehicle I.D.#: 1GCGC24R1YR181174  
 Tire Size: LT245/75 R16 Year: 2000 Odometer: 250447

\*(All Measurements Refer to Impacting Side)



GWWR F 4100  
 R 6000  
 Tot. 8600

Vehicle Geometry -- mm (in.)

o <u>1889.1 (74.375)</u>	b <u>1835.2 (72.25)</u>
c <u>5562.6 (219.0)</u>	d <u>1327.2 (52.25)</u>
e <u>3327.4 (131.0)</u>	f <u>908.05 (35.75)</u>
g <u>673.1 (26.5)</u>	h <u>1405.5 (55.375)</u>
i <u>441.33 (17.375)</u>	j <u>647.7 (25.5)</u>
k <u>609.6 (24.0)</u>	l <u>793.75 (31.25)</u>
m <u>1587.5 (62.5)</u>	n <u>1619.3 (63.75)</u>
o <u>1009.7 (39.75)</u>	p <u>82.55 (3.25)</u>
q <u>762 (30.0)</u>	r <u>444.5 (17.5)</u>
s <u>466.73 (18.375)</u>	t <u>1844.7 (72.625)</u>
Wheel Center Height Front	<u>351.95 (14.25)</u>
Wheel Center Height Rear	<u>355.13 (14.375)</u>
Wheel Well Clearance (FR)	<u>895.35 (35.25)</u>
Wheel Well Clearance (RR)	<u>952.5 (37.5)</u>
Frame Height (FR)	<u>390.53 (15.375)</u>
Frame Height (RR)	<u>685.8 (27.0)</u>
Engine Type	<u>8 CYL. GAS</u>
Engine Size	<u>5.7L</u>

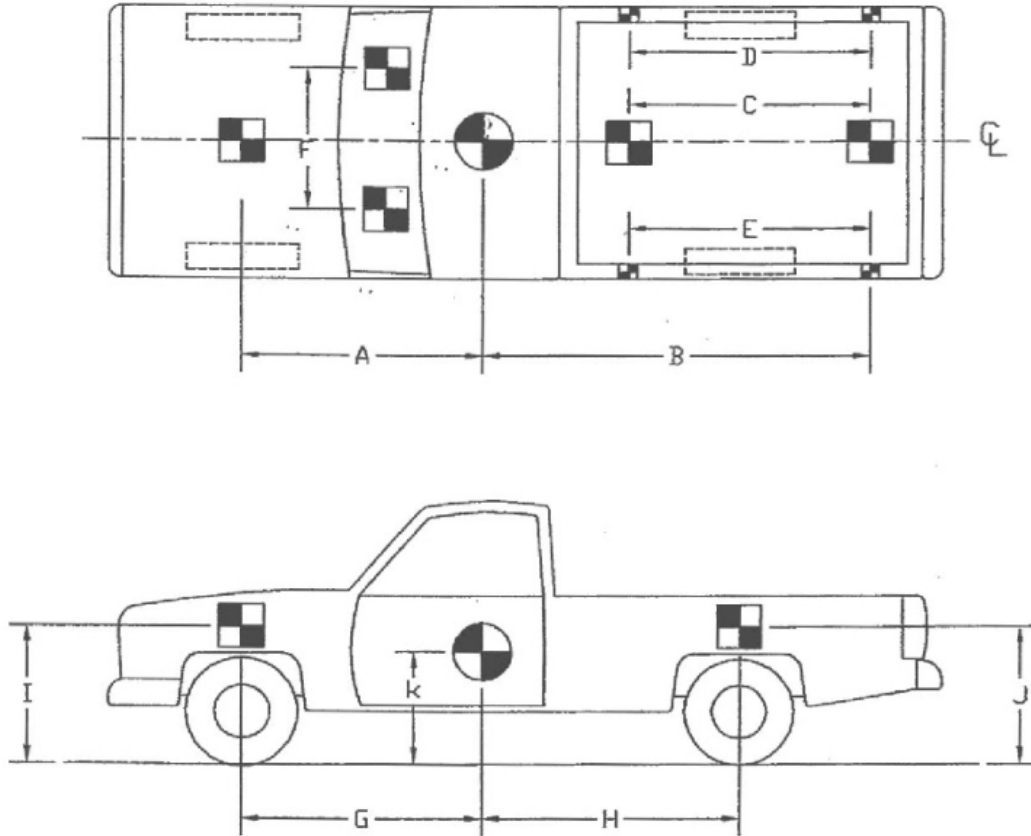
Transmission Type:

Automatic  
 RWD

Weights kg (lbs)	Curb	Test Inertial	Gross Static
W-front	<u>1233.3 (2719)</u>	<u>(2614)</u>	<u>1185.7 (2614)</u>
W-rear	<u>932.13 (2055)</u>	<u>843.68 (1860)</u>	<u>843.68 (1860)</u>
W-total	<u>2165.5 (4774)</u>	<u>2029.4 (4474)</u>	<u>2029.4 (4474)</u>

Note any damage prior to test: None

Figure 172. Vehicle Dimensions, Test USPBN-1



TEST #: <u>USPBN-1</u>					
TARGET GEOMETRY-- mm (in.)					
A	<u>1607</u>	(63.25)	E	<u>2153</u>	(84.75)
I	<u>997</u>	(39.25)	F	<u>1216</u>	(47.875)
B	<u>2362</u>	(93.0)	J	<u>1054</u>	(41.5)
C	<u>1229</u>	(48.375)	G	<u>1407</u>	(55.375)
K	<u>673</u>	(26.5)	H	<u>1921</u>	(75.625)
D	<u>2153</u>	(84.75)			

**Figure 173. Vehicle Target Locations, Test USPBN-1**

## **10.7 Data Acquisition Systems**

Three data acquisition systems, two accelerometers and one rate transducer, were used to measure the motion of the vehicle. The output data from all three devices was analyzed and plotted using the “DynaMax 1 (DM-1)” computer software program and a customized Microsoft Excel spreadsheet.

### **10.7.1 Accelerometers**

One triaxial piezoresistive accelerometer system with a range of  $\pm 200$  g's was used to measure the acceleration in the longitudinal, lateral, and vertical directions at a sample rate of 10,000 Hz. The environmental shock and vibration sensor/recorder system, Model EDR-4M6, was developed by Instrumented Sensor Technology (IST) of Okemos, Michigan and includes three differential channels as well as three single-ended channels. The EDR-4 was configured with 6 MB of RAM memory and a 1,500 Hz low pass filter. The “DynaMax 1 (DM-1)” computer software program and a customized Microsoft Excel spreadsheet were used to analyze and plot the accelerometer data.

Another triaxial piezoresistive accelerometer system with a range of  $\pm 200$  g's was also used to measure the acceleration in the longitudinal, lateral, and vertical directions at a sample rate of 3,200 Hz. The environmental shock and vibration sensor/recorder system, Model EDR-3, was developed by Instrumented Sensor Technology (IST) of Okemos, Michigan. The EDR-3 was configured with 256 kB of RAM memory and a 1,120 Hz low pass filter. The “DynaMax1 (DM-1)” computer software program and a customized Microsoft Excel spreadsheet were used to analyze and plot the accelerometer data.

Finally, a third accelerometer system was also used to measure the acceleration in the longitudinal, lateral, and vertical directions at a sample rate of 10,000 Hz. The environmental shock and vibration sensor/recorder system, a two-Arm piezoresistive accelerometer, was developed by Endevco of San Juan Capistrano, California. Three accelerometers were used to measure each of the longitudinal, lateral, and vertical accelerations independently. Data was collected using a Sensor Input Module (SIM), Model TDAS3-SIM-16M, which was developed by Diversified Technical Systems, Inc. (DTS) of Seal Beach, California. The SIM was configured with 16 MB SRAM memory and 8 sensor input channels with 250 kB SRAM/channel. The SIM was mounted on a TDAS3-R4 module rack. The module rack is configured with isolated power/event/communications, 10BaseT Ethernet and RS232 communication, and an internal back-up battery. Both the SIM and module rack are crashworthy. The “DTS TDAS Control” computer software program and a customized Microsoft Excel worksheet were used to analyze and plot the accelerometer data.

### **10.7.2 Rate Transducers**

An Analog Devices, Inc. model ADXRS300 rate gyro with a range of  $\pm 1200$  degrees/sec in each of the three directions (pitch, roll, and yaw) was used to measure the rotational rates of motion of the test vehicle. The rate transducer was internally mounted on EDR-4M6, and therefore was also rigidly attached to the vehicle near its center of gravity. Rate transducer signals were stored in the internal memory of EDR-4M6.

An additional angular rate sensor was also used. The ARS-1500 has a range of 1,500 degrees/sec in each of the three directions (pitch, roll, and yaw) and was used to measure the rates of rotation of the test vehicle. The angular rate sensor was mounted on an aluminum block

inside the test vehicle at the center of gravity and recorded data at 10,000 Hz to the SIM. The raw data measurements were then downloaded, converted to the proper Euler angles for analysis, and plotted. The “DTS TDAS Control” computer software program and a customized Microsoft Excel worksheet were used to analyze and plot the angular rate sensor data.

### **10.7.3 High-Speed Photography**

For test no. USPBN-1, five high-speed VITcam digital video cameras and five digital video cameras were used. Camera details, lens information, and camera operating speeds are shown along with a schematic of the camera locations in Figure 174.

The VITcam videos were analyzed using Image Express MotionPlus and Redlake Motion Scope software. Camera speed and camera divergence factors were considered in the analysis of the high-speed videos.

### **10.7.4 Pressure Tape Switches**

Five pressure-activated tape switches, spaced at 2-m (6.56-ft) intervals, were used to determine the speed of the vehicle before impact. Each tape switch fired a strobe light which sent an electronic timing signal to the data acquisition system as the right-front tire of the test vehicle passed over it. The test vehicle speed was then determined from the electronic timing mark data recorded using the “Test Point” software. Strobe lights and high-speed film analysis are used only as a backup in the event that vehicle speed cannot be determined from the electronic data.

USPBN-1 Camera Summary

No.	Type	Operating Speed (frames/sec)	Lens	Lens Setting
2	Vitcam CTM	500	12.5 mm Fixed	
3	Vitcam CTM	500	Sigma 24-135 mm	24 mm
5	Vitcam Gigabit	500	Sigma 70-200 mm	85 mm
6	Vitcam Gigabit	500	Sigma 24-70 mm	35 mm
7	Vitcam Gigabit	500	Sigma 50 mm Fixed	
1	JVC-GZ-MC500 (Everio)	29.97		
3	JVC-GZ-MC40u (Everio)	29.97		
4	JVC-GZ-MC40u (Everio)	29.97		
5	JVC-GZ-MC27u (Everio)	29.97		
7	Canon-ZR90	29.97		

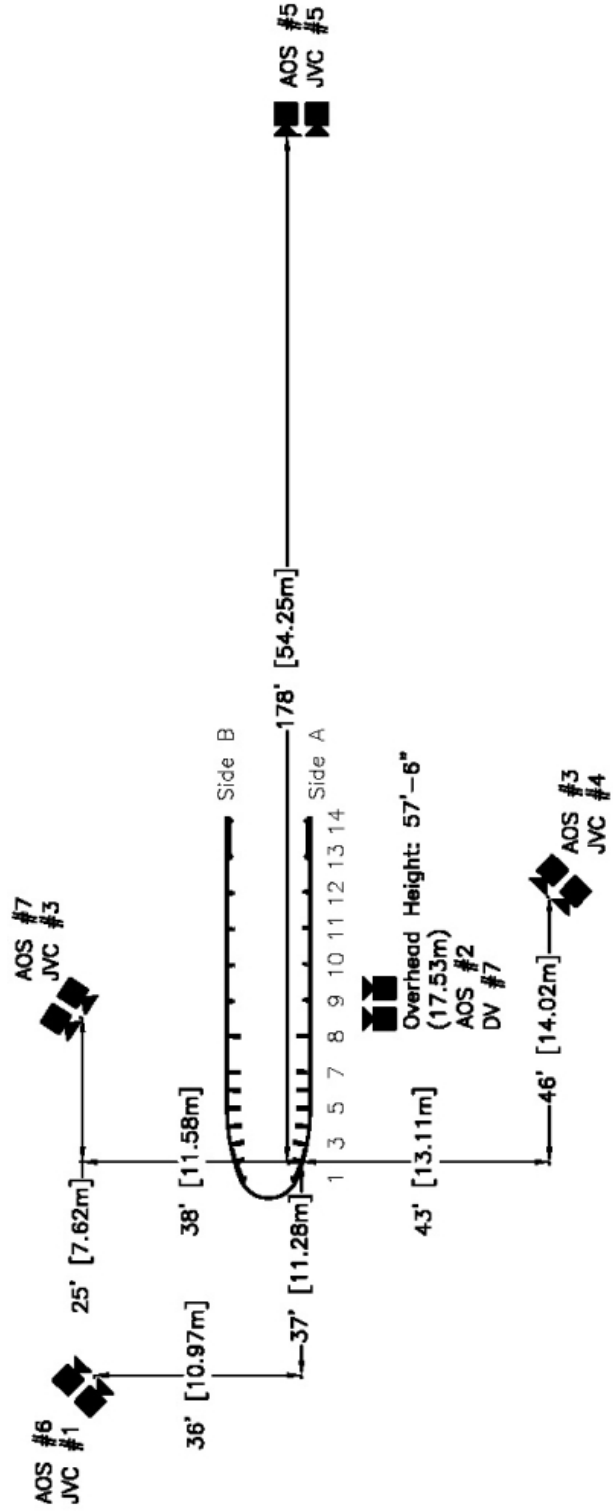


Figure 174. Locations of High Speed Cameras, Test USPBN-1

## 10.8 Crash Test No. USPBN-1

Test no. USPBN-1 was conducted according to NCHRP Report No. 350 Test Designation 3-38. The 4,474-lb (2,029-kg) pickup truck impacted the test article at a speed of 63.2 mph (101.7 km/h) and an angle of 22.6 degrees. The target critical impact point was the centerline of post no. 2, as shown in Figure 175. Actual vehicle impact with the barrier system occurred approximately 4 in. (101.6 mm) downstream of the target location. A summary of the test results and sequential photographs are shown in Figure 176. Additional sequential and documentary photographs are shown in Figures 177 through 187.

### 10.8.1 Weather Conditions

Test No. USPBN-1 was conducted on November 26, 2008 at approximately 1:30 pm. The weather conditions were reported as shown in Table 22.

**Table 22. Weather Conditions, Test No. USPBN-1**

Temperature	52 °F (11 °C)
Humidity	38%
Wind Speed	3 mph (5 km/hr)
Wind Direction	320° from True North
Sky Conditions	Sunny
Visibility	10 Statute Miles
Pavement Surface	Dry
Previous 3-Day Precipitation	0 in. (0 mm)
Previous 7-Day Precipitation	0 in. (0 mm)

### 10.8.2 Test Description

Following the initial impact with the pickup truck, the thrie beam rail immediately began to deform inward. At approximately 0.038 sec, the left front of the pickup truck impacted post no. 3 on the right side, or side A, causing the bolts to fracture and the post no. 3 to break away. At 0.058 sec, post no. 4 on the right side had broken away. As the pickup penetrated farther into

the barrier, post no. 5 broke away at approximately 0.076 sec. At 0.096 sec, the wood blockout on post no. 2 broke, which separated the rail from post no. 2. After post no. 6 broke at 0.110 sec, post no. 1 on the right side broke at approximately 0.112 sec, which also eliminated the cable anchor on the right side. Even with the released anchor, the rail continued to wrap around the pickup as it penetrated farther into the system.

Next, post no. 7 broke in the strong axis at approximately 0.144 sec. Post no. 2 finally broke at approximately 0.210 sec, due to the impact with post no. 1, and the rail began to deform over to post no. 1 on the left side of the system. Also, the rail began to drop on the driver's side of the pickup at 0.210 sec. At approximately 0.270 sec, the front end of the pickup was near the end of the slotted rail at post no. 8, and a buckle point formed in the non-slotted rail near post no. 9, causing the rail to begin to drop on the passenger's side of the pickup. This buckle caused the rail to drop to the ground, and the pickup truck began to override the rail. The truck continued to travel up and over the rail until the left-front corner of the truck contacted the ground at approximately 0.728 sec. The momentum of the truck continued forward, while the left-rear of the truck impacted posts no. 11 and 12 on the left side, or side B, of the system at 0.892 sec. This impact caused the pickup to begin rolling over, and the pickup rolled over top of post nos. 13 and 14 on the left side of the system before coming to rest on its roof approximately 15 ft (4.6 m) downstream of the system. The trajectory of the pickup truck during the crash test and the final position of the vehicle are provided in Figures 181 and 182.

### **10.8.3 Vehicle Damage**

The moderate vehicle damage, occurring as a result of the vehicle climbing over the system and rolling over upon impact, is shown in Figures 186 and 187. Minor undercarriage



damage was observed on the vehicle. Both the front bumper and the hood had scrapes and dents across the entire front end. The grill and both headlights broke off completely. Also, the front windshield and the driver's-side door were broken and cracked due to the roof of the truck being crushed inward from the rollover. The driver's side of the truck received moderate damage as the front fender was dented inward, the front suspension was broken, and the driver's door was pushed out of the frame. In the rear, the driver's-side rear tire was gashed, and the box shifted with respect to the cab. Also, there was a dent and gash near the gas cap of the truck. The passenger's side of the truck had minor damage as there were minor dents on the box, the door was slightly out of the frame, and there were scrapes and dents on the front fender. It is noted that it was difficult to determine the amount and extent of the damage caused by the interaction with the guardrail as opposed to damage caused with the vehicle overriding the system and the subsequent rollover of the vehicle. Also, complete occupant compartment deformations and the corresponding locations are provided in Appendix B.

#### **10.8.4 Barrier Damage**

Barrier damage was extensive, as shown in Figures 183 through 185. Most of the post damage occurred to the right side of the system, or the impact side of the system, Side A. The first eight posts on the right side of the system were fractured and broke away. BCT post no. 1 fractured through the hole at ground level. The universal steel breakaway post nos. 2 through 8 all broke away as the bolts fractured. None of the breakaway posts had any noticeable soil gap except for post no. 2, which had a soil gap of 2 1/2 in. (64 mm). Post nos. 9 and 10 on the right side of the system both bent downstream in the weak axis and were not connected to the thrie beam rail. Post no. 11 was twisted clockwise slightly and was not connected to the rail. Post no.

12 was not damaged but was not connected to the rail. Post no. 13 did not have any damage and was still connected to the rail. Finally, post no. 14 was still connected to the rail but was broken through the hole at ground level. On the left side of the system, only post nos. 11 and 12 received damage, as they were both bent over in the weak axis from impact with the rear driver's side of the pickup.

The damage to the three beam guardrail in the system consisted of bucking and tearing of the guardrail. Buckling of the rail on the right side occurred near post no. 2, around post nos. 7 and 8, and at post no. 9. Buckling of the rail on the left side occurred at post no. 1. On right side, there were tears in the rail at the splice at post no. 1, in the upper slot at post no. 2, at the splice at post no. 5, and at the bottom of the rail at post no. 6. Also, there were kinks and scuff marks all along the right side of the barrier from post no. 2 through post no. 8 due to interaction with the pickup truck. On the left of the system, there was a dent between post nos. 7 and 8, and the slots at post no. 11 and 12 were deformed. Also, the rail was buckled at post no. 1 on the left side of the barrier.

#### **10.8.5 Occupant Risk Values**

The occupant impact velocities and 0.010-sec average occupant ridedown accelerations were calculated from both the DTS and the EDR-3 and are summarized in Table 23. It is noted that the occupant impact velocities (OIVs) and occupant ridedown accelerations (ORAs) were within the suggested limits provided in NCHRP Report No. 350. The THIV and PHD values were determined to be 24.6 ft/s (7.5 m/s) and 11.37 g's, respectively from the DTS rate transducer. The results of the occupant risk, as determined from the accelerometer data, are also

summarized in Figure 176. The recorded data from both the accelerometers and the DTS rate transducer are shown graphically in Appendix C.

**Table 23. Summary of OIV, ORA, THIV, and PHD Values, Test USPNB-1**

Evaluation Criteria		Transducer System	
		EDR-3	DTS
OIV [ft/s (m/s)]	Longitudinal	-23.68 (-7.22)	-21.05 (-6.42)
	Lateral	9.55 (2.91)	2.68 (0.82)
ORA [g's]	Longitudinal	-11.92	-11.36
	Lateral	5.69	6.03
THIV [ft/s (m/s)]		--	24.6 (7.5)
PHD [g's]		--	11.37

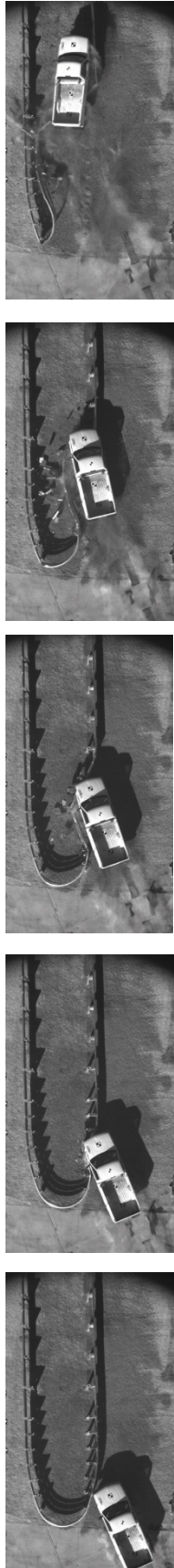
### 10.8.6 Discussion of Results

Following test USPNB-1, a safety performance evaluation was conducted, and the fracturing bolt, steel-post bullnose barrier system was determined to be unacceptable for test designation no. 3-38 impact conditions according to the NCHRP Report No. 350 criteria. The bullnose barrier failed to contain and stop the test vehicle in a controlled manner due to vehicle vaulting and override of the system. Detached elements and debris from the test article did not penetrate or show potential for penetrating the occupant compartment. As a result of vehicle rollover, there was deformation of, or intrusion into, the occupant compartment that could have caused serious injury. The vehicle did not remain upright during and after collision. The vehicle's trajectory did not intrude into adjacent traffic lanes. However, the vehicle trajectory behind the test article was unacceptable as the test vehicle overrode the guardrail and became airborne in the median area behind the bullnose system. In summary, test USPNB-1 failed to

meet several of the safety performance criteria due to the pickup truck overriding the guardrail and its subsequent rollover.



**Figure 175. Impact Location, Test USPBN-1**



0.000 sec	0.078 sec	0.172 sec	0.280 sec	0.546 sec
<ul style="list-style-type: none"> <li>• Test Agency .....MwRSF</li> <li>• Test Number .....USPBN-1</li> <li>• Date .....11/26/2008</li> <li>• NCHRP 350 Test Designation .....3-38</li> <li>• Test Article .....Bullnose Median Barrier</li> <li>• Key Elements .....Universal Breakaway Steel Posts</li> <li>• Type of Soil .....Grading B AASHTO M147-65 (1990)</li> <li>• Test Vehicle <ul style="list-style-type: none"> <li>Type/Designation.....2000P</li> <li>Make and Model.....2000 GMC C2500</li> <li>Curb .....4,774 lbs</li> <li>Test Inertial.....4,474 lbs</li> <li>Gross Static.....4,474 lbs</li> </ul> </li> <li>• Impact Conditions <ul style="list-style-type: none"> <li>Speed .....63.2 mph</li> <li>Angle (trajectory).....22.6 deg</li> <li>Target Impact Location.....Centerline of post no. 2</li> <li>Actual Impact Location .....4 in. downstream of centerline post 2</li> </ul> </li> <li>• Exit Conditions <ul style="list-style-type: none"> <li>Speed .....NA</li> <li>Angle .....NA</li> <li>Vehicle Snagging .....None</li> </ul> </li> <li>• Post-Impact Trajectory <ul style="list-style-type: none"> <li>Vehicle Stability .....Unsatisfactory/Rollover</li> <li>Vehicle Stopping Distance.....77' 9 1/2" downstream and 15' 4 3/4" left of impact as measured to driver's-side front tire</li> </ul> </li> </ul>	<ul style="list-style-type: none"> <li>• Occupant Impact Velocity (DTS) <ul style="list-style-type: none"> <li>Longitudinal.....-21.05 ft/s &lt; 39.37 ft/s</li> <li>Lateral .....2.68 ft/s &lt; 39.37 ft/s</li> </ul> </li> <li>• Occupant Ridedown Acceleration (DTS) <ul style="list-style-type: none"> <li>Longitudinal.....-11.36 g's &lt; 20 g's</li> <li>Lateral .....6.03 g's &lt; 20 g's</li> </ul> </li> <li>• Occupant Impact Velocity (EDR-3) <ul style="list-style-type: none"> <li>Longitudinal.....-23.68 ft/s &lt; 39.37 ft/s</li> <li>Lateral .....9.55 ft/s &lt; 39.37 ft/s</li> </ul> </li> <li>• Occupant Ridedown Acceleration (EDR-3) <ul style="list-style-type: none"> <li>Longitudinal.....-11.92 g's &lt; 20 g's</li> <li>Lateral .....5.69 g's &lt; 20 g's</li> </ul> </li> <li>• THIV (not required).....24.6 ft/s &lt; 39.37 ft/s</li> <li>• PHD (not required).....11.37 g's &lt; 20 g's</li> <li>• Test Article Damage .....Significant</li> <li>• Maximum Deflection <ul style="list-style-type: none"> <li>Permanent Set .....NA</li> <li>Dynamic .....NA</li> </ul> </li> <li>• Vehicle Damage.....Significant <ul style="list-style-type: none"> <li>VDS [24] .....11-L&amp;T-4</li> <li>CDC [25].....11FDAO3</li> </ul> </li> <li>• Maximum Deformation .....1 in. at center of the occupant compartment</li> <li>• Angular Displacement <ul style="list-style-type: none"> <li>Roll.....-219 degrees</li> <li>Pitch .....-25 degrees</li> <li>Yaw .....-54 degrees</li> </ul> </li> </ul>			

**Figure 176. Summary of Test Results and Sequential Photographs, Test USPBN-1**



0.000 sec



0.200 sec



0.050 sec



0.300 sec



0.100 sec



0.400 sec



0.150 sec



0.500 sec

Figure 177. Additional Sequential Photographs, Test USPBN-1



0.000 sec



0.500 sec



0.200 sec



0.620 sec



0.250 sec



0.870 sec



0.360 sec



1.280 sec

Figure 178. Additional Sequential Photographs, Test USPB-1





0.000 sec



0.320 sec



0.130 sec



0.410 sec



0.210 sec



0.490 sec



0.280 sec



0.600 sec

Figure 179. Additional Sequential Photographs, Test USPBN-1



0.000 sec



0.140 sec



0.050 sec



0.190 sec



0.100 sec



0.250 sec

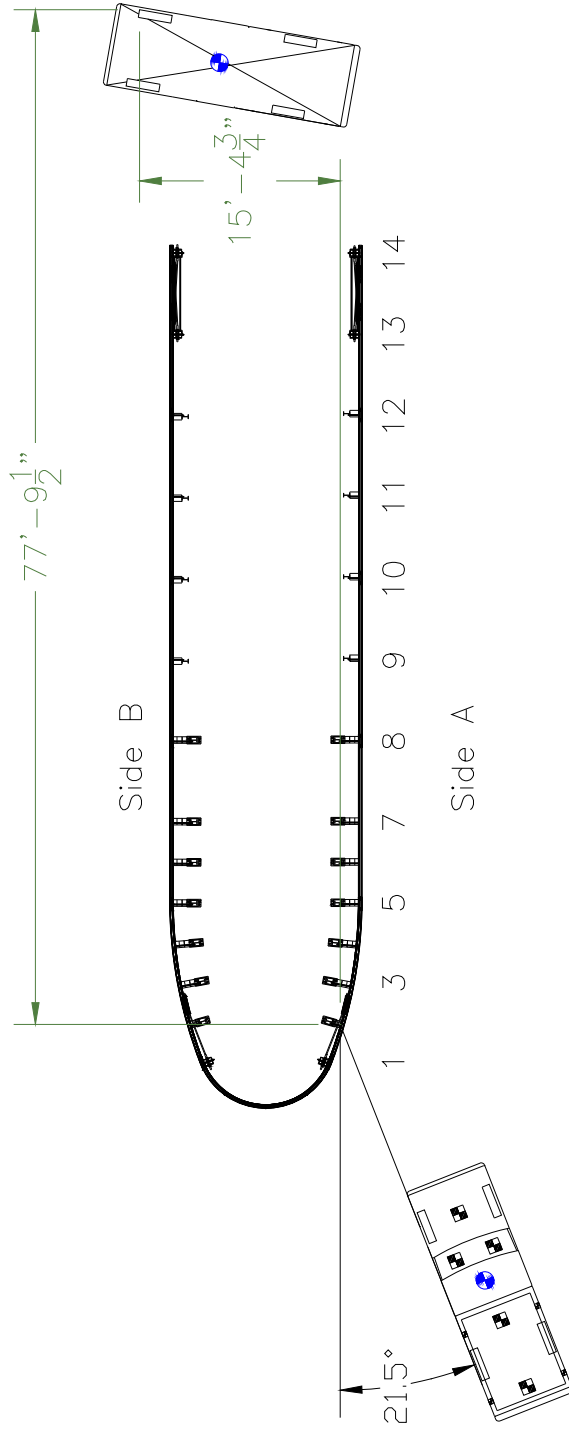


0.120 sec

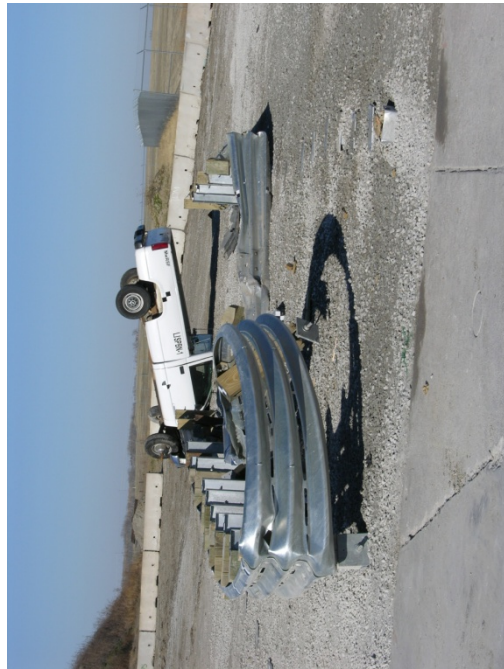


0.400 sec

Figure 180. Additional Sequential Photographs, Test USPB-1



**Figure 181. Vehicle Trajectory, Test USPNB-1**



**Figure 182. System Damage and Vehicle Final Position, Test USPBN-1**



**Figure 183. System Damage, Test USPBN-1**



**Figure 184. System Damage, Test USPB-N-1**



**Figure 185. System Damage, Test USPB-N-1**



**Figure 186. Vehicle Damage, Test USPBN-1**





**Figure 187. Vehicle Damage, Test USPBN-1**

## **11 COMPARISON OF CRASH TESTS USING TEST DESIGNATION NO. 3-38**

### **11.1 Comparison of Crash Tests Designation No. 3-38**

Following the unsuccessful crash test on the fracturing bolt, steel-post, bullnose barrier system, a thorough investigation was performed in order to determine the likely cause for the unsatisfactory outcome. To assist with this investigation, a comparison was made between test USPBN-1 and prior test designation 3-38 crash tests on both the previous wood-post and steel-post, bullnose barrier systems, as detailed in Table 24. In addition, a comparison of the time-sequential photographs for the fracturing bolt, steel-post bullnose test (test no. USPBN-1) and the wood-post bullnose (test no. MBN-8) is provided in Figures 188 through 191. From these comparisons, two factors were believed to have contributed to the vehicle climbing over the barrier system described herein.

First, the fracturing bolt posts did not absorb sufficient energy to safely capture and contain the vehicle. The posts broke away quickly and did not rotate much in the soil, which allowed the pickup to penetrate farther into the system. A comparison of the fracture times for the wood and steel posts is provided in Table 25. From this comparison, it appears that the fracturing-bolt, steel posts, except for post no. 2, broke away quicker than the wood counterparts. Second, post no. 2 remained intact significantly longer than the wood counterpart, thus causing the pickup truck to redirect more than that observed in the previous wood-post bullnose testing. Due to these factors, the pickup truck penetrated faster and farther downstream into the system than that observed in previous testing and did not achieve similar lateral penetration, as provided in Table 26. The front end of pickup was not sufficiently captured before contacting the end of the slotted rail near post no. 8. A buckle formed in the non-slotted rail section located near post

no. 9, which caused the rail to buckle toward the ground. This behavior allowed the pickup truck to climb up and over the rail.

As a result of the failed test, design changes were deemed necessary to allow for the successful containment or redirection of the pickup truck. Several design modifications are recommended in Chapter 13.

**Table 24. General Behavior and Comparison of Test Designation No. 3-38 Tests**

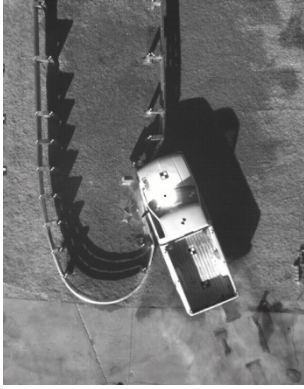
Test No.	Post Type	Facts
MBN-8	Wood CRT Posts	<ul style="list-style-type: none"> <li>- Test passed as the slotted rail pocketed around and captured the pickup.</li> <li>- The rail completely wrapped around the pickup by the time the front end of the pickup reached post #7.</li> <li>- The rail ended up wrapping around post #8.</li> <li>- The anchorage, post #1, broke away approximately 154 ms.</li> <li>- The CRT wood posts broke at the bottom hole, thus absorbing energy by moving soil.</li> </ul>
SBN-1	Steel Hinged Posts	<ul style="list-style-type: none"> <li>- The anchorage, post #1, held on until 240 ms.</li> <li>- Pickup redirected instead of pocketing around post #8.</li> </ul>
SBN-2	Steel Hinged Posts	<ul style="list-style-type: none"> <li>- Post #1 was changed to a wood BCT post.</li> <li>- The anchorage, post #1, broke away quicker, held on approximately 90 ms.</li> <li>- Pickup pocketed into system, got inside of post #8 similar to MBN-8.</li> <li>- However, rail began to drop at approximately 214 ms when front end of pickup was near post #7.</li> <li>- Pickup ramped up on debris/posts causing the rail to drop</li> </ul>
USPBN-1	Fracturing Bolt Steel Posts	<ul style="list-style-type: none"> <li>- The anchorage, post #1, held on until approximately 132 ms.</li> <li>- Post #2 held on longer than previous wood post testing.</li> <li>- Pickup did not pocket nearly as much and the rail did not wrap around the pickup until after post #8.</li> <li>- After post #8, the rail is non-slotted and the rail buckled to the ground at approx. 210 ms.</li> <li>- Posts did not absorb as much energy, no soil gaps and posts broke away quicker.</li> </ul>



0.150 sec



0.300 sec



0.050 sec



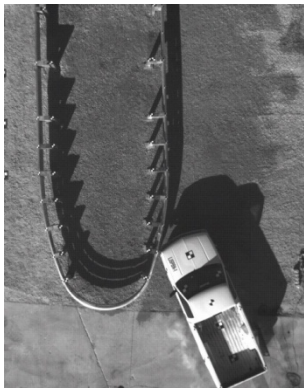
0.250 sec



0.000 sec



0.200 sec



0.100 sec



0.150 sec

**Figure 188. Sequential Photographs, Test USBN-1**



0.150 sec



0.100 sec



0.050 sec



0.000 sec



0.350 sec



0.300 sec



0.250 sec



0.200 sec

Figure 189. Sequential Photographs, Test MBN-8



0.075 sec



0.050 sec



0.025 sec



0.100 sec



0.175 sec



0.150 sec



0.125 sec



0.100 sec

Figure 190. Sequential Photographs, Test USBN-1



0.000 sec



0.025 sec



0.050 sec



0.075 sec



0.100 sec



0.125 sec



0.150 sec



0.175 sec

**Figure 191. Sequential Photographs, Test MBN-8**

**Table 25. Comparison of Fracture Times for Wood and Steel Posts**

<b>MBN-8 (Wood Posts)</b>	
<b>Post #</b>	<b>Time Broke (ms)</b>
1	154
2	54
3	54
4	82
5	126
6	**

<b>USPBN-1 (Steel Posts)</b>	
<b>Post #</b>	<b>Time Broke (ms)</b>
1	132
2	106*
3	38
4	58
5	78
6	110

\*= Time Blockout Broke

\*\* = Time Uncertain

**Table 26. Comparison of Pickup Location versus Time**

<b>Timing of the front end of the pickup to reach each post position</b>			
<b>At post #</b>	<b>Test MBN-8</b>	<b>Test USPBN-1</b>	<b>Test SBN-2</b>
3	36	32	32
4	72	56	62
5	118	92	96
6	184	122	132
7	252	168	178

\*\* Times in msec



## 12 SUMMARY AND CONCLUSIONS

### 12.1 Summary

The study began with an extensive literature review of previous breakaway steel posts to find potential candidates for use as the universal breakaway steel post. A literature review of CRT wood post testing revealed the need for additional testing in order to determine the strength and behavior of the CRT wood posts for use in selecting a new universal breakaway steel post. As a result, CRT wood posts were tested and evaluated in a rigid sleeve using three different axes of impact.

After determining the properties of the CRT wood posts, brainstorming was used to generate new breakaway steel post concepts that could eventually replace the CRT wood post. Several steel tubular and steel W8x10 (W203x14.9) post options were investigated. In addition, other breakaway posts were considered and consisted of a steel fracturing bolt concept, and posts manufactured with brittle materials, including fiber reinforced plastic and cast iron. From these initial post concept candidates, the list was narrowed down to five concepts for use in a testing and evaluation program, as described as the round 1 bogie testing.

For the first round of bogie testing, a steel tube in steel tube concept, a steel tube in steel tube with a through bolt concept, a fiber reinforced plastic (FRP) tube, a fracturing bolt (slipbase) concept, and a circular fillet weld concept were all tested and evaluated. Although most of the concepts showed some promise, the number of concepts was narrowed down to the two most-promising designs. Both the fracturing bolt and circular fillet weld concepts demonstrated good potential for use as the universal breakaway steel post, and thus, they were included in a second round of bogie testing.

The second round of bogie testing involved five bogie tests on revised designs for the circular fillet weld and fracturing bolt concepts. These two concepts were modified to better match the properties of the CRT wood posts. After the second round of bogie testing, it was determined that the fracturing bolt concept best matched the properties of the CRT wood post. Thus, the fracturing bolt post was chosen for use as the universal breakaway steel post.

Previously, the fracturing bolt post had been tested in soil, while the wood CRT post had been tested in a rigid sleeve. As a result, it was decided to test and evaluate the CRT wood posts in soil to determine whether the dynamic performance of the fracturing bolt post compared with that observed for the CRT wood post when placed in soil. From this soil testing, it was determined that fracturing bolt reasonably compared with the soil behavior obtained for the CRT posts. However, it was noted that the fracturing bolt post concept had never been tested at an oblique (diagonal) angle. As a result, the fracturing bolt post needed to be tested at an oblique angle to make certain that it matched the strength and behavior of the CRT wood post. Since minor refinements were made to the fracturing bolt post, it was also retested in a strong-axis impact in a third round of bogie testing.

For third round of bogie testing, the fracturing bolt post was impacted in both a strong axis and a diagonal (45-degree) axis. From this testing, the strength of the fracturing bolt post was found closely matched the targeted strength level for each impact angle. Also, the post broke away cleanly for each impact angle, similar to the behavior observed for the wood posts. Thus, the fracturing bolt post was deemed ready for evaluation through full-scale crash testing when used in a thrie beam bullnose system.

Before the full-scale crash testing, initial LS-DYNA simulation modeling of the fracturing bolt post was performed. A simulation of the fracturing bolt post was created that generally matched the behavior observed in the actual bogie testing for three different axis of impact. For all three impact scenarios, the fracturing bolt post simulation model broke away similar to what was observed in the bogie testing. Thus, it was believed that this model could eventually be used in the simulation of a full-scale crash test or for use in evaluating post design modifications.

Lastly, test no. USPBN-1 was conducted according to NCHRP Report No. 350 Test Designation 3-38. The steel-post, bullnose system was impacted at the critical point at the centerline of post no. 2. Actual vehicle impact with the barrier system occurred approximately 4 in. (101.6 mm) downstream of the target location. The 4,474-lb (2,029-kg) pickup truck impacted the barrier at a speed of 63.2 mph (101.7 km/h) and an angle of 22.6 degrees.

Following test no. USPBN-1 (test designation no. 3-38), a safety performance evaluation was conducted, and the fracturing-bolt, steel-post, bullnose barrier was determined to be unacceptable according to the NCHRP Report No. 350 criteria. The failure of test USPBN-1 to meet all of the safety performance criteria was directly attributed to the pickup truck overriding the guardrail near post no. 7 on the right side of the system. Following a comparison between test no. USPBN-1 and the previous tests run according to test designation nos. 3-38 on the bullnose system, two factors were believed to have contributed to the vehicle climbing over the system. First, the fracturing bolt posts did not absorb enough energy to safely capture and contain the vehicle. The posts did not rotate much in the soil and broke away quickly, which allowed the pickup to penetrate more into the system. Second, post no. 2 remained intact longer than the

wood counterparts, thus causing the pickup truck to redirect more than that observed in the previous testing on the wood-post, bullnose barrier.

## 13 RECOMMENDATIONS

### 13.1 Future Work

Following the failure of test no. USPBN-1, MwRSF researchers and MnDOT officials discussed the future plan for this research project. As such, it was determined that this project should follow one of two approaches. First, it was determined that several changes could be implemented into the bullnose system, and then the pickup truck crash test could be re-run in order to evaluate those design modifications. Second, this research and development project could be refocused to utilize more computer simulation modeling, component testing, and bogie testing in order to better understand the effect that various features and design modifications have on overall system performance.

#### 13.1.1 - Plan No. 1 – Implement Modifications and Re-run Full-Scale Crash Test

For the first option, it was proposed that design modifications be implemented into the steel-post, bullnose system. Then, once any changes were incorporated into the design, the pickup truck test would be re-run according to the test no. 3-38 impact conditions.

Following an evaluation of the test results from test no. USPBN-1 as well as a comparison results with prior crash tests performed according to test designation no. 3-38, several design modifications were brainstormed in order to improve barrier performance. The potential design modifications included:

- 1) changing post no. 2 from a breakaway steel post to a wood BCT post, as used in the wood-post, bullnose system;
- 2) reducing the soil embedment depth by 6 in. (152 mm) for each breakaway steel post);
- 3) adding another slotted thrie-beam rail section along each side of the barrier; and
- 4) increasing the structural capacity for the fracturing-bolt steel post about its strong axis of bending.

It should be noted that the implementation of these design changes will not ensure that the steel-post, bullnose system will perform in an acceptable manner when evaluated with test designation no. 3-38. However, the researchers believed that that safety performance of the steel-post, bullnose barrier should be improved if some or all of the noted design modifications were incorporated.

Some of the noted modifications were conceived in order to provide increased energy absorption capacity for the breakaway steel posts, thus allowing for improved vehicle-rail interlock on the front end and increased vehicle capture. As such, it is recommended that post no. 2 be changed back to a wood BCT post in order to provide similar fracture times and vehicle penetration into the interior of the bullnose system, as compared to the successful test no. MBN-8.

For option 1, the fracturing-bolt, breakaway steel post could be strengthened by replacing 3/8-in. (9.5-mm) diameter, grade 5 bolts with 7/16-in. (11.1-mm) diameter, grade 5 bolts. With this change, the clear distance between the bolts in the strong-axis direction could be reduced from 10 13/16 in. (275 mm) to 10 in. (254 mm). For the weak axis, the bolts would still utilize a 2 1/2-in. (64-mm) clear distance, thus slightly increasing the post strength about the weak axis. The post capacity about the diagonal (45-degree) axis would increase as well. The post embedment depth in the soil should also be reduced to 40 in. (1,016 mm) in order to promote more rotation and energy absorption prior to post fracture. However, the soil would require sufficient compaction in order to ensure that the posts would break away. With these changes, the fracturing-bolt, steel-post, bullnose system would have increased potential for capturing the 2000P pickup truck at the TL-3 impact conditions of NCHRP Report No. 350.

### **13.1.2 - Plan No. 2 – Refocus Effort on More Research and Development**

For the second option, it was proposed that the research and development study be refocused to include more component and bogie testing as well as LS-DYNA computer simulation modeling before additional full-scale vehicle crash testing was performed. Using this option, researchers would obtain a better understanding as to why test no. USPBN-1 failed. Researchers would also be more able to determine how sensitive the barrier system would be to the proposed design changes. However, this effort would likely require considerable research funding and time before confidence would exist for predicting actual crash test behaviors or for evaluating the effect of design changes. In addition, a longer research period would be needed under this option versus the alternative approach discussed under option no. 1.

## 14 REFERENCES

1. Bielenberg, B.W., Faller, R.K., Reid, J.D., Rohde, J.R., Sicking, D.L., and Keller, E.A., *Concept Development of a Bullnose Guardrail System for Median Applications*, Final Report to the Midwest States' Regional Pooled Fund Program, MwRSF Research Report No. TRP-03-73-98, Midwest Roadside Safety Facility, University of Nebraska-Lincoln, Lincoln, Nebraska, May 1998.
2. Bielenberg, B.W., Faller, R.K., Reid, J.D., Rohde, J.R., Sicking, D.L., Keller, E.A., and Holloway, J.C., *Phase II Development of a Bullnose Guardrail System for Median Applications*, Final Report to the Midwest States' Regional Pooled Fund Program, MwRSF Research Report No. TRP-03-78-98, Midwest Roadside Safety Facility, University of Nebraska-Lincoln, Lincoln, Nebraska, December 1998.
3. Bielenberg, B.W., Faller, R.K., Reid, J.D., Rohde, J.R., Sicking, D.L., Keller, E.A., Holloway, J.C., and Supencheck, L.L., *Phase III Development of a Bullnose Guardrail System for Median Applications*, Final Report to the Midwest States' Regional Pooled Fund Program, MwRSF Research Report No. TRP-03-95-00, Midwest Roadside Safety Facility, University of Nebraska-Lincoln, Lincoln, Nebraska, June 2000.
4. Ross, H.E., Jr., Sicking D.L., and Zimmer, R.A., *National Cooperative Highway Research Report 350: Recommended Procedures for the Safety Performance Evaluation of Highway Features*. Transportation Research Board, Washington, D.C., 1993.
5. Bielenberg, B.W., Faller, R.K., Rohde, J.R., and Reid, J.D., *Evaluation of an Existing Steel Post Alternative for the Thrie Beam Bullnose Guardrail System*, Letter Report to the Midwest States' Regional Pooled Fund Program, MwRSF Research Report No. TRP-03-193-07, Midwest Roadside Safety Facility, University of Nebraska-Lincoln, Lincoln, Nebraska, August 2007.
6. Hascall, J.A., Faller, R.K, Reid, J.D., Sicking, D.L., and Kretschmann, D.E., *Investigating the Use of Small-Diameter Softwood as Guardrail Posts (Dynamic Test Results)*, Final Report to the Forest Products Laboratory – U.S. Department of Agriculture, MwRSF Research Report No. TRP-03-179-07, Midwest Roadside Safety Facility, University of Nebraska-Lincoln, Lincoln, Nebraska, March 2007.
7. Hinch, J.A., Owings R.P., and Manhard G.A., *Safety Modifications of Turned-Down Guardrail Terminals, Volumes 1, 2, and 3*, Final Report to the Federal Highway Administration, Ensco, Inc., Springfield, VA, June 1984.
8. Bronstad, M.E., and Michie, J.D., *Breakaway Cable Terminals for Guardrails and Median Barriers*, NCHRP Research Results Digest 84, Transportation Research Board, Washington, D.C., March 1976.



9. Bronstad, M.E., and Michie, J.D., *Modified Breakaway Cable Terminals for Guardrails and Median Barriers*, NCHRP Research Results Digest 102, Transportation Research Board, Washington, D.C., May 1978.
10. Bronstad, M.E., *A Modified Foundation for Breakaway Cable Terminals*, NCHRP Research Results Digest 124, Transportation Research Board, Washington, D.C., November 1980.
11. Arens, S.W., Faller, R.K., Rohde, J.R., and Polivka, K.A., *Dynamic Impact Testing of CRT Wood Posts in a Rigid Sleeve*, Final Report to the Minnesota Department of Transportation, MwRSF Research Report No. TRP-03-198-08, Midwest Roadside Safety Facility, University of Nebraska-Lincoln, Lincoln, Nebraska, January 2008.
12. Rohde, J.R., Hascall, J.A., Polivka, K.A., Faller R.K., and Sicking, D.L., *Dynamic Testing of Wooden Guardrail Posts – White and Red Pine Species Equivalency Study*, Final Report to the Midwest States' Regional Pooled Fund Program, MwRSF Research Report No. TRP-03-154-04, Midwest Roadside Safety Facility, University of Nebraska-Lincoln, Lincoln, Nebraska, September 2004.
13. Strongwell Corporation, 2008, <http://www.strongwell.com/>
14. Dutta, P.K., *Investigations of Plastic Composite Materials for Highway Safety Structures*, US Army Corps of Engineers Cold Regions Research & Engineering Laboratory, CRREL Report 98-7, Hanover, New Hampshire, August 1998.
15. Advanced Fiber Products, 2008, <http://www.afpfiberglass.com/>
16. Sicking, D.L., Rohde, J.R., and Reid, J.D., *Design and Development of Steel Breakaway Posts*, Transportation Research Record 1720, Paper No. 00-0628, Transportation Research Board, National Research Council, Washington, D.C., 2000.
17. DynaMax User's Manual, Revision 1.75, Instrumented Sensor Technologies, Inc., Okemos, Michigan, April 1993.
18. The DADiSP Worksheet, Data Analysis and Display Software, User Reference Manuals, Version 4.0, DSP Development Corporation, Cambridge, Massachusetts, December 1991.
19. Society of Automotive Engineers (SAE), *Instrumentation for Impact Test – Part 1 – Electronic Instrumentation – SAE J211/I MAR95*, New York City, NY, 1999.
20. Livermore Software Technology Corp., LS-DYNA, <http://www.lstc.com/index.htm>
21. Electrophysics, Moisture Meter Model MT700, Operating Instructions & Information, Ontario, Canada.

22. Hiser, N.R. *Slip Base Modeling for Cable Guardrail Systems*, A Thesis Presented to the Faculty of The Graduate College at the University of Nebraska-Lincoln, April 2003.
23. Hinch, J., Yang, T.L., and Owings, R., *Guidance Systems for Vehicle Testing*, ENSCO, Inc., Springfield, VA 1986.
24. *Vehicle Damage Scale for Traffic Investigators*, Second Addition, Technical Bulletin No. 1, Traffic Accident Data (TAD) Project, National Safety Council, Chicago, Illinois, 1971.
25. *Collision Deformation Classification - Recommended Practice J224 March 1980*, Handbook Volume 4, Society of Automotive Engineers (SAE), Warrendale, Pennsylvania, 1985.

**15 APPENDICES**

## Appendix A. Bogie Testing Results

### A.1 Test Summary Information

A summary sheet for every bogie test is provided in this section. Summary sheets include acceleration, velocity, and displacement versus time plots, as well as force and energy versus deflection plots.

**Table A-1. Post Testing Summary**

<b>UBSP Test Parameters</b>
UBSP: Universal Breakaway Steel Post Concepts
Test: Impact in standard strong soil at 0, 45, and 90 degrees with respect to strong axis
Accelerometer: EDR-3 Data
Bogie Mass (Weight): 1,841 lbs (835.1 kg)
Bumper Height: 24 7/8 in. (632 mm)
Post Length: 72 in. (1,829 mm)
Soil: 135 lb/ft <sup>3</sup> (2163 kg/m <sup>3</sup> ) NCHRP 350 (AASHTO 147-65 (1990) Grade B)

**Table A-2. Post Testing Results Reference**

Test No.	Velocity		Impact Angle	Post Type	Figure Number
	mph	ft/s			
UBSP-1	19.5	28.5	0	Steel Tube in Steel Tube	Figure A-1
UBSP-2	19.3	28.3	90	Steel Tube in Steel Tube	Figure A-2
UBSP-3	19.7	28.9	0	FRP Tube	Figure A-3
UBSP-4	19.6	28.7	90	FRP Tube	Figure A-4
UBSP-5	19.4	27.6	0	Fracturing Bolt	Figure A-5
UBSP-6	18.5	27.1	90	Fracturing Bolt	Figure A-6
UBSP-7	19.4	23.6	0	Circular Fillet Weld	** No Data
UBSP-8	20.2	29.6	90	Circular Fillet Weld	Figure A-7
UBSP-9	19.9	29.2	0	Fracturing Bolt -Revision	Figure A-8
UBSP-10	19.1	28.0	90	Fracturing Bolt - Revision	Figure A-9
UBSP-11	19.7	28.9	90	Circular Fillet Weld - Revision	Figure A-10
UBSP-12	18.7	27.4	0	Circular Fillet Weld - Revision	Figure A-11
UBSP-13	18.7	27.4	0	Fracturing Bolt - Revision	Figure A-12
UBSP-14	19.1	28.0	0	CRT Wood Post	Figure A-13
UBSP-15	20.5	30.1	0	CRT Wood Post	Figure A-14
UBSP-16	20.2	29.6	90	CRT Wood Post	Figure A-15
UBSP-17	20.6	30.2	90	CRT Wood Post	Figure A-16
UBSP-18	20.0	29.3	45	CRT Wood Post	Figure A-17
UBSP-19	20.0	29.3	45	CRT Wood Post	Figure A-18
UBSP-20	19.0	27.9	0	Fracturing Bolt – 2 <sup>nd</sup> Revision	Figure A-19
UBSP-21	19.6	28.7	45	Fracturing Bolt – 2 <sup>nd</sup> Revision	Figure A-20

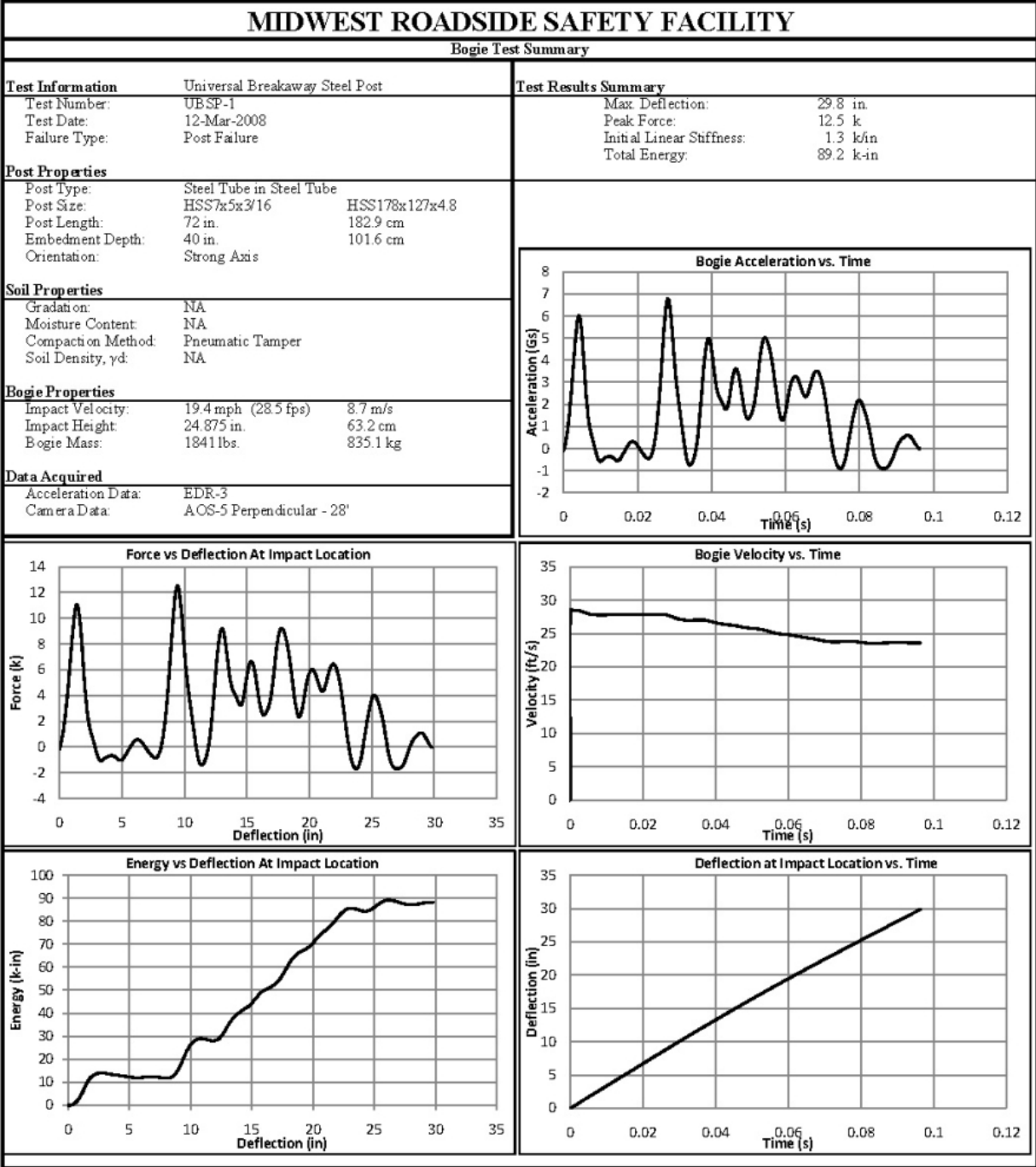


Figure A-1. Results of UBSP-1 (EDR3)

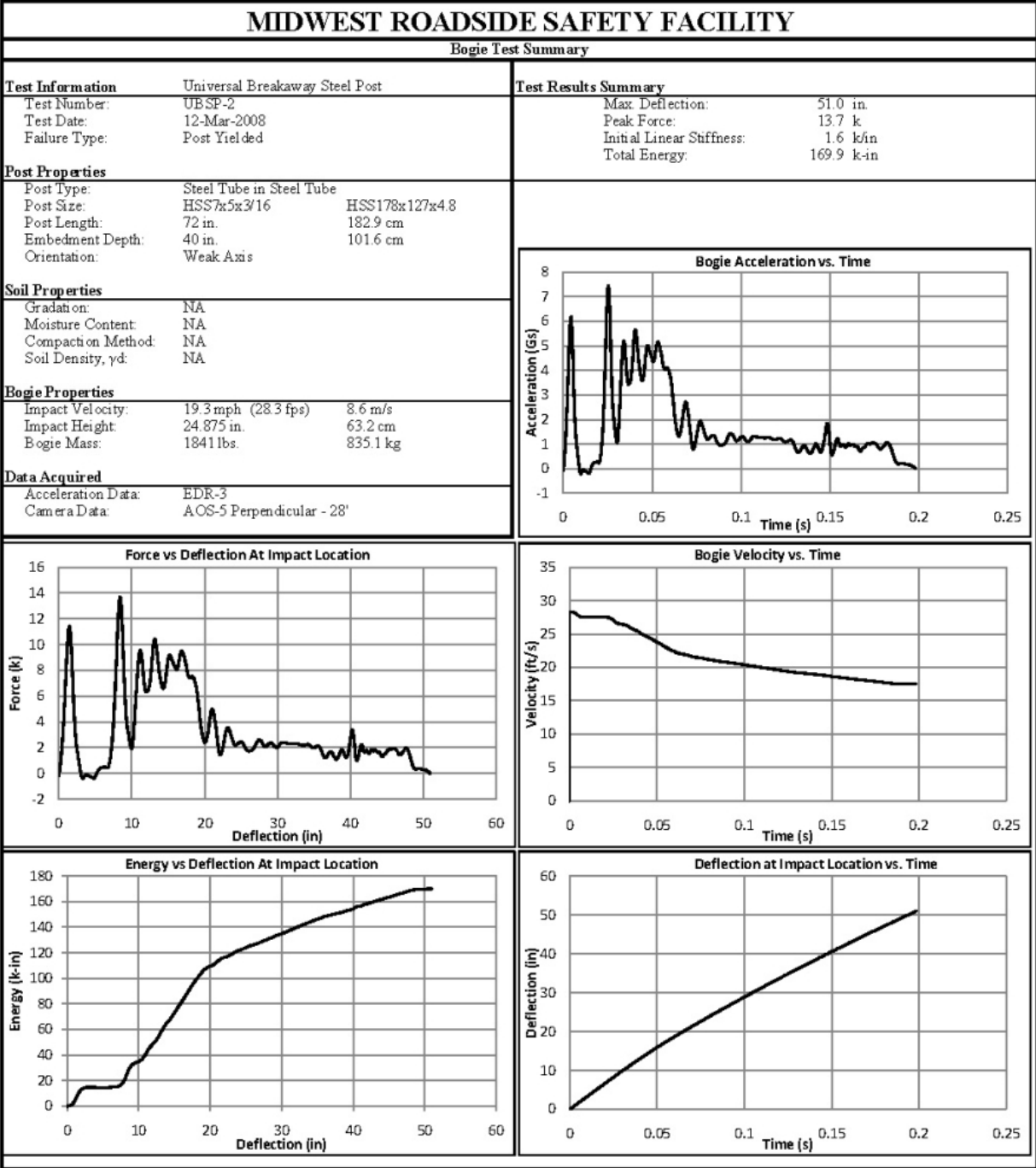


Figure A-2. Results of UBSP-2 (EDR3)

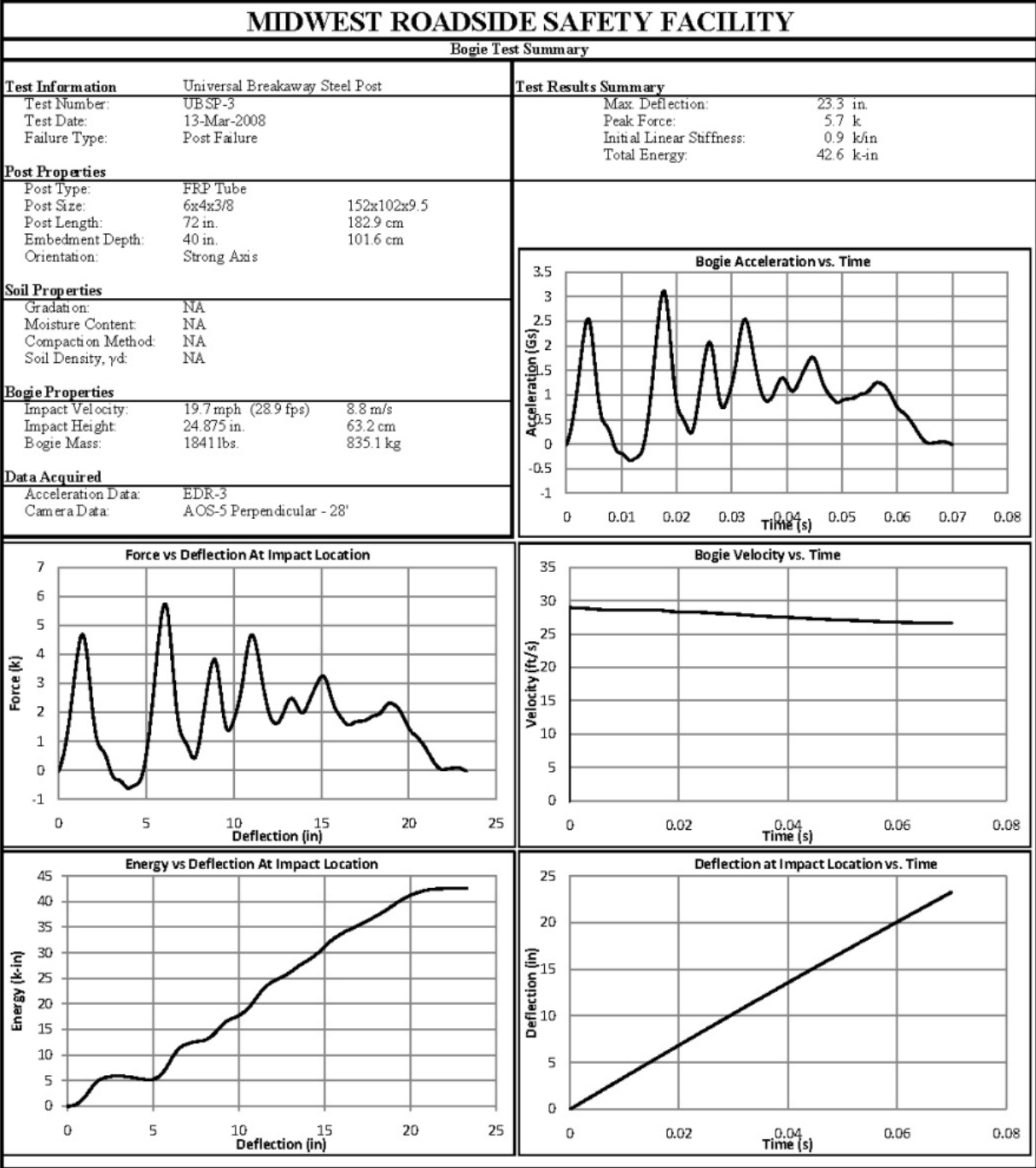


Figure A-3. Results of UBSP-3 (EDR3)

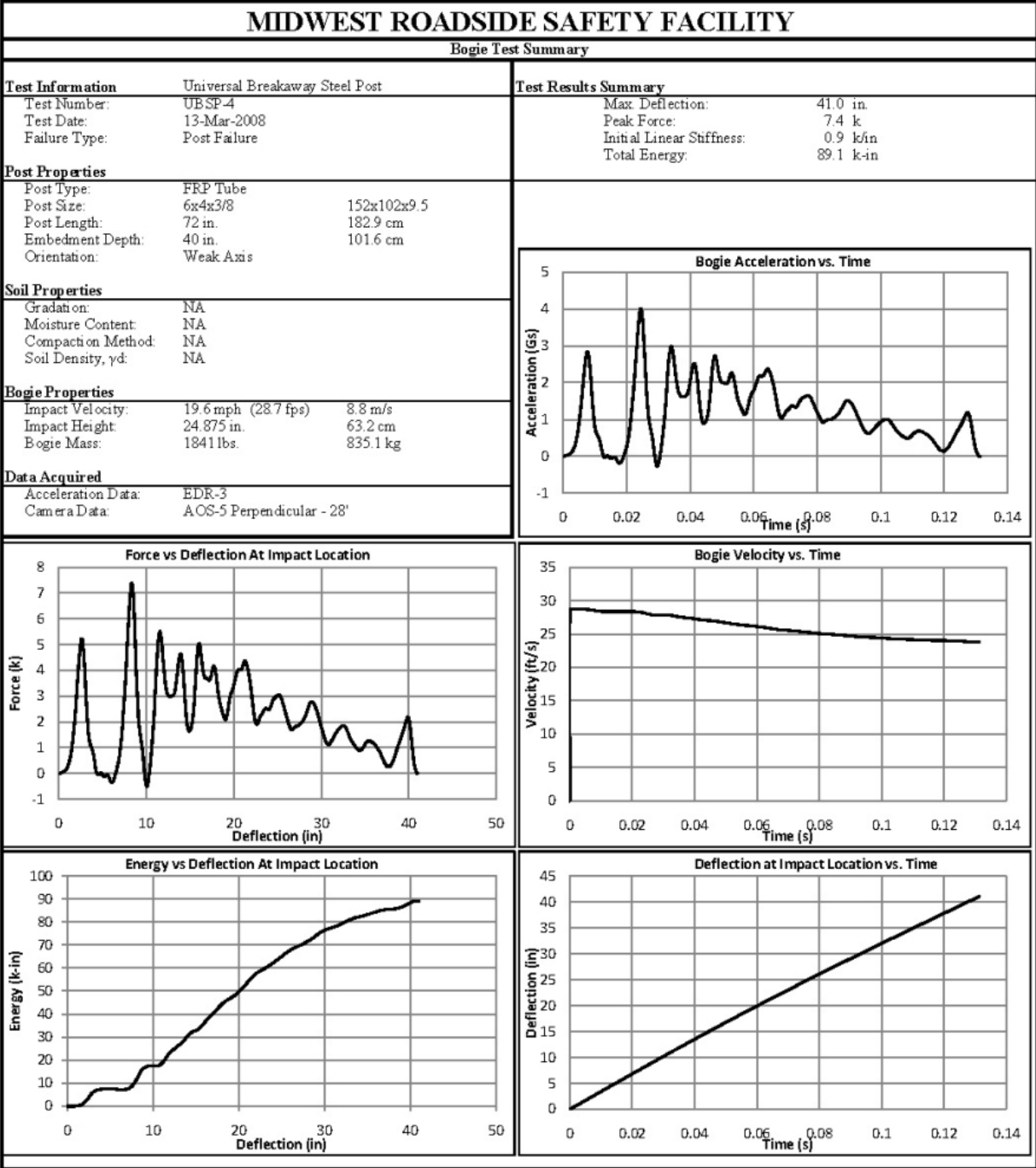


Figure A-4. Results of UBSP-4 (EDR3)



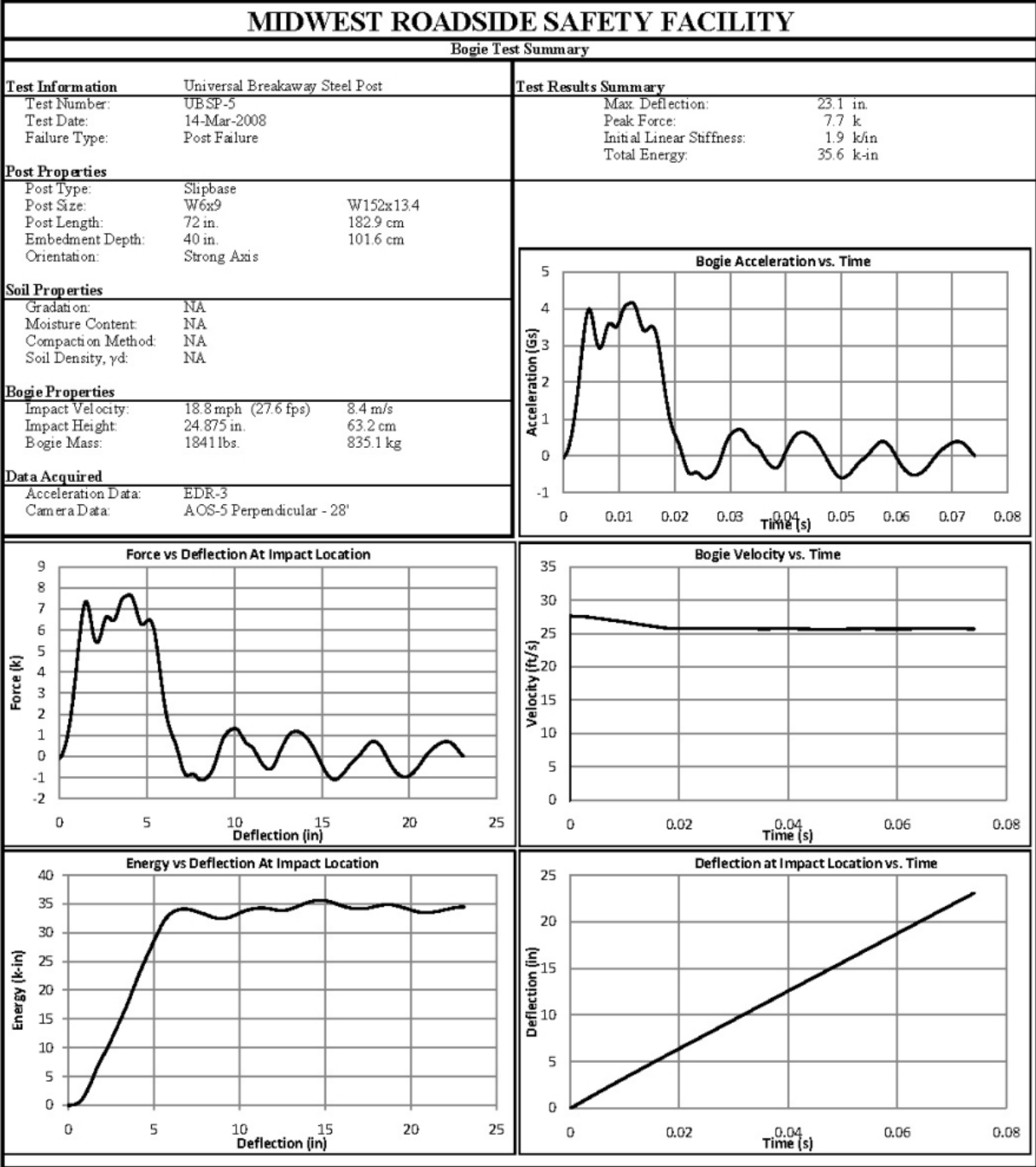


Figure A-5. Results of UBSP-5 (EDR3)

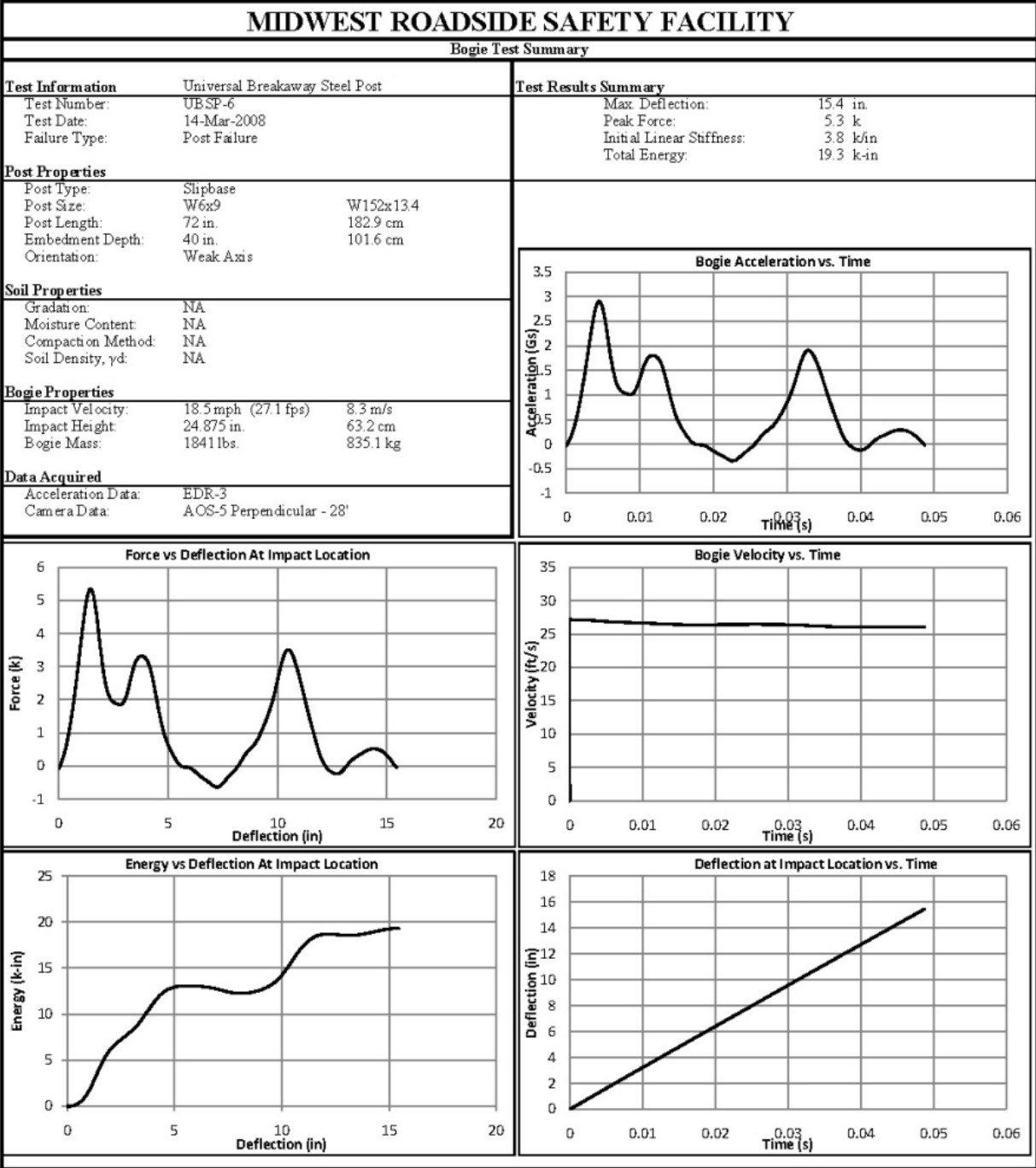


Figure A-6. Results of UBSP-6 (EDR3)

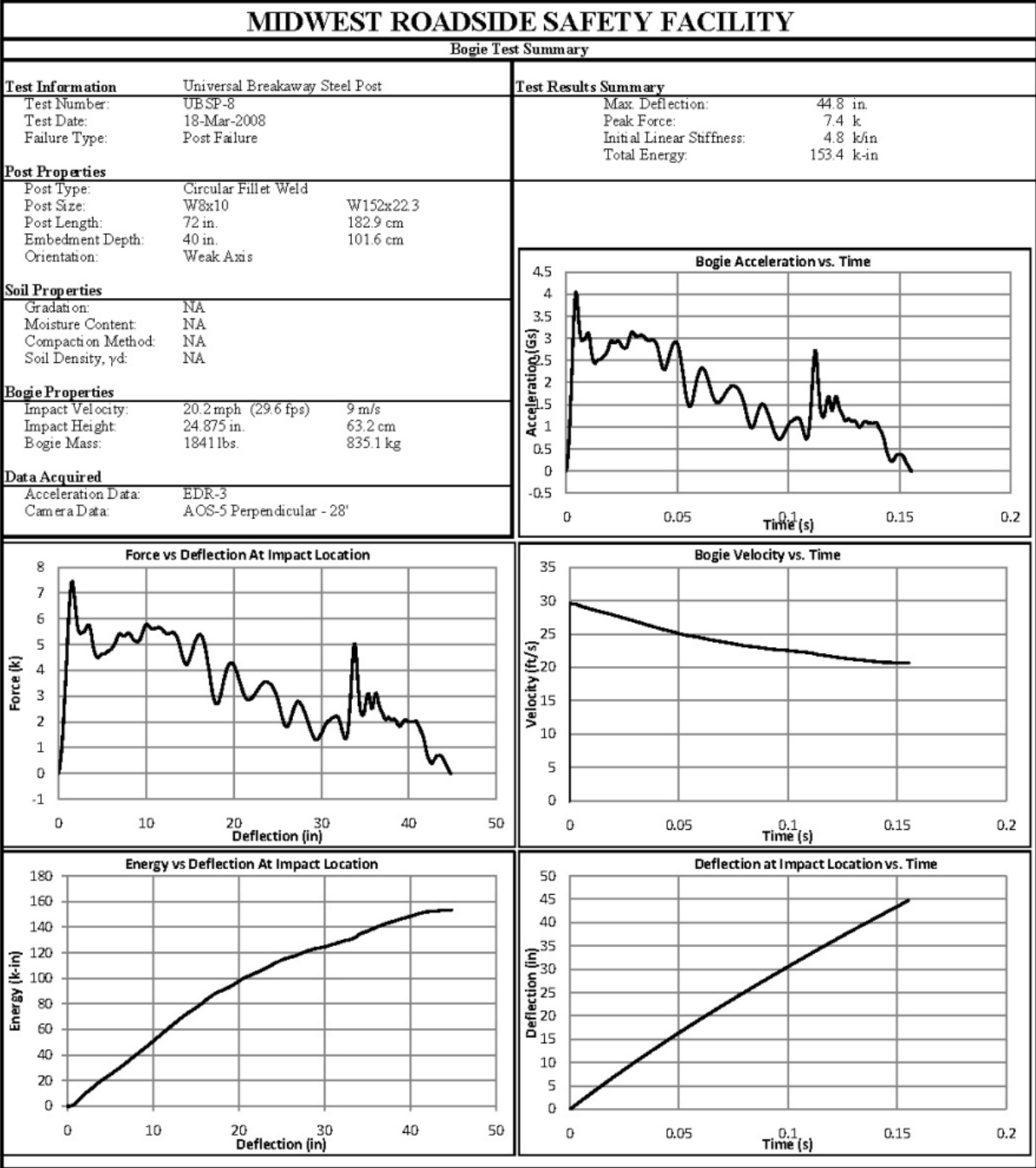


Figure A-7. Results of UBSP-8 (EDR3)

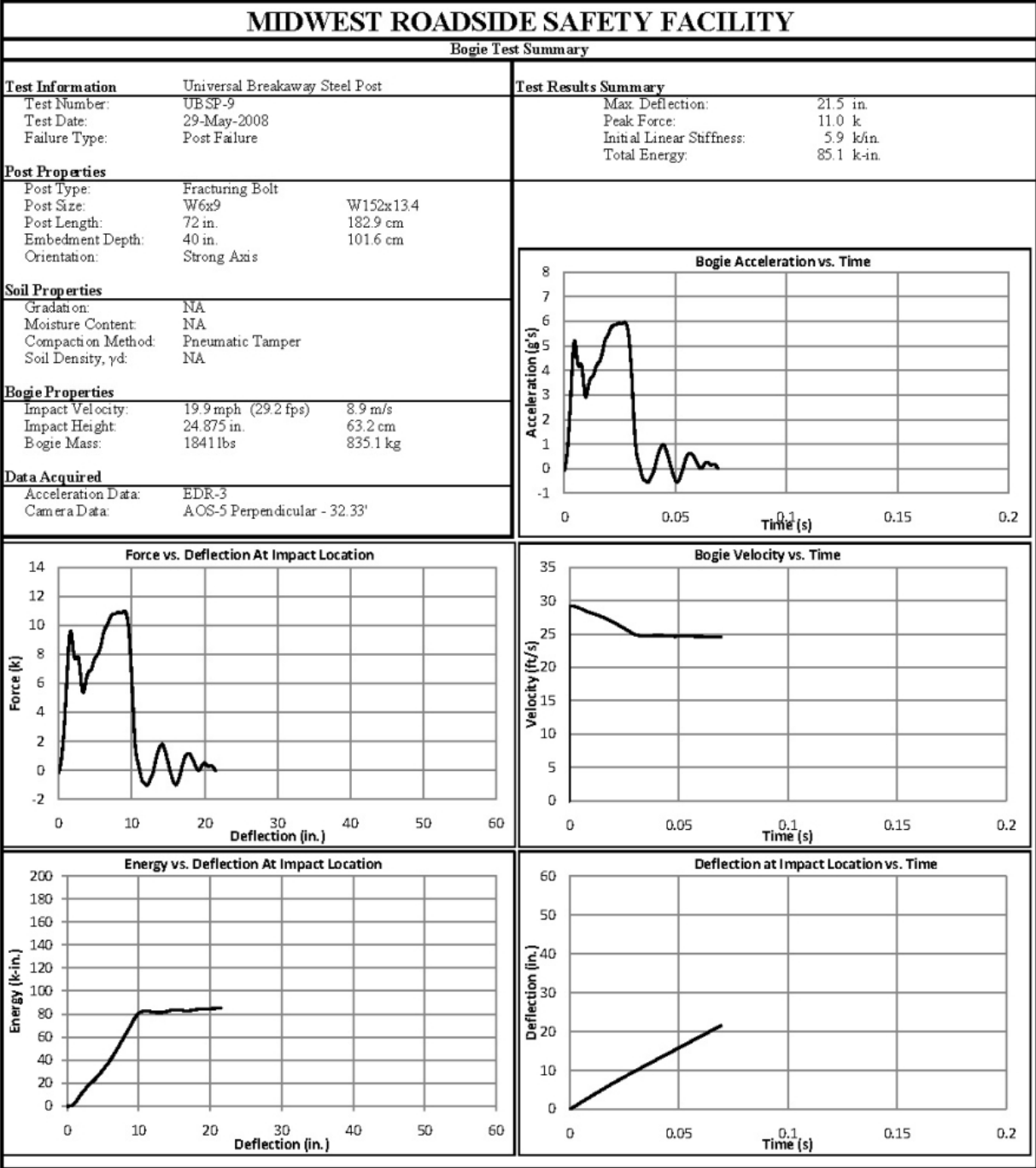


Figure A-8. Results of UBSP-9 (EDR3)

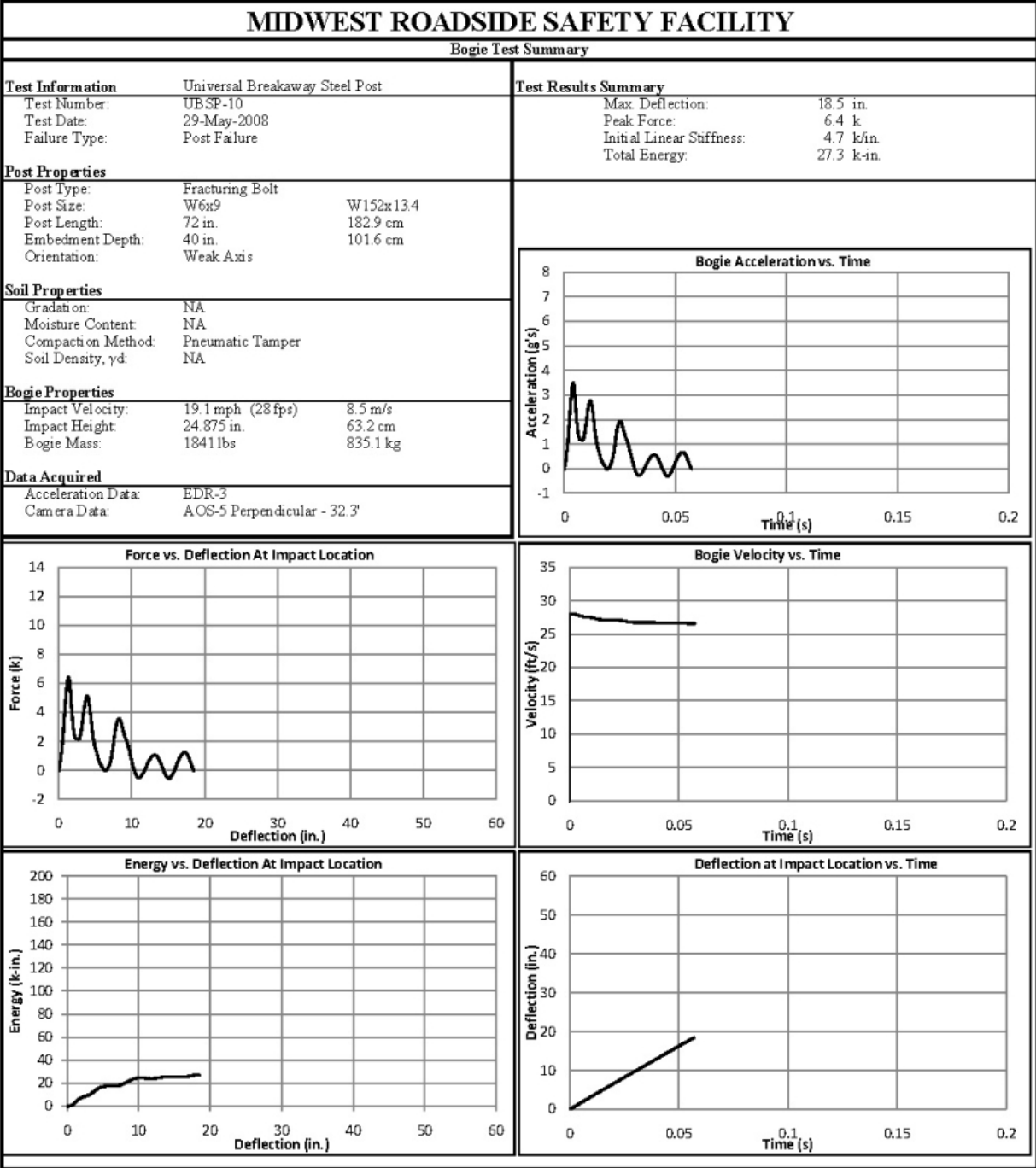


Figure A-9. Results of UBSP-10 (EDR3)

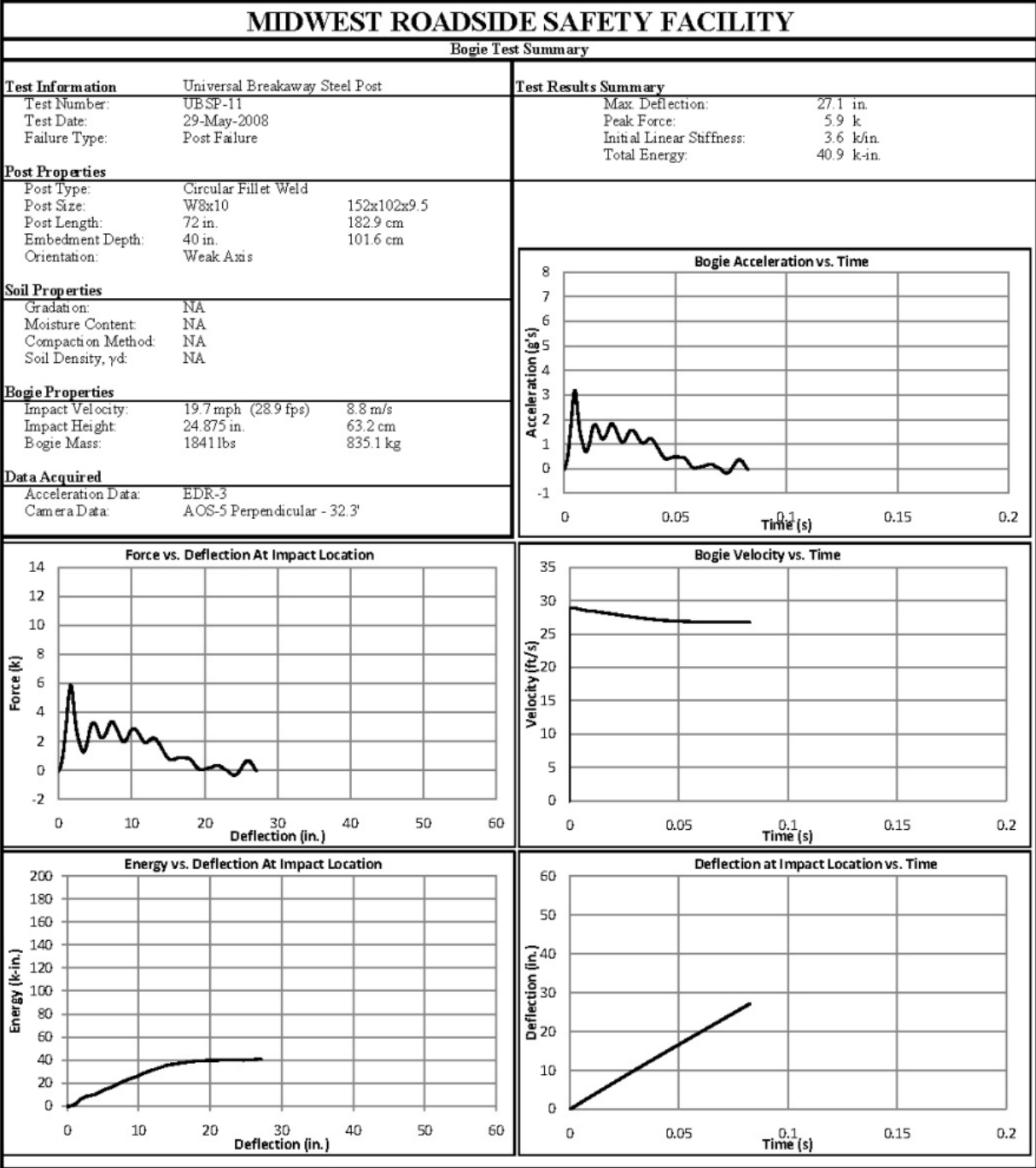


Figure A-10. Results of UBSP-11 (EDR3)

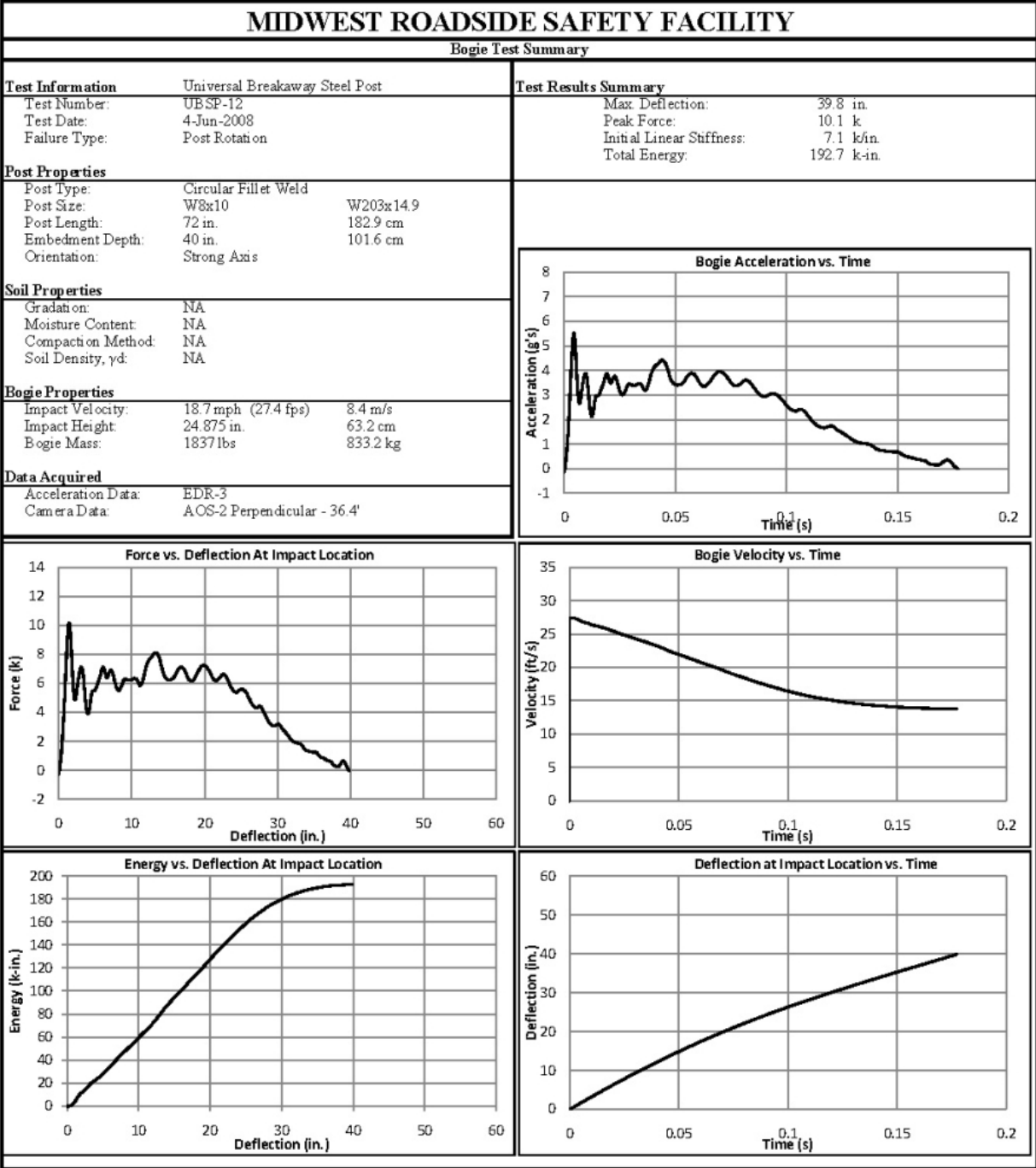


Figure A-11. Results of USBP-12 (EDR3)

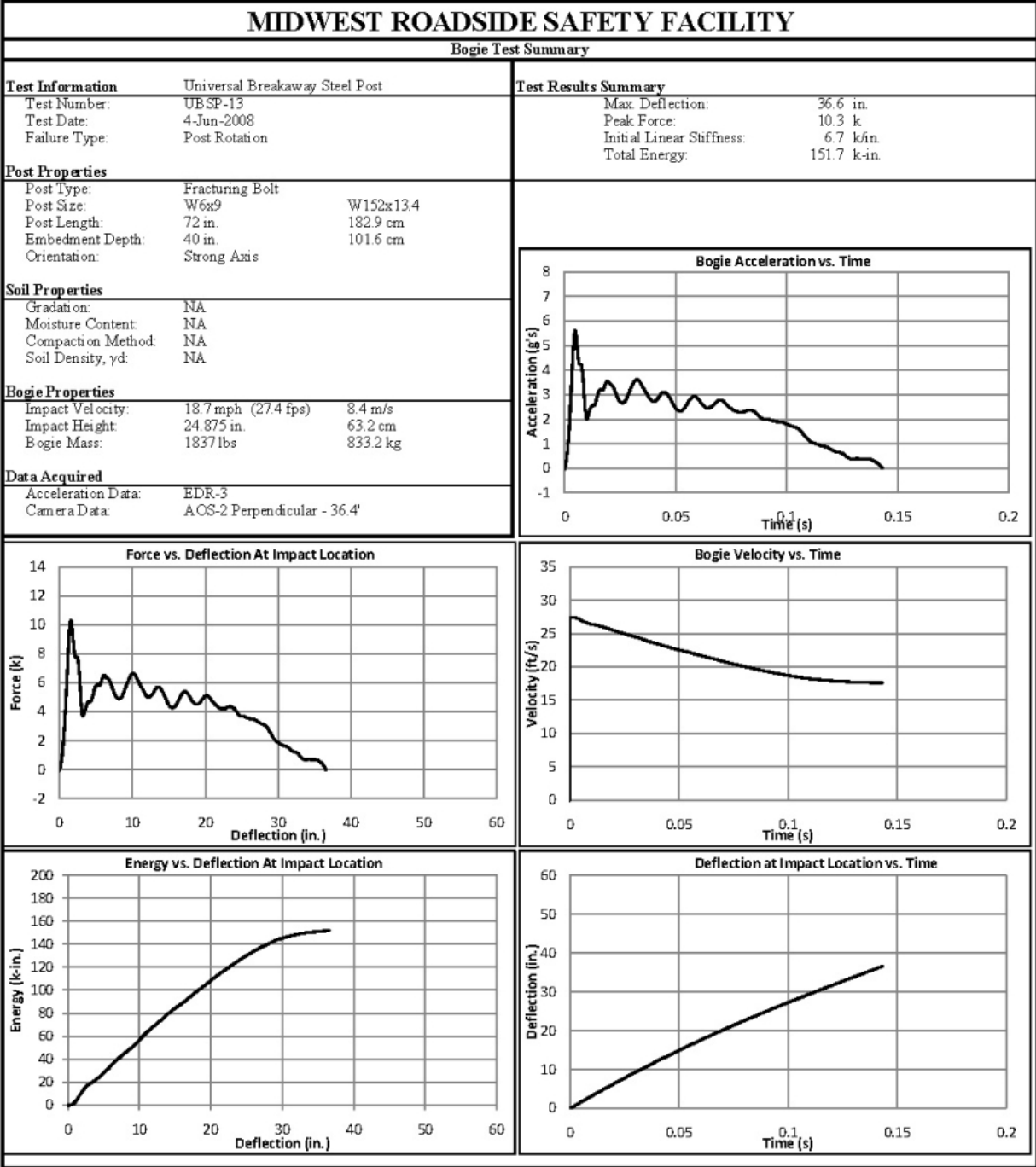


Figure A-12. Results of UBSP-13 (EDR3)



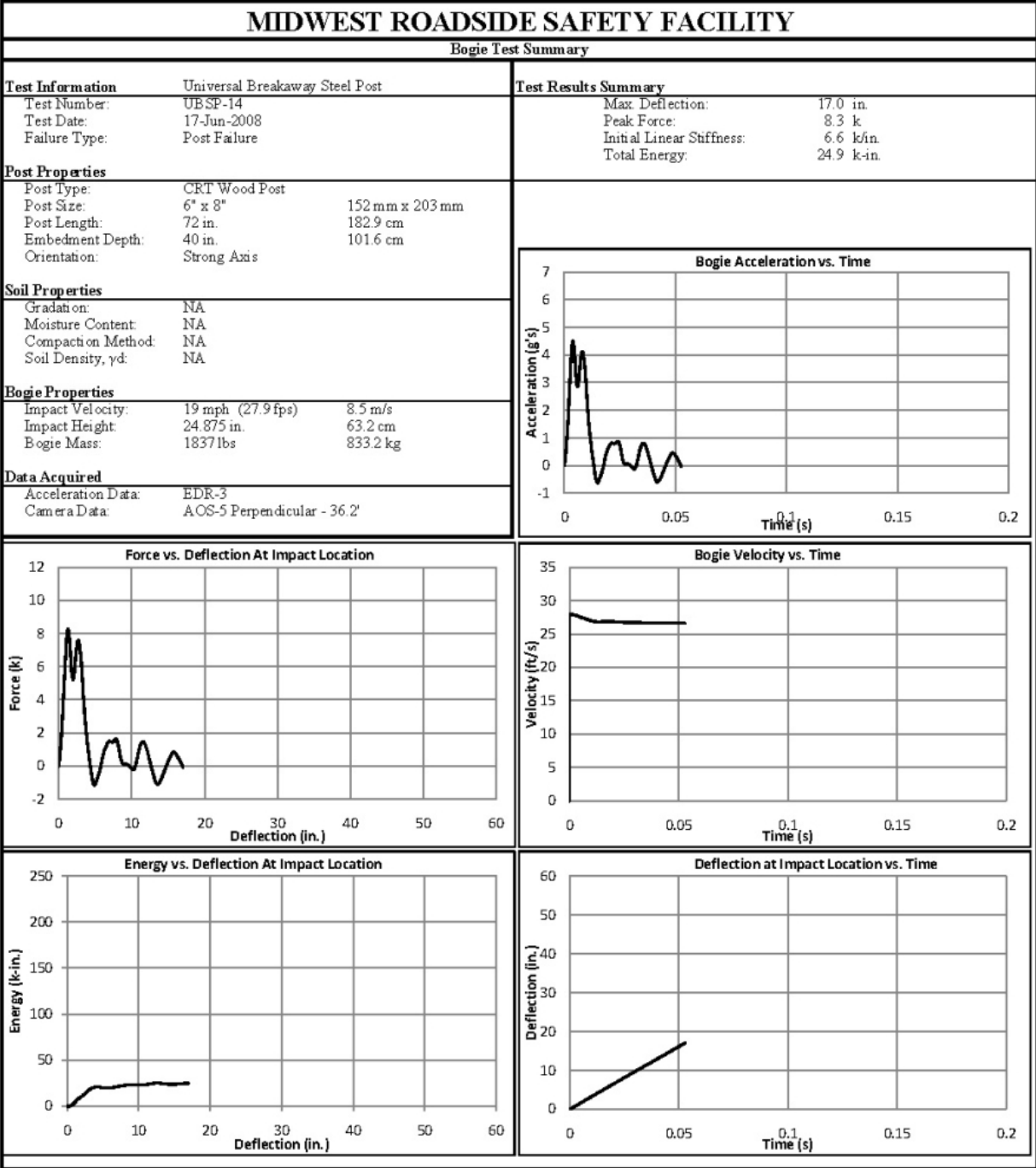


Figure A-13. Results of UBSP-14 (EDR3)

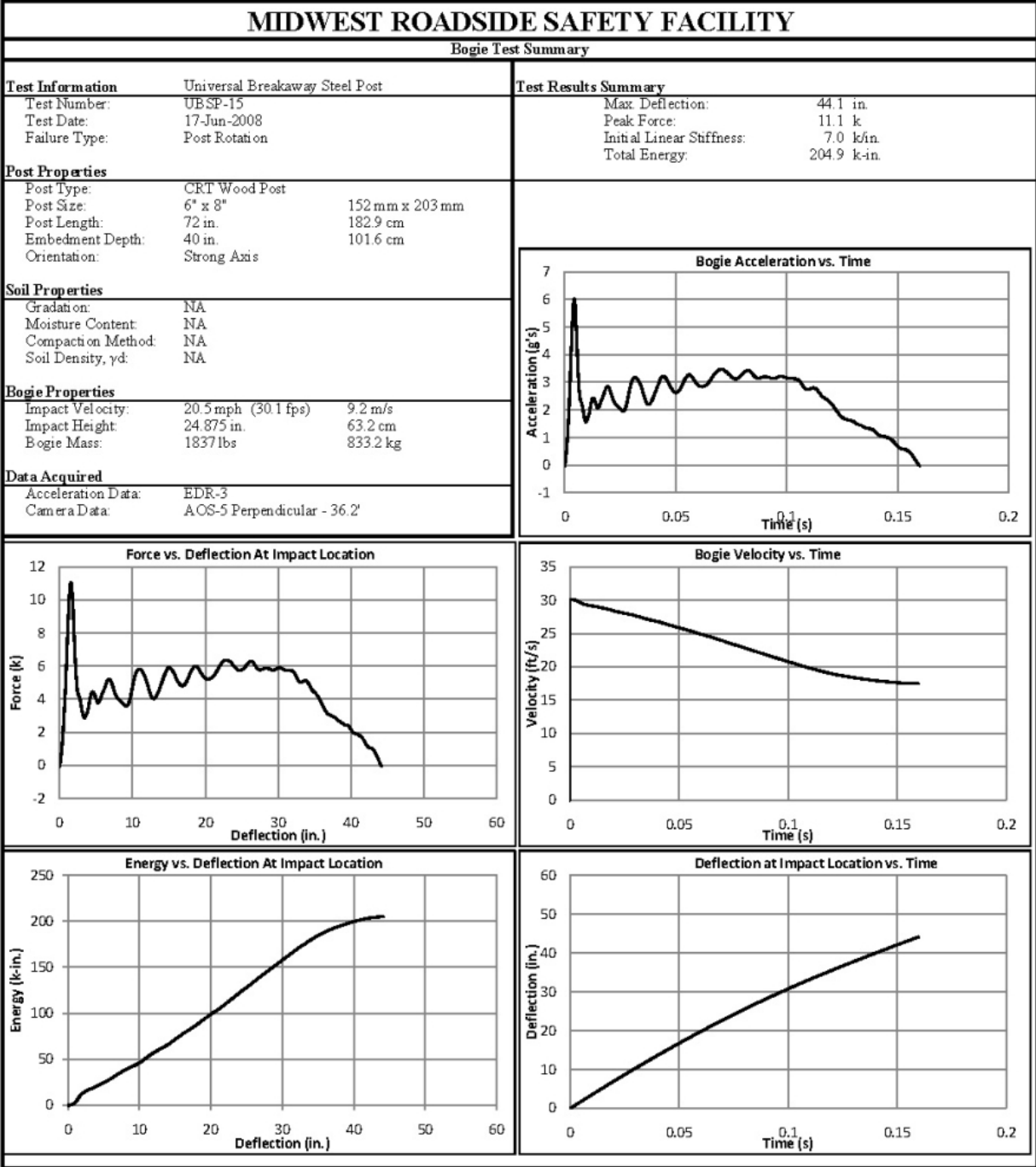


Figure A-14. Results of UBSP-15 (EDR3)

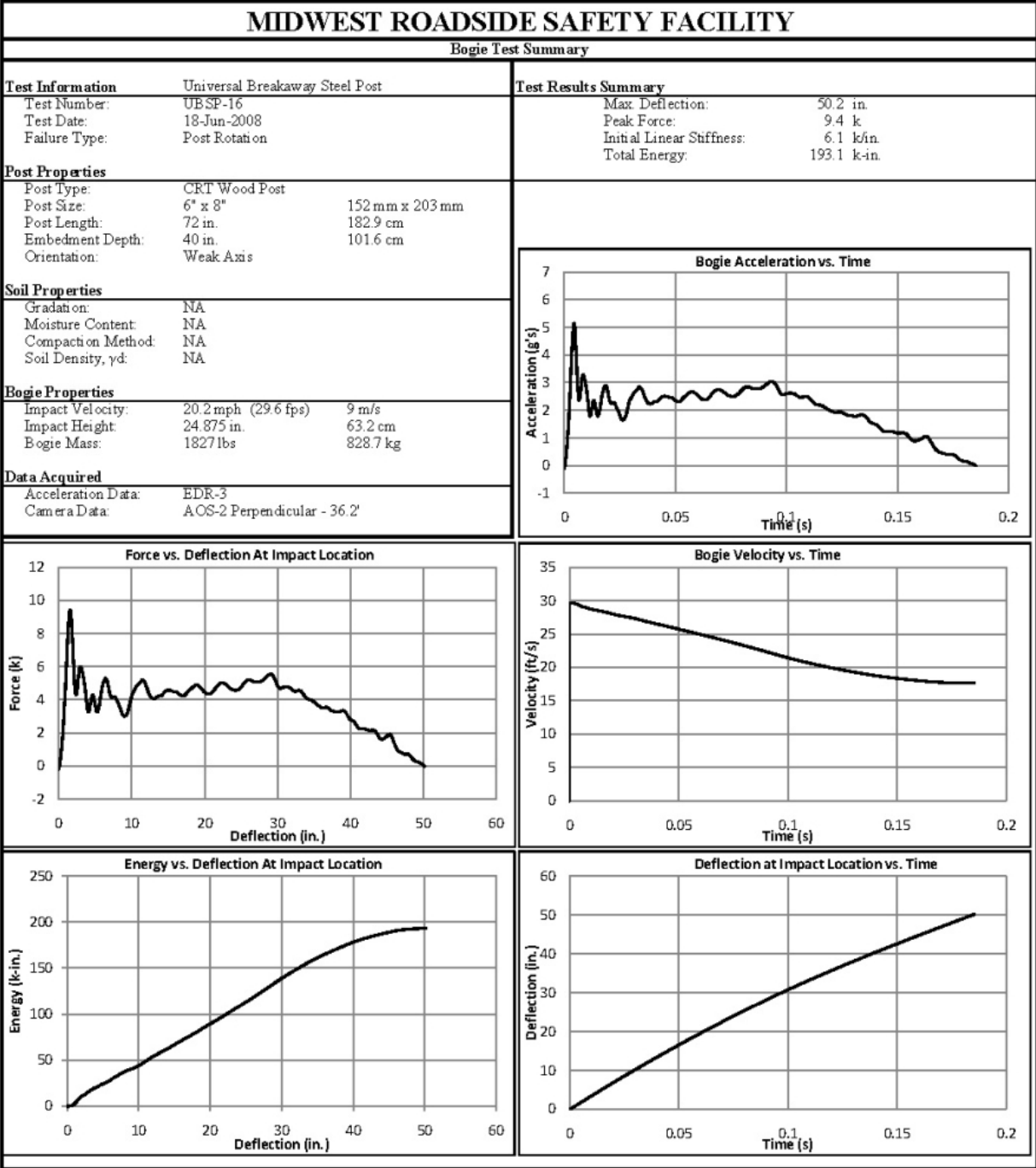


Figure A-15. Results of UBSP-16 (EDR3)

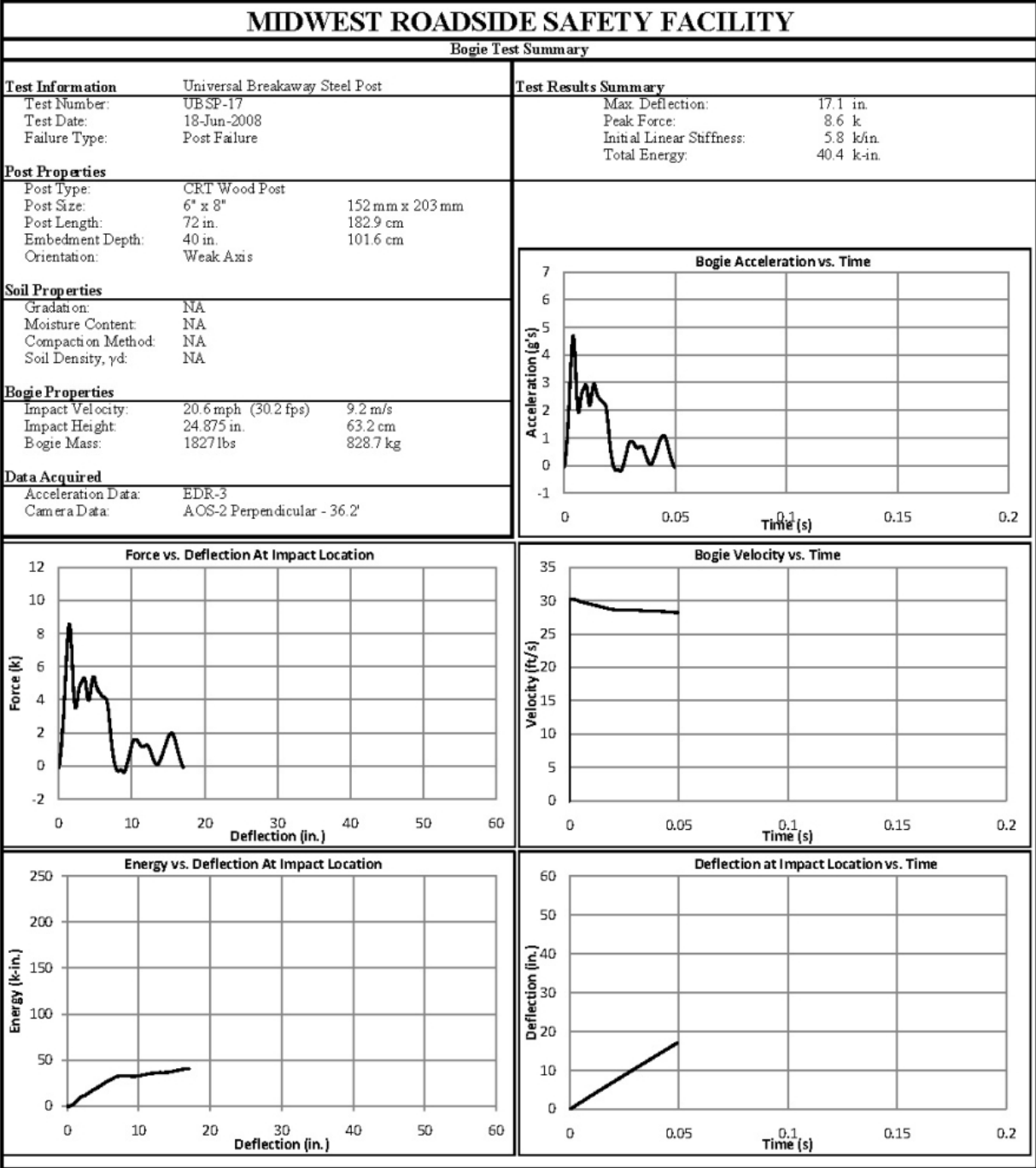


Figure A-16. Results of UBSP-17 (EDR3)

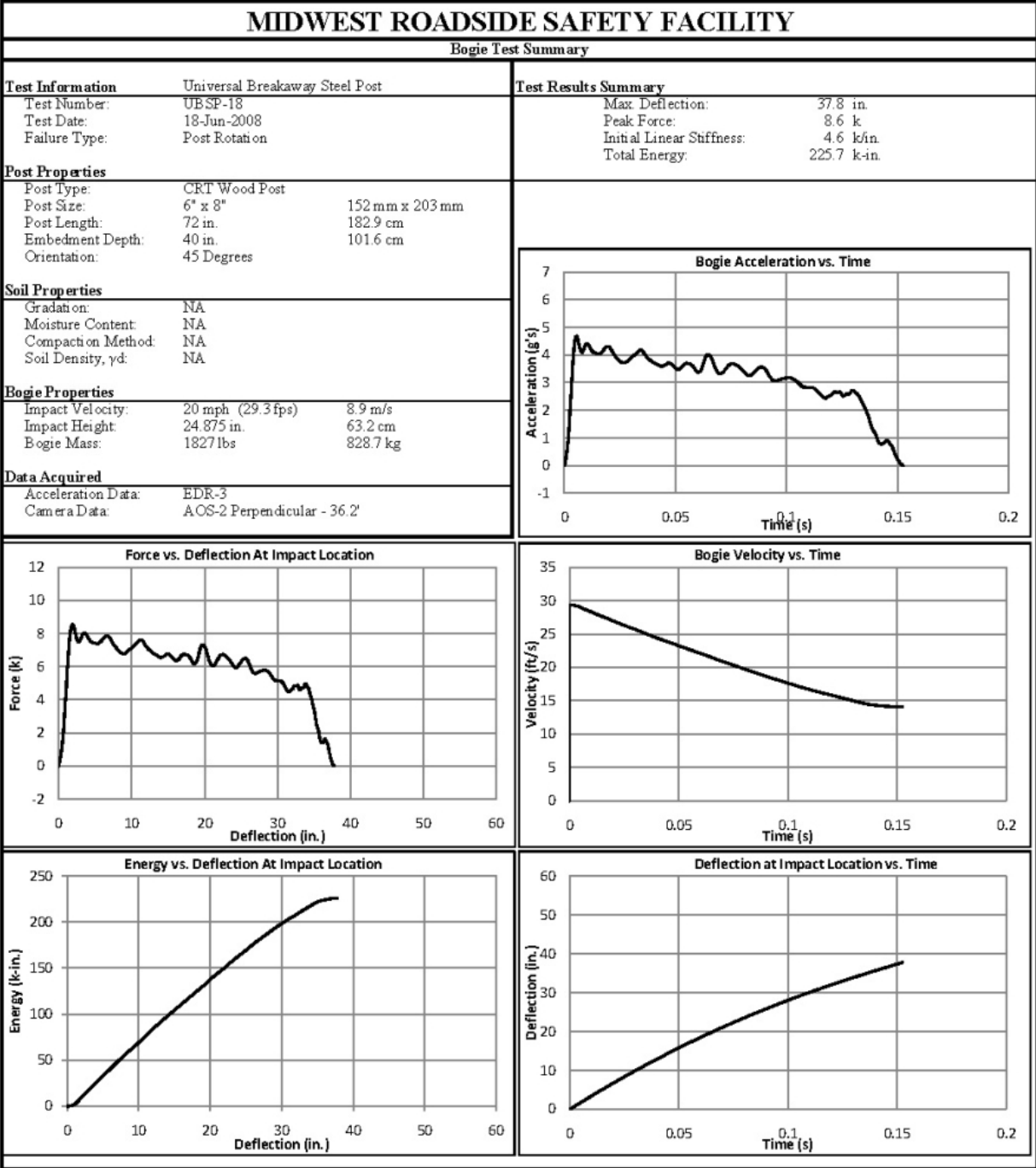


Figure A-17. Results of UBSP-18 (EDR3)

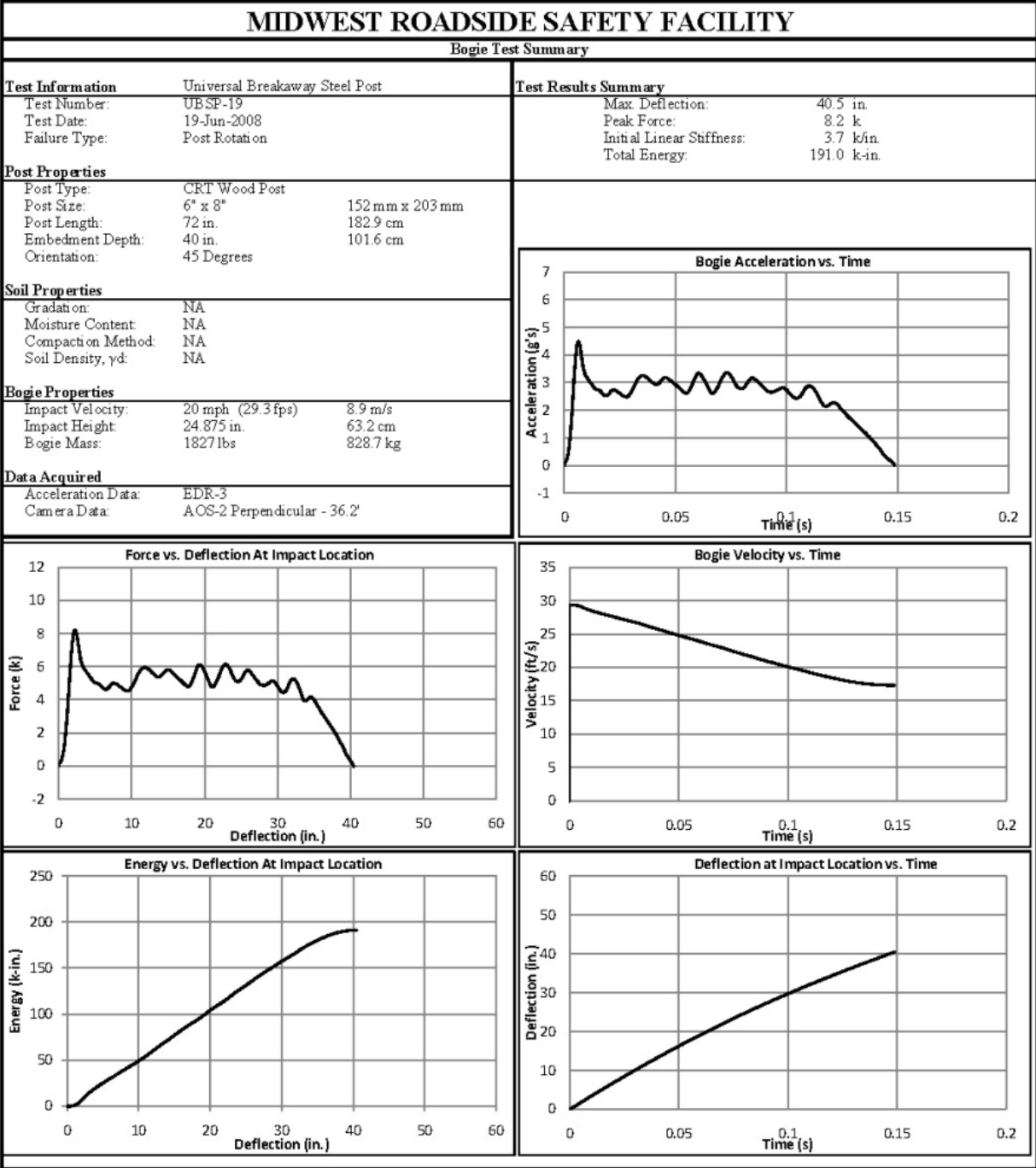


Figure A-18. Results of UBSP-19 (EDR3)

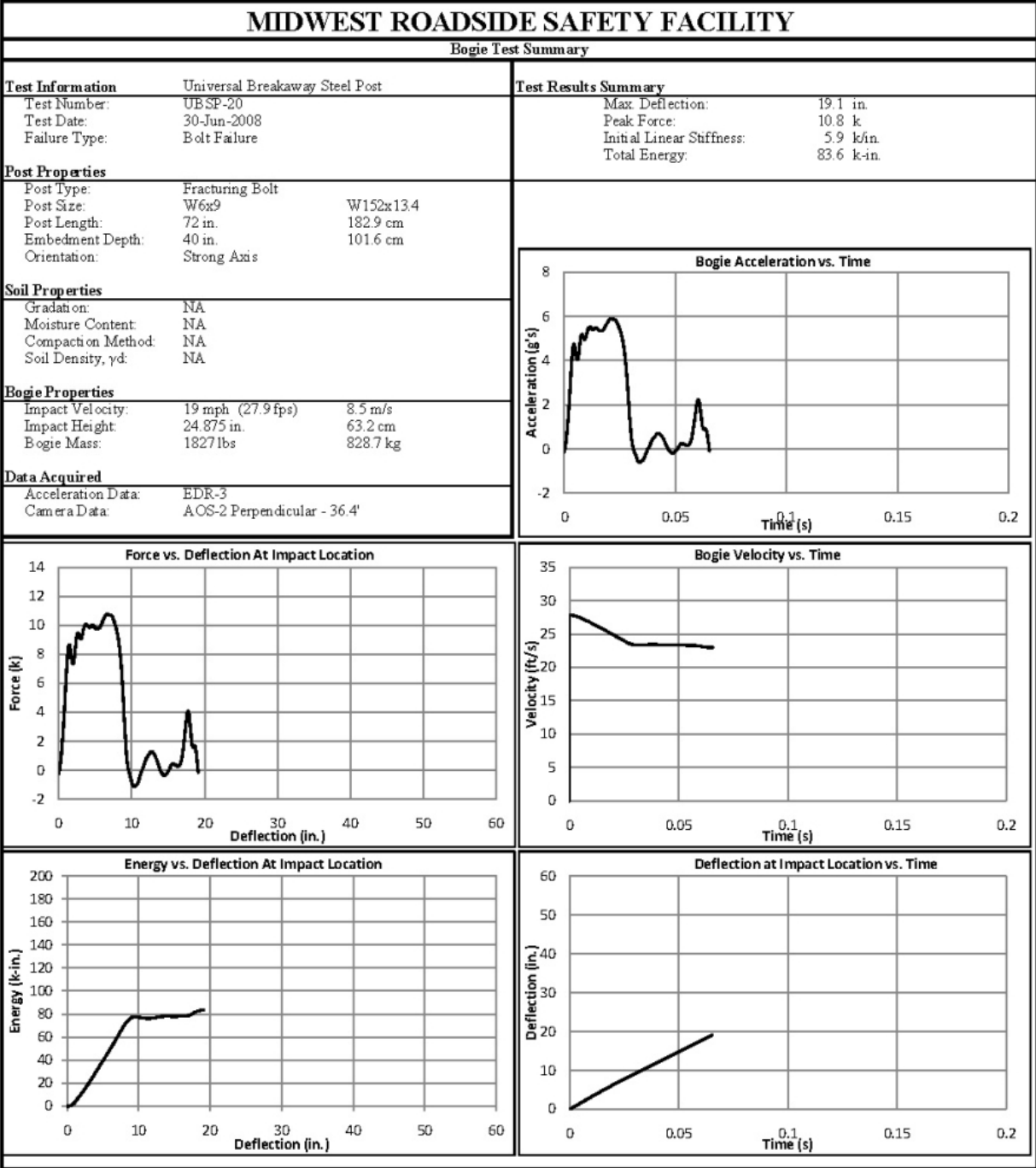


Figure A-19. Results of UBSP-20 (EDR3)

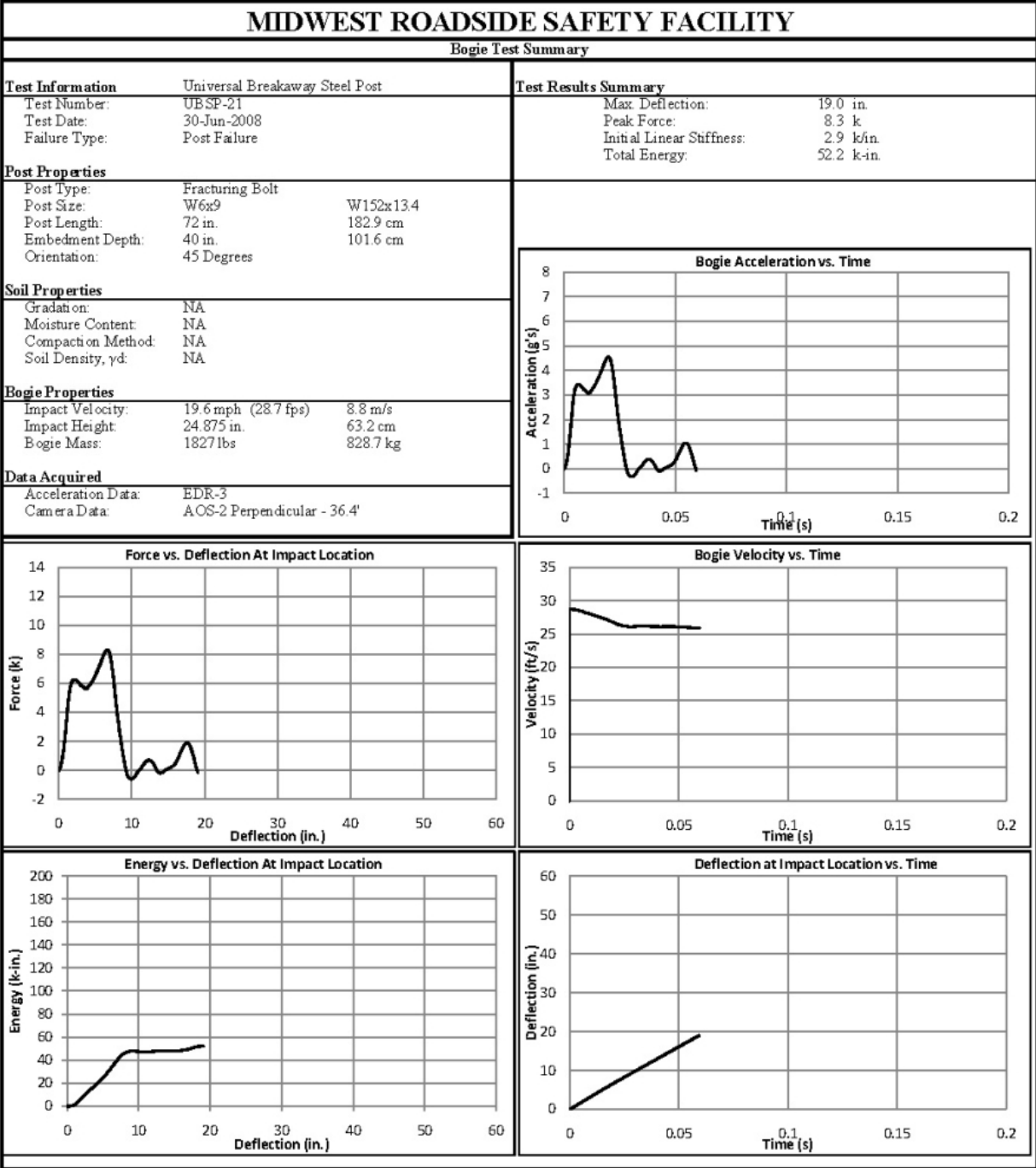


Figure A-20. Results of UBSP-21 (EDR3)



**Appendix B. Occupant Compartment Deformation, Test USPBN-1**

Figure B-1. Occupant Compartment Deformation Data, Set 1, Test USPBN-1

Figure B-2. Occupant Compartment Deformation Data, Set 2, Test USPBN-1

Figure B-3. Occupant Compartment Deformation Index (OCDI), Test USPBN-1

VEHICLE PRE/POST CRUSH INFO  
 Set-1

TEST: USPBN-1  
 VEHICLE: 2000 Chevy C2500

Note: If impact is on driver side need to enter negative number for Y

POINT	X	Y	Z	X'	Y'	Z'	DEL X	DEL Y	DEL Z
1	32.5	-30.25	-1.5	32.25	-30.25	-1.25	-0.25	0	0.25
2	36.25	-24.25	-0.25	36	-24	0	-0.25	0.25	0.25
3	36	-16.5	-0.5	36	-16.25	-0.25	0	0.25	0.25
4	28.75	-5.5	1	28.75	-5.5	0.5	0	0	-0.5
5	30.5	-30.5	-4.75	30.25	-30.5	-5	-0.25	0	-0.25
6	32	-24.5	-4.5	32	-24.5	-4.25	0	0	0.25
7	32.25	-17	-4.5	32.25	-17	-5	0	0	-0.5
8	28.5	-7.25	-2.75	28.5	-7.5	-3	0	-0.25	-0.25
9	26	-30.25	-7.75	26	-30.5	-7.75	0	-0.25	0
10	26.5	-25.25	-7.75	26.5	-25.25	-7.5	0	0	0.25
11	27	-19.75	-7.5	26.75	-19.75	-7.5	-0.25	0	0
12	25.5	-13	-7	25.5	-12.75	-7	0	0.25	0
13	23.25	-6.5	-3	23.25	-6.5	-3.25	0	0	-0.25
14	23	-1	-2.5	23	-1	-2.5	0	0	0
15	18.5	-30	-9.25	18.5	-30.25	-10	0	-0.25	-0.75
16	18.5	-23.25	-8.75	18.5	-23.5	-9	0	-0.25	-0.25
17	17.75	-16	-8.75	17.75	-16.25	-9	0	-0.25	-0.25
18	16	-6.25	-3.25	16	-6.25	-3.75	0	0	-0.5
19	15.75	-0.75	-3	15.75	-0.75	-3	0	0	0
20	12	-30	-9.25	12	-30.25	-10	0	-0.25	-0.75
21	12.5	-21.75	-8.75	12.25	-21.75	-9	-0.25	0	-0.25
22	12.25	-14	-8.5	12.25	-14.25	-9.5	0	-0.25	-1
23	9.5	-6	-3.75	9.5	-6	-4.25	0	0	-0.5
24	8.25	-0.75	-3.25	8.25	-0.75	-4	0	0	-0.75
25	1.25	-30	-9	1.25	-30.25	-9.75	0	-0.25	-0.75
26	0.5	-21.5	-8	0.5	-21.75	-7.5	0	-0.25	0.5
27	0.75	-15.25	-7.5	0.75	-15.5	-7.5	0	-0.25	0
28	1	-6.5	-4.25	1	-6.5	-4.5	0	0	-0.25
29	1	-1	-3.75	1	-1	-4	0	0	-0.25
30									

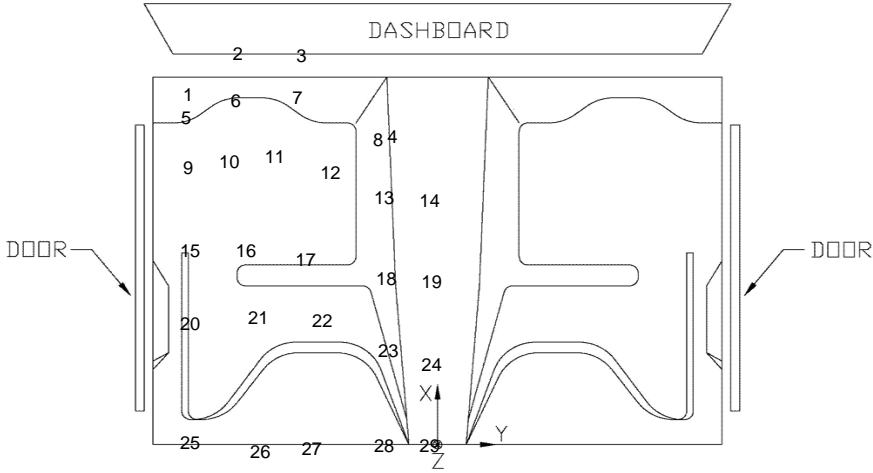


Figure B-1. Occupant Compartment Deformation, Set 1

VEHICLE PRE/POST CRUSH INFO  
 Set-2

TEST: USPBN-1  
 VEHICLE: 2000 Chevy C2500

Note: If impact is on driver side need to  
 enter negative number for Y

POINT	X	Y	Z	X'	Y'	Z'	DEL X	DEL Y	DEL Z
1	52	-20.25	-1.25	51.75	-20.25	-1.5	-0.25	0	-0.25
2	55.75	-14.25	0	55.5	-14	0	-0.25	0.25	0
3	55.5	-6.5	-0.5	55.5	-6.25	-0.5	0	0.25	0
4	48.25	4.5	0.5	48.25	4.5	0.5	0	0	0
5	50	-20.5	-4.25	49.75	-20.5	-4.5	-0.25	0	-0.25
6	51.5	-14.5	-4.5	51.5	-14.5	-4.5	0	0	0
7	51.75	-7	-4.25	51.75	-7	-4.5	0	0	-0.25
8	48	2.75	-3	48	2.5	-3.5	0	-0.25	-0.5
9	45.5	-20.25	-7.25	45.5	-20.5	-7.75	0	-0.25	-0.5
10	46	-15.25	-7.25	46	-15.25	-7.75	0	0	-0.5
11	46.5	-9.75	-7.25	46.25	-9.75	-7.75	-0.25	0	-0.5
12	45	-3	-7	45	-2.75	-7.25	0	0.25	-0.25
13	42.75	3.5	-3.25	42.75	3.5	-3	0	0	0.25
14	42.5	9	-2.75	42.5	9	-2.25	0	0	0.5
15	38	-20	-8.75	38	-20.25	-9	0	-0.25	-0.25
16	38	-13.25	-8.5	38	-13.5	-8.75	0	-0.25	-0.25
17	37.25	-6	-8.5	37.25	-6.25	-9	0	-0.25	-0.5
18	35.5	3.75	-3.5	35.5	3.75	-4.25	0	0	-0.75
19	35.25	9.25	-3.25	35.25	9.25	-3.75	0	0	-0.5
20	31.5	-20	-8.75	31.5	-20.25	-8.5	0	-0.25	0.25
21	32	-11.75	-8.5	31.75	-11.75	-8.5	-0.25	0	0
22	31.75	-4	-8.5	31.75	-4.25	-9.5	0	-0.25	-1
23	29	4	-3.75	29	4	-4.75	0	0	-1
24	27.75	9.25	-3.5	27.75	9.25	-4.25	0	0	-0.75
25	20.75	-20	-8.25	20.75	-20.25	-9	0	-0.25	-0.75
26	20	-11.5	-7.5	20	-11.75	-7.25	0	-0.25	0.25
27	20.25	-5.25	-7.25	20.25	-5.5	-7	0	-0.25	0.25
28	20.5	3.5	-4.25	20.5	3.5	-4.25	0	0	0
29	20.5	9	-3.75	20.5	9	-3.5	0	0	0.25
30									

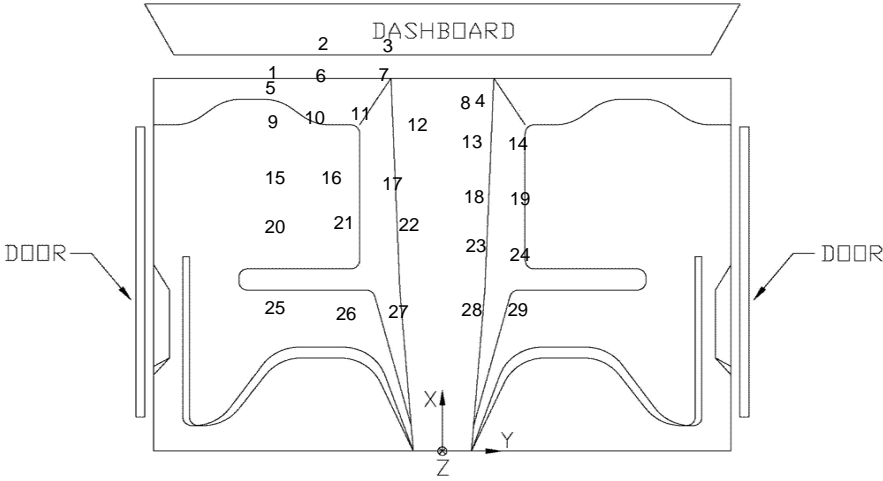


Figure B-2. Occupant Compartment Deformation, Set 2

**Occupant Compartment Deformation Index (OCDI)**

Test No. USPBN-1  
 Vehicle Type: 2000 Chevy G2500

OCDI - XXABCDEFGHI

XX = location of occupant compartment deformation

A = distance between the dashboard and a reference point at the rear of the occupant compartment, such as the top of the rear seat or the rear of the cab on a pickup

B = distance between the roof and the floor panel

C = distance between a reference point at the rear of the occupant compartment and the motor panel

D = distance between the lower dashboard and the floor panel

E = interior width

F = distance between the lower edge of right window and the upper edge of left window

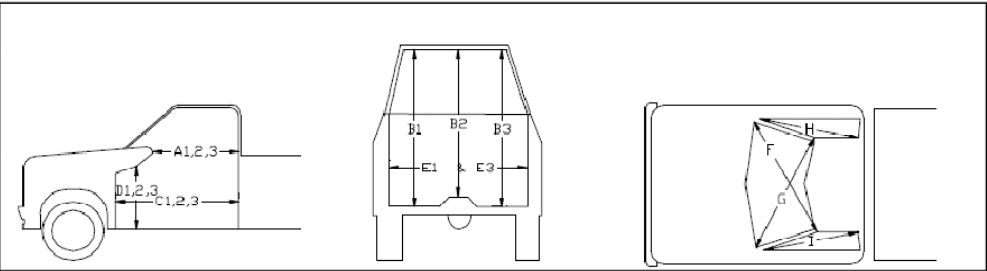
G = distance between the lower edge of left window and the upper edge of right window

H = distance between bottom front corner and top rear corner of the passenger side window

I = distance between bottom front corner and top rear corner of the driver side window

**Severity Indices**

- 0 - if the reduction is less than 3%
- 1 - if the reduction is greater than 3% and less than or equal to 10%
- 2 - if the reduction is greater than 10% and less than or equal to 20%
- 3 - if the reduction is greater than 20% and less than or equal to 30%
- 4 - if the reduction is greater than 30% and less than or equal to 40%



where,  
 1 = Passenger Side  
 2 = Middle  
 3 = Driver Side

**Location:**

Measurement	Pre-Test (in.)	Post-Test (in.)	Change (in.)	% Difference	Severity Index
A1	46.75	46.50	-0.25	-0.53	0
A2	47.25	47.50	0.25	0.53	0
A3	47.50	47.75	0.25	0.53	0
B1	43.25	38.50	-4.75	-10.98	2
B2	39.75	33.75	-6.00	-15.09	2
B3	44.50	41.00	-3.50	-7.87	1
C1	59.25	60.00	0.75	1.27	0
C2	54.75	55.00	0.25	0.46	0
C3	58.25	58.50	0.25	0.43	0
D1	21.75	21.50	-0.25	-1.15	0
D2	17.25	17.00	-0.25	-1.45	0
D3	22.25	22.00	-0.25	-1.12	0
E1	62.25	62.25	0.00	0.00	0
E3	63.50	63.50	0.00	0.00	0
F	54.25	54.00	-0.25	-0.46	0
G	57.50	58.00	0.50	0.87	0
H	41.50	43.00	1.50	3.61	1
I	41.25	43.25	2.00	4.85	1

Note: Maximum severity index for each variable (A-I) is used for determination of final OCDI value

Final OCDI: XXABCDEFGHI  
 LF 0 2 0 0 0 0 0 1 1

**Figure B-3. Occupant Compartment Deformation Index (OCDI)**

### **Appendix C. Accelerometer Data Analysis, Test USPBN-1**

Figure C-1. Graph of Longitudinal Deceleration – Filtered Data, Test USPBN-1

Figure C-2. Graph of Longitudinal Occupant Impact Velocity – Filtered Data, Test USPBN-1

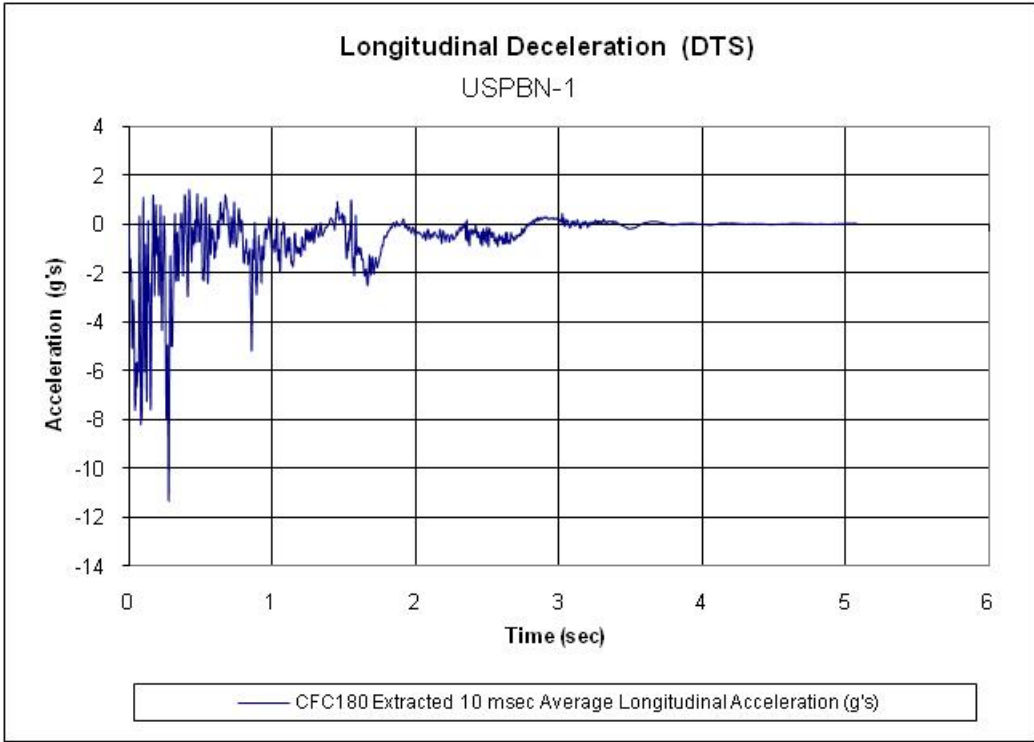
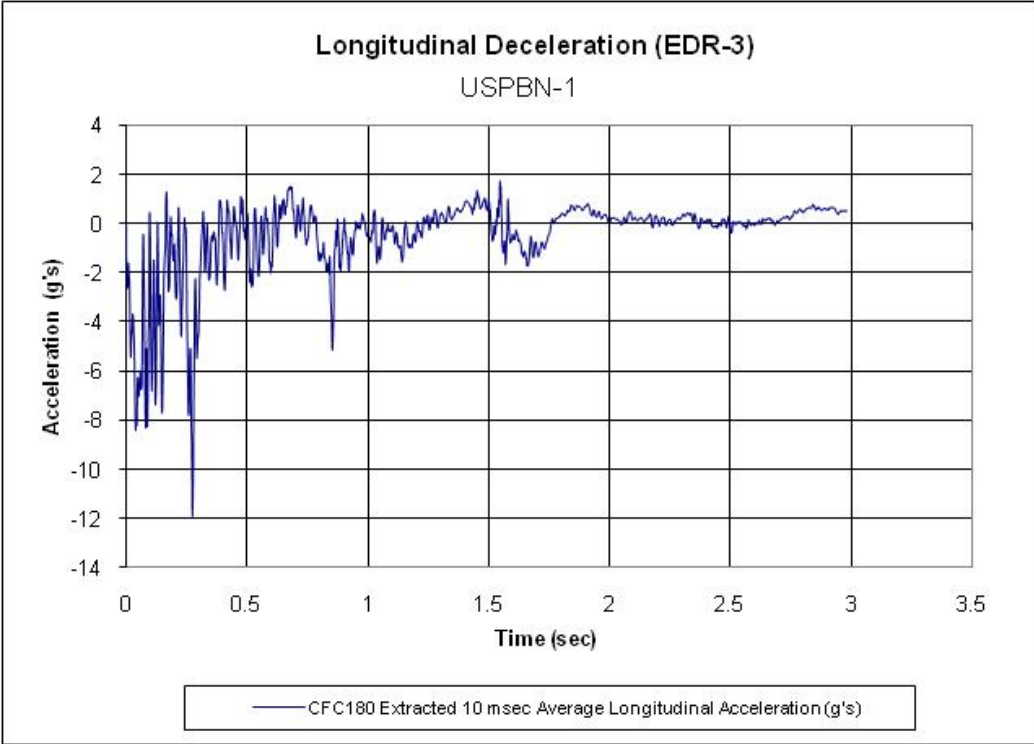
Figure C-3. Graph of Longitudinal Occupant Displacement – Filtered Data, Test USPBN-1

Figure C-4. Graph of Lateral Deceleration – Filtered Data, Test USPBN-1

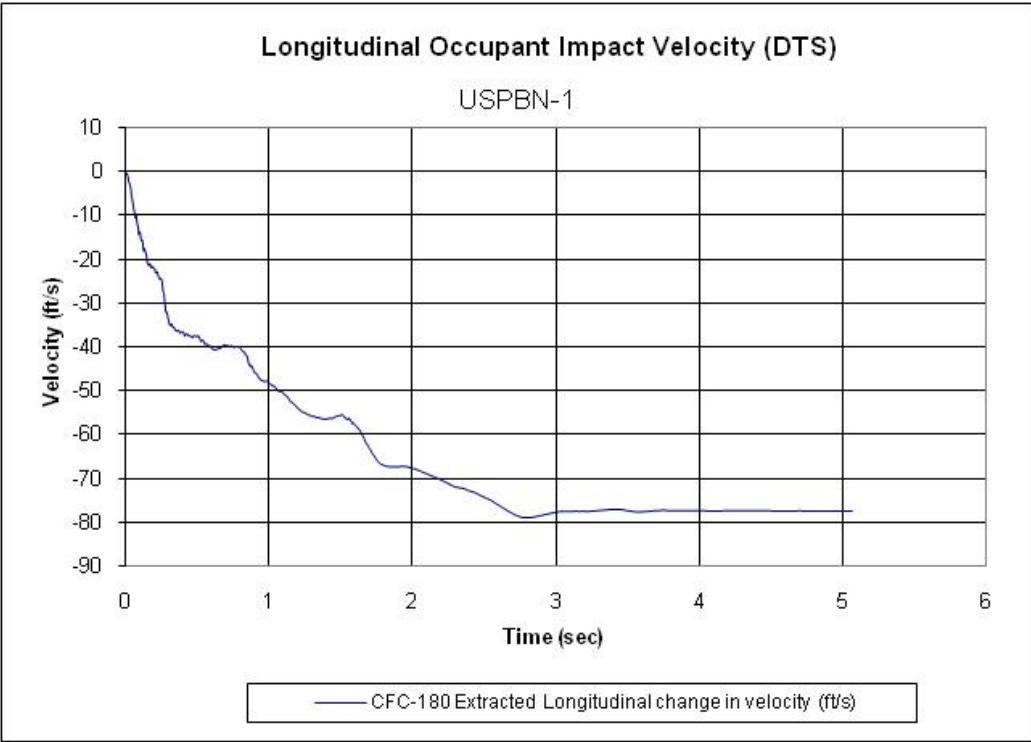
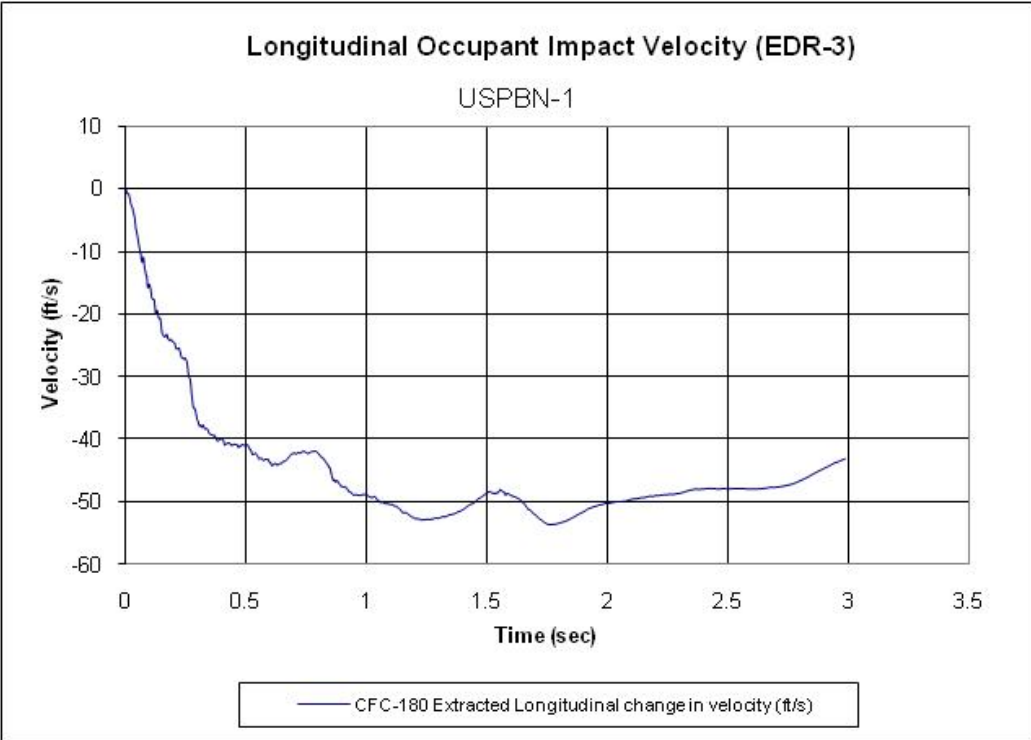
Figure C-5. Graph of Lateral Occupant Impact Velocity – Filtered Data, Test USPBN-1

Figure C-6. Graph of Lateral Occupant Displacement – Filtered Data, Test USPBN-1

Figure C-7. Rate Transducer Data, Test USPBN-1



**Figure C-1. Graph of Longitudinal Deceleration – Filtered Data, Test USPBN-1**



**Figure C-2. Graph of Longitudinal Occupant Impact Velocity – Filtered Data, Test USPBN-1**

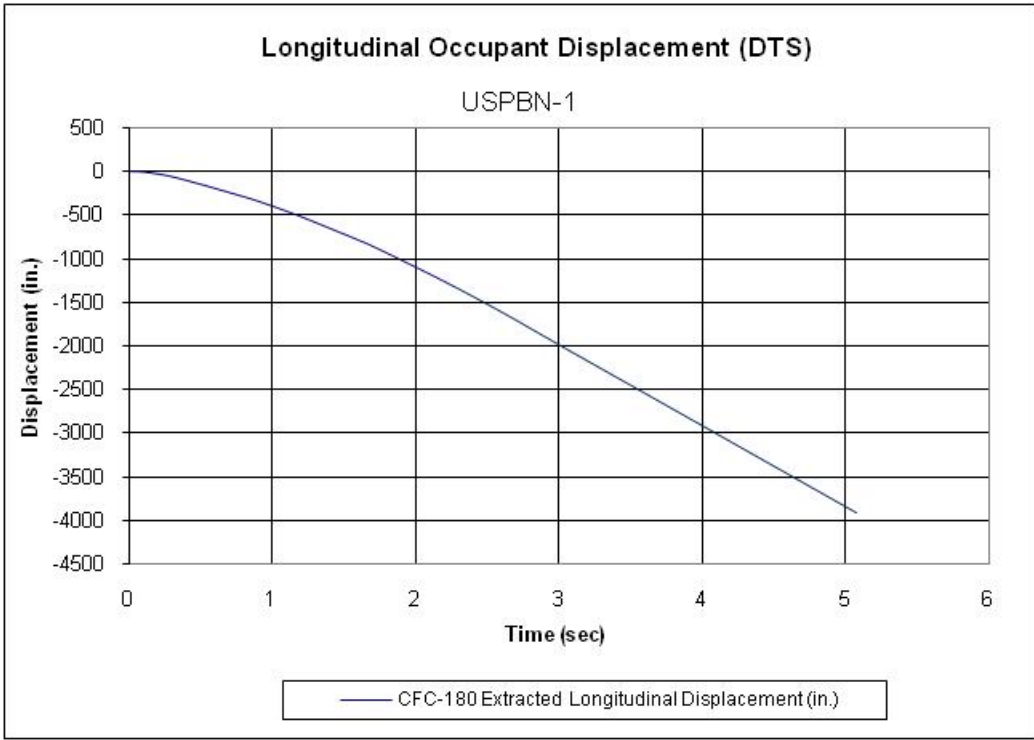
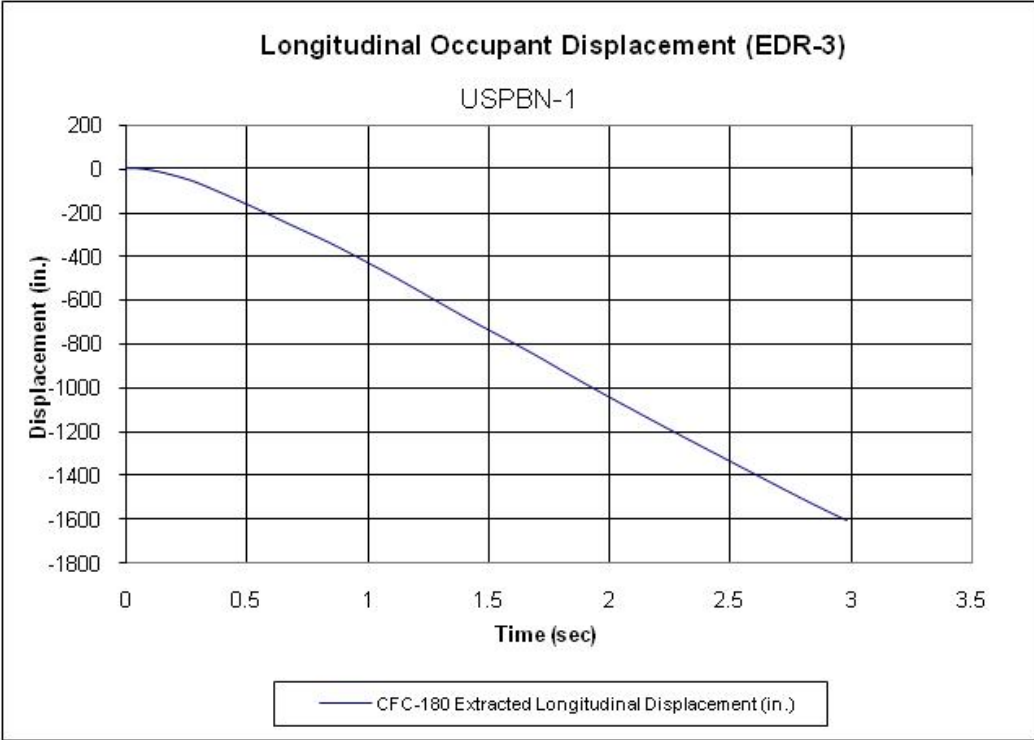
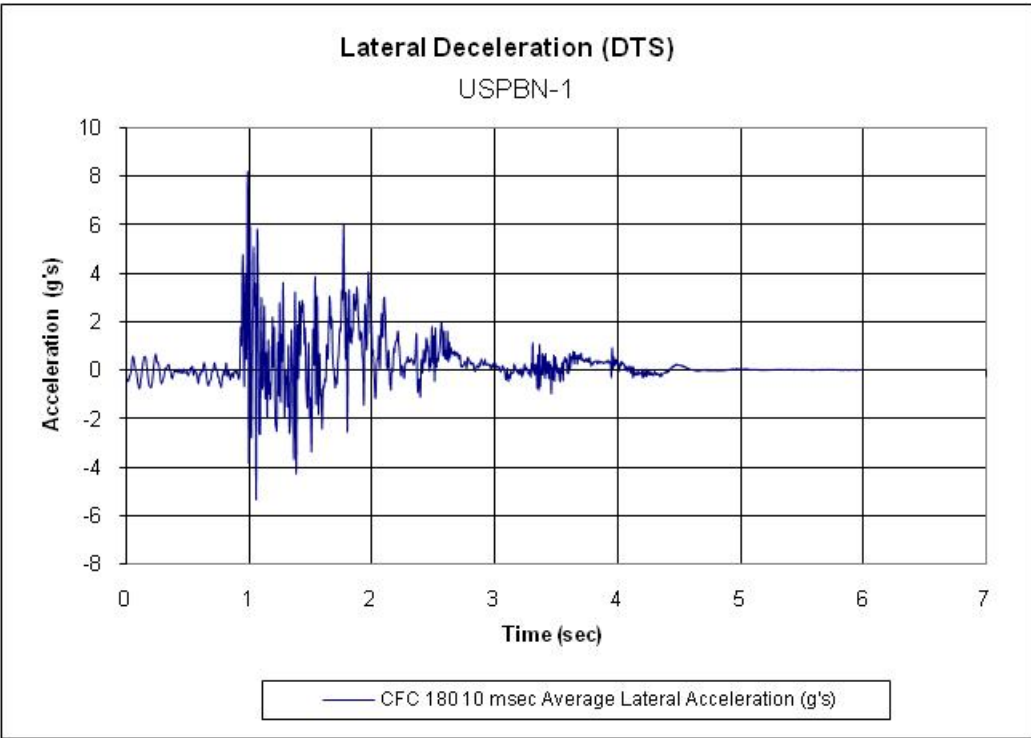
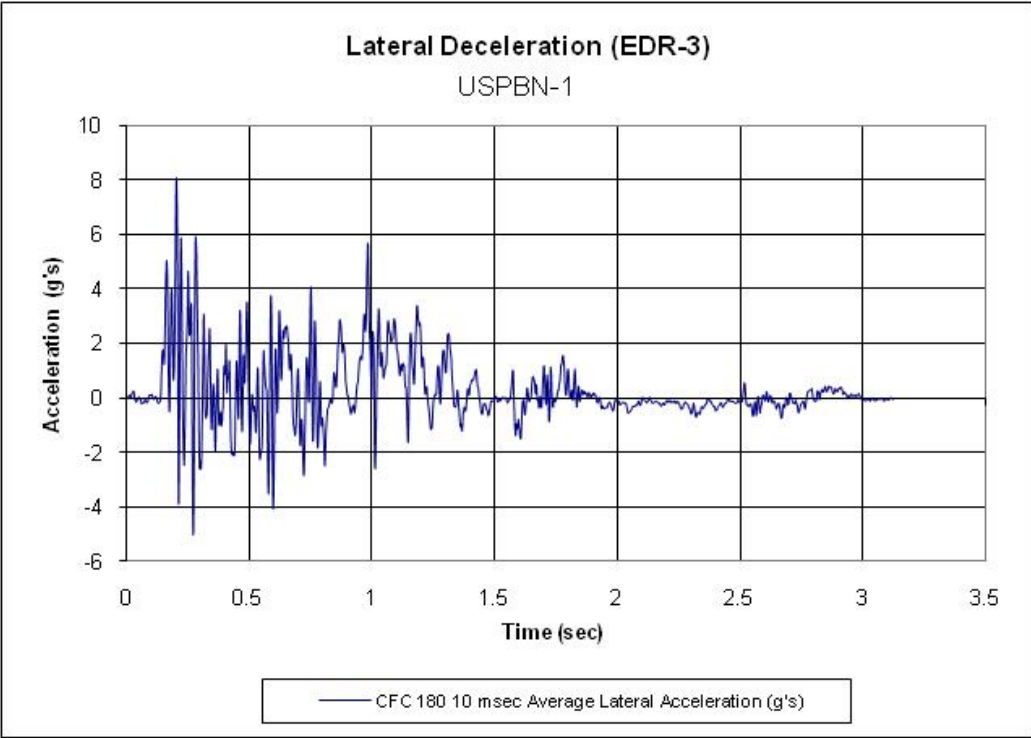


Figure C-3. Graph of Longitudinal Occupant Displacement – Filtered Data, Test USPBN-1





**Figure C-4. Graph of Lateral Deceleration – Filtered Data, Test USPBN-1**

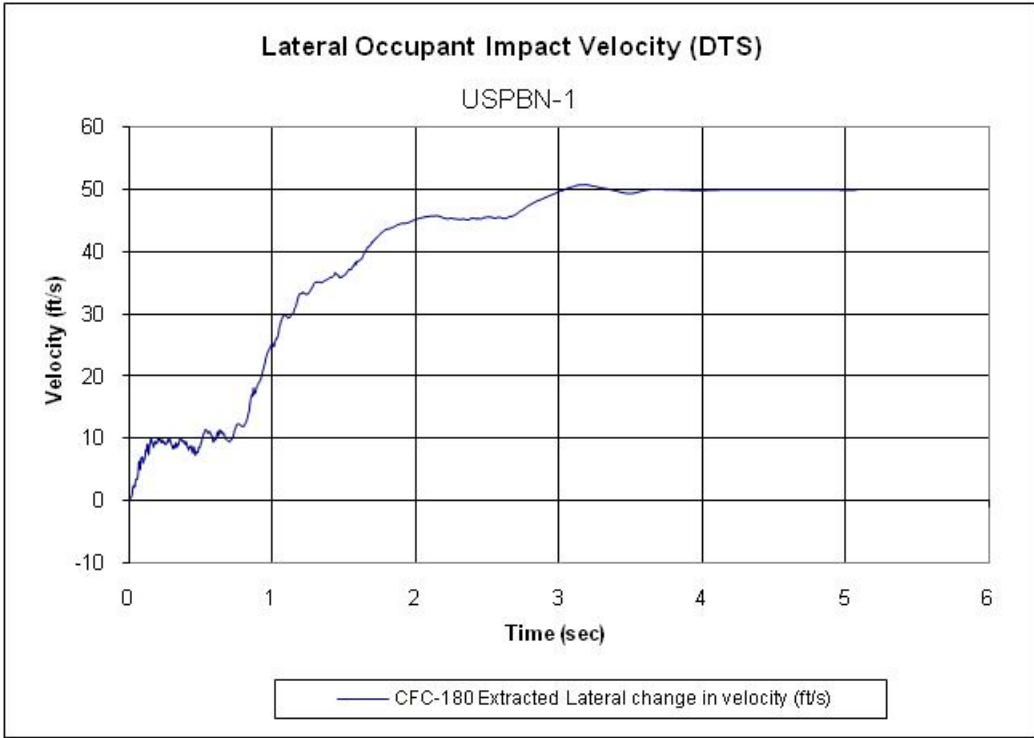
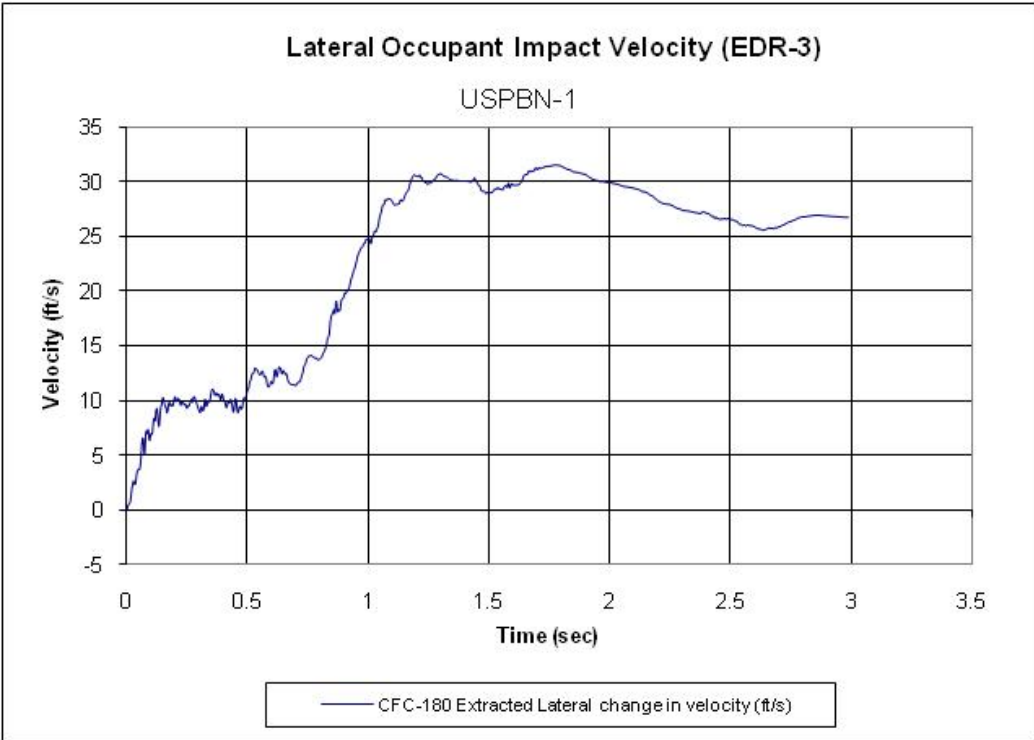
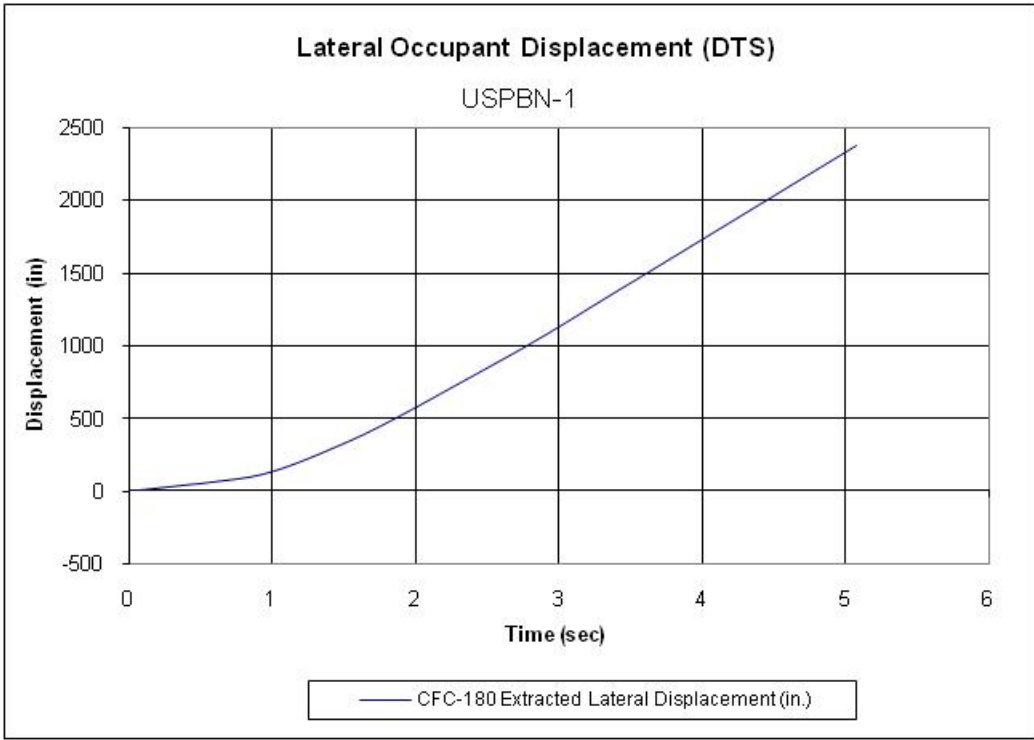
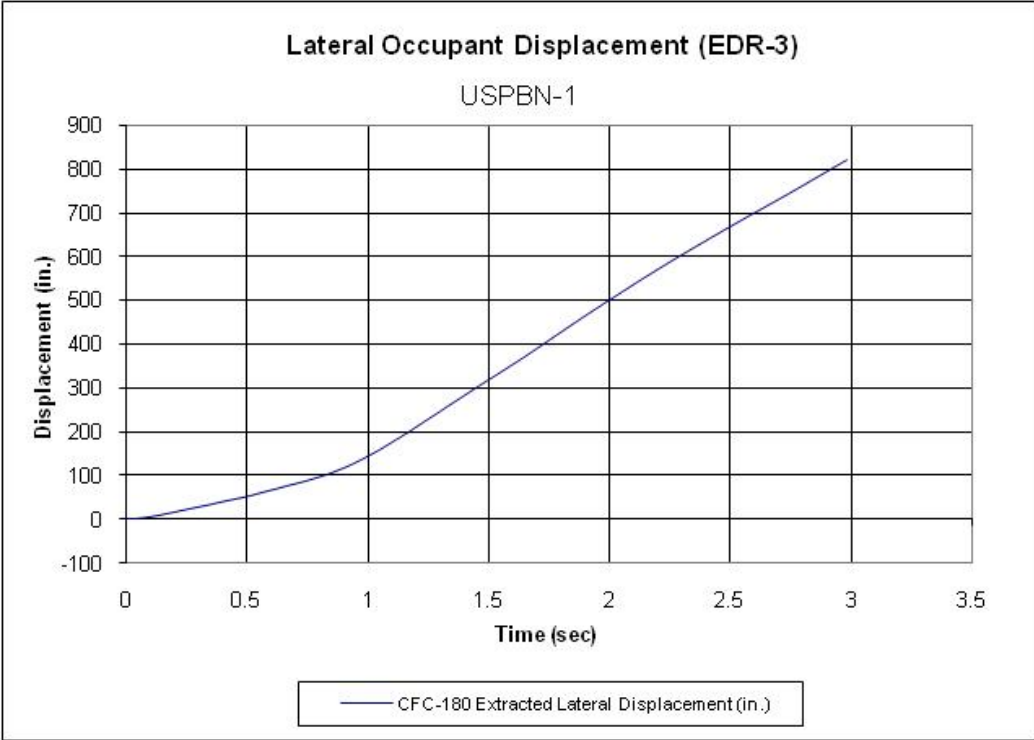


Figure C-5. Graph of Lateral Occupant Impact Velocity – Filtered Data, Test USPBN-1



**Figure C-6. Graph of Lateral Occupant Displacement – Filtered Data, Test USPBN-1**

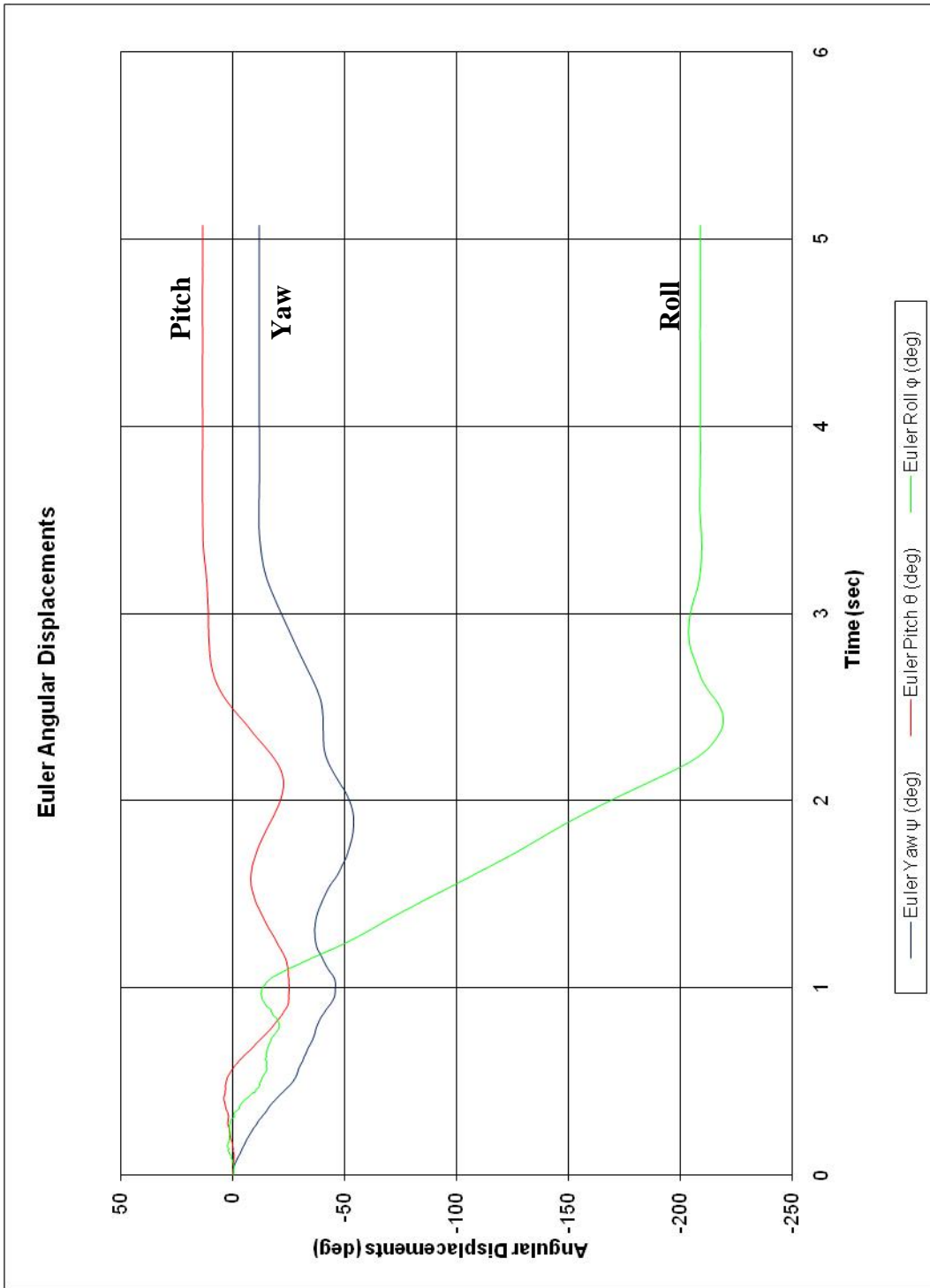


Figure C-7. Rate Transducer Data, Test USPBN-1

## **Appendix D. Summary of Test USPBN-1 in Metric Units**

Figure D-1. Summary of Test Results and Sequential Photographs (Metric), Test USPBN-1

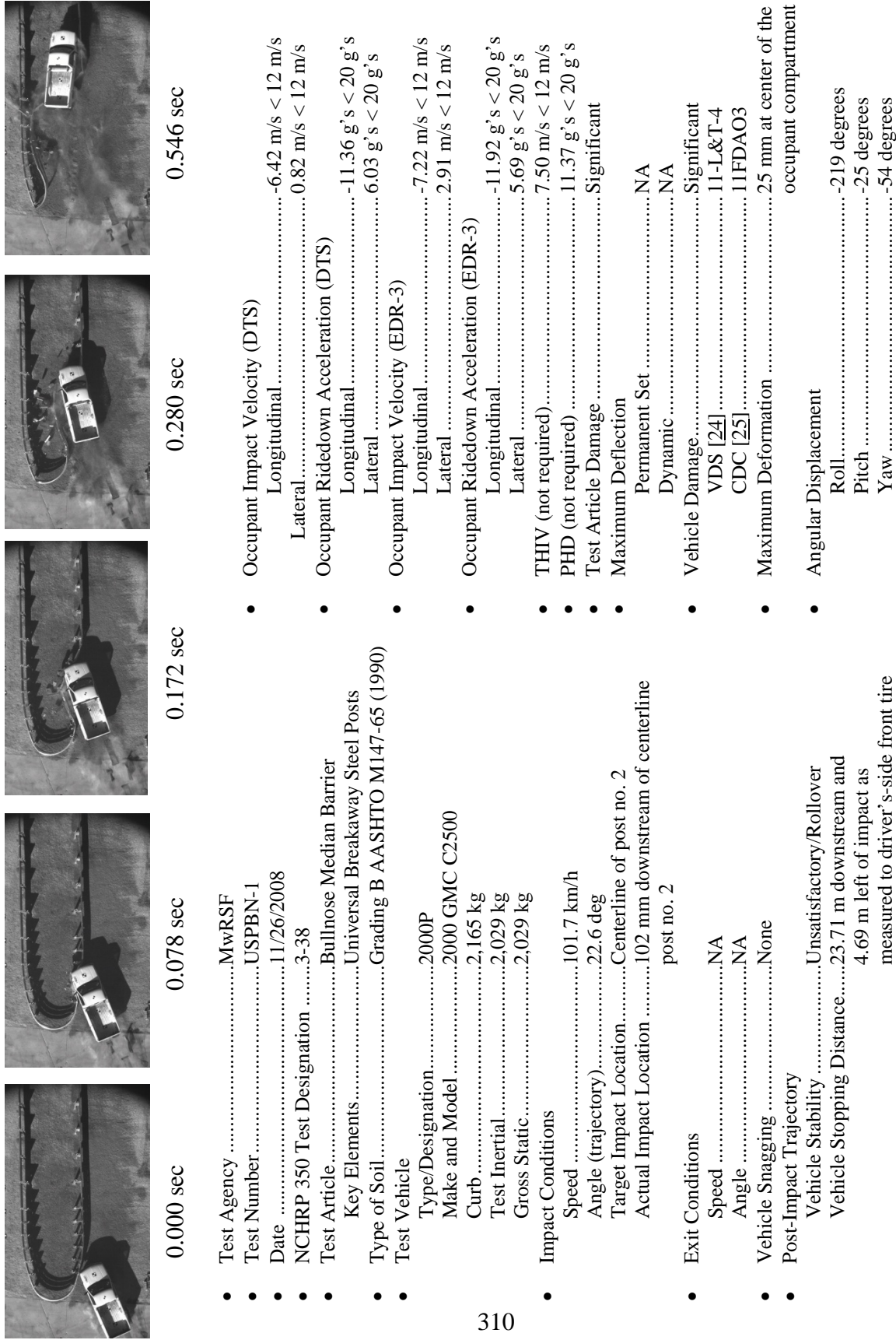


Figure D-1. Summary of Test Results and Sequential Photographs (Metric), Test USPBN-1

**END OF DOCUMENT**